Regulation of Pulmonary Vascular Remodelling by Double-Stranded RNA

Helena Adele Turton

Submitted towards the degree of Doctor of Philosophy

Division of Clinical Medicine

School of Medicine and Population Health

University of Sheffield

December 2023

Acknowledgments

Firstly, I would like to extend my deepest thanks to my supervisor, Dr Roger Thompson, whose guidance, and expertise played a crucial role in shaping this challenging but rewarding PhD journey. Your meticulous feedback, and dedication to my academic development have been appreciated throughout. Thank you for allowing me to pursue this PhD alongside my staff research assistant position.

I would like to thank my supervisor Professor Sheila Francis for your feedback and for being an excellent role model to me and all women in STEM. I would also like to thank my supervisor Professor Allan Lawrie for your invaluable research expertise. I also thank Professor Allan Lawrie for creating a vibrant working environment in the form of the Pulmonary Vascular Research Group. I am thankful to all past and present members of the group. I am particularly grateful to Dr Laura West and Ms Nadine Arnold for their time given towards my *in vivo* experiments. I am lucky enough to say that these colleagues became great friends, providing encouragement, laughter, and a listening ear throughout the ups and downs of life. My thanks also goes out to the wider community of the Division of Clinical Medicine including Ms Fiona Wright and Mr Sam Caughran for their histology contributions. A huge thank you to my funder, British Heart Foundation (BHF). This work was specifically funded by BHF Intermediate Clinical Fellowship granted to Dr Roger Thompson (FS/18/13/13328).

My friendship groups outside of work have been fundamental in this PhD journey too. I would like to thank my oldest friends, Meg, Hannah, and Sophie for being so caring and supportive, particularly through my final year. Milly and Ellen whose friendship I particularly cherish. Laura, Kate, and Suze for creating much-needed adventure weekends. And thank you to all my netball and yoga friends who provided a space for healthy competition and relaxation outside of work.

A huge thank you to Mum, Craig and Sophie for your endless love and support. Thank you to our newest family member, Elsie, who has already brought so much joy, and at times when I needed it the most. Though he is no longer with us in person, I would like to thank my Dad, whose love, support, and outlook on life continues to inspire me.

This work is dedicated to the memory of my Dad whose influence will forever shape my academic and personal journey.

Abstract

Double-stranded (ds)RNA signalling pathways are components of innate immunity associated with pro-inflammatory cytokine and type I interferon production. The role of dsRNA pathway activation in the pulmonary vasculature is not clear. Previous evidence of dsRNA conferring protection in animal models of pulmonary hypertension (PH) contrasts with the dogma that inflammation drives pulmonary vascular remodelling. This apparent paradox was explored in this thesis.

The role of synthetic dsRNA (poly(I:C)) in a Sugen hypoxic (SuHx) mouse model of PH was investigated. Prophylactic intraperitoneal poly(I:C) had no effect on the severity of PH or vascular remodelling in this model. To investigate whether the timing and route of administration of dsRNA impacted outcomes, experiments assessed the effect of prior administration of intranasal poly(I:C) in the SuHx model. A single instillation of intranasal poly(I:C)-induced lung inflammation and subsequent exposure to SuHx enhanced pulmonary vascular remodelling and haemodynamic estimates of pulmonary vascular resistance.

This thesis also explored whether a genetic predisposition to pulmonary vascular remodelling (*EIF2AK4* mutation) altered responses to dsRNA. *EIF2AK4* encodes for GCN2, and loss-of-function mutations are associated with pulmonary veno-occlusive disease, a rare sub-type of PH. In human pulmonary artery endothelial cells with GCN2 deficiency, poly(I:C) enhanced release of TNFα. However, mice with global knockout of GCN2 did not have an exaggerated PH phenotype following exposure to intranasal poly(I:C) and hypoxia.

Together these data favour the hypothesis that canonical pro-inflammatory pathway activation by dsRNA is associated with enhanced pulmonary vascular remodelling. Specifically, previous exposure to dsRNA-induced lung inflammation may act as a potential driver in PAH pathogenesis, while dsRNA activation of endothelial cells may promote a pro-inflammatory phenotype in the context of GCN2 deficiency. Further work is required to associate prior viral lung inflammation with PH and to investigate the potential role of TNFα in PVOD pathogenesis.

Publications in association with this thesis

Turton, H., Thompson, R., & Farkas, L. **RNA Signalling in Pulmonary Arterial Hypertension — A Double-Stranded Sword**. *International Journal of Molecular Sciences*. 2020.

Turton, H., ..., Lawrie, A., & R., Thompson. **Prior lung inflammation induced by intranasal double-stranded RNA does not exacerbate pulmonary hypertension in a mouse model.** *ERJ Open Research.* 2023. *(Conference paper)*.

Schwiening, M., … **Turton, H**., & Soon, E. **Unpicking the Effects of General Control Non-depressible 2 (GCN2) Deficiency in Pulmonary Veno-Occlusive Disease.** American Thoracic Society 2023. *(Conference paper)*.

Publications as a Research Assistant

Contributing authorship:

Turton, H., Pickworth, J., Paterson, G., Lawrie, A., Baillie, K., & R Thompson**. Soluble P-Selectin and von Willebrand Factor Rise in Healthy Volunteers Following Non-Exertional Ascent to High Altitude.** *Frontiers in Physiology*. 2022.

Zawia, A., …, **Turton, H.,** & Thompson, R., & Lawrie, A. **Altered Macrophage Polarization Induces Experimental Pulmonary Hypertension and Is Observed in Patients with Pulmonary Arterial Hypertension.** *Arteriosclerosis, Thrombosis, and Vascular Biology*. 2021.

Keir, H., … **Turton, H.,** & Chalmers, J. **Dipeptidyl peptidase-1 inhibition in patients hospitalised with COVID-19: a multicentre, double-blind, randomised, parallel-group, placebo-controlled trial.** *The Lancet Respiratory Medicine*. 2022.

Durrington, C., …**Turton, H.,** & R. Thompson. **Assessing the Repeatability of NT-proBNP Testing Using Laboratory and Point of Care Testing in PAH (REPEAT-PAH*). American Thoracic Society 2023*. (*Conference paper)*.

Consortium authorship:

Angyal, A., *et al.* **T-cell and antibody responses to first BNT162b2 vaccine dose in previously infected and SARS-CoV-2-naive UK health-care workers: a multicentre prospective cohort study**. *The Lancet Microbe*. 2021.

Zheng, B., *et al*. **Determinants of recovery from post-COVID-19 dyspnoea: analysis of UK prospective cohorts of hospitalised COVID-19 patients and community-based controls.** *The Lancet Regional Health – Europe*. 2023.

Evans, R., et al. **Clinical characteristics with inflammation profiling of long COVID and association with 1-year recovery following hospitalisation in the UK: a prospective observational study.** *The Lancet Respiratory medicine*. 2022.

Jackson, C., et al. **Effects of sleep disturbance on dyspnoea and impaired lung function following hospital admission due to COVID-19 in the UK: a prospective multicentre cohort study.** *The Lancet Respiratory medicine*. 2023.

Copyright Notice

Table of Contents

List of figures

List of tables

Abbreviations

α-SMA	Alpha smooth muscle actin
ABEVG	Miller's elastin stain with alcian blue and Curtis' modified van Gieson
ADAR	Adenosine deaminases acting on RNA
ANOVA	Analysis of variance
Ao	Aortic
AP1	Activator protein 1
ATF4	Activating transcription factor 4
BOECs	Blood outgrowth endothelial cells
BMP	Bone morphogenetic protein
BMPR2	Bone morphogenetic protein receptor type 2
CSA	Cross-sectional area
CO	Cardiac output
Ct	Threshold cycle
CT	Computerised tomography
CTEPH	Chronic thromboembolic pulmonary hypertension
CXCL	Chemokine ligand
DAMPs	Damage associated molecular patterns
dCt	Ct target gene normalised to Ct reference gene, delta Ct
ddCt	dCt target sample normalised to dCt reference sample, delta delta Ct
DEGs	Differentially expressed genes
dP/dt	Delta pressure/delta time; change in pressure over time
dsRNA	Double stranded RNA
ECs	Endothelial cells
eIF2α	Eukaryotic translation initiation factor 2
EIF2AK4	Eukaryotic initiation factor 2α kinase 4
EMCV	Encephalomyocarditis virus
ePVR	Estimated pulmonary vascular resistance
FDR	False discovery rate
GAPDH	Glyceraldehyde 3-phosphate dehydrogenase
GCN2	General control nonderepressible 2
GM-CSF	Granulocyte macrophage colony-stimulating factor
GO	Gene ontology
HIV	Human immunodeficiency virus
Hx	Hypoxia
IFN	Interferon
IFNAR1	Interferon Alpha And Beta Receptor Subunit 1
IL	Interleukin
IPAH	Idiopathic pulmonary arterial hypertension
ISR	Integrated stress response
IRF3	Interferon regulatory factor 3
KEGG	Kyoto Encyclopaedia of Genes and Genomes
KO	Knockout
LPS	Lipopolysaccharide
LV	Left ventricle
LVEDP	Left ventricular end diastole pressure
LVEDV	Left ventricular end diastole volume

MAPK	Mitogen-activated protein kinase
MCT	Monocrotaline
MDA5	Melanoma differentiation-associated protein 5
miRNA	MicroRNA
MMC	Mitomycin-C
mmHg	Millimetres of mercury
mPAP	Mean pulmonary artery pressure
mRNA	Messenger ribonucleic acid
NF-κB	Nuclear factor kappa-light-chain-enhancer of activated B cells
Nx	Normoxia
PA	Pulmonary artery
PAECs	Pulmonary artery endothelial cells
PAH	Pulmonary arterial hypertension
PASMCs	Pulmonary artery smooth muscle cells
PAMPs	Pathogen associated molecular patterns
PCH	Pulmonary capillary hemangiomatosis
PCR	Polymerase chain reaction
PERK	Protein kinase R-like endoplasmic reticulum kinase
P-eIf2α	Phosphorylation of eIF2α
PDE-5	Phosphodiesterase type 5
PH	Pulmonary hypertension
PKR	Protein kinase R
PI3K	Phosphoinositide 3-kinases
Poly(I:C)	Polyinosinic-polycytidylic acid
PRRs	Pattern recognition receptors
PVOD	Pulmonary veno-occlusive disease
RV	Right ventricle
RVESP	Right ventricular end-systolic pressure
RVH	Right ventricular hypertrophy
RVU	Relative volume units
RT-qPCR	Reverse transcription with quantitative polymerase chain reaction
SDS-PAGE	Sodium dodecyl sulphate - polyacrylamide gel electrophoresis
Sec	Seconds
SEM	Standard error of the mean
siRNA	Small interfering RNA
SMCs	Smooth muscle cells
SuHx	Sugen 5416/hypoxia
RLR	Retinoic acid-inducible gene-I -like receptors
TAPSE	Tricuspid Annular Plane Systolic Excursion
TGFβ	Transforming growth factor beta
TNF	Tumour necrosis factor
TLR	Toll-like receptor
TRAIL	TNF-related apoptosis-inducing ligand; TNFSF10
VWF	Von Willebrand Factor

1. Introduction

1.1 Pulmonary arterial hypertension

1.1.1 Clinical classification of pulmonary hypertension and pulmonary arterial hypertension

Pulmonary hypertension (PH) is a medical term that encompasses many diseases but all patients with PH are definitively diagnosed by an elevated mean pulmonary arterial pressure (mPAP) of ≥20mmHg at rest (Simonneau et al., 2019). The change in definition from a mPAP of ≥25 mmHg to ≥20mmHg at rest was made in light of reports that showed that the upper limit in healthy individuals was <20mmHg, as determined by two standard deviations above the mPAP (i.e., 14.0 ±3.3 mmHg). In addition, patients with borderline mPAP (20-25mmHg) typically have adverse outcomes (Douschan et al., 2018; Lamia et al., 2017; Simonneau et al., 2019).

PH patients present with dyspnoea at rest and during exercise, fatigue, syncope, chest pain, peripheral oedema, and ascites. Physiologically, symptoms occur due to abnormally high pressures and resistance in the pulmonary circulation that leads to decreased blood flow and abnormal gaseous exchange in the lungs. PH is classified into 5 groups according to clinical, aetiological, and pathological features. These classifications of PH include group 1 PH, pulmonary arterial hypertension (PAH); group 2 PH, PH due to left heart disease; group 3 PH, PH due to chronic lung disease and/or hypoxia; group 4 PH, chronic thromboembolic PH (CTEPH) and group 5 PH, PH with unclear or multifactorial mechanisms. PH is a progressive and life-threatening

condition, and only group 1 and 4 PH patients have access to clinically available drug therapies (Kiely et al., 2013).

Pulmonary artery hypertension (PAH) or group 1 is a very rare disorder that is haemodynamically characterized by a sustained mPAP ≥20mmHg at rest, with a normal pulmonary artery wedge pressure (PAWP ≤15mmHg) and increased pulmonary vascular resistance (PVR ≥ 3 wood units) (Simonneau et al., 2019). This increased right ventricular afterload ultimately leads to right heart failure and death (Machado et al., 2009). Group 1 PH (PAH) is comprised of a diverse range of disorders and the aetiologies, pathophysiological mechanisms, and clinical features form the basis for the clinical subclassifications of PAH. In turn, the subclassifications of PAH also begin to inform therapeutic management in clinic (Simonneau et al., 2019). The subclassifications of group 1 PH (PAH) are as follows: idiopathic (group 1.1), heritable (group 1.2), drug and toxin associated PAH (group 1.3), other disorders associated with PAH (i.e., connective tissue disease, HIV, portal hypertension, congenital heart disease or schistosomiasis) (group 1.4), PAH long-term responders to calcium channel blockers (group 1.5), PAH with overt features of venous/capillary involvement (group 1.6), and persistent PH of the new-born syndrome (group 1.7) (Simonneau et al., 2019). Epidemiologically, PAH is a rare disorder with the prevalence ranging from 15-50 per million in the United States and Europe (Beshay et al., 2020).

1.1.2 Pathogenesis of pulmonary arterial hypertension

Irrespective of the underlying causes, PAH patients harbour similar pathophysiological features which include sustained vasoconstriction of pulmonary arterioles, progressive and obliterative pulmonary vascular remodelling contributing to increased pulmonary pressure and resistance, thus leading to abnormal blood flow and poor gaseous exchange. Pulmonary vascular remodelling affects all layers (intima, media and adventitia) of the vasculature, exhibiting a cancer-like phenotype of excessive proliferation and apoptosis resistance (Thenappan et al., 2018). Specific histological features of pulmonary vascular remodelling include apoptotic resistant endothelial cells, endothelial, smooth muscle and fibroblast proliferation, medial hypertrophy, concentric and eccentric fibroid change, plexiform lesions, dilated and thrombotic lesion formation and perivascular inflammatory infiltrates (figure 1.1) (Galiè et al., 2009; Rabinovitch, 2008). Until recently the contribution of adventitia in pulmonary vascular remodelling was overlooked. The principal component of the adventitia layer is fibroblasts. Other constitutes include immunomodulatory cells, vasa vasorum and adrenergic nerves. Some suggest that the adventitia is the principal 'injury-sensing tissue' of the pulmonary vascular layers in which fibroblasts may be the first vascular wall cells to exhibit evidence of activation in response to vascular injury or stress. Activation of the adventitia influences fibroblast proliferation, expression of contractile and extracellular matrix deposition and secretion of cytokines, chemokines, reactive oxygen species, all of which contribute to pulmonary vascular remodelling and vascular tone (Tobal et al., 2021). PAH is often referred to as a pre-capillary disease as pathological lesions affect the small (<50μm diameter) distal pulmonary arteries (Tuder et al., 2007). Pulmonary veins in PAH are not typically remodelled, although a

spectrum between arterial and venous remodelling may exist (Dorfmüller et al., 2010). Identification of triggers and drivers of pulmonary vascular remodelling are emerging within the PH research community, but most have not been successfully targeted for therapy.

Current therapies only exploit known vasoconstrictor pathways, rather than targeting mechanisms of pulmonary vascular remodelling. The key vasoconstrictor pathways include endothelin, nitric oxide, and prostacyclin (Sitbon & Morrell, 2012). Very few PAH patients (<10%) are long term responders to calcium channel blockers (vasodilators) (i.e. PH group 1.5), therefore mortality for non-responders remains very poor (Sitbon et al., 2005). There are reports evidencing the breadth and complexity of triggers and drivers in PAH pathogenesis (figure 1.2) (Thompson & Lawrie, 2017). Drivers of PAH have been described as both acquired and heritable. Proposed acquired drivers include disrupted transcriptional regulation by somatic genetic mutations, DNA and histone acetylation and miRNA expression, mitochondrial metabolic dysfunctions, hypoxia, drug and toxins, inflammation, shear stress and pathogens such as viruses (Thompson & Lawrie, 2017). Heritable or predisposed drivers include genetic mutations and sex hormones (Thompson & Lawrie, 2017). A landmark study by Lane et al (2000) identified bone morphogenic protein receptor type 2 (*BMPR2)* mutations as a cause of familial PAH. *BMPR2* mutations are the most common genetic cause, accounting for ~80% of heritable PAH and ~20% of idiopathic PAH (Lane et al., 2000). Other prominent mutations in PAH include *ALK1/ACVRL1, BMP9, SMAD1, KCNK3.* With exception of *KCNK3,* all of these mutated genes are involved in BMPR2 signalling (Ma et al., 2013; Sahay, 2019). However, it is becoming increasingly clear that the pathogenesis of PAH is multifactorial, requiring additional

vascular insults on top of genetic predisposition or acquired risk factors. A ‘multiple-hit’ hypothesis has been proposed in the context of PAH disease (Geraci et al., 2010).

However, an overarching theme of PAH pathogenesis is inflammation and PAH has been described in part as a disease of altered immunity. For example, PAH is associated with multiple autoimmune diseases (i.e. systemic sclerosis, systemic lupus erythematosus), suggesting dysregulated immunity may trigger pulmonary vascular disease (Simonneau et al., 2019). Interestingly, perivascular inflammation and enhanced circulating inflammation cytokines such as IL-1β, -6, -10, GM-CSF have been measured in cases of PAH without co-existing inflammatory disease or infections, such as idiopathic PAH patients (Cracowski et al., 2014). Proinflammatory phenotypes have also been linked to genetic predisposition, where BMPR2 deficient pulmonary artery endothelial cells (PAECs) exhibit enhanced proinflammatory cytokine expression in response to stimuli such as LPS and TNFα (Sawada et al., 2014; Soon et al., 2010). Pro-inflammatory cytokines and interferon are also known signalling products of viral RNA recognition via toll-like receptors(Lee et al., 2018). These data begin to highlight the complementary themes between known drivers of pulmonary vascular remodelling in PAH, inflammation, and innate anti-viral responses.

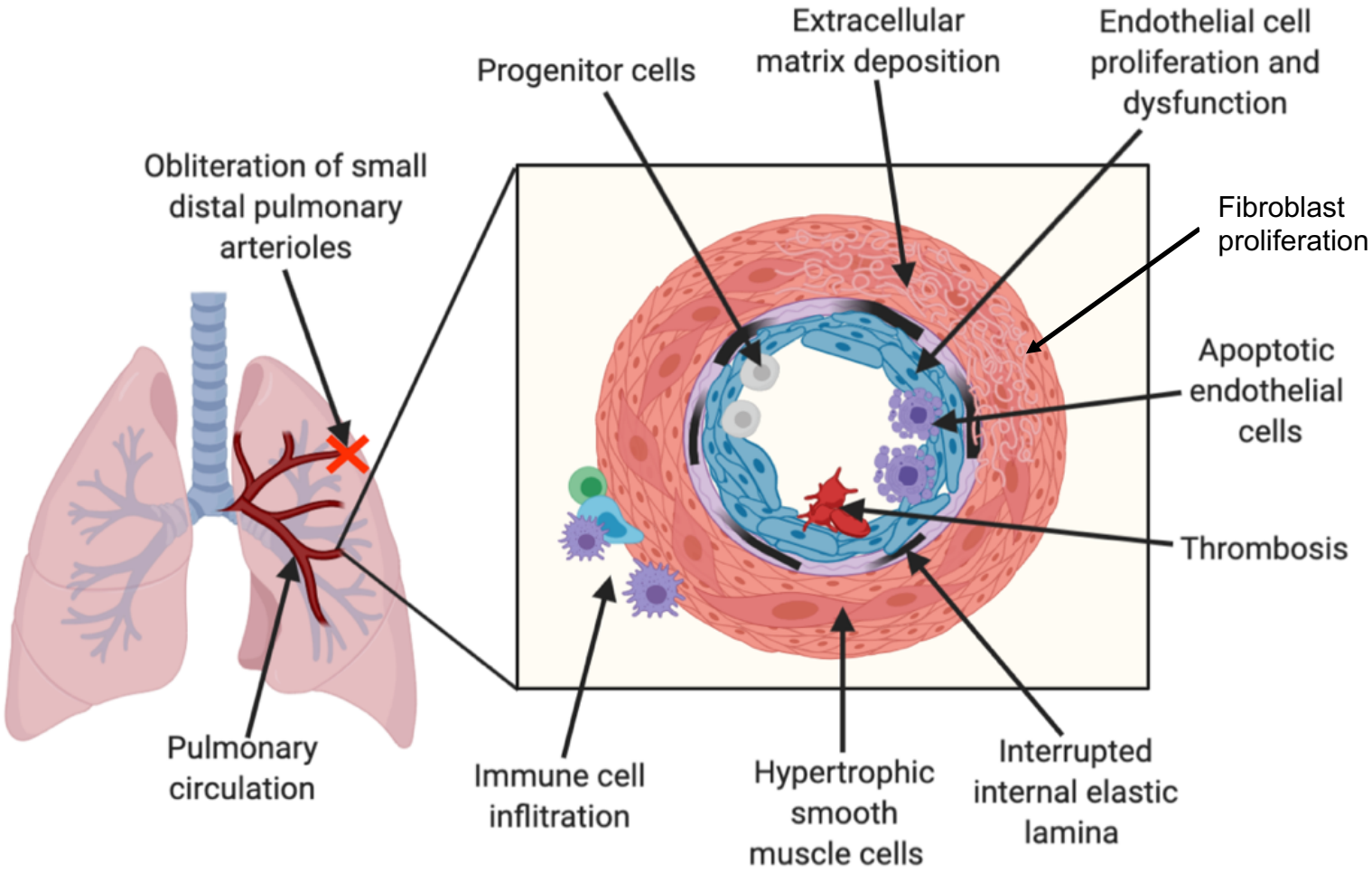

Figure 1.1. Schematic illustrating the pathological characteristics of pulmonary vascular remodelling in PAH.

Initial vasoconstriction and cell injury leads to excessive proliferation and evasion of apoptosis in endothelial cells. Proliferation of smooth muscle cells and fibroblasts further contributes to progressive and obliterative remodelling in pre-capillary arterioles. Image created in Biorender.com.

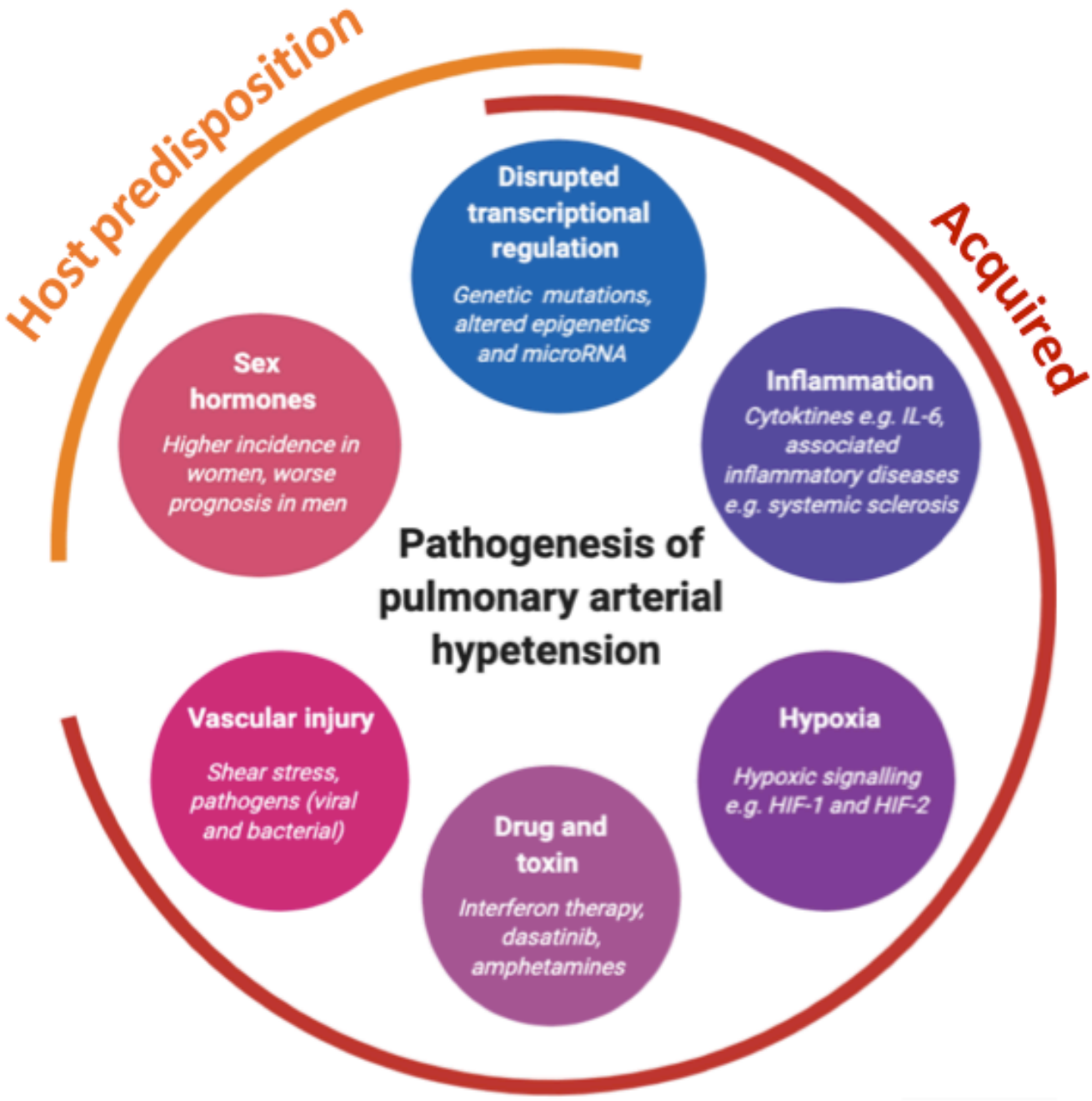

Figure 1.2. Pathogenesis of PAH.

Although the exact triggers or drivers of PAH remain unclear, there are several known risk factors and drivers of PAH pathogenesis. These drivers can be predispositions and acquired factors, or both, as a multiple hit hypothesis has been proposed in the pathogenesis of PAH. Risk factors which predispose an individual to the development of PAH include gender and heritable genetic mutations in genes such as *BMPR2* and *EIF2AK4* (eukaryotic initiation factor 2α kinase 4). Somatic gene mutations of *BMPR2* and its signalling intermediates are contributing disease drivers. Other acquired factors of PAH pathogenesis include inflammation, hypoxia, drugs/toxins and vascular injury from shear stress or pathogens. Image created in Biorender.com.

1.1.3 A subclassification of PAH: Pulmonary veno-occlusive disease

Pulmonary veno-occlusive disease (PVOD) is a cause of PH and is a very rare subtype of group 1 PAH, forming group 1.6 (Simonneau et al., 2019). Group 1.6 is named 'PAH with overt features of venous/capillary involvement (PVOD/ pulmonary capillary hemangiomatosis (PCH)). As the name suggests, PVOD is characterised as a post-capillary disease with significant pulmonary venous remodelling but also with pre-capillary involvement. The defining pathological feature of PVOD is the fibrous intimal proliferation and muscular hyperplasia of septal and pre-septal venules (Simonneau et al., 2019). Other PVOD diagnostic features from lung CT include centrilobular ground-glass opacities and enlarged mediastinal lymph nodes. In addition, pulmonary function tests exhibit diminished lung diffusing capacity for carbon monoxide and severe hypoxemia (Liang et al., 2016). PVOD has an extremely low incidence rate of 0.1 cases per million per year, however, the poor morbidity and high risk of mortality to a patient is significant. With the widespread pulmonary vascular remodelling localised to both the venous and arteriole systems of the pulmonary circulation, it is unsurprising that the prognosis of a PVOD patient is particularly dismal. PVOD prognosis is lower than that of idiopathic PAH patients. Specifically, the 1-year mortality rate after PVOD diagnosis has been reported to be as high as 75% (Saito et al., 2017). PVOD patient outcomes are particularly poor due to the risk of vasodilator therapy causing fatal pulmonary oedema (Palmer et al., 1998), and because of this, lung transplantation remains the treatment of choice. In addition, PVOD is commonly mistaken for PAH, despite different pathological features. An extremely low incidence rate of 0.1 cases per million per year, non-specific respiratory symptoms, similar haemodynamic features to PAH, and the reluctance to obtain lung biopsies due to a

risk of bleeding contribute to misdiagnoses (Hajouli et al., 2019). However, the identification of *EIF2AK4* (eukaryotic initiation factor 2α kinase 4) mutations to be causal in the pathogenesis of PVOD by Eyrie et al (2014) has informed the change in guidelines to definitively diagnose PVOD. Now, genetic screening (i.e., *EIF2AK4* mutation present) is the gold standard in PVOD diagnosis, as opposed to the previous histological definitive diagnosis from a contraindicated lung biopsy.

1.1.3.1 Genetic susceptibility (i.e., *EIF2AK4* mutations) in PVOD pathogenesis

Biallelic mutations in the *EIF2AK4* gene cause autosomal-recessive heritable PVOD in familial cases (Eyries et al., 2014). Sporadic PVOD has also been described in the context of acquiring *EIF2AK4* homozygous recessive mutations (Eyries et al., 2014). In more detail, whole exome sequencing demonstrated that mutations in *EIF2AK4* were present in all familial PVOD cases and in 25% of the sporadic PVOD cases (Eyries et al., 2014). The full penetrance of *EIF2AK4* in familial cases and the presence of sporadic *EIFA2K4* mutations supports a major causal role for *EIF2AK4* in the pathogenesis of PVOD. In addition, co-occurrence of a frame shift mutation in *BMPR2* and a novel splice mutation in *EIF2AK4* was identified in hereditary PAH (HPAH) (Eichstaedt et al., 2016; Liang et al., 2016; Tenorio et al., 2015). Likewise, *EIF2AK4* mutations have been identified in autosomal-recessive pulmonary capillary hemangiomatosis (PCH) (the other disorder in PAH group 1.6) in familial and sporadic cases (Best *et al*, 2014). The exact role of *EIF2AK4* loss-of-function mutations in the pathogenesis of PVOD is still unknown, however GCN2, the protein encoded by *EIF2AK4,* is a well characterised kinase of the integrated stress response (ISR) and involved in cellular adaptation to stress (details given in section 1.1.3.2).

1.1.3.2 *EIF2AK4*- encoding GCN2 protein in the integrated stress response

One way in which cells adapt to stress and restore cellular homeostasis is via the activation of the integrated stress response (ISR). The ISR is a highly conserved pathway including 4 kinases, one of which is the previously mentioned GCN2 protein. The other three kinases are: interferon-induced double-stranded RNA-dependent eIF2α kinase (PKR encoded by *EIF2AK2*), PKR-like endoplasmic reticulum resident kinase (PERK encoded by *EIF2AK3*) and heme-regulated inhibitor kinase (HRI encoded by *EIF2AK1*) (Donnelly et al., 2013). Each kinase has a unique domain to sense its respective stress condition and is activated by a diverse range of intracellular or extracellular stimuli. Specifically, activation of GCN2 by amino acid deprivation, PKR by double stranded (ds)RNA, PERK by endoplasmic reticulum protein folding stress, and HRI by heme deficiency occurs in the ISR (Pakos-Zebrucka et al., 2016). All ISR kinases dimerize and auto-phosphorylate upon stimuli activation. All ISR kinases function to phosphorylate the α subunit of eukaryotic translation initiation factor 2 (eIF2α) at serine 51, ultimately suppressing translation and specifically 5' cap-dependent translation (Donnelly et al., 2013). However, homozygous mutation of serine 51 on eIFα prevents eIF2α phosphorylation, permitting normal mRNA translation even under ER stress or glucose deprivation (Scheuner et al., 2001). Phosphorylated eIF2α (P-eIf2α) mediates the inhibition of eIF2B activity and reduces eIF2-GDP to eIF2-GTP exchange, leading to reduced $tRNAi^{Met}$ (transfer RNA for initiation of methionine) binding to ribosome, attenuating protein synthesis (Pakos-Zebrucka et al., 2016). Changes in eIF2α phosphorylation have previously been linked to altered cytokine responses in the context of pulmonary vascular cells. PAH-associated BMPR2 deficiency enhanced the inflammatory chemokine, GM-CSF (granulocyte macrophage colony-stimulating factor), in response to an inflammatory

stimulus (TNFα) and exacerbated PH via prolonged p38-activation of MAPK signalling (Sawada et al., 2014).

In addition to global suppression of 5' cap-dependent translation, a few mRNA transcripts, namely activating transcription factor 4 (ATF4), are preferentially translated in attempt to resolve cellular homeostasis (Pakos-Zebrucka et al., 2016). This preferential translation of *ATF4* occurs due to the unique presence of one or more upstream open reading frames (uORFs) in its 5′ untranslated region of the gene. ATF4 is a transcription factor that forms homo- or hetero- dimers that bind to DNA to control the expression its gene targets. One of ATF4's gene targets is growth arrest and DNA damage-inducible protein (GADD34) (Clavarino et al., 2012). GADD34 functions in a negative feedback loop process where it forms a complex with protein phosphatase 1 (GADD34–PP1) to promote termination of the ISR by the dephosphorylation of eIF2α (Clavarino et al., 2012). Other examples of preferentially translated genes during ISR activation are ATF5 and CHOP. This upregulated gene translation promotes oxidative stress, inflammation, cell survival, autophagy, and apoptosis processes as mechanisms for recovery or to signal towards cell death (Pakos-Zebrucka et al., 2016). The full process of the ISR is illustrated in figure 1.3.

The exact role of *EIF2AK4* loss-of-function mutations in the pathogenesis of PVOD is still unclear. Yet, the varied age of onset PVOD and incomplete penetrance of *EIF2AK4* mutations does suggest that additional genetic or environmental factors (i.e., hits) may be required for disease initiation and progression (Eyries et al., 2014). The following original reports have begun to elicit the role of *EIF2AK4* loss-of-function mutations in the pathogenesis of PVOD.

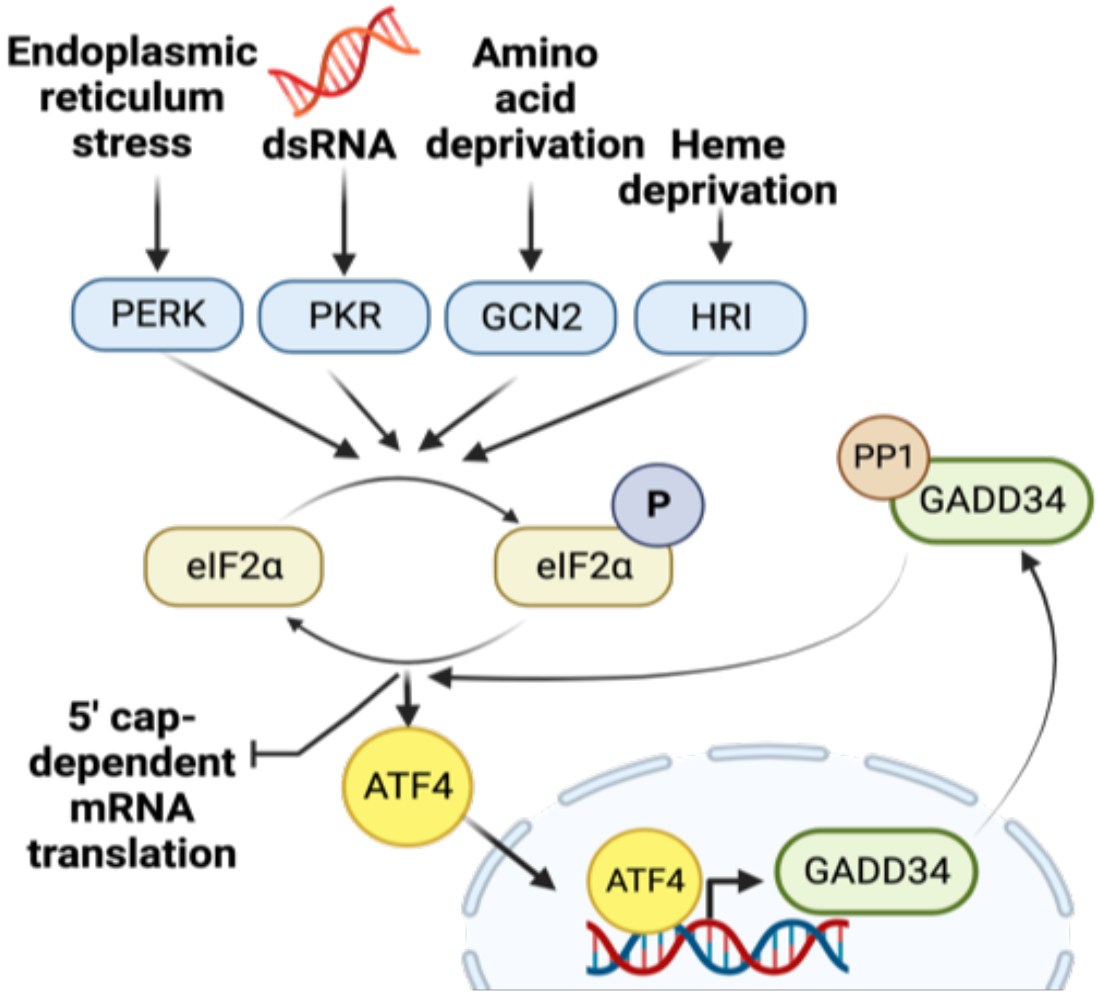

Figure 1.3. Integrated stress response.

As adapted from Pakos-Zebrucka et al (2016), this illustrates pathways within the integrated stress response (ISR). A variety of cellular stimuli which are specific to each of the four ISR kinases activate this pathway. Upon their respective stimulation, the ISR kinases (GCN2, PKR, PERK and HRI) homodimerize and auto-phosphorylate mediating signalling pathways. GCN2 is activated by amino acid deprivation. PKR is activated by dsRNA (derived from exogenous, endogenous, and synthetic sources). PERK is activated by endoplasmic reticulum stress. HRI is activated by heme deprivation, and unlike the other ISR kinase, HRI is predominantly localised in erythroid cells. All kinase activation leads to the phosphorylation of eIF2α mediating the inhibition of 5' cap-dependent translation in a process of post-transcriptional regulation. In addition, to restore cellular homeostasis, specific mRNAs are selectively translated due to unique presence of one or more upstream open reading frames, including the translation of ATF4, ATF5, CHOP and GADD34. GADD34 is important role in the negative feedback loop which mediates de-phosphorylation of P- eIF2α to cease the activation of this pathway. ATF4 is a transcription factor which gene targets are implicated in restoring cellular homeostasis or determining the cell for death signals. Image created in Biorender.com.

1.1.3.3 Mechanism of action of *EIF2AK4* mutations in PVOD

To date, few studies have investigated how the loss-of-function *EIF2AK4* (encoding GCN2) mutations contribute to pulmonary vascular remodelling and pathogenesis of PVOD. Exclusively in PAECs, GCN2 inhibition with 2662034 compound decreased BMP-9 induced SMAD1/5/8 phosphorylation (Manaud et al., 2020). This process was unaffected in pulmonary artery smooth muscle cells (PASMCs). In addition, GCN2 knockdown via siRNA in PAECs significantly enhanced the important hallmark of pulmonary vascular remodelling; PAECs proliferation (Manaud et al., 2020). GCN2 knockdown via siRNA in PAECs also enhanced the expression of the anti-apoptotic survivin (Manaud et al., 2020). In addition, GCN2 inhibition with 2662034 compound reduced BMP9 and rapamycin-induced SMAD1/5/8 phosphorylation in PAECs; rapamycin which is a known inhibitor of mTORC1 (Manaud et al., 2020). Validating these results using a mitomycin-c (MMC)-exposed rat model of PVOD, Manaud et al (2020) reported unaffected BMPR2 protein expression, significantly decreased SMAD1/5/8 phosphorylation, and significantly increased SMAD2/3 phosphorylation. These data evidence a GCN2/BMP/TGF-β axis in human and animal models of PVOD and *in vitro*.

In another relevant cell type, PASMCs from PVOD donors, with a confirmed *EIF2AK4* mutation and reduced GCN2 protein expression demonstrated significantly reduced ATF3 protein expression and significantly increased phosphorylation of p38 MAPK compared to control donor PASMCs (Chen et al., 2021). Increased mRNA expression of *col1a1* and *col1a2* in PASMCs of PVOD donors was determined to be GCN2-ATP-p38 MAPK dependent and a pharmacological inhibitor of p38 improved ventricular hypertrophy, pulmonary vascular remodelling, and right ventricular end systolic

pressure (RVESP) and tricuspid annular plane systolic excursion (TAPSE) in an MMC-exposed rat compared to control (Chen et al., 2021). Interestingly, p38 MAPK signalling has been implicated in double stranded (ds)RNA signalling in mouse embryonic fibroblasts. Specifically, IL-6 release in response to dsRNA or EMCV infection was determined to be p38 MAPK-dependent (Iordanov et al., 2000). More detail on dsRNA signalling is in section 1.2.

Unintuitively, reduced GCN2 protein expression in PASMCs of PVOD donors was concurrent with unaffected levels of phosphorylation of eIF2α (Chen et al., 2021). This unexpected result was also reported in Manaud et al (2020) which reported unaffected levels of phosphorylation of eIF2α in lung from hereditary and sporadic PVOD patients and MMC-exposed rat, all of which had confirmed GCN2 deficiencies. Exclusively in the MMC-exposed rat model of PVOD, and not in the lungs of hereditary and sporadic PVOD patients, the protein expression of PERK and PKR (i.e., other ISR kinases) were significantly and progressively increased as determined by weekly protein expression analysis over a 5-week period of MMC exposure in rats (Manaud et al., 2020). These data infer biological compensation of the ISR in the context of GCN2 deficiency which potentially may contribute to PVOD pathogenesis. Notably, PKR which is overexpressed in an MMC-exposed rat (with confirmed reduced GCN2 protein expression), is a cytosolic receptor of dsRNA. The significant role of dsRNA signalling in pulmonary vascular remodelling and PAH is evidenced in section 1.2, 1.3 and 1.4.

These converging data regarding ISR, GCN2 deficiency, changes in PKR expression and dsRNA signalling inspired some subsequent research questions in this thesis to

explore the potential interplay between GCN2 deficiency and the dsRNA signalling pathway in pulmonary vascular cells (data shown in chapter 5 and 6).

1.1.3.4 Environmental risk factors in PVOD

The pathogenesis of PVOD is largely unknown but in a small number of cases environmental factors are directly associated with the development of PVOD. Occupational exposure to organic solvents (and concurrent tobacco exposure) or treatment of diseases with specific chemotherapies are high risk factors associated with PVOD development (Montani et al., 2015).

Mitomycin-C (MMC) is a chemotherapy used to treat cancer but evidence of MMC-induced PVOD has been observed in human disease and animal models. Specifically, Joselson and Warnock (1983) documented a case study of PVOD after chemotherapy treatment including MMC. More robustly, a prospective study including cases of MMC-associated PVOD subsequent to squamous anal cancer in the French Pulmonary Hypertension Registry allowed comparisons of estimated incidence in the MMC-treated cancer population with PVOD versus the general population with PVOD (Perros et al., 2015). Perros et al (2015) reported that the incidence of PVOD in the cancer treated MMC population was >5000 higher than those with idiopathic PVOD. A single dose of 4mg/kg of MMC in male and female rats significantly increased mPAP, total pulmonary vascular resistance and right ventricular hypertrophy and induced pulmonary vascular remodelling with significant venous and capillary involvement further validating the PVOD patient data (Perros et al., 2015). This MMC model was also determined to be molecularly relevant, as like hereditary PVOD, patients that show no expression of GCN2, MMC-exposed rats had decreased protein levels of

GCN2 in a dose dependent manner, decreased phosphorylation of Smad1/5/8 and unaffected levels of BMPR2 (Perros et al., 2015). Furthermore, Smad-3 dependent signalling has been attributed to pulmonary vascular endothelial-to-mesenchymal transition (a hallmark of pulmonary vascular remodelling) in MMC-exposed PVOD rats and PVOD patients (Zhang et al., 2021). This MMC-induced model of PVOD rats was novel as reported by Perros et al (2015) and other research groups have chosen to use this PVOD model ever since.

The occupational exposure of trichloroethylene (chlorinated organic solvent) has also been proposed as a risk factor in PVOD pathogenesis (Montani et al., 2015). In a case-control study comparing PVOD and PAH patients, a significant trichloroethylene exposure was found in 42% of PVOD patients compared to 3% of PAH patients (Montani et al., 2015). Interestingly, trichloroethylene exposure PVOD was associated with an older age of disease onset and absence of *EIF2AK4* mutations. This was compared to PVOD patients harbouring *EIF2AK4* mutations that typically were younger in age at disease onset and had no history of trichloroethylene exposure (Montani et al., 2015). Notably, the trichloroethylene exposure was concurrent with tobacco exposure supporting a multi-hit model of pathogenesis (Montani et al., 2015). Trichloroethylene's mode of action in PVOD pathogenesis has largely not been investigated but Caliez et al (2020) demonstrated that trichloroethylene induces vascular permeability in the process of endothelial dysfunction.

1.1.3.5 Autoimmune and inflammatory disorder risk in PVOD

Although data are exclusively in case reports, the association of autoimmune and inflammatory disorders with PVOD pathogenesis is still notable. For example, PVOD has been diagnosed in combination with sarcoidosis, Langerhans' cell granulomatosis, and Hashimoto's thyroiditis (Hamada et al. 2000; Hoffstein, Ranganathan, and Mullen 1986; Kokturk et al. 2005).

As stated in all previous sections of this chapter, there is residing evidence for inflammation as a key driver and/or trigger of pulmonary vascular remodelling and PAH pathogenesis, but the specific contributions of inflammation in disease are still debated. This thesis specifically researches the contributions of innate immunity associated with dsRNA signalling in pulmonary vascular remodelling and PAH pathogenesis.

1.2. Double-stranded (ds)RNA signalling

1.2.1 Innate immunity

In the past two decades, researchers have come to understand that innate immunity is not only fundamental as the first line of defence from external pathogens such as virus, but innate immune signalling can contribute to pathogenesis of disease, as well as possessing the ability to protect from cellular injury and regulate tissue homeostasis. Stemming from Janeway's concept of "pattern recognition receptors" (PRRs) that bind "pathogen-associated molecular patterns" (PAMPs), ongoing research has found that PRRs also recognize internal "damage-associated molecular

patterns" (Janeway & Medzhitov, 2002). Whereas PAMPs are debris that came from processing of pathogens by the immune system, "damage-associated molecular patterns" (DAMPs) are frequently part of the structural and functional components of our own cells and tissues, which are often released during tissue injury. Bacterial lipopolysaccharides (LPS) and viral derived nucleic acids such as exogenous dsRNA are examples of PAMPs (Janeway & Medzhitov, 2002). Extracellular DAMPs include hyaluronan, heparan sulfate, fibronectin, and Tenascin C. In addition to these extracellular molecules, DAMPs can also be derived from intracellular material released when cells are so severely injured that they undergo apoptosis or necrosis (Schaefer, 2014). Double stranded RNA derived from mitochondrial transcripts, repetitive elements in the form of short and long interspersed elements (SINEs and LINEs) and human endogenous retroviruses serve as intracellular DAMPs via several PRRs (Karikó et al., 2004).

Synthetic dsRNA also binds to PRRs in eukaryotic cells. Synthetic dsRNA in the form of polyinosinic:polycytidylic acid (poly(I:C)) is commonly used experimentally and is used in established lung injury/viral models in murine (Gan et al., 2018; Gao et al., 2021; Harris et al., 2013; Stowell et al., 2009). A specific synthetic form of dsRNA called rintatolimod is sold under the tradename of Ampligen® (Mitchell, 2016). Rintatolimod selectively binds to toll-like receptor 3 (TLR3) and has both immunomodulatory and antiviral properties which have shown to be beneficially in chronic fatigue syndrome and some cancers (El Haddaoui et al., 2022; Mitchell, 2016). In addition, Ampligen® is currently being used in a phase II clinical trial to treat long Covid-19 (AMP-158; FDA approved). These data above begin to highlight the

contradictory properties (i.e., inflammation and protective immunomodulation) of synthetic dsRNA in their respective settings.

1.2.2 RNA sensors

1.2.2.1 Toll like receptor 3 (TLR3) and endosomal dsRNA receptors

Localized to extracellular membranes or in intracellular compartments, toll-like receptors (TLRs) are a specific type of PRR, and can sense PAMPs and DAMPs (Chaturvedi & Pierce, 2009). Toll-like receptor 3 (TLR3) has been established as a central PRR for all sorts of RNA molecules. The acidic endosomal localization of TLR3 is relevant as dsRNA is a common intermediate of many virus' replication cycles in the host cell. Interestingly, non-viral nucleic acids, such as endogenous mRNA released from necrotic cells also trigger the TLR3 pathway (Karikó et al., 2004). Likewise, poly(I:C) is used extensively in research as a TLR3 ligand (Alexopoulou et al., 2001; Farkas et al., 2019; Lee et al., 2018; Zhou et al., 2013). Structural analysis of dsRNA bound to TLR3 revealed that 40–50 base-pair duplexes bind to a TLR3 dimer (Liu et al., 2008). An alternative model suggests TLR3 dimers could also bind shorter duplexes, although application of various lengths of dsRNA to murine dendritic cells required duplexes of more than 90 base-pairs to invoke signalling (Pirher et al., 2008). TLR3 can also sense incomplete stem structures, such as in vitro transcribed RNAs, and is therefore capable of responding to single stranded RNA depending on its length and secondary structure (Jelinek et al., 2011). In addition, TLR3 is expressed on a wide variety of cell types, including on the endosomes and lysosomes of fibroblasts, epithelial tissues, endothelial, smooth muscle and immune cells (Nishiya & DeFranco, 2004; Seya et al., 2005).

The mechanisms by which extracellular dsRNA is delivered to endosomal TLR3 remain incompletely understood. However, it is known that nucleic acids are hydrophilic and cannot pass directly through the plasma membrane. Rather, nucleic acids are delivered into the cell by endocytosis, the *de novo* production of internal membranes generated from the plasma membrane phospholipid bilayer (Doherty & McMahon, 2009). Clathrin-dependent endocytosis, scavenger receptors and CD41 in human airway epithelial cells have been shown to be important in extracellular dsRNA internalization (Dieudonné et al., 2012; Itoh et al., 2008; H. K. Lee et al., 2006). It is not only the unique localization of endosomal receptors that helps prevent potential self-nucleic acid recognition and subsequent autoimmune disease. TLR3, and other endosomal TLRs (TLR7, TLR8 and, in mice, TLR13), are also strictly regulated, trafficked and processed before a ligand can bind (Ewald et al., 2011; Horton & Farris, 2012; Pope & Huang, 2009). Unlike plasma membrane bound TLRs, endosomal TLRs reside in the endoplasmic reticulum, before dsRNA stimulation mediates controlled exiting of TLR to endosomes via the chaperone membrane protein, Unc93b1 (Tabeta et al., 2006) (figure 1.4). Intracellular localization of TLR3, and perhaps the processing of TLR3 adjacent to phagosomes containing apoptotic cells is also governed by a distinct regulatory domain within the TLR itself called the cytoplasmic linker region (Funami et al., 2004; Nishiya et al., 2005). Other regulatory processes to circumvent self-recognition include endosomes containing pH-activated proteases called cathepsins and asparagine endopeptidase, important for TLR3 processing and recognition (Ewald et al., 2011).

1.2.2.2 Cytosolic dsRNA receptors

TLR3 deficient mice have been shown to produce an inflammatory response in the form of TNFα and IL-1β production after poly(I:C) treatment (López et al., 2004). These observations led to the identification of dsRNA recognition by cytosolic sensors called RIG-I-like receptors (RLRs). These receptors likely mediate sequential responses to dsRNA together with the endosomal recognition receptors. RLRs include retinoic acid inducible gene-I (RIG-I), melanoma differentiation-associated gene-5 (MDA-5), and laboratory of genetics and physiology-2 (LGP2) (Kawai & Akira, 2009).

PKR, an integrated stress response kinase (as discussed in section 1.1.3.2), can also induce the production of pro-inflammatory cytokines and type I interferon (IFN) via viral dsRNA recognition. PKR regulates numerous signalling pathways as an adaptor and/or via its kinase activity (Galabru & Hovanessian, 1987). PKR has been shown to be an intermediate of the TLR3 signalling pathway and also is an activator of canonical NF-κB and MAPK pathways contributing to type I IFN production (Jiang et al., 2003; Zamanian-Daryoush et al., 2000) (figure 1.4). Double-stranded RNA of over 33 base pairs is thought to be necessary to activate PKR, although shorter duplexes with single-stranded tails also induced PKR auto-phosphorylation (Manche et al., 1992; Zheng & Bevilacqua, 2004). A variety of other RNA-binding proteins and DExD/H box helicases have also been implicated in recognition of cytosolic dsRNA, for example, Leucine-Rich Repeat Flightless-Interacting Protein 1 (LRRFIP1), 2',5'-oligoadenylate synthetase (OAS)-RNase L pathway and Adenosine deaminases acting on RNA (ADARs) (Yang et al., 2010) .

1.2.2.3 cGAS/STING signalling

Other less characterized responses to nucleic acids include cytosolic cGAS (cyclic GMP-AMP synthase), and STING signalliing cGAS recognition of DNA is well characterized in literature but questions surrounding the cGAS /STING recognition of viral RNA still remain. One report suggests that the RNA-containing dengue virus liberates mitochondrial DNA that can be sensed by the cGAS/STING pathway, enhancing the anti-viral response (Sun et al., 2017). Despite activation by different nucleic acids, reports indicate that STING and mitochondrial anti-viral signalling protein (MAVS) have a connected type I IFN response, in which MAVS recruits STING in the form of a physical interaction, in response to ssRNA (Nazmi et al., 2012). As of yet, no one has provided evidence for a similar interaction in response to dsRNA.

1.2.3 Intracellular signalling mediated by dsRNA

Agonists binding to TLRs trigger the dimerization of cytoplasmic signalling domains called Toll/interleukin 1 receptor (TIR) that provide a scaffold to recruit cytosolic TIR domain-containing adaptors that propagate intracellular signalling (Meylan et al., 2004). It was originally proposed that all TLRs, including TLR3, had an essential adaptor molecule called myeloid differentiation primary response 88 (MyD88) (Itoh et al., 2008). This has now been disproven and TLR3 immune responses have been shown to be mediated by the TIR-domain containing adaptor protein inducing interferon beta (TRIF) pathway exclusively, inducing type I IFN and pro-inflammatory cytokines (Kawai & Akira, 2006). TRIF can induce several pathways, ultimately activating IRF3, AP1 and NF-κB transcription factors via different binding-motifs (figure 1.4) (Meylan et al., 2004). The c-terminal of TRIF contains Rip homotypic interaction

motif which activates members of the receptor interacting (RIP) family and the N-region of TRIF contains three TRAF-6 binding domains (Kawai & Akira, 2006). RIP1 and TRAF6 are indispensable in TLR3-mediated NF-κB activation by inducing the liberation and translocation of NF-κB into the nucleus via the activation of IκB kinase complex (Meylan et al., 2004; Sato et al., 2003). A TRIF-independent branch of TLR3 signalling has also been suggested (Hoebe et al., 2003; Yamashita et al., 2012). Specifically, dsRNA-stimulated dimerization of TLR3 has shown to lead to transient recruitment of proto-oncoprotein c-Src to enhance cell migration, proliferation and adhesion (Yamashita et al., 2012) (figure 1.4). MDA5 and RIG-I pathways are activated upon ligand binding and/or synergy with TLR3 recognition. Signal transduction is mediated by caspase activation recruitment domains (CARDs) located at the N-terminal of RLRs (figure 1.4). MAVs is the adaptor molecule that induces production of IRF3 and NF-ΚB target genes (Lurescia, Fioretti and Rinaldi, 2018). RLRs and TLRs share downstream pathways, where TBK1 and IKKε phosphorylation of IRF 3 and 7 promotes expression of type I IFN (i.e. IFNα and IFNβ), and IKKi complex phosphorylation of NF-ΚB promotes pro-inflammatory cytokine production (Bakshi et al., 2017). Proinflammatory cytokines and chemokines induced by dsRNA signalling include IL-6, IL-8, IL-10, IL-12, TNF-α, IL-1β, CXCL10 (IP-10). This further results in the production of interferon-stimulated genes (ISGs) such as PKR and 2'5'OAS in a positive feedback loop to mediate an antiviral state and/or signalling to cell death. Specifically, PKR, RNase L, IRF3 and c-Jun N-terminal kinase are some of the components of the pro-apoptotic pathways activated by dsRNA, whilst NF-κB promotes survival (Gantier & Williams, 2007). In addition, pro-inflammatory cytokines, and chemokines act as stimulants and chemoattractants of neutrophils, macrophages, T and B cells and natural killer cells (Chen et al., 2021)

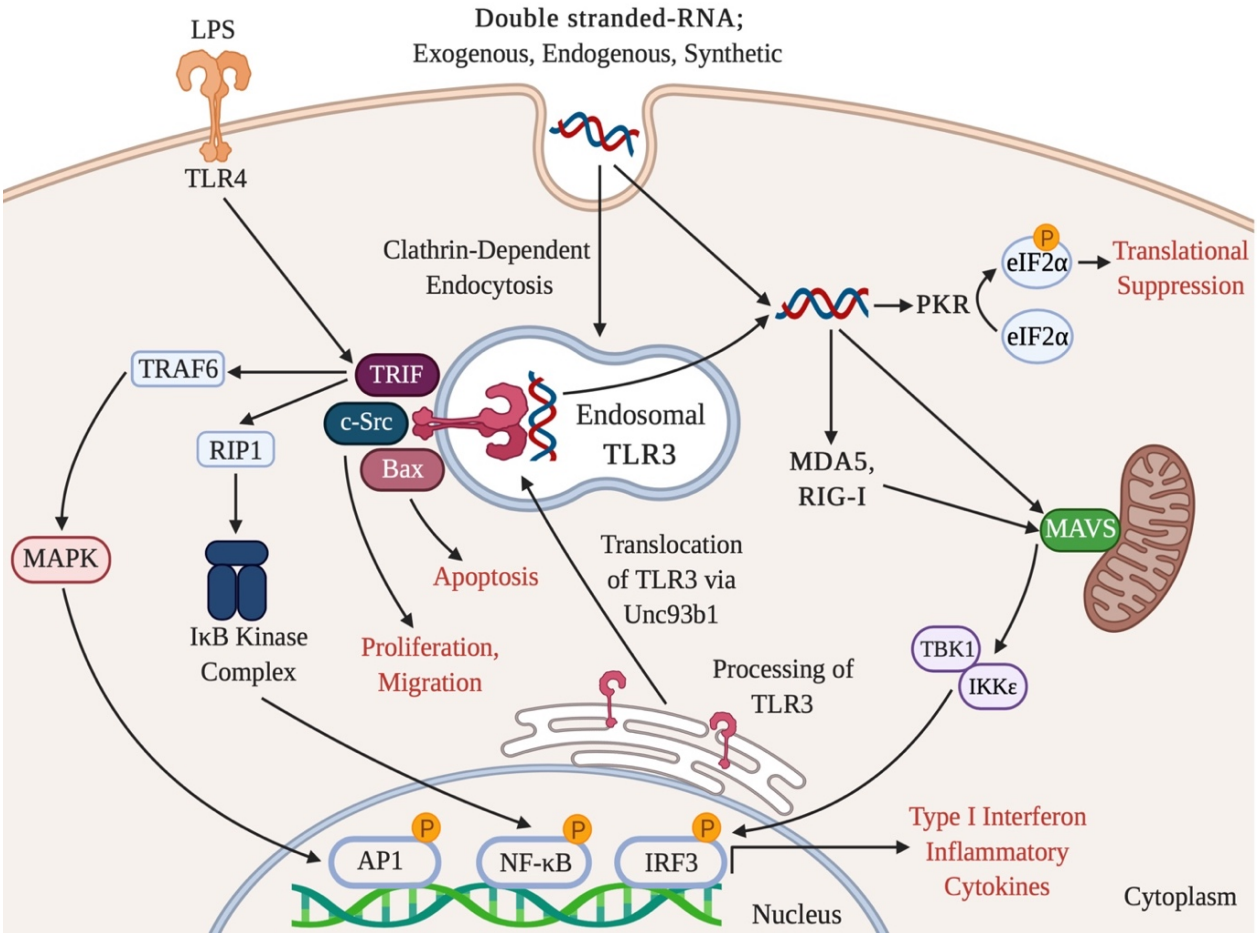

Figure 1.4. Double stranded (ds)RNA signalling pathways. Double stranded-RNA (dsRNA) derived from virus, mRNA liberated from necrotic cells and synthetic polyinosinic:polycytidylic acid are recognized by TLR3. TLR3 is located in acidic endosomes formed during clathrin-dependent endocytosis. TLR3 signalling occurs via TRIF, an adaptor that can also be recruited by TLR4. TRIF activates NF-κB and AP1 to induce transcription of type I interferon and pro-inflammatory cytokines. Apoptosis and proliferation can be induced by TRIF-independent TLR3 signalling via BAX and c-SRC respectively. Cytosolic receptors can respond to dsRNA independently of TLR3 or in a synergistic manner and these include retinoic acid inducible gene-I (RIG-I) and melanoma differentiation antigen 5 (MDA-5). These signal via the mitochondrial anti-viral signalling protein (MAVS) to activate interferon regulatory factor 3 (IRF3). RNA can also suppress translation via activation of protein kinase R (PKR), which in turn phosphorylates eukaryotic initiation factor 2-alpha (EIF2α). Abbreviations: TRIF, TIR-domain-containing adapter-inducing interferon-β (TRIF); TRAF6, Tumour necrosis factor receptor (TNFR)-associated factor 6; MAPK, mitogen-activated protein kinase; RIP-1, receptor-interacting protein 1; AP-1, Activator protein 1; BAX, BCL2 Associated X Protein; TBK1, TANK-binding kinase; IKK, inhibitor of nuclear factor-κB (KB) kinase. Created with BioRender. (Turton, Thompson and Farkas, 2020).

1.3. Evidence of dsRNA signalling pathways in features of vascular remodelling

1.3.1 TLR3 deficiency in tissue repair

The above discussion illustrates highly regulated cellular responses to dsRNA. Emerging evidence implicates these pathways in non-inflammatory tissue repair, remodelling, and homeostasis. Importantly, it is the dysregulation of tissue repair pathways that form the basis of aberrant tissue remodelling. Specifically, it is thought that an initial acute pulmonary vascular injury followed by its abnormal repair initiates progressive pulmonary vascular remodelling in the context of PAH.

Moreover, TLR3 deficiency has been shown to play repair and remodelling roles in the lung parenchyma and the systemic vasculature. Specifically, Cole et al (2011) demonstrated that TLR3 deficiency was associated with enhanced elastic lamina damage following carotid artery injury and early onset atherosclerosis in hyperlipidaemic mice. O'Dwyer et al (2013) revealed protective repair pathways mediated by TLR3. They observed that TLR3 knockout mice had increased levels of pro-fibrotic cytokines and collagen deposition than wild type mice in a bleomycin-induced model of pulmonary fibrosis (O'Dwyer et al., 2013). Furthermore, TLR3 deficient mice failed to regenerate hair follicles after wounding, while in the eye, activation of TLR3 suppressed neovascularisation in models of age-related macular degeneration (Lin et al., 2011; Yang et al., 2008).

In the heart, the regeneration of neonatal mouse heart tissue was impaired in TLR3 deficient animals following myocardial infarction (Wang et al., 2018). This phenotype

was attributed to reduced proliferation of TLR3 deficient cardiomyocytes while poly(I:C) promoted glycolysis and proliferation in a YAP1-dependent manner (Wang et al., 2018). Other cardiac roles for TLR3 have been reported in post-viral infection myocardial injury and post-ischemia/reperfusion (I/R) injury (Abston et al., 2013; Chen et al., 2014; Hardarson et al., 2007). Hardarson et al. (2007) reported that TLR3 deficient mice were more susceptible to encephalomyocarditis virus (EMCV), with increased mortality compared to wild type. In EMCV-infected mice, serum analysis showed higher cardiac troponin I levels in TLR3-/- mice, compared to littermate controls, suggesting a direct EMCV-induced myocardial injury (Hardarson et al., 2007). In a different model that used coxsackievirus B3 (CVB3), TLR3 deficient mice were less effective at eliminating the virus in the acute phase and developed more severe chronic myocarditis with greater cardiac dysfunction, inflammation and fibrosis than wild type mice (Abston et al., 2013). In comparison to these protective effects of myocardial TLR3 against virus, demonstrated that both TLR3 and TRIF deficient mice exhibited significant reduced infarct size and improved left ventricular function, 24 hours after I/R injury (Chen et al. 2014). TRIF deficient mice had marked decreases in myocardial caspase 3 activity, indicative of apoptosis, after I/R injury (Chen et al. 2014).

A further interesting observation in cardiomyocytes demonstrated that TLR3 regulation of tissue homeostasis could also occur without dsRNA stimulation. Gao et al (2019) revealed the role for TLR3 in the regulation of potassium channels and cardiac electrophysiological homeostasis that was not dependent on downstream immune signals. TLR3-deficient mice had prolonged QT intervals, associated with reduced amplitude of current intensity compared to control cells and this was independent of

MyD88 and TRIF signalling and unaffected by poly(I:C) stimulation (Gao et al., 2019). TLR3 protein predominantly resided in the endoplasmic reticulum of cardiomyocytes, which express small amounts of the UNC93B1 chaperone protein, and was found to be important for potassium channel synthesis (Gao et al., 2019). This work indicates a tissue-specific role in the context of limited endosomal TLR3 trafficking, but whether this is important in other cells or whether TLR3 is involved in the stabilization of other proteins remains unknown. The work above implicates TLR3 as a regulator of tissue repair in several organs and in the systemic vasculature. In addition, work by Farkas et al (2019) have extended these observations to the context of vascular remodelling in pulmonary hypertension. This work is discussed in detail in section 1.4.1 and forms a basis for subsequent research questions in this thesis.

1.3.2 DsRNA signalling in apoptosis and proliferation

Imbalances between cell death and proliferation are central in the vascular remodelling of PAH. Many believe that initial EC apoptosis propagates apoptosis-resistant EC proliferation in development of plexiform lesions and liberates endogenous growth factors to promote SMC proliferation (Sakao et al., 2009). There is now evidence to suggest that apoptosis and proliferation are regulated by the components of the dsRNA signalling pathway. For example, apoptosis, via FADD-caspase 8 mediated death signalling and upregulation of p53 was induced by dsRNA activation of PKR (Balachandran et al., 1998; Gil & Esteban, 2000). Poly(I:C) has also been shown to induce TLR3-dependent apoptosis by up to 40% in human umbilical vein cord endothelial cells (HUVECs) compared to untreated cells (R. Sun et al., 2011). Cell proliferation via mitosis is governed by the cell cycle. Cell cycle analysis has shown

that mutated PKR induces cell cycle arrest, promoting a longer G1 phase and less engagement in the S phase (Zamanian-Daryoush et al., 1999). Yang et al. (2006) revealed pro-proliferative and IL-1α stimulatory effects of dsRNA in human vascular SMCs but indicated vascular SMCs to possess species-specific actions, as mouse vascular SMCs failed to respond to poly(I:C) in a proliferative manner. On the contrary, in both prophylactic and therapeutic poly(I:C) treatment in SuHx rat models, the number of apoptotic and proliferative cells in the pulmonary artery were significantly reduced (Farkas et al., 2019). Other work has revealed protective effects of poly(I:C) associated with alterations in apoptosis susceptibility. In the brain, poly(I:C) reduced infarct volume by 57.2% compared to untreated mice subjected to an ischemic/reperfusion injury (Zhang et al., 2015). This protection was dependent upon TLR3 and was associated with reduced apoptosis in microglial cells (Zhang et al., 2015). Furthermore, recognition of endogenous dsRNA by TLR3 has been proposed to effect apoptosis. For example, endogenous dsRNA liberated from lung tissue or necrotic neutrophils, activated TLR3 in the absence of exogenous virus and increased apoptosis in lung tissue, in mice models of hyperoxia lung injury (Murray et al., 2008).

In addition to direct cellular effects of dsRNA mediated by PKR or TLR3, downstream activation of interferon stimulated genes and release of interferon may also influence proliferation. When studying the effect of IFN in vascular remodelling, Bauer and Bauer (2012) revealed *in vitro* IFNα treatment on human PAECs inhibited proliferation. Likewise, vascular SMCs showed attenuated proliferation when treated with IFNβ (Schirmer et al., 2010). Conversely, other interferon stimulated genes may enhance proliferation. For example, TRAIL is a protein ligand and although it is implicated in apoptosis, it can also promote proliferation. TRAIL is induced by IFN and is specifically

a target gene of the interferon regulatory factor, IRF9 (Schirmer et al., 2010; Tsuno et al., 2009). Interestingly, TRAIL expression was increased in explanted PASMCs from idiopathic PAH and in vascular remodelled lesions in monocrotaline (MCT) rat models of PAH (Hameed et al., 2012). Additionally, explanted PASMCs treated with recombinant TRAIL induced proliferation and migration in a dose-dependent manner (Hameed et al., 2012). Reinforcing TRAIL's significance in pro-proliferation, blocking endogenous TRAIL with preventative and therapeutic anti-TRAIL antibody in MCT models significantly reduced proliferative biomarker PCNA in small pulmonary arterioles (Hameed et al., 2012)

1.3.3 DsRNA signalling in angiogenesis

Double stranded-RNA receptors and signalling pathways also exert substantial effects on EC function. An important function of ECs is angiogenesis, which is the name given to the development of new blood vessels from existing vasculature. In pulmonary vascular disease, angiogenesis is usually impaired leading to pulmonary vascular rarefaction and pruning. Research into angiogenesis has focused on protein growth factors that promote or restrict angiogenesis, such as vascular endothelial growth factor, bone morphogenic proteins, angiopoietins, and various cytokines and chemokines. Yet in the recent years, work has shown that angiogenesis is also regulated by the innate immune system. For example, shockwave therapy (SWT)-models of angiogenesis in ischemic tissue induced *TLR3* and *IFNβ1* in a time-dependent manner and liberated endogenous RNA from ECs (Holfeld et al., 2016). Furthermore, angiogenesis induced by SWT was abolished in TLR3-deficient mice in hind limb ischemia models (Holfeld et al., 2016). By contrast, Schirmer et al (2010)

revealed mice deficient in the downstream effector of TLR3, IFNAR1, induced arteriogenesis, when assessed by the same approach of assessing the percentage of restored perfusion in the femoral artery. This implies TLR3 is necessary for normal endothelial function, whereas downstream signalling via IFNAR1 is not required for the development of angiogenesis.

1.3.4 DsRNA signalling in endothelial dysfunction

RNA signalling also influences the barrier function of vascular endothelial cells. Zimmer et al (2011) revealed that poly(I:C) treatment impaired aortic endothelial cell vasodilation in a TLR3-dependent manner and impaired reendothelialization after a denuding carotid artery injury in wild type mice. Both tissue TLR3 activation and TLR3 stimulation in endothelial progenitor cells impaired reendothelialization (Zimmer et al., 2011). These detrimental effects of poly(I:C)-induced TLR3 activation are in contrast to findings by Cole et al (2011). Cole and colleagues showed that poly(I:C) significantly reduced neointima formation in response to carotid collar injury and these vascular protective effects of poly(I:C) were ablated in TLR3-deficent mice. TLR3 activation was also protective in the medial layer of the arterial wall (Cole et al., 2011). The contradictive findings may be attributed to differences in poly(I:C) dosage and administration regimes, analysis of reendothelialization in whole versus cross-sectional carotid artery sections and in the technique to create carotid injury. Cole et al (2011) used an arterial injury model involving a perivascular collar injury model that did not affect SMC integrity, as opposed to, Zimmer et al (2011) who performed electrical endothelial denudation which did not maintain vascular cell integrity.

1.4 Double stranded RNA signalling in PAH pathogenesis

1.4.1 TLR3 in PAH

Farkas *et al* (2019) showed TLR3 knockout mice developed more severe PH as assessed by increased RVESP and pulmonary artery muscularization, in the well-established PH model of chronic hypoxia and SU5416 (SuHx) mice, compared to wildtype mice. These pre-clinical models have translational relevance as reduced TLR3 expression has been observed in PH patients. Farkas et al (2019) showed reduced TLR3 expression in lung vascular lesions of PAH patients. Interestingly, these ECs with reduced TLR3 expression did not cease production of pro-inflammatory cytokines, such as IP-10, in response to poly(I:C). Rather, dsRNA signalling was shown to occur through the alternate RNA receptors, RIG-I and MDA5 (Farkas et al., 2019). Interestingly, the TLR3 agonist, poly(I:C), increased TLR3 expression in rat lung ECs in an IL-10 dependent manner. Prophylactic high-dose poly(I:C) treatment (10 mg/kg three times a week) in the SuHx rat model reduced RVESP and the number of vascular occlusions but had no significant effect on medial wall thickness or cardiac output (Farkas et al., 2019). Therapeutic poly(I:C) attenuated established PH when administered 3 weeks after initiation of the disease with hypoxia and SU5416. These data suggest that TLR3 has a protective role in PAH and that the TLR3-agonist, poly(I:C), can restore TLR3 levels in TLR3 deficient endothelial cells, thus restoring protective anti-remodelling signals mediated via this pathway. Likewise, poly(I:C) was protective when promoting BMPR2 expression in ECs as downregulation of BMPR2 signalling is associated with PAH pathogenesis (Bhagwani et al., 2023). Reduced

expression of TLR3 and BMPR2 in ECs were also concurrent with reduced expression of p53 (Bhagwani et al., 2023).

However, potential detrimental consequences associated with activating dsRNA signalling and subsequent type I IFN and proinflammatory cytokine response are largely reported in pulmonary vascular remodelling in PAH pathogenesis and are outlined below (section 1.4.3).

1.4.2 PKR in PAH

PKR, another pattern recognition receptor has shown to have a regulatory role in murine models of PH. Specifically the activation of PKR (i.e., phosphorylation of PKR) was significantly increased in the SuHx and MCT rat model of PH (Li et al., 2021). Moreover, the inhibition of PKR activity via compound C16 was injected intraperitoneally, one week prior to the induction of SuHx and MCT significantly reduced RVESP, right ventricular hypertrophy and percentage of pulmonary vascular remodelling (Li et al., 2021). Likewise, PKR knockout mice exposed to SuHx had significantly decreased RVESP, right ventricular hypertrophy and pulmonary vascular remodelling compared to SuHx wildtype mice (Li et al., 2021). The beneficial action of PKR depletion in a SuHx mouse was attributed to the repression of apoptosis-associated speck-like protein containing CARD (ASC) activation to inhibit high mobility group box 1 (HMGB1) and IL-1β release (Li et al., 2021).

1.4.3 Interferon response in PAH

Double stranded RNA recognition via TLR3 is a potent inducer of type I IFN. Type I IFNs present in humans include IFN-α and IFN-β. Type I IFN acts in a paracrine manner to elicit an anti-viral response via production of IFN stimulation genes and induction of innate and adaptive immune responses. However, excessive type I IFN activation may contribute to the pathogenesis of autoimmune diseases. The strong association between PAH and autoimmune diseases such as lupus erythematosus and systemic sclerosis could implicate excess IFN activity in PAH pathogenesis (Simonneau et al., 2019). Eloranta et al (2010) revealed increased serum levels of interferon-inducible protein-10 (IP-10) and IFN-α in systemic sclerosis patients with PAH and lung fibrosis. A contradictory finding, by Bauer et al (2014), reported IFNα to prevent and reverse PH in mice models, highlighting potential interspecies variation in IFN signalling.

Exogenous elevated levels of IFN in the context of α or β IFN therapy for non-PAH diseases such as hepatitis C and multiple sclerosis have also been linked to the development of PAH (Papani et al., 2017; Savale et al., 2014; Tsuchiya et al., 2017). Papani et al (2017) revealed a significant increase in the incidence of PAH in an IFN α or β therapy population, derived from a health insurance USA database, when compared to the baseline incidence rate of PAH in the general population. Interestingly, reports suggests that the type of IFN therapy is associated with the delay between initiation of IFN therapy and PAH diagnosis. Savale et al (2014) identified the majority (73%) of PAH diagnoses were within 3 years after initiation of IFNα therapy. Conversely, the majority (80%) of patients receiving IFN-β therapy were diagnosed 5–

10 years after commencement of exposure (Savale et al., 2014). The association between IFN therapy and PAH was strengthened by data on haemodynamic parameters, functional class, and diffusion capacity testing during and after IFN treatment. For example, 48% of patients receiving IFN-α therapy exhibited a clinically relevant $\geq$15% reduction in diffusion capacity for carbon monoxide testing at 24 weeks post-treatment when compared to baseline (Foster et al., 2013). Likewise, PVR was significantly increased at median IFN treatment duration (7.4 months), before returning to baseline after IFN discontinuation at 7.7 months. Likewise, resolution of functional class and 6-minute walk test to baseline levels (treatment naïve) were observed after IFN discontinuation (Foster et al., 2013). Studies like these contributed to type I IFN being identified as a risk factor of PAH at the PH World Symposium in 2013 (Simonneau et al., 2013). However, a key limitation when studying patients diagnosed with hepatitis C and receiving subsequent IFN therapy, is the often-associated co-morbidities such as liver cirrhosis and portal hypertension that are also known risk factors of PAH. Therefore, hepatitis C itself and its associated diseases perhaps triggers the development of asymptomatic PAH before IFN therapy (Tsuchiya et al., 2017).

IFN has long been linked to the release of endothelin-1 in vascular cells (Woods et al., 1998, 1999; Wort et al., 2001). First identified by Yanagisawa et al (1988), endothelin-1 is now known to be a potent vasoconstrictor that is predominantly released from vascular ECs and possesses pro-mitogenic properties. Endothelin-1 is implicated in the progression of increased PVR and pulmonary vascular remodelling in PAH (Chester & Yacoub, 2014; Kim et al., 2000). IFN-α treatment activated PASMCs to release endothelin-1 (Badiger et al., 2011). Given the relationship of between viral

RNA signalling and its downstream effectors of IFN and subsequent endothelin-1, George et al (2012) investigated this in PASMCs. The TLR3 agonist, poly(I:C), significantly enhanced endothelin-1 by 4-fold in PASMCs. Additionally, PASMCs released increased amounts of poly(I:C)-induced endothelin-1 when primed with TNFα compared to the control (George et al., 2012). As poly(I:C)-induced activation of TLR3 is a potent inducer of IFN, they postulated that endogenous IFN acts in an autocrine manner to synergise with TNFα and add to endothelin-1 production (George et al., 2012). To directly investigate the effect of type I IFN signalling on the development of PAH, George et al (2014) subjected IFNAR1-/- and wildtype mice to chronic hypoxia. Protective effects of IFNAR1-/- in response to hypoxia were measured via a significant reduction in RVESP, muscularised pulmonary vessels and serum endothelin-1 levels. To add, increased IFNAR1 protein expression was measured in human PAH lung. IP-10 and endothelin-1, important mediators of inflammation and vasoconstriction in PAH, were reduced in LPS-treated IFNAR1-/- mice compared to LPS-treated wildtype mice, suggesting that LPS-induced endothelin-1 release is dependent on IFNAR1 (George et al., 2014).

Whether produced by exogenous or endogenous dsRNA activation of TLR3, autoimmune disease or via therapeutic administration of IFN, there is a lot of evidence to suggest excessive IFN may be involved in the development of PAH. Interestingly, a role for excessive IFN levels in PAH appears to oppose the previously discussed hypothesis by Farkas et al (2019) that TLR3 activation may play a protective role in PAH. Activation of TLR3 would be expected to increase interferon levels and, by extension, endothelin levels. Therefore, strategies to enhance TLR3 signalling may require synergistic targeting of excessive interferon activity.

1.4.4 Pro-inflammatory cytokines in PAH

Double stranded RNA signalling is also a potent inducer of proinflammatory cytokines, and such cytokines have been implicated in the pathogenesis of PAH. For example, circulating levels of pro-inflammatory cytokines were significantly higher in idiopathic PAH when compared to control (Itoh et al. 2006; Soon et al. 2010). Likewise, altitude-exposed TNF-α over-expressing in mice, specifically in alveolar type II cells, had significantly increased right and left ventricular systolic pressures and right ventricular hypertrophy when compared to control (Fujita et al., 2001). Similarly, TNF-Tg female mice developed progressive and obliterative pulmonary vascular remodelling and exhibited increased pulmonary pressures (Bell et al, 2020).

PAH patients had significantly higher levels of serum IL-1β, -2, -4, -6, -8, -10, and -12p70 and TNF-α compared with healthy controls (Soon et al., 2010) but arguably IL-6 contributions to pathogenesis of PAH are predominantly reported in literature when compared to other cytokines and are strongly evidenced both animal models and humans. By various approaches of IL-6 depletion in transgenic murine models and knockdown of IL-6 and its receptor in murine, reports show a consistent reduction in pulmonary pressures, cardiac function, pulmonary vascular remodelling, and right ventricular hypertrophy in models of PH (Maston et al., 2018; Savale et al., 2014; Tamura et al., 2018). Conversely, overexpression of IL-6 enhanced murine models of PH (Golembeski et al., 2005; Steiner et al., 2009). Likewise, PAH patients had elevated serum IL-6 levels and was predictive for patient mortality(Hirsch et al., 2023; Soon et al., 2010).

1.5 Research hypothesis

Together, these data suggest that dsRNA can regulate hallmarks of vascular remodelling such as apoptosis, proliferation, impaired wound healing/tissue repair and angiogenesis, and endothelial cell dysfunction. Whilst most of these processes can be regulated by the canonical dsRNA signalling pathway associated with pro-inflammatory cytokines and type I interferon and have the potential to contribute to deleterious vascular disease outcomes, there are instances in literature where dsRNA signalling is associated with an anti-inflammatory profile, vascular repair, and disease protection.

Overall, the role of inflammation in the pathogenesis of pulmonary vascular remodelling and PAH is unclear. In particular, the role of dsRNA signalling as part of the innate immune response in pulmonary vascular remodelling and pulmonary arterial hypertension is contradictory and under-researched. Therefore, future work is required to elucidate if dsRNA signalling is deleterious or protective in pulmonary vascular remodelling and pulmonary arterial hypertension. In particular a synthetic form of dsRNA, poly(I:C), has shown to be protective in a rat model of PH (Farkas et al., 2019), but its feasibility as a potential therapeutic in PAH still remains unclear as the mechanism of action, route of administration, and its potential associated adverse outcomes and reproducibility of these data have not been investigated. Moreover, the effects of poly(I:C) have not been investigated in combination with genetic mutations (such as *EIF2AK4* encoding for GCN2) associated with PAH pathogenesis in the under researched area of PVOD. As PAH pathogenesis is considered multifactorial, and GCN2's associations with another integrated stress response kinase, PKR, and

PKR's known binding to dsRNA, the effects of poly(I:C) in the context of GCN2 deficiency in pulmonary vascular remodelling and PAH warrants further investigation.

The main hypothesis of this work is that dsRNA signalling has an important role in pulmonary vascular remodelling and PAH with the context of dsRNA signalling being crucial to PAH pathogenesis prior to proposing a future therapy.

I will use the synthetic form of dsRNA, poly(I:C), throughout this work to activate dsRNA signalling.

I will test this hypothesis using the following aims:

1. Investigating the effects of intraperitoneal poly(I:C) as a therapeutic in a SuHx mouse model of PH
2. Investigating the effects of previous exposure to poly(I:C)-induced lung inflammation on the SuHx mouse model of PH
3. Investigating the effects GCN2 deficiency in dsRNA signalling in endothelial cells
4. Investigating the effects of GCN2 knockout in a Hx mouse model of PH with previous exposure to intranasal poly(I:C)

2. Methods

In vitro models

2.1 Ethical approval for human samples

Derivation and storage of blood outgrowth endothelial cells (BOECs) from blood samples taken from healthy donors at the Pulmonary Vascular Disease Unit, Royal Hallamshire Hospital, Sheffield was approved by the Yorkshire and Humber Research Ethics Committee as part of the STH-Obs study (Sheffield Teaching Hospitals Observational Study of Patients with Pulmonary Hypertension, Cardiovascular and other respiratory diseases; 18/YH/0441). Healthy donors gave informed consent to participate. Cells were stored in an HTA-licenced biorepository.

2.2 Endothelial cell culture and maintenance

2.2.1 Human pulmonary artery endothelial Cells

Human pulmonary artery endothelial cells (hPAECs) (CC-2530, batch number of 4 different donors: 18TL155113, 0000708987, 19TL217385, 21TL228096) were purchased from Lonza, Switzerland. Lonza provided donor clinical characteristics (Appendix Table 1). The cryopreserved hPAECs were thawed in a 37 ˚C water bath and cultured in 75cm^2 Corning™ tissue culture treated flask (ThermoFisher) containing endothelial cell growth medium-2 BulletKit™ (EGM™-2) (Lonza). EGM™-2 contained endothelial cell growth basal medium -2 (EBM™-2) (Lonza) supplemented with EGM™-2 SingleQuots™ (Lonza). Supplements added to one 500ml bottle of EBM™-2 included 5% (v/v) of foetal bovine serum (FBS), 0.2 ml Hydrocortisone, 2ml human fibroblast growth factor (hFGF), 0.5 ml vascular endothelial growth factor

(VEGF), 0.5 ml insulin-like growth factor-I (IGF-1), 0.5 ml ascorbic acid, 0.5 ml human epidermal growth factor (hEGF), 0.5 ml gentamicin sulfate-amphotericin (GA-1000), and 0.5 ml Heparin. Cultures were maintained in a humidified incubator at 21% O_2, 5% CO_2 at 37 ˚C. Cells demonstrated characteristic endothelial cell cobblestone morphology and were previously validated by the supplier, with positive staining positive for the endothelial markers, von Willebrand Factor and CD31.

2.2.2 Human blood outgrowth endothelial cells (BOECs)

Previously generated healthy donor-derived blood outgrowth endothelial cells (BOECs) were kindly donated by Professor Allan Lawrie, Imperial College London, formerly University of Sheffield. BOECs are generated from circulating endothelial progenitors in adult peripheral whole blood, all of which, have the capacity to differentiate into mature endothelial cells upon isolation, expansion, and culture. The protocol included taking approximately 50ml of blood from the participant and placing it into a 50ml falcon containing 2ml of sodium citrate. Citrated blood was then diluted 1:1 in PBS before layering 15ml of diluted blood onto Ficoll-Paque™ PLUS (ThermoFisher), in several 50ml falcons, for separation of mononuclear cells from blood via density gradient centrifugation at 400xg for 30 minutes at room temperature with the break off. The mononuclear cells, contained in the 'buffy coat', was removed by Pasteur pipette, and diluted 1:1 in PBS and centrifuged at 300xg for 20 minutes at room temperature. The cell supernatant was removed, and the cell pellet was resuspended in EGM™-2 media containing BulletKit™ supplements (Lonza) and 20% (v/v) FBS (Gibco™, ThermoFisher). This cell suspension was plated onto Type I collagen (ThermoFisher) coated 25cm^2 Corning cell culture flasks (ThermoFisher). Cells were maintained in EGM™-2 media containing BulletKit™ supplements (Lonza)

and 20% FBS (v/v) (Gibco™, ThermoFisher) and media was changed in the first 24 hours after preparation and then every 3 days thereafter. Endothelial cell colonies appeared more than 10 days after initial preparation and when 70-80% confluency was reached, cells were trypsinised and transferred to multiple 75cm^2 cell culture flasks (ThermoFisher). BOECs exhibit characteristics of mature endothelial cells such as cobblestone morphology and endothelial cell-specific markers, such as CD31. Prior to this development in experimental biology, primary endothelial cells largely were derived from explanted organs and therefore somewhat inaccessible. BOECs which originate from early progenitor cells are believed to have a role in postnatal neogenesis, a process of generating new blood vessels which is implicated in PAH pathogenesis and airway inflammation. BOECs were stained for endothelial biomarkers of CD31 and vWF to validate endothelial cell type (figure 2.1).

2.2.3 Cell phenotyping by immunofluorescent staining

Indirect immunofluorescent staining with endothelial-specific markers were used to validate in house generation of healthy donor derived BOECs (figure 2.1), prior to use in subsequent experiments as a primary endothelial cell surrogate (Toshner et al., 2013). BOECs were cultured onto coverslips before 4% (w/v) paraformaldehyde was applied to fix the cells. After several PBS washes, fixed cells were blocked and permeabilised with 0.1% (v/v) Triton X-100 (Sigma) in PBS for 15 minutes at room temperature, prior to blocking of cells in 1% (w/v) BSA (Sigma), 0.1% (v/v) Tween (Sigma, USA) in PBS for 1 hour at room temperature. Polyclonal rabbit anti-human von Willebrand factor (vWF) (Dako), polyclonal Rat anti-mouse CD31(BioLegend) and monoclonal mouse anti-human smooth muscle actin (SMA) (Dako) antibodies were

diluted (1:250) in blocking buffer and applied overnight at 4°C. After removal of surplus primary antibodies and several PBS washes, Alexa Fluor 488 goat anti-rabbit IgG (H+L) (Invitrogen Ltd., UK) and Alexa Fluor 555 goat anti-mouse IgG (H+L) (Invitrogen Ltd., UK) were diluted (1:1000) in blocking buffer and added to cells for 1 hour at room temperature. Vectashield mounting medium with DAPI (Vector Laboratories) was used to mount coverslips to the centre of microscope slides before they were stored at 4˚C in the dark. Indirect immunofluorescent staining of an autofluorescence control (no 1° and 2° antibody), positive control (PAECs supplied by Lonza), and control for primary antibody specificity (no 1° antibody) were conducted in parallel under the same conditions. Indirect immunofluorescence was visualised using Zeiss system, Axio Observer.Z1 with fluorescent cameras, Axiocam MRm (figure 2.1.), and analysed using Zen (Zeiss) software.

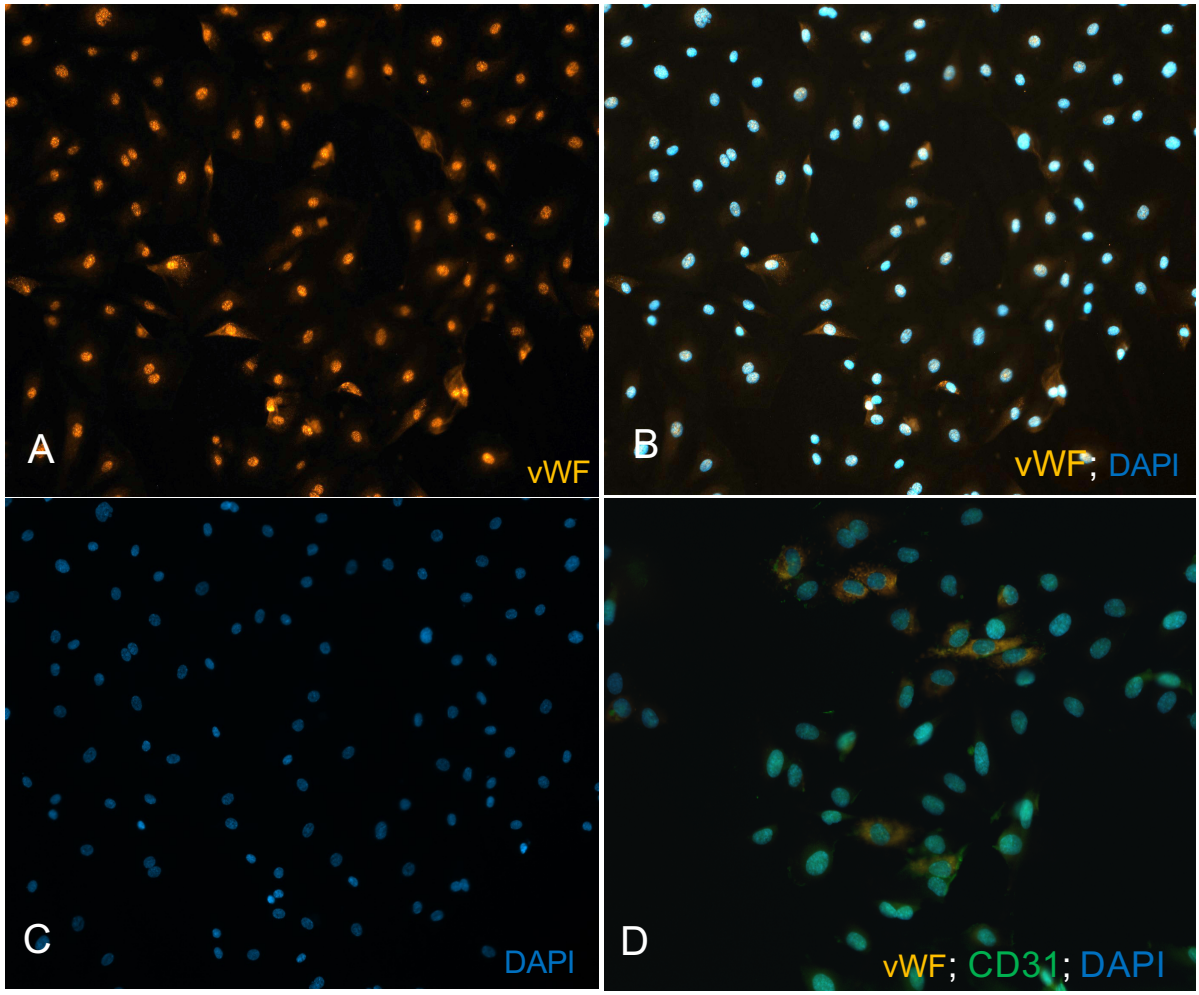

Figure 2.1 Immunophenotyping of blood outgrowth endothelial cells (BOECs). Endothelial cell specific biomarker vWF (A) and CD31 (D) were used to stain BOECs for validation of endothelial-like cell type. DAPI (B-D) stained nuclei of cells. This was achieved by indirect immunofluorescent scanning and visualised using Zeiss system, Axio Observer.Z1 with fluorescent cameras, Axiocam MRm.

2.3 Materials

2.3.1 Polyinosinic:polycytidylic acid (poly(I:C))

Low molecular weight (LMW) polyinosinic:polycytidylic acid (poly(I:C)) (InvivoGen and Tocris Bioscience) was used to stimulate hPAECs, BOECs and in mouse models of PH. Poly(I:C)-LMW is comprised of separate inosine and cytidine homopolymers bound together to form average nucleotide sizes of 0.2kb to 1kb and base sizes were validated by RNA agarose gel electrophoresis and visualised using an UV transilluminator (figure 2.2). Poly(I:C)-LMW, from both suppliers (InvivoGen and Tocris Bioscience), were cell culture and endotoxin tested by the supplier. Poly(I:C) was prepared by solubilising 25mg of lyophilized poly(I:C)-LMW in 1ml of sterile endotoxin-free physiological water (NaCl 0.9% (v/v)) supplied by manufacturer. After resuspension, aliquots of stock concentrations of 25mg/ml poly(I:C)-LMW were stored at -20 ˚C and freeze-thaw cycles were avoided.

For *in vitro* experiments, stock poly(I:C) was diluted in EGM^{TM}-2 containing 0.5% (v/v) FBS (Lonza) to produce working concentrations of 25μg/ml or 0.25μg/ml.

For *in vivo* experiments, stock poly(I:C) was diluted in sterile saline to produce working concentrations for administration into mouse models of PH and their appropriate controls. See below (section 2.13.2) for specific concentrations and dosing schedule of poly(I:C) in mouse studies.

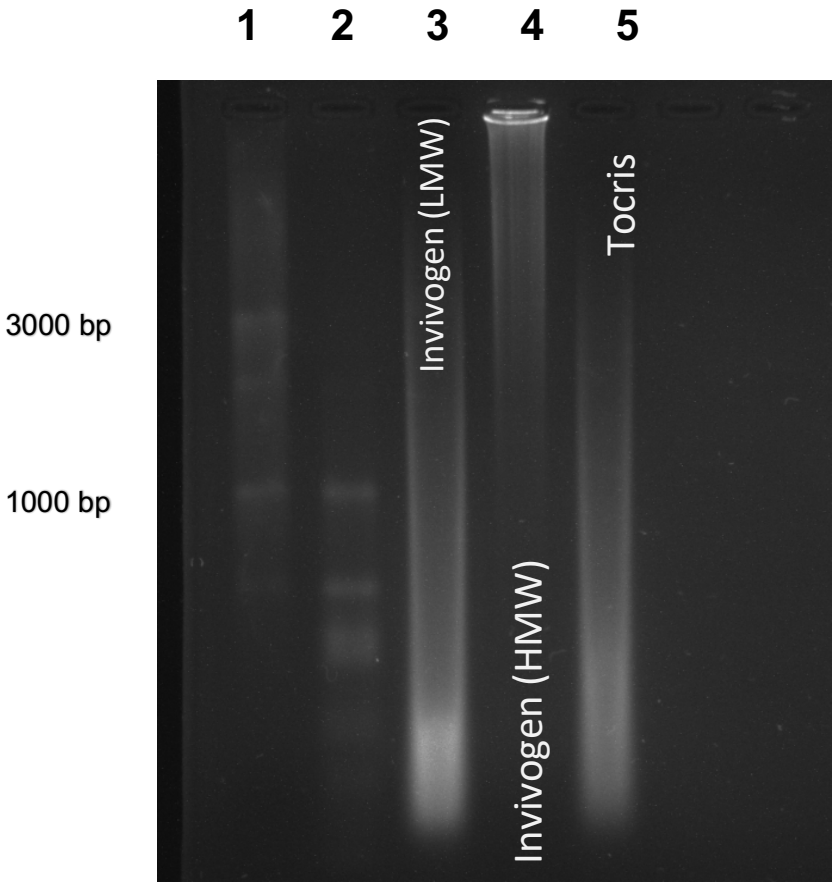

Figure 2.2. Image of a UV illuminated native RNA 1.2% (w/v) agarose gel in TAE buffer electrophoresis. This image validates low molecular weight poly(I:C) purchased from Invivogen and Tocris Bioscience.

Lane 1; dsRNA ladder (New England Biolabs; size range: 500 bases - 9,000 bases; N0362S; 10uL. Lane 2; low Range dsRNA ladder (New England Biolabs; size range: 1000 bases - 50 bases; N0364S; 10uL. Lane 3; LMW poly(I:C) purchased from Invivogen. Lane 4 contains HMW poly(I:C) purchased from Invivogen. Lane 5; poly(I:C) purchased from Tocris Bioscience and confirms LMW base sizes of dsRNA.

2.4 Transient transfection via siRNA

Small interfering (si)RNA oligonucleotides targeting *GCN2, PKR,* and non-targeting controls were obtained from Dharmacon and purchased in the SMARTpool format where four siRNA sequences for the same gene target are pooled together (table 2.1). Human PAECs and BOECs were transfected using lipofectamine-based RNAimax reagent following manufacturer's instructions (Invitrogen™, ThermoFisher). When conducting knockdown of a single gene i.e., *EIF2AK4 (GCN2)* or *EIF2AK2 (PKR*)*,* or simultaneous double knockdown i.e., *EIF2AK4* (GCN2) and *EIF2AK2* (*PKR*), siRNA (100nM) and Lipofectamine™ RNAiMAX transfection reagent (Invitrogen™, ThermoFisher) were gently mixed by inverted the tub in Opti-MEM (reduced serum media of Eagle's Minimum Essential Media, buffered with HEPES and sodium bicarbonate) and incubated for 20 mins to form complexes. Growth media was removed, and cells were washed twice with PBS, before lipofectamine: siRNA complexes were then transferred onto sub-confluent (70-80%) hPAECs or BOECs in 75cm^2 cell culture flasks, where complexes were diluted further in Opti-MEM to a final siRNA concentration of 20nM. This standard transfection approach, rather than reverse transfection, provided successful gene knockdown efficiencies. Cells were transfected for 72 hours in normoxic conditions in the incubator at 37 ˚C and 5% CO_2. Opti-MEM containing lipofectamine: siRNA complexes was replaced with EGM^{TM}-2 containing 5% FBS (Lonza) after 6 hours of transfection.

Table 2.1 List of siRNA target sequences.

siRNA target	Target sequence(s):
Non-targeting control	UGGUUUACAUGUCGACUAA
EIF2AK4 (GCN2)	CAGCAGAAAUCAUGUACGA, GCAAUUCUGUGGUGCAUAA, GACCAUCCCUAGUGACUUA, GGAAAUUGCUAGUUUGUCA
EIF2AK2 (PKR)	GUAAGGGAACUUUGCGAUA, GCGAGAAACUAGACAAAGU, CGACCUAACACAUCUGAAA, CCACAUGAUAGGAGGUUUA

2.5 Gene expression analysis

Gene expression quantification was conducted via the chronological processes of RNA extraction, cDNA synthesis (reverse transcription) and quantitative polymerase chain reaction (RT-qPCR). Total RNA was extracted from transfected and unstimulated or poly(I:C)-stimulated hPAECs and BOECs using 500µl TRIzol per 50,000 cells plated in 12-well cell culture plates. Cell lysates from two technical replicates (2 wells of a 12-well plate) were pooled together in the same RNA isolation preparation. RNA was isolated using the spin column-based RNA isolation kit of Direct-zol™ RNA Miniprep (Zymo Research). At room temperature, RNA from samples in TRIzol were directly transferred to spin column and a series of ethanol-based washes and centrifugations allowed RNA to bind to the column, before nuclease-free water was used to elute total

RNA. Total RNA (500ng) determined via ThermoScientific™ NanoDrop™ 2000 spectrophotometer, was used to perform reverse transcription by using a High-Capacity RNA-to-cDNA kit (ThermoFisher) and Veriti™ 96-Well Thermal Cycler (ThermoScientific). In addition to determining RNA concentrations, the NanoDrop™ 2000 spectrophotometer also provided quality assurance of the RNA. Workflow was halted if samples did not meet quality assurance criteria of: A260/280 value of 1.8-2.2 and A260/230 $\geq$ 1.8. The thermal cycler program steps in the synthesis of cDNA were as follows: 1) 25˚C for 10 minutes, 2) 37˚C for 60 minutes, 3) 95 ˚C for 5 minutes, before storing at -20 ˚C. Over ice, complementary DNA was diluted (1:10) using RNase-free water and pipetted into a 384 qPCR well-plate in triplicate. Gene expression levels in hPAECs and BOECs were quantified by TaqMan hydrolysis probes labelled with 6-carboxyfluorescein (Applied Biosystems, UK). The following TaqMan primer/probes were used: *EIF2AK4* (*GCN2*), *EIF2AK2* (*PKR), IL-6, IP-10, TNF-*α*, MDA5, TLR3,* β*-actin* and *GAPDH*. Each RT-qPCR reaction totalled 10µl and consisted of 5µl of TaqMan™ Fast Advanced Master Mix, 0.5µl TaqMan primer/probe and 4.5µl of diluted cDNA. The qRT-PCR plate was sealed and centrifuged at 300 xg for 2 minutes to eliminate bubbles and loaded into QuantStudio™ 7 Flex Real-Time PCR System with Design & Analysis Software 2.0. RT-qPCR running parameters included: 1) pre-incubation; 95 ˚C, 20 seconds for 1 cycle, 2) amplification; 95 ˚C (denaturing) for 1 second, 60 ˚C (annealing) for 20 seconds, before a 2.19 ˚C/second raise in temperature to 95 ˚C (elongation); these steps occurred for 40 cycles, 3) melting curve, 95-97 ˚C, continuous for 1 cycle, 4) cooling, 40˚C, 30 seconds for 1 cycle. Threshold cycle (Ct) values for each gene of interest were obtained for each sample and normalised to the corresponding housekeeping gene (e.g., *GAPDH* or β-*actin*) Ct values of that sample to provide delta Ct (ΔCt). The Ct value defines the

number of cycles required for the fluorescent signal to reach a threshold. To calculate relative changes in gene expression (fold change) the $2^{-\Delta\Delta ct}$ method was used which is the relative difference in ΔCt to the experimental sample to the control sample. In the case of my experiments the control sample was cells treated with a non-targeting siRNA and unstimulated.

2.6 Luminex assay

Cytokine levels in a fixed volume (50µl) of cell supernatant derived from hPAECs and BOECs deficient in GCN2 and/or PKR, with and without, 24-hour stimulation of poly(I:C), were quantified using Luminex xMAP technology in coordination with ProcartaPlex magnetic bead-based fluorescent multiplexed immunoassays (ThermoFisher), according to the manufacturer instructions. ProcartaPlex Simplex immunoassays detected IP-10 and IL-6 and ProcartaPlex high sensitivity kit detected TNF-α (ThermoFisher). The principles of this immunoassay are based on specific epitope binding of an antibody to a specific antigen in combination with magnetic beads being uniquely dyed with infrared fluorophores of differing intensities. In an 'ELISA-like' approach, the triplicate analyte samples and standards of known concentrations were sandwiched between capture antibodies attached to magnetic beads diffused with fluorescent dye mixtures and biotinylated detector antibodies (figure 2.3). When the antigen is immobilised, streptavidin-phycoerythrin conjugates, which have a strong affinity for biotin were added to each well. High sensitivity kits included an additional application of two amplification reagents. Washes were conducted between each application and incubation of bead, antibody, or metabolite, ensuring magnetic plate was attached. All immunoassays were run on a Luminex® 200™ according to manufacturer's instructions. Magnetic beads pass through a red

laser to excite internal dye to identify bead set corresponding to a target of interest, whilst a green laser excites phycoerythrin. The fluorescent intensity of phycoerythrin is proportion to the amount of analyte bound. Data was exported from Luminex software and was fitted to a seven-point standard curve generated using five-parameter logistic regression in GraphPad Prism Version 9.3.1.

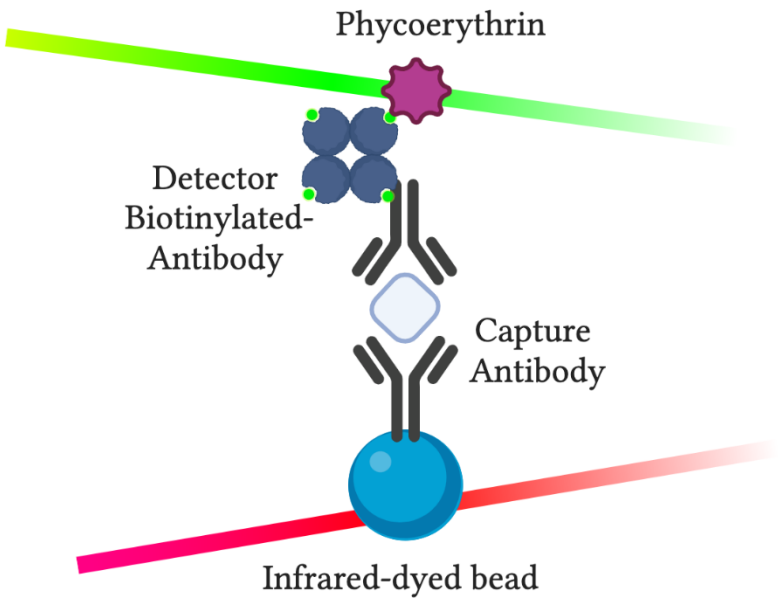

Figure 2.3. Principles of Luminex technology.

A red laser excites the bead, and the infrared emissions enable identification of the relevant analyte, while the green laser allows quantification of fluorescence. Original image created in Biorender.com

2.7 Western blotting

Protein was extracted from transfected (si*GCN2*, si*PKR* or siCTL) BOECs and hPAECs with and without poly(I:C)-stimulation using 250 µL of M-PER ™ Mammalian Protein Extraction Reagent, containing Halt Phosphatase Inhibitor Cocktail (ThermoFisher) and Halt Protease Inhibitor Cocktail, EDTA free (ThermoFisher), per 2.5 x 10^5 cells in a 25cm^2 cell culture flask. Total protein concentration was determined by Pierce™ 660nm Protein Assay Kit (ThermoFisher), in accordance with manufacturer instructions. Pierce™ Bovine Serum Albumin Standard Pre-Diluted Set (ThermoFisher) was used to generate protein standards that included seven standards between 0-2000µg/ml. In triplicates, protein lysates were diluted (1:5) in nuclease-free water before Pierce™ reagent was added to samples and protein standards and incubated for 10 minutes at room temperature. The clear plate was read in a spectrophotometer at 660nm. Unknown protein concentrations were interpolated from protein standard curve and dilution factor was applied to calculate volume required to yield 30µg. To total 40µl, 30µg of protein samples were reduced using 4µL 10X Bolt™ Reducing Agent (ThermoFisher) in 10µL 4X Bolt™ LDS Sample Buffer (ThermoFisher) and added to ≤ 26µL of deionized water. Samples were subsequently heated at 70℃ for 10 minutes. In the immunoblots, protein solution and Chameleon® Duo Pre-stained Protein Ladder (Li-cor) were separated by SDS-PAGE using Bolt™ 4-12% Bis-Tris Plus Gels, 10-well (ThermoFisher). Proteins were transferred to polyvinylidene difluoride (PVDF) membranes, as part of Mini iBlot™ 2 Transfer Stacks (ThermoFisher; 0.2-µm pore size, low fluorescence) using iBlot 2 Dry Blotting System (ThermoFisher). Immunoblots were blocked in Odyssey® Blocking Buffer in TBS (Li-cor) for 1 hour, before primary antibodies (Table 2.2) in Odyssey® Blocking Buffer in TBS diluted (1:1) in PBS were incubated overnight at 4 ˚C. Immunoblots were rinsed

(3 x 10 minutes each wash) with TBS-Tween 0.1% before appropriate secondary fluorophore-conjugated antibodies (LI-COR) (Table 2.2) in Odyssey® Blocking Buffer in TBS diluted (1:1) in PBS were applied. GADPH was used as the loading control. Immunoreactivity was detected using Odyssey® Fc (LI-COR) using the principle of near-infrared fluorescence at wavelengths of 700nm or 800 nm. Dosimetry of bands were measured using Image Studio Lite software.

Table 2.2. List of antibodies used with corresponding sources

Target	Host	Dilution	Source	Secondary Antibody
GCN2	Rabbit mAb anti-GCN2 #3302	1:250	Cell Signalling Technology	IRDye® 680RD Goat anti-Rabbit IgG #925-68073
PKR	Rabbit pAb anti-PKR #18244-1-AP	1:1000	Proteintech	IRDye® 680RD Goat anti-Rabbit IgG #925-68073
GAPDH	Mouse mAb anti-GAPDH #D4C6R	1:1000	Cell Signalling Technology	IRDye® 800CW Goat anti-Mouse IgG #926-32210

2.8 Caspase 3/7 assay

The Caspase-Glo 3/7 assay (Promega) was used to assess apoptosis-specific caspase 3 and 7 activity in hPAECs-deficient in GCN2 and/or PKR, with and without,

24-hour stimulation of poly(I:C). The assay was conducted according to manufacturer instructions. Caspases 3 and 7 are cysteine proteases which are downstream effector caspases, rather than initiator caspases, in a type of programmed cell death called apoptosis. Therefore, this assay uses caspase 3/7 as a surrogate biomarker for apoptosis activity. Using triplicates of 5 x 10^3 PAECs per 0.32cm^2 well, equal amounts of caspase 3/7 reagent was added to cell supernatant to provide a luminogenic caspase 3/7 substrate that contains a tetrapeptide DEVD sequence. Subsequently, hPAECs were lysed to facilitate caspase 3/7 cleavage of pro-luciferin DEVD substrate. The thermostable luciferase has now a readily available substrate, devoid of DEVD, and in the presence of ATP can produce light. The luminescent production is directly proportional to caspase 3/7 activity. To eliminate technical variability, all reagents were adequately thawed to room temperature and substrate was added for 1 hour, and peak luminescent signal was recorded. The 96 well-plate was read using luminometer plate reader.

2.9 Cell viability assay

CellTitre-Glo luminescent cell viability assay was purchased from Promega to determine the number of viable cells, via quantification of ATP, in hPAECs- deficient in GCN2 and/or PKR, with and without, 24-hour stimulation of poly(I:C) and this was conducted according to manufacturer instructions. The assay uses a reagent containing luciferin and a thermostable luciferase dependent on the presence of ATP. Using triplicates of 5 x 10^3 PAECs per 0.32cm^2 well, equal amounts of CellTiter-Glo reagent were added to cell supernatant to mediate cell lysis whilst importantly inhibiting endogenous ATPases released during cell lysis. The stable LucPpe2-derived luciferase catalyses the mono-oxygenation of luciferin in the presence of ATP to

produce light. Cells were incubated for 10 minutes to produce a stable signal. Care was taken during this assay to ensure a consistent temperature of reagents, seeding of $5x10^3$ per $0.32cm^2$ for samples, and seeding of 625- $2x10^4$ cells to generate 7-point standard curve was conducted as consistently and accurately as possible. The 96 well-plate was read using a luminometer plate reader, and sample luminescent recordings were interpolated from a standard curve to generate absolute numbers of viable metabolically active cells, where the luminescent output was proportional to cell number.

2.10 RNA-sequencing

2.10.1 Principles and wet lab methodology

Human PAECs that were treated with siRNA targeting non-homologous control gene and *EIF2AK4* (encoding GCN2 protein), with and without stimulated poly(I:C) stimulation (Invivogen; 25µg/ml) for 4 hours, were subjected to RNA harvest via Trizol. RNA was purified via Direct-zol RNA Miniprep (Zymo Research) as described in section 2.5. RNA lysates were sent on dry ice for poly(A) selected messenger (m)RNA sequencing at external company Novogene (Cambridge). The workflow consisted of sample preparation with quality assurance, RNA library preparation, sequencing of mRNA on platform Illumina NovaSeq 6000 sequencing system before fastq files were sent for in-house bioinformatics analysis. Bioinformatic analysis was kindly completed by Dr Roger Thompson.

In more detail, Illumina technologies required high quality RNA as evaluated by RNA integrity number (≥ 4.0 out of 10 using Agilent 2100 technology) and RNA purity (A260/280 value of 1.8-2.2 and A260/230 $\geq$ 1.8 using NanoDrop technology). To

measure differential gene expression, messenger RNA was exclusively sequenced. To do this, a mRNA library was prepared by enriching for poly(A) selection via poly(T) oligo attached magnetic beads before mRNA was fragmented using divalent cations under elevated temperature. RNA was converted into complementary DNA (cDNA) via first and second strand cDNA synthesis and 3' ends of cDNA are adenylated to prevent ligation to each other. In preparation of cDNA hybridisation to flow cell (where sequencing occurs), indexing adapters (oligonucleotides sequences complementary to the flow cell and allows for sample identification) were also attached. To validate and enrich for cDNA consisting of indexing adapters on both ends, PCR was performed, and the library was quantified, and quality checked before normalization and pooling prior to sequencing.

Messenger RNA (mRNA) sequencing was performed using Illumina NovaSeq 6000 Sequencing System at a read length of paired end 150 base pairs. The principles of this technology include sequencing-by-synthesis and reversible dye-terminators that enable the identification of single bases as they are introduced into DNA strands. This occurs by immobilising single stranded cDNA library onto the flow cell via complementary base pair binding to oligonucleotides on the surface of the flow cell. Subsequent cluster regeneration can occur via bridge amplification and hundreds of identical strands form. Simultaneously tens of millions of clusters are sequenced-by-synthesis via the incorporation of four fluorescently labelled deoxynucleotide triphosphates (dNTPs) which corresponds to A, C, T and G bases. The nucleotide fluorescent label serves as a terminator for polymerization, and so, at each dNTP incorporation, the fluorescent dye is excited by a light source to emit a fluorescent signal to identify the base. The fluorescent label is then enzymatically cleaved to allow

incorporation of the next nucleotide, owing to a highly accurate base-by-base sequencing readout. The number of sequencing cycles determines the length of the read. Forward and reverse are paired and mapped to reference genome where all sequence reads are quantified, and sequencing differences are identified in parallel.

2.10.2 RNA sequencing data analysis

The bioinformatic pipeline of 'nf-core/rnaseq' allowed the input of FastQ files and performed quality control, adapter trimming, and genome alignment and read quantification (Patel et al., 2023). Specifically, MultiQC v1.11 aggregated quality control results from several bioinformatic analyses (i.e., Salmon, FastQC and cutadapt) to generate a general statistic table containing mapped aligned (%), mapped aligned (millions), duplicate reads (%), average GC content (%), average sequence length (bp), total sequences (millions) before and after trimming and the total base pairs (trimmed) (Appendix table 2).

Using DESeq2 bioinformatic package in R, principal component analysis (PCA) and heat map of sample-to-sample distances reduced dimensionality of the data to aid with data visualisation. Thereafter DESeq2 bioinformatic package in R measured differential expressed genes in pairwise comparisons and data are presented in ranked tables and volcano plots where adjusted *p* values are reported. The DESeq2 analysis was carried out in R on the date of 30th March 2023.

All differential expressed genes within a pairwise comparison was subjected to over representation analysis using the website: WebGestalt. Enrichment ratios were ranked

and respective false discovery rate (FDR) at a threshold of $p<0.05$ were reported. The FDR method of Benjamin-Hochberg method was used.

In vivo models

2.11 Ethical approval for animal studies

All regulated animal procedures were approved by The University of Sheffield Ethics Committee and performed in accordance with UK legislation under the Animals (Scientific Procedures) Act 1986. Work was carried out under Professor Allan Lawrie's project licence (PPL 70/8910 and PP9603995), Dr Helen Marriott's project licence (P4802B8AC) and my personal licence (PIL 44450).

2.12 Husbandry

Mice were housed in cages of up to 6 individuals in a controlled environment where a 12-hour light/dark cycle at 22 ˚C and a constant air pressure was maintained. Animals were fed standard laboratory chow (Harlan 18% protein rodent diet). Animal care was kindly performed by the University of Sheffield Biological Services Unit staff.

2.13 Experimental design of animal studies

2.13.1 Sample size

An online power calculator was used to inform the sample size for all animal experiments conducted in this thesis. A sample size of at least 3 animals per group was used to provide $\geq$80% power (i.e., type II error) to detect differences in cardiac pressures of 5mmHg with a standard deviation of 2mmHg with a 95% confidence interval (i.e., type I error). Additional animals were used in some experiments to

increase power and/or sensitivity and to obtain sufficient lung tissue for morphometric analysis. Animals were given a unique identifier where they were randomised blindly based on weights to achieve a similar weight distribution across all groups where possible.

2.13.2 Sugen-hypoxic pulmonary hypertension mouse model

As adapted from Ciuclan et al (2011), SU5416 (Semaxinib; Sugen) in combination with normobaric hypoxia (10% oxygen or F_IO2 0.1) was used to generate a pulmonary hypertension model in mouse (SuHx). Initially developed as an anticancer drug, SU5416 is a small molecule selective inhibitor of vascular endothelial growth factor (VEGF) receptors (Ciuclan et al., 2011). SU5416 exacerbates chronic hypoxia induced PH in rodents and mediates complex vascular remodelling and cardiac indices. Potential mechanisms by which SU5416 increases pulmonary vascular remodelling include inducing the synthesis and deposition of extracellular matrix, inducing pulmonary EC death contributing to later EC proliferation and reducing phosphorylated Akt expression implicated in VEGF-dependent endothelial cell survival (Ciuclan et al., 2011). Experimental mice were injected subcutaneously with SU5416 suspended in 0.5% (v/v) carboxymethylcellulose sodium, 0.9% (v/v) sodium chloride, 0.4%(v/v) polysorbate 80, and 0.9% benzyl alcohol (v/v) in deionized water (Sigma) (Vitali et al., 2014). SuHx mice were injected using 25G needle once weekly with SU5416 at 20 mg/kg body weight per dose. Mice were exposed to normobaric hypoxia (10% O_2) inside a ventilated plexiglass chamber in which nitrogen was injected under the control of an Oxycycler controller for 3 weeks. To prevent carbon dioxide retention, CO_2 was removed by soda lime that lined the bottom of the hypoxic chamber.

2.13.3 Prophylactic intraperitoneal poly(I:C) in SuHx mouse model

Adapted from Farkas et al (2019), who used prophylactic poly(I:C) in rat models of PH, poly(I:C)-LMW (Invivogen) was diluted in sterile saline to provide bi-weekly intraperitoneal injections of 2mg/kg or 10mg/kg in C57BL/6J mice (Jackson Laboratories) that were subjected to SuHx (figure 2.4). This was accompanied by saline control.

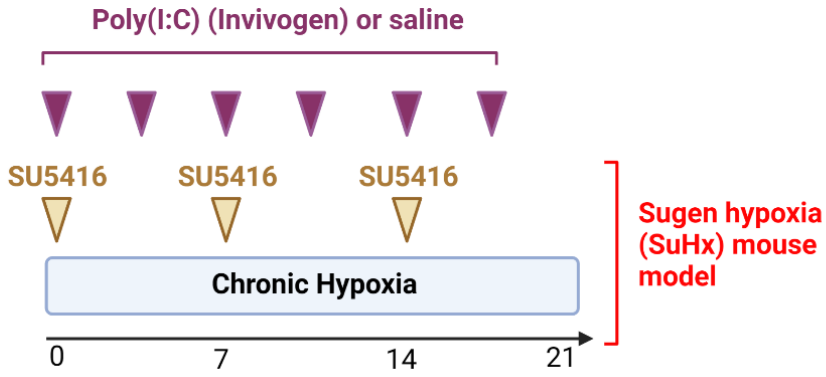

Figure 2.4. Experimental design for bi-weekly prophylactic intraperitoneal injections of poly(I:C) or saline vehicle in SuHx C57BL/6J mice.

Poly(I:C) purchased from Invivogen was diluted in saline and administered bi-weekly at dose of 2.5mg/kg or 10mg/kg. Original image created in Biorender.com.

In the attempt to further optimise poly(I:C) dosing schedules in SuHx mice, poly(I:C)-LMW (Tocris Biosciences) was diluted in sterile saline to provide thrice-weekly intraperitoneal doses of 10mg/kg in C57BL/6J mice (Jackson Laboratories) (figure 2.5). This was accompanied by saline control.

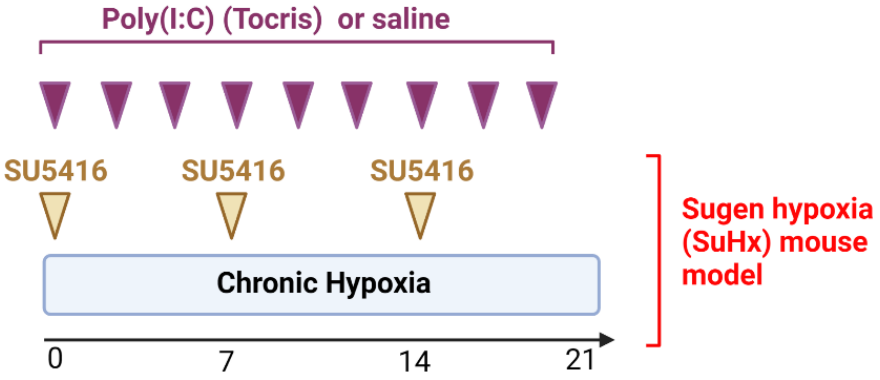

Figure 2.5. Experimental design for thrice-weekly prophylactic intraperitoneal injections of poly(I:C) or saline vehicle in SuHx C57BL/6J mice.

Poly(I:C) purchased from Tocris Biosciences was diluted in saline and administered thrice weekly at 10mg/kg. Original image created in Biorender.com.

At the end of the above studies, all mice were anesthetized and underwent non-recovery surgery to yield haemodynamic data via cardiac catheterisation before tissues were taken for histology.

2.13.4. Intranasal installation of poly(I:C)

To non-invasively deliver poly(I:C) to the upper and lower respiratory tract of C57BL/6J, GCN2 -/- and control mice, the well-established technique of intranasal instillation was used (figure 2.6, 2.7 and 2.8). Mice were anesthetized under 1.5–2.0% isoflurane delivered in 100% oxygen with a flow of 2.0 L/min before the animal was held by the scruff to enable the pipetting of 100µg of poly(I:C) (Invivogen) in 50µl of sterile saline in one (figure 2.6 and 2.8) or two (figure 2.7) dosing regimens. Poly(I:C) was delivered drop-by-drop at the nostrils at the time of inhalation. Some mice were sacrificed to yield lung tissues for assessment of immunological and cellular responses at different time points whilst others were exposed to SuHx or Hx alone (figure 2.6 and 2.7). The length time between intranasal poly(I:C) and SuHx or Hx induction is shown

in figure 2.6, 2.7 and 2.8. The PH phenotype was assessed by cardiac catheterisation, lung histology and right ventricular hypertrophy at 21 days after initial PH induction.

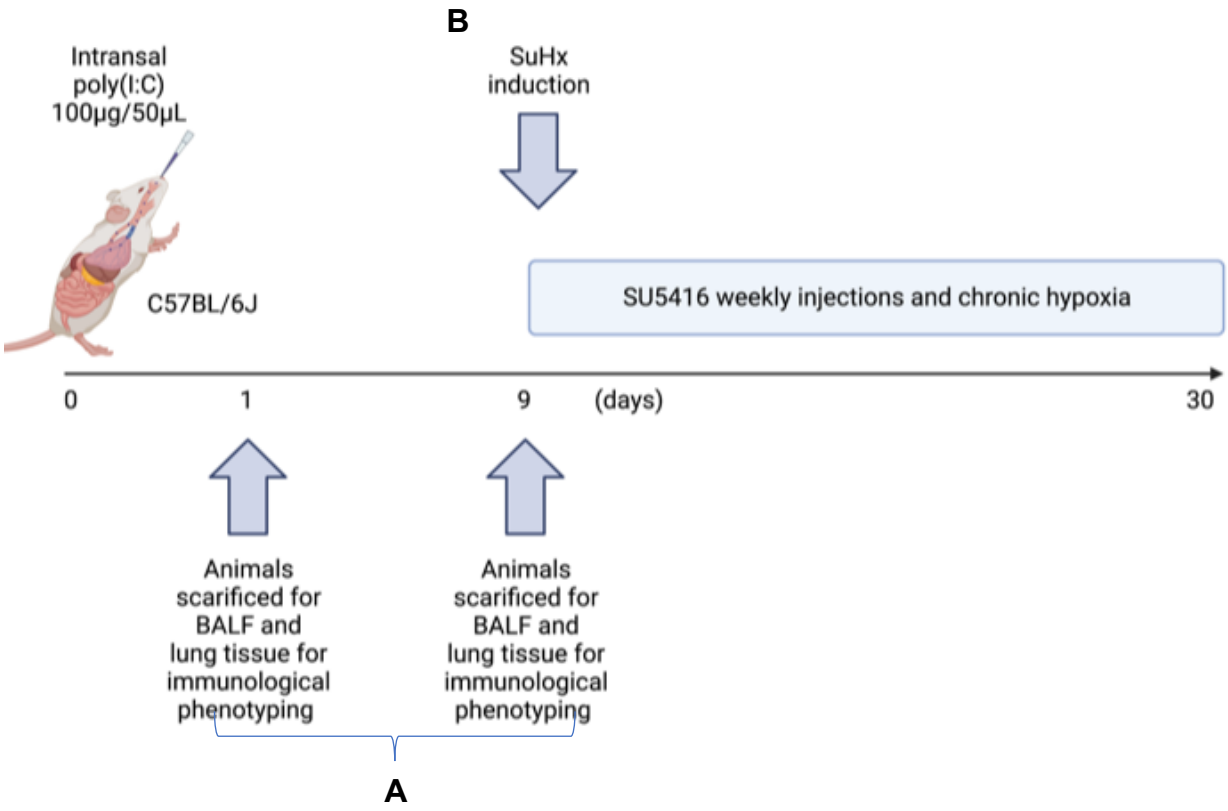

Figure 2.6. Experimental design of a single exposure of intranasal instillation of poly(I:C) (100µg/50µl) prior to SuHx induction model.

A). C57BL/6J mice immunological responses were assessed at 24 hours and 9 days post 100µg of poly(I:C) (Invivogen) in 50µl of sterile saline intranasal instillation via bronchoalveolar lavage fluid total cell counts, cytospin differential cell counts and supernatant cytokine analysis (CBA) and lung tissue analysis (details below).

B) Other C57BL/6J mice were exposed to intranasal instillation of poly(I:C) (Invivogen) at day 0 before sugen-hypoxia was induced on day 9. The PH phenotype was assessed by cardiac catheterisation, lung histology and right ventricular hypertrophy on day 30.

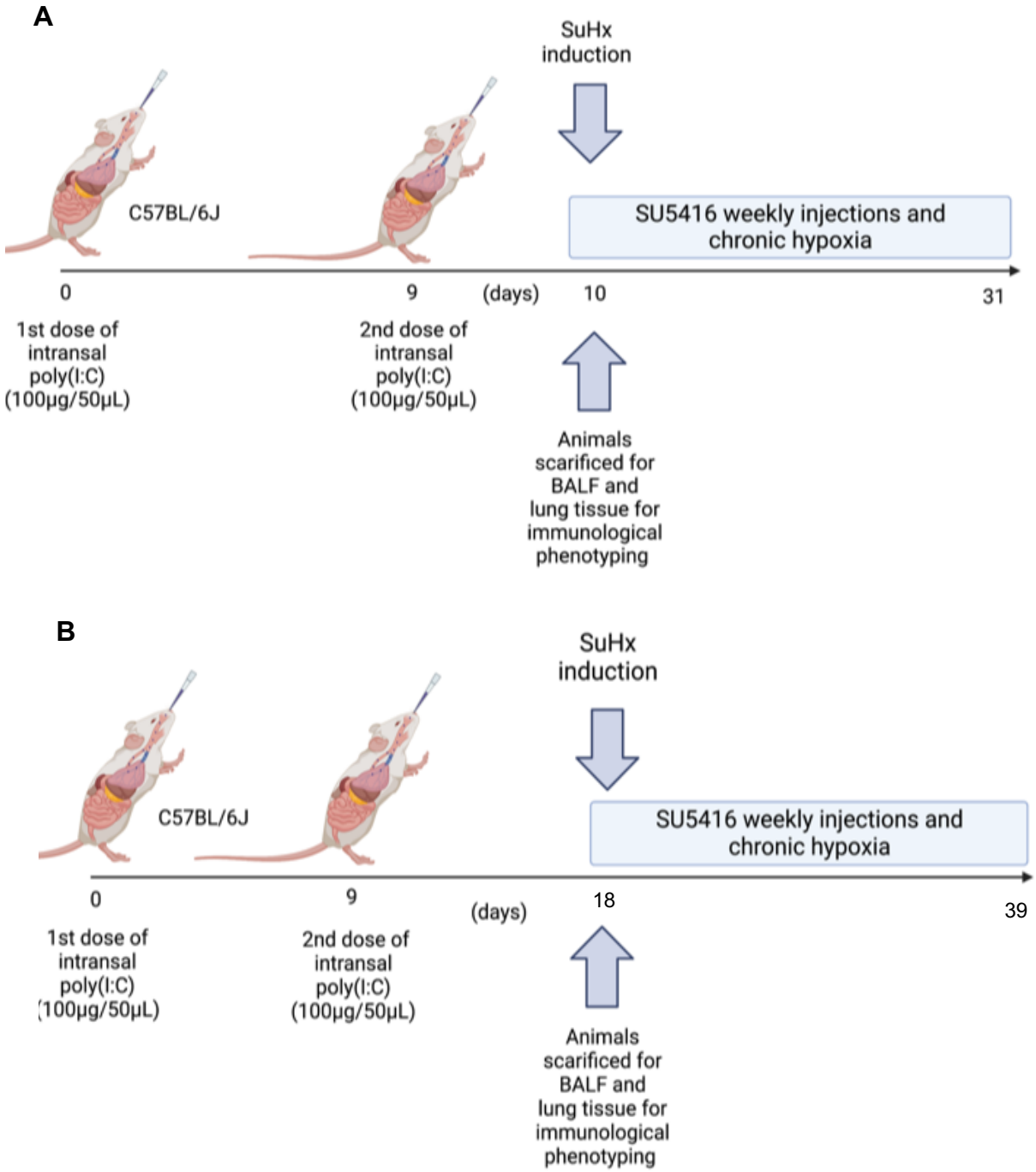

Figure 2.7 Experimental design of repeated exposure of intranasal instillation of poly(I:C) 100µg/50µl at 24 hours (a) – and 9 days (b) - prior to SuHx induction model.

A). C57BL/6J mice were instilled with 2 doses of intranasal poly(I:C) 100µg/50µl on day 0 and 9 before SuHx induction on day 10 (i.e., 24 hours after the 2nd poly(I:C) instillation). The PH phenotype was assessed by cardiac catheterisation, lung histology and right ventricular hypertrophy on day 31.

B) C57BL/6J mice were instilled with 2 doses of intranasal poly(I:C) 100µg/50µl on day 0 and 9 before SuHx induction on day 18 (i.e., 9 days after the 2nd poly(I:C) instillation). The PH phenotype was assessed by cardiac catheterisation, lung histology and right ventricular hypertrophy on day 39.

2.13.5. GCN2 knockout mouse in SuHx with prior intranasal exposure to poly(I:C)

GCN2 homozygous knockout (B6.129S6-*Eif2ak4*$^{tm1.2Dron}$/J; GCN2 -/-) mice were kindly donated by Dr Elaine Soon, University of Cambridge. GCN2-/- mice and their littermate controls were instilled with one dose of intranasal poly(I:C) (100μg/50 μl) on day 0 and on day 9 SuHx was induced, and thereafter, exposed to a 3-week duration of SuHx (figure 2.8). Endpoint measurements of cardiac catheterisation and lung tissue for vascular morphometry were taken.

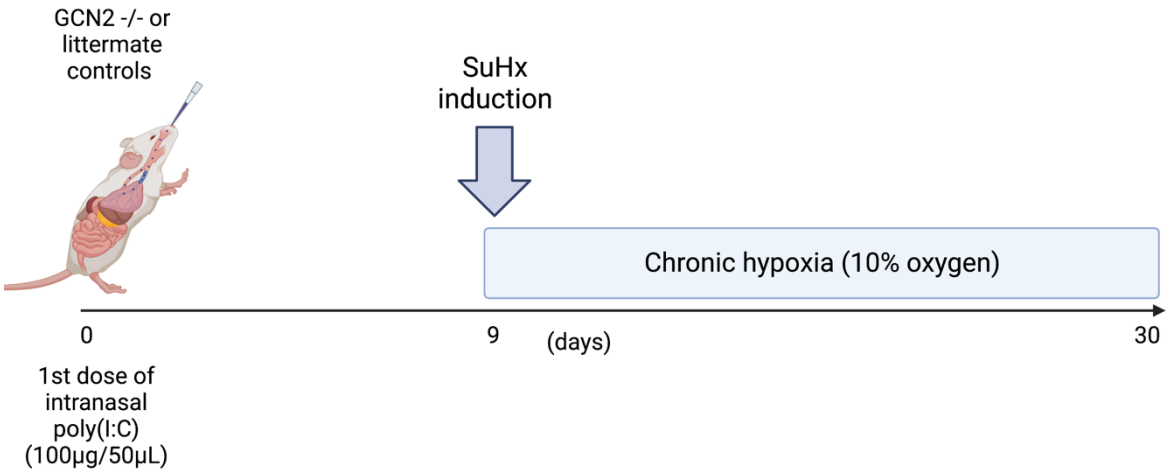

Figure 2.8. Experimental design of a single exposure of intranasal instillation of poly(I:C) (100μg/50μl) prior to SuHx induction model in GCN2 -/- and littermate control mice.

GCN2 -/- mice and littermate control mice were exposed to intranasal instillation of poly(I:C) (Invivogen) at day 0 before sugen-hypoxia was induced on day 9. The PH phenotype was assessed by cardiac catheterisation, lung histology and right ventricular hypertrophy on day 30.

2.14 Bronchoalveolar lavage fluid (BALF) collection from mice

To measure markers of inflammation in the lower and upper respiratory tract after intranasal poly(I:C) or saline (control) instillation, mice were subjected to bronchoalveolar lavage. Mice were killed by an overdose of intraperitoneal sodium pentobarbitone (ThermoFisher) and killing was confirmed by exsanguination via cardiac puncture. Bronchoalveolar lavage fluid (BALF) collection was kindly performed by Mr Carl Wright by inserting a catheter in the trachea of mouse to facilitate installation of ice-cold saline (3 x 1ml) into the bronchioles. The instilled fluid was gently retracted to maximise BALF retrieval and to minimise shearing forces. BALF collection was centrifuged at 300xg for 5 minutes at 4˚C. Cell supernatant was removed and frozen for subsequent cytokine measurements by cytokine bead array (see section 2.15). RMPI media (ThermoFisher) containing 10% (v/v) FBS (Gibco^{TM}, ThermoFisher) was used to re-suspend bronchoalveolar cells. A total cell count was determined by haemocytometer and differential cell counts were calculated from fractions of leukocyte populations identified by morphology on cytospins stained with Diff-Quik (Merck) (figure 2.9).

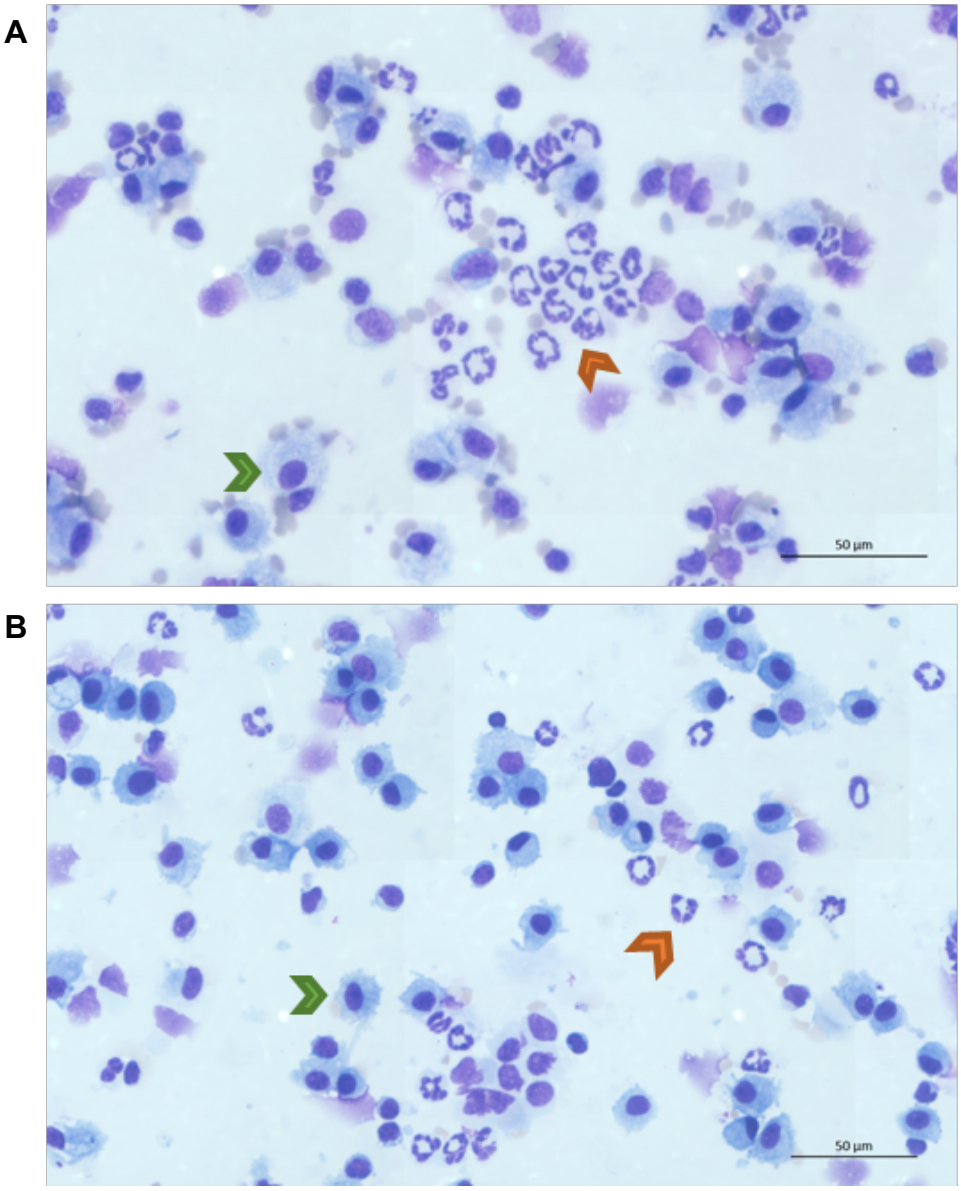

Figure 2.9. Representative images of bronchoalveolar cells stained with Diff-Quik on cytospin preparations 24 hours post – one dose (a) or two doses (b) of intranasal instillation poly(I:C) (100µg/50µl) from C57BL/6J mice.

Orange arrowhead indicates a neutrophil. Green arrowhead indicates a macrophage. Cytospin slides were visualized and scanned using x64 magnification using a Zeiss multi-slide scanning microscope.

2.15 Cytokine bead array (CBA)

To simultaneously measure multiple cytokines in BALF supernatant that were harvested from C57BL/6J mice previously instilled with intranasal poly(I:C) or saline, a flow cytometry approach was taken. Specifically, a cytokine bead array (CBA) (BD Biosciences) was used to assess concentrations of IL-6, TNFα and KC. The CBA was kindly conducted by Mrs Sue Clark in the Core Flow Cytometry Facility at the University of Sheffield. The Cytek Aurora flow cytometry machine with 488nm laser was used to measure cytokines indirectly by sandwiching the cytokine of interest between a bead with unique fluorescent intensity that corresponds to the protein of interest and a detector antibody which is complementary to your protein of interest. The detector antibody and fluorescent bead bound to the cytokine is passed through a laser (480nm) and the amount of fluorescence is directly proportional to the amount of protein present in the sample.

2.16 Macrophage and neutrophil staining in mouse lung

The left lungs of intranasal poly(I:C) or saline instilled mice were resected and perfused with PBS before being processed for formalin fixation, paraffin embedding and cutting (further details in section 2.18). Lung slides were dehydrated with decreasing alcohols, and endogenous peroxidases were blocked with hydrogen peroxidase prior to immunostaining. Lung slides were immunostained for Ly6G, a protein that is exclusively expressed on neutrophils. The primary antibody used was a rat monoclonal anti-mouse Ly6G (1:150 in PBS; NBP2-00441; Biotechne Limited). The secondary antibody of anti-rat IgG was raised in goat and goat serum was used to block background signal. Secondary antibody reagents were used as part of

ImmPRESS® horse radish peroxidase kit (Vector Laboratories). Lung slides were also immunostained for iNOS, a biomarker for macrophages with a M1 phenotype. The primary antibody used was a rabbit polyclonal anti-mouse iNOS (1:100 in PBS; ab15323; abcam) in combination with a secondary horse anti-rabbit IgG conjugated to horseradish peroxidase (Vector Laboratories). A goat polyclonal anti-mouse MMR/CD206 primary antibody (1:100 in PBS; AF2535; Biotechne Limited) was used to immunostain for macrophages with a M2 phenotype. Secondary antibody reagents were used as part of ImmPRESS® horse radish peroxidase kit for horse anti-goat IgG Vector Laboratories) in combination with horse serum to block background signal. DAB (3,3′-Diaminobenzidine) substrate kit (Abcam) was used as per manufacturer's instruction was used as the substrate to horseradish peroxidase before slide mounting with DPX mountant and imaging of slide using Zeiss multi-slide scanning microscope.

2.17 Pulmonary hypertension phenotyping

To assess for the pulmonary hypertension phenotype in all animal models discussed above, cardiac catheterisation, pulmonary vascular morphometry and right ventricular hypertrophy were performed. All are discussed in further detail below.

2.17.1 Cardiac catheterisation

Cardiac catheterisation was used to continuously measure pressures and volume in the heart chambers of mouse models of PH to assess ventricular haemodynamics. Clinically, haemodynamic parameters are measurements that provide definitive diagnosis and indication of prognosis in PAH patients. Cardiac catheterisation is the gold standard method for PH diagnosis.

As adapted from Ma et al (2016), right ventricular haemodynamic measurements were collected by advancing a 1F research mouse pressure volume catheter (PVR-1030) (Millar Instruments) into the RV via isolation and venotomy of the external right jugular vein during a closed chest surgical procedure. Left ventricular and aortic measurements haemodynamic measurements were collected by advancing a 1F research mouse pressure volume catheter (PVR-1045) (Millar Instruments) into the LV via isolation and arteriotomy of the carotid artery during a closed chest surgical procedure in mouse. The catheters were previously calibrated using blood resistivity (cuvette) calibration method. Both catheters consist of a single pressure sensor and four ring electrodes along its length. High-frequency low-amplitude constant current is passed through the outer pair of electrodes, to excite the ventricular space, whilst the inner pair of electrodes measures a time-varying conductance between the two during a cardiac cycle (Pacher et al., 2008). Under the principles of ohm's equation, conductance is inversely proportional to the amount of conductive material at that site (Pacher et al., 2008). For example, during systole, blood volume is reduced and the conductance increases. Using the Baan's equation, the ventricular volume can be obtained from the known values of measured and parallel conductance, blood resistance and the distance between electrodes. All haemodynamic parameters were recorded in spontaneously breathing experimental mice under 1.5–2.0% isoflurane anaesthesia delivered in 100% oxygen with a flow of 2.0 L/min. Pressure-volume loop recordings were acquired by MPVS Ultra® Pressure-Volume Loop System in combination with LabChart 7 software (ADinstruments). Analysis of pressure-volume loops (discussed below) were carried out in LabChart 7 (ADinstruments). Cardiac catheterisation was completed by me and with the kind help of Dr Laura West.

2.17.2 Pressure-volume loops of cardiac cycle

LabChart 7 software plots pressure (mmHg) on Y axis and volume (RVU) on the x axis (figure 2.10) when conducting cardiac catheterisation. Pressure-volume loops are utilised to assess haemodynamic and contractility parameters (table 2.3 and 2.4). Haemodynamic parameters refer to the flow of blood and contractility parameters refer to the ability of the myocardium to contract. The end-systolic pressure-volume relationship (ESPVR) is an important measure when assessing contractility (or inotropy). ESPVR indicates the maximal pressure that can be developed by the ventricle at any given volume (figure 2.12). Therefore, shallower slopes of ESPVR indicate lesser cardiac inotropy and steeper slopes indicate greater inotropy. ESPVR has been shown to correlate with dP/dt_{max} which is the maximal rate of rise in ventricular pressure (Morimont et al., 2012).

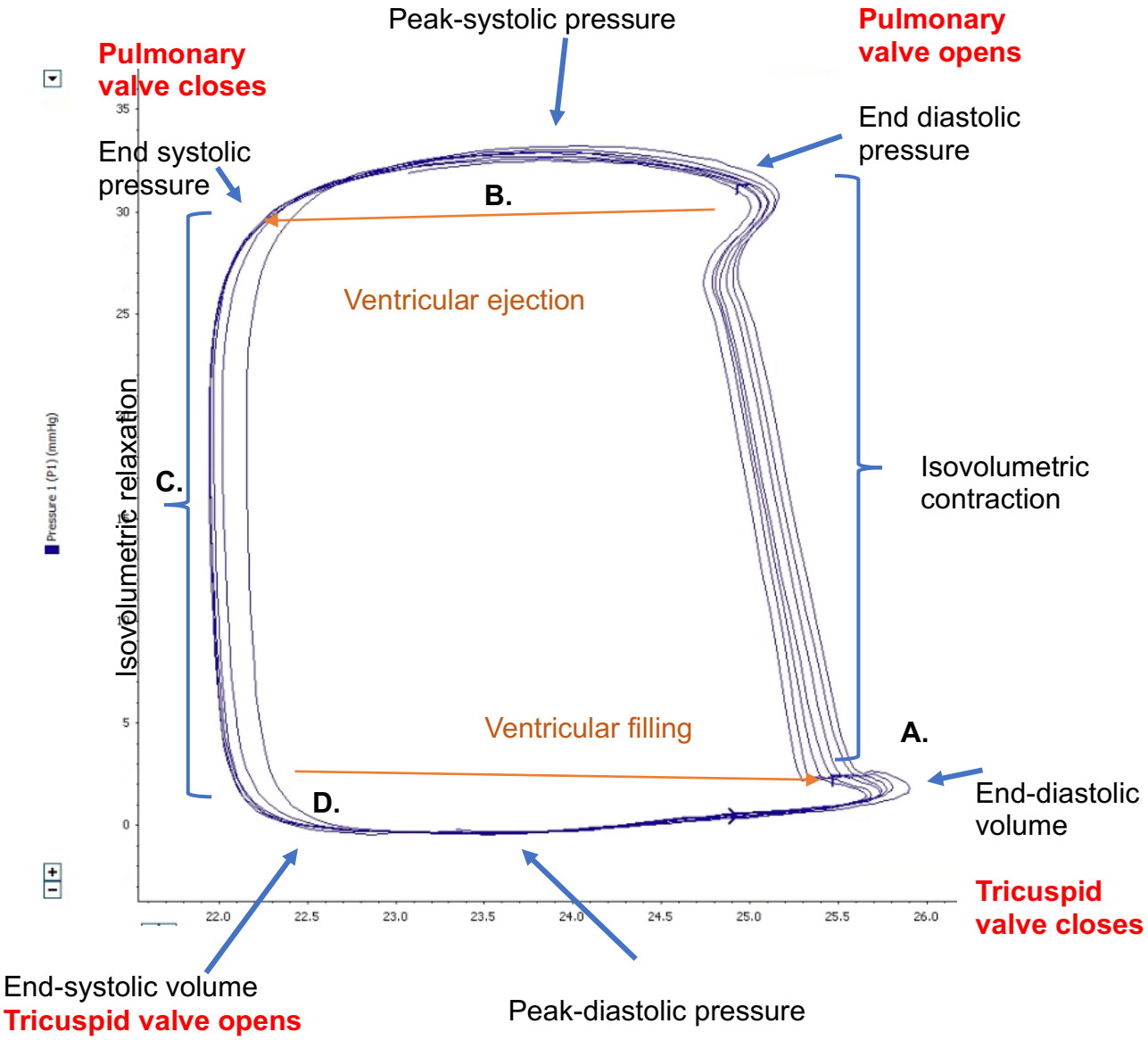

Figure 2.10. Pressure-volume loops of seven cardiac cycles taken between two inspirations recorded in a spontaneous breathing C57BL/6J SuHx model under 1.5–2.0% isoflurane anaesthesia.

Y axis represents cardiac pressures (mmHg), and x axis represents cardiac volume (RVU). A) The right ventricle begins to contract; the tricuspid valve closes and the right ventricular pressure increases. B) At the point in which the right ventricular pressure exceeds the pulmonary artery, the pulmonary valve opens, and blood ejection begins. During this ejection phase, ventricular pressure continues to rise (peak systolic pressure) before pressure begins so fall and pulmonary valve closes to inhibit backflow into the right-side of the heart. C) The ventricle relaxes isovolumetrically and all valves close. D). When the right ventricular pressure falls below the right atrium pressure, the tricuspid valve opens, and ventricular filling occurs. This cycle is continually repeated. Alterations in the pressure-volume relationship indicate cardiac contractility and compliance/stiffness differences.

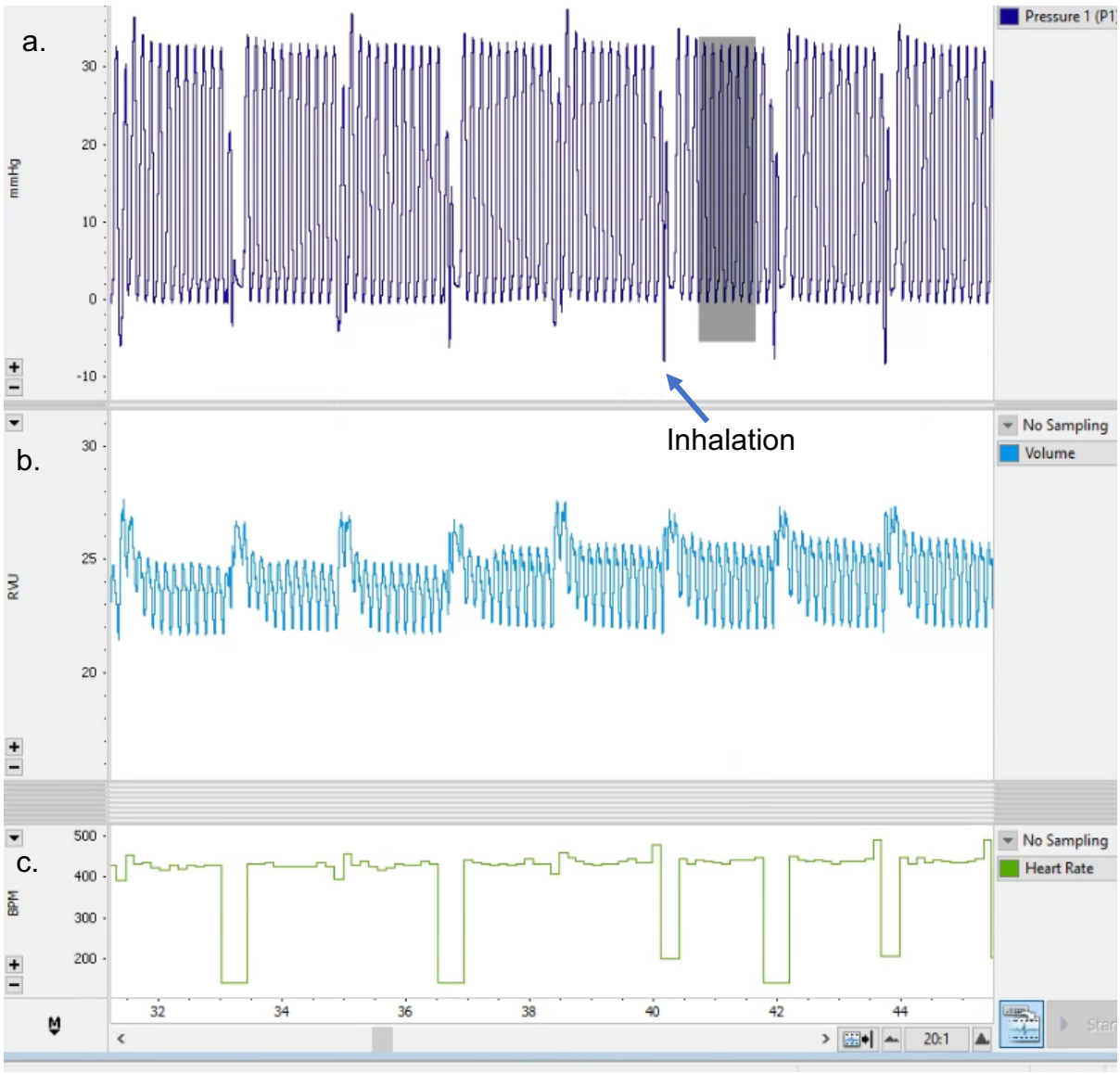

Figure 2.11. An example of pressure-volume loop analysis: right ventricular pressure (mmHg) (A), volume (RVU) (B) and heart rate (bpm) (C) channels in Labchart 7 which correspond to above pressure-volume loop figure (i.e., figure 2.10).

Seven cardiac cycles have been highlighted in channel 1, all of which were analsysed in Labchart 7 and the average of all loops were taken forward in my analysis. Of note, loop data analysis did not include the point of mouse inhalation due to the associated artificially changes in pressure and volume. Pressure-volume loops were exclusively analysed from animals with heart rates of >400 beat per minute to minimise effects of anaesthesia on cardiac function.

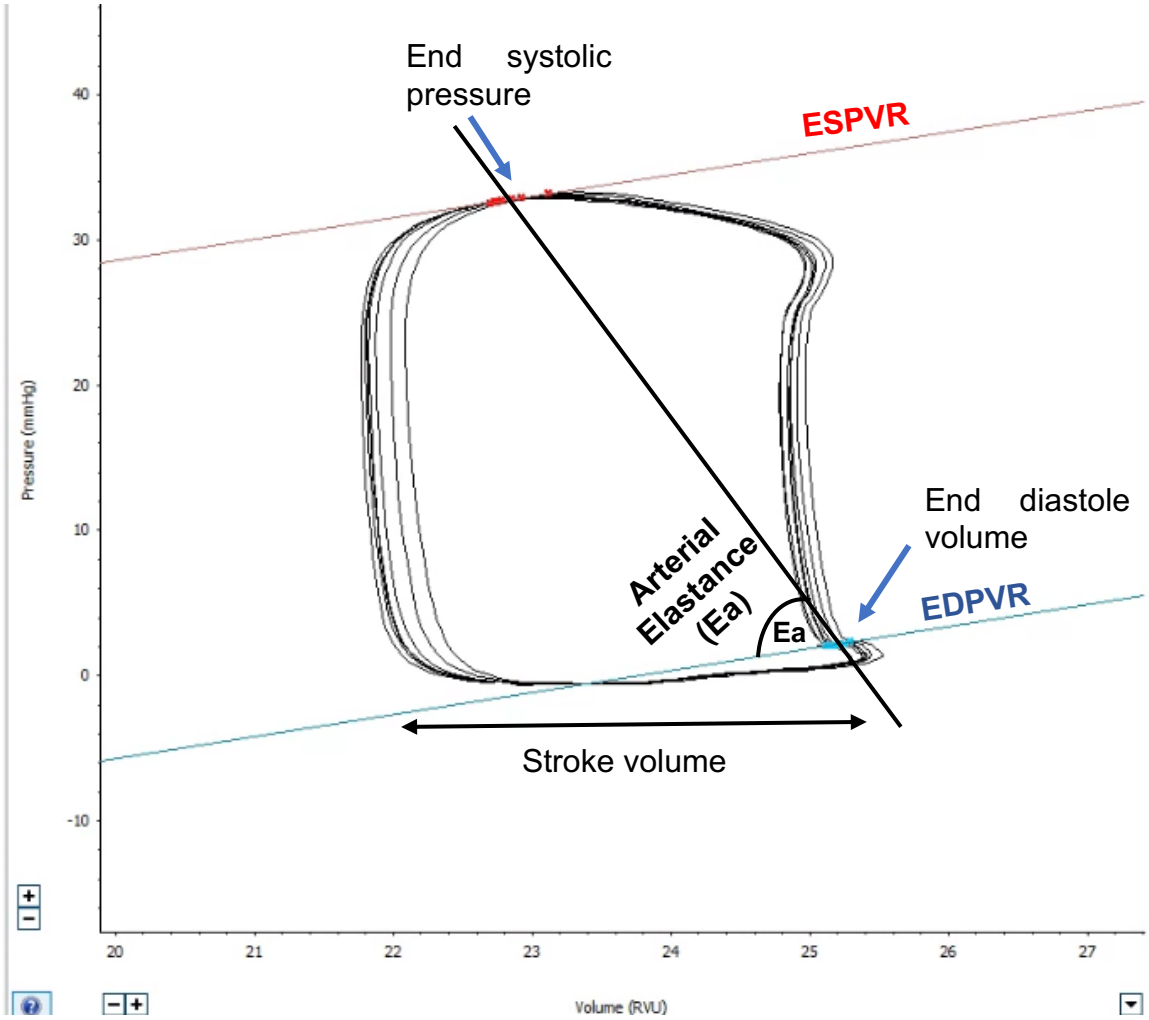

Figure 2.12. Loop view in Lab chart 7 corresponding to above analysis of right ventricular pressure-volume loop.

Each loop has its own unique end-systolic pressure (red dots) and end-diastolic volume points (blue dots). These individual points are used to establish the end-systolic pressure-volume relationship (ESPVR; red line) which is important when assessing load-independent measures of cardiac contractility. The slope of the ESPVR represents the endo-systolic elastance (Ees). The end-diastolic pressure-volume relationship (EDPVR; blue line) is important when referring to ventricular compliance/stiffness. For accurate ESPVR and EDPVR measurements, temporary blood flow cessation via inferior vena cava occlusion (IVC) must be performed. However, a laparotomy is required for a vena cava occlusion (IVC) and at the time of experiments I was not efficient in performing cardiac catheterisation and laparotomy simultaneously. Instead, I reported dP/dt_{max} which is a load dependent measure of contractility. In a model of PAH, it is expected that the contractile measurement of dP/dt_{max} increase and stroke volume decrease.

Table 2.3. Definitions and units given to haemodynamic parameters measured by right cardiac catheterisation and recorded in all *in vivo* experiments.

Haemodynamic parameter	Units	Definition
Right ventricular end-systolic pressure (RVESP)	mmHg	Pressure at the completion of right ventricular contraction when pulmonary valve closes; surrogate for pulmonary artery pressure
RV dP/dt_{max}	mmHg/sec	Maximal rate of rise of ventricular pressure per contraction
ePVR *	mmHg/RVU/min	Resistance against blood flow from the pulmonary artery to the left atrium
ePVRi †	mmHg/RVU/min/g	Resistance against blood flow from the pulmonary artery to the left atrium normalized to animal weight

*This was calculated using measurements from RV and LV cardiac catheterisation using the equation: estimated mean pulmonary artery pressure (emPAP) (mmHg)– LVEDP (mmHg))/LV cardiac output (RVU) (Arnold et al., 2019). emPAP was derived using the following equation: (RVESP x 0.61) + 2 mmHg (Chemla et al., 2004). Cardiac output was derived from LV stroke volume (RVU) x heart rate (bpm). †In the case of ePVRi, the following equation was used: estimated mean pulmonary artery pressure (emPAP) (mmHg) – LVEDP (mmHg))/LV cardiac index (RVU/g) (Arnold et al., 2019). LV cardiac index is calculated by: (LV stroke volume x heart rate)/weight (g).

Table 2.4. Definitions and units given to haemodynamic parameters measured by left cardiac catheterisation and recorded in all *in vivo* experiments.

Haemodynamic parameter	Units	Definition
Left ventricular end-diastolic pressure (LVEDP)*	mmHg	Pressure at the end of left ventricular relaxation; surrogate for left atrial pressure
LV dP/dt_{max}	mmHg/sec	Maximal rate of rise of ventricular pressure per contraction
Left ventricular end-diastolic volume (LVEDV)	RVU	Volume at the end of left ventricular relaxation
LV stroke volume	RVU	Difference between the left end-diastolic and end-systolic volumes
LV cardiac output (CO)	RVU/min	Amount of blood pumped out of the left ventricle within one minute
Aortic (Ao) blood pressure	mmHg	Mean pressure within the aortic root

*In PAH patient definitive diagnosis via right heart catheterisation, pulmonary capillary wedge pressure is used to estimate LVEDP.

2.18 Immunohistochemistry to assess pulmonary vascular remodelling

2.18.1 Lung, heart, and blood tissue harvest

After haemodynamic and contractility measurements were taken, animals were sacrificed by cardiac puncture and death confirmed by cervical dislocation. Blood taken during cardiac puncture was put into 1.5ml Eppendorf tubes, allowed to clot and centrifuged at 2000 xg at room temperature for 15 minutes. Serum was aliquoted and transferred to -80 ˚C for storage. Lung was removed for pulmonary vascular morphometry and heart for Fulton Index (section 2.19). Lung and heart tissue were

removed *en bloc*. A lateral incision underneath the diaphragm and the frontal rib cage was excised to expose heart and lungs. Via blunt dissection, the muscle and connective tissue surrounding the trachea were removed before the trachea was cut and the descending aorta was removed to allow the heart and lungs to be freely resected. 5ml of PBS in a syringe with a 21G needle attached was inserted into the right ventricle to perfuse the lungs. The right lung was ligated using suture and sections of lung were removed and placed in RNAlater™ stabilization solution (ThermoFisher) for subsequent RNA analysis and other lung sections were placed in a cryovial and frozen in liquid nitrogen for subsequent protein analysis. The remaining right lung was ligated using suture and a catheter was inserted into the trachea to deliver 10% neutral buffered formalin to fix and inflate the left lung. The left lung was placed into 50ml of 10% neutral buffered formalin for at least 24 hours before it was replaced by PBS prior to processing, embedding, cutting, and mounting onto glass microscope slides.

2.18.2 Tissue fixing and processing and cutting

The left lung was decanted from PBS storage and a scalpel blade was used to cut the lung into 4 pieces across the short axis. The lung was dehydrated by increasing alcohol exposure and then processed into paraffin using a Leica TP1020 Semi-enclosed Benchtop Tissue Processor (Leica Microsystems) according to the manufacturer's instructions. Lungs were went embedded into paraffin blocks using moulds and placed on a cold surface to solidify. Blocks containing the lung tissue were cut into section of 5μm thickness via microtomy and then placed onto polysine glass microscope slides. Slides were left to air dry before staining was performed. Some of this work was kindly performed by Ms Fiona Wight, Mr Sam McCaughran and Ms Julie Porter.

2.18.3 Specific immuno- and tinctorial stains

Formalin-fixed paraffin-embedded (FFPE) lung sections were stained with Alcian blue Elastin Van Gieson (ABEVG) to detect elastin fibres. Indirect immunostains for α-smooth muscle actin (α-SMA) (1:150; Dako, M0851; smooth muscle marker) and von Willebrand factor (1:300; Dako, A0082; endothelial cell marker) were also used. ImmPRESS enzyme polymer reagent kit (Vector Laboratories) containing secondary antibody (IgG), complementary to the primary antibody host, and conjugated to horseradish peroxidase were applied in the indirect immunostaining process. DAB (3,3′-Diaminobenzidine) substrate kit (Abcam) was used as per manufacturer's instruction where horseradish peroxidase catalyses the oxidation reaction of DAB and converts DAB into an insoluble brown precipitate that can be visualised easily using microscopy. All tissues were counterstained with haematoxylin before dehydration via increasing concentrations of alcohol and xylene treatments, before DPX mountant was used to fix sections to glass slides. This was kindly performed by Ms Fiona Wight, Mr Sam McCaughran, and Ms Julie Porter.

2.18.4 Pulmonary vascular morphometry and quantification

The degree of remodelling was assessed in small pulmonary arteries and arteriole less than 50 μm in diameter by calculating the ratio of the media to the cross-sectional area of the whole vessel (media/ CSA) in sections stained with α-SMA and by assessing the degree of muscularisation in sections stained with ABEVG. Vessels were classified as muscularised (>50% double elastic lamina per vessel) or non-

muscularised (<50% double elastic lamina per vessel), then expressed as a percentage of muscularised vessels to total pulmonary vessels.

2.19 Right ventricular hypertrophy assessment

Right ventricular hypertrophy was assessed by Fulton's Index (RV/(LV+S)) as a marker of pulmonary hypertension. Atriums were removed and the right ventricle was dissected from the left ventricle and septum and then weighed.

2.20 Statistical analysis

All statistical analysis was performed using GraphPad Prism Version 9.3.1 software. Normality distribution of all data sets were tested by the Shapiro-Wilk test and the appropriate statistical testing was applied thereafter. In the case of comparing the mean or median of two groups, a *t*-test or Mann-Whitney test were used, in parametric and non-parametric tests, respectively. When comparing the mean or median of more than two groups, a one-way ANOVA or Kruskal-Willis test were used, in parametric and non-parametric tests respectively. Two-Way ANOVA was used compare the means of two groups when considering two independent variables within an experiment. Tukey post-hoc multiple comparison testing was performed to compare means after one-way and two-way ANOVA. In the case of handling non-normal data with two independent variables, a Kruskal-Willis test with post hoc Bonferroni testing was used to correct for multiple comparisons. Data are expressed as mean values with standard error of the mean (SEM) for standardisation purposes. Statistical significance was accepted when $p \leq 0.05$, with the exception of differentially expressed genes obtained RNA-sequencing at threshold of $p<0.1$.

3. The investigation of poly(I:C) as a potential prophylactic therapeutic in a Sugen-hypoxia mouse model of pulmonary hypertension

3.1 Introduction

Double stranded (ds)RNA can originate from various sources (i.e., exogenous, endogenous, and synthetic). Exogenous sources, such as dsRNA viruses, are described as pathogen associated molecular patterns (PAMPs) while endogenous sources are described as damage associated molecular patterns (DAMPs) (Janeway & Medzhitov, 2002). A synthetic form of dsRNA is polyinosinic:polycytidylic acid; poly(I:C). Regardless of the derivation of dsRNA, it is sensed by pattern recognition receptors (PRRs) such as Toll-like receptors (TLRs) and retinoic acid-inducible gene-I (RIG-)-like receptors (RLRs). In addition, dsRNA can also be recognised by dsRNA-binding proteins such as adenosine deaminases acting on RNA (ADAR) (Turton et al., 2020). Recognition of dsRNA via PRRs activates signalling cascades that ultimately phosphorylate transcription factors such as NF-κB, IRF3 and AP1 to induce transcription of pro-inflammatory cytokines and type I interferon (Turton et al., 2020). The dsRNA signalling pathway is a key regulatory process of the innate immune system, and the dysregulation of this pathway is often implicated in disease pathogenesis. Specifically, dysregulation of dsRNA signalling has been implicated in pulmonary vascular remodelling due to effects on endothelial cell and smooth muscle cell proliferation and apoptosis, angiogenesis, and cytokine production (Turton et al., 2020).

Some *in vivo* effects of the dsRNA signalling pathway are presented by Farkas et al*,* (2019). They showed that a poly(I:C) receptor, TLR3, was reduced in the endothelium of lung vascular lesions in patients with pulmonary arterial hypertension (PAH) and in experimental pulmonary hypertension (PH) in a Sugen-hypoxia (SuHx) rat model. Furthermore, exaggerated PH was measured in TLR3 -/- mice following SuHx exposure. Farkas *et al* (2019) showed that TLR3 deficiency in pulmonary arterial endothelial cells (PAECs) from PAH patients promoted apoptosis and increased endothelin-1 and IL-6 mRNA expression in rat lung *in vitro.* These data imply that TLR3 has a homeostatic role where signalling via TLR3 prevents PAECs apoptosis. This is particularly important given the notion of early endothelial cell apoptosis as a prerequisite to increased vascular cell proliferation in pulmonary vascular remodelling (Rafikova et al., 2019; Thompson & Lawrie, 2017).

Farkas et al (2019) also showed that prophylactic and therapeutic dosing regimens of intraperitoneal poly(I:C) prevented and reduced pulmonary PH, pulmonary vascular remodelling, and right ventricular failure in the SuHx rat model of pulmonary hypertension. These beneficial effects of the known inflammatory inducer, poly(I:C), in the rat model of PH is surprising given the dogma surrounding the damaging role of inflammation in PAH pathogenesis (Rabinovitch, 2008; Zhong & Yu, 2022). However, Farkas et al (2019) postulates that the induction of TLR3 expression and anti-inflammatory IL-10 explain the protective effects of high-dose prophylactic poly(I:C) treatment in a SuHx rat model of PH. Specifically, Farkas et al (2019) showed increased TLR3 and IL-10 mRNA expression after poly(I:C) treatment in rat lung $CD117^{+}$ endothelial cells and increased IL-10 protein in the lungs of SuHx rats. TLR3's regulation of vascular protection was also studied by the study by Cole *et al* (2012)

and O'Dwyer et al (2013). Specifically, Cole et al (2011) demonstrated that TLR3 deficiency was associated with enhanced elastic lamina damage following carotid artery injury and early onset atherosclerosis in hyperlipidaemic mice. O'Dwyer et al (2013) revealed protective repair pathways mediated by TLR3. They observed that TLR3 knockout mice had increased levels of pro-fibrotic cytokines and collagen deposition than wildtype mice in a bleomycin-induced model of pulmonary fibrosis.

The prophylactic and therapeutic effects of intraperitoneal poly(I:C) (thrice weekly 10mg/kg) treatment were observed in a SuHx rat model of PH, but it remains unclear if this therapeutic benefit and the underpinning mechanisms are conserved in mouse models of PH. Investigating if the therapeutic benefit of intraperitoneal poly(I:C) is conserved in SuHx mice is the essential prerequisite work to prospective experiments which would investigate the mechanism of action of intraperitoneal poly(I:C) in commercially available TLR3 KO mice exposed to a SuHx model of PH, where the TLR3 KO rat is not commercially available. And so, this chapter of my thesis will investigate the therapeutic action of prophylactic intraperitoneal poly(I:C) on PH in a SuHx mouse model. Due to the strong beneficial effects of prophylactic poly(I:C) on haemodynamic parameters and pulmonary vascular remodelling in rats shown in Farkas *et al* (2019), I hypothesised that prophylactic poly(I:C) would effectively reduce the severity of a SuHx mouse model of PH.

I investigated the hypothesis through the following aims:

1. Investigate the potential side effects of intraperitoneal poly(I:C) in a SuHx mouse model of pulmonary hypertension
2. Investigate the cross-species conservation of prophylactic intraperitoneal poly(I:C) in a SuHx mouse model of pulmonary hypertension via cardiac catheterisation and pulmonary vascular morphometry
3. Optimise the dose of prophylactic intraperitoneal poly(I:C) in a SuHx mouse model of pulmonary hypertension

Results

3.2 Significant weight loss in C57BL/6J mice exposed to Sugen-hypoxia and treated with bi-weekly intraperitoneal poly(I:C)

In rodent PH models, treatments given alongside agents that induce PH are considered prophylactic (Callegari et al., 2019). To assess cross-species conservation of the beneficial effects of prophylactic intraperitoneal poly(I:C) (thrice-weekly 10mg/kg) previously observed in rats (Farkas et al., 2019), in combination with optimising the dosage regimen of poly(I:C), I subjected 12-week-old male C57BL/6J mice to three-week SuHx exposure and injected prophylactic bi-weekly doses of intraperitoneal synthetic dsRNA (poly(I:C)) supplied by Invivogen at 2.5mg/kg or 10 mg/kg (figure 3.1.a). Poly(I:C) doses of 2.5mg/kg were previously tolerated in the animal models of cancer, ocular inflammation, and acute lung injury by Pulko et al. (2009), Crowley et al. (2018), Gan et al. (2018), respectively.

First and foremost a potential therapy must be safe and produce minimal adverse effects. Therefore, I investigated the effects of intraperitoneal poly(I:C) (2.5mg/kg and 10mg/kg bi-weekly) in SuHx mice on the specific sickness behaviour measure of weight loss.

The weight of all animals was recorded on day 0 (baseline), prior to induction of SuHx and the first injection part of the bi-weekly poly(I:C) doing regimen. Thereafter, weights were recorded weekly. Throughout this 21-day experiment, SuHx exposure alone had no significant effect on mean weight when compared to baseline weight (figure 3.1.b). On day 7, 2.5mg/kg and 10mg/kg doses of poly(I:C) in SuHx mice significantly reduced

mean weight by 3.2 % and 5.7%, respectively, when compared to baseline weight (figure 3.1.b-c). The weight of SuHx mice injected with 2.5mg/kg or 10mg/kg poly(I:C) had improved by day 14 and no significant differences in mean weight were measured when compared to respective baseline weights (figure 3.1.b). On day 21, before PH endpoint assessment, weights of SuHx mice injected with bi-weekly 10mg/kg poly(I:C) were significantly reduced by 6.2% compared to baseline (figure 3.1.b). In comparison, SuHx mice injected with saline or bi-weekly 2.5mg/kg poly(I:C) weights were not significantly different compared to their respective baseline mean weight on day 21 of the experiment (figure 3.1.b-c).

During daily welfare checks, animals did not display any other features of sickness behaviour such as under conditioning, reduced breathing rate, presence of grimace or piloerection or reduction in natural or provoked behaviour.

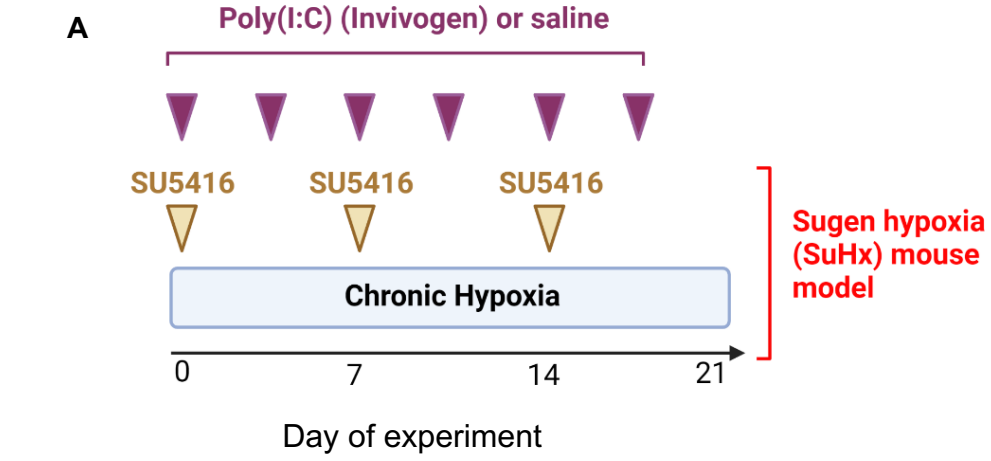
A
Poly(I:C) (Invivogen) or saline
SU5416
SU5416
SU5416
Sugen hypoxia (SuHx) mouse model
Chronic Hypoxia
0
7
14
21
Day of experiment

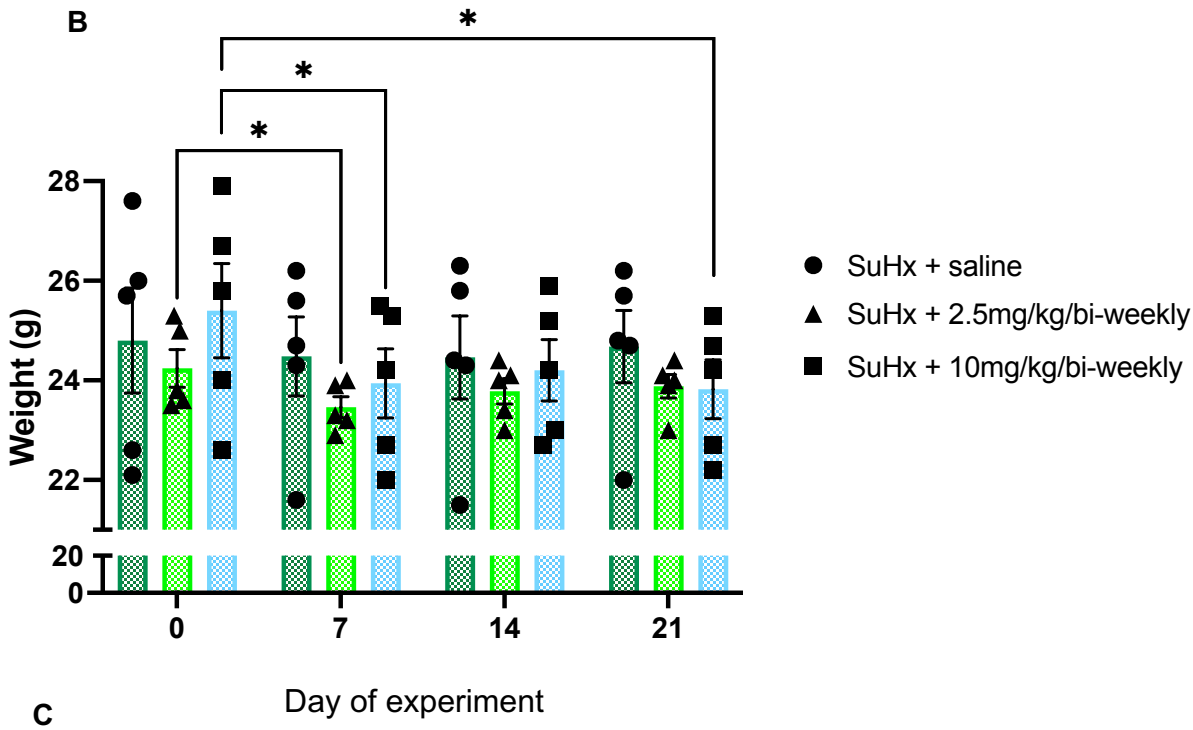
B
*
*
*
Weight (g)
28
26
24
22
20
0
0
7
14
21
Day of experiment
SuHx + saline
SuHx + 2.5mg/kg/bi-weekly
SuHx + 10mg/kg/bi-weekly

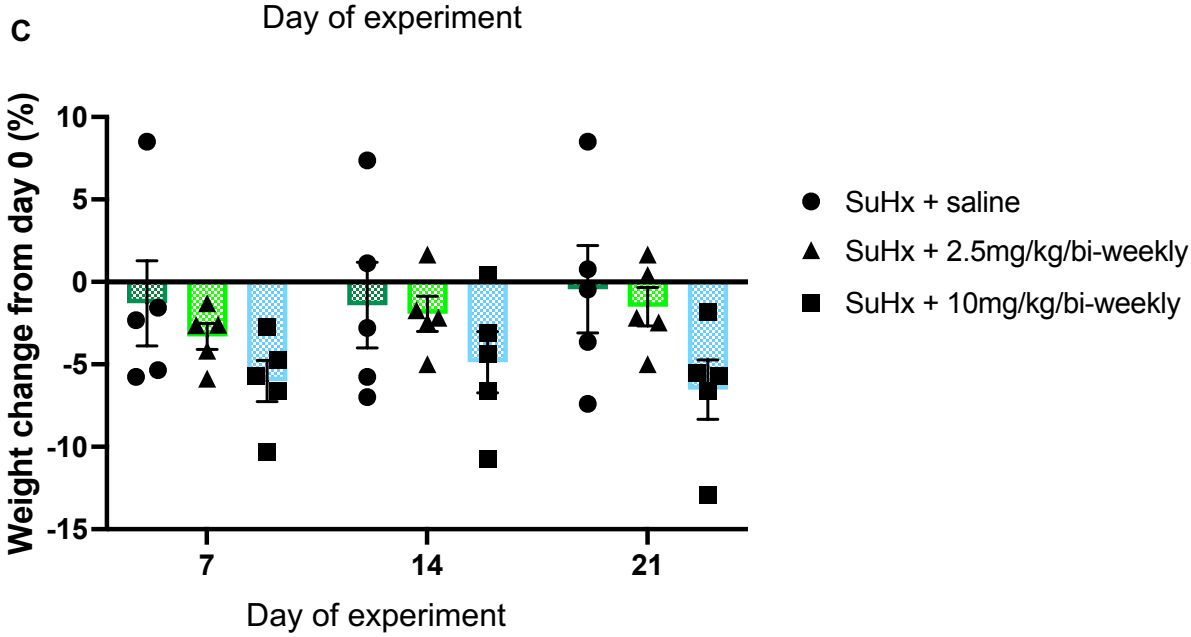
C
Weight change from day 0 (%)
10
5
0
-5
-10
-15
7
14
21
Day of experiment
SuHx + saline
SuHx + 2.5mg/kg/bi-weekly
SuHx + 10mg/kg/bi-weekly

Figure 3.1. Weight loss in C57BL/6J mice treated with bi-weekly intraperitoneal poly(I:C) (Invivogen) and exposed to Sugen-hypoxia.

Bi-weekly intraperitoneal poly(I:C) (supplied by Invivogen) (2.5mg/kg or 10mg/kg) or saline control injections were given during a three-week SuHx exposure in male C57BL/6J mice aged 12 weeks at the point of SuHx induction. Experimental design was created in Biorender.com (A). Weights of animals were recorded weekly, and graphs present absolute weight (g) (B) and percentage weight change (delta) from day 0 (C). Normality testing conducted. Data show mean ± SEM. One-way ANOVA, Tukey's multiple comparisons testing. *, $p < 0.05$. n=5. SuHx; Sugen-hypoxia.

3.3 Prophylactic bi-weekly intraperitoneal poly(I:C) (Invivogen) injections did not prevent the development of pulmonary hypertension or pulmonary vascular remodelling in Sugen-hypoxia C57BL/6J mice

Cardiac catheterisation (figure 3.2-4) was performed to measure the haemodynamic effects of bi-weekly intraperitoneal poly(I:C) injections in SuHx mice. Normoxic and SuHx mice received bi-weekly intraperitoneal saline injections as a control. Animals were subsequently sacrificed for lung and heart pathology to assess pulmonary vascular remodelling and Fulton's Index, respectively, to further assess the PH phenotype.

SuHx mice injected with bi-weekly intraperitoneal saline developed significantly increased RVESP compared to normoxic control (mean increase of 8.89 mmHg) (figure 3.2.b). In addition, RV dP/dt_{max} (figure 3.2.c) and ePVRi (figure 3.4.b) were significantly increased in SuHx mice compared to normoxic control. Also, in concordance with the haemodynamic diagnostic definition of PAH, LVEDP (mmHg) was unaffected in the SuHx mouse compared to normoxic control (figure 3.3.b). SuHx mice injected with bi-weekly intraperitoneal saline also developed a significant reduction in LV stroke volume (figure 3.4.c), LVEDV (figure 3.3.d), LV cardiac output (figure 3.3.e) when compared to normoxic controls.

Bi-weekly intraperitoneal poly(I:C) (2.5mg/kg or 10mg/kg) in SuHx mice did not affect any pressure, volume or contractility parameter assessed by right and left cardiac catheterisation when compared to SuHx saline mice (figure 3.2-4).

Likewise, the significant increase in percentage of pulmonary vessels muscularised (figure 3.6.a) and pulmonary cross-sectional area/medial ratio (figure 3.6.b) in SuHx mice were unaffected by bi-weekly intraperitoneal poly(I:C) (2.5mg/kg or 10mg/kg) when compared to SuHx saline controls. Representative images of the respective pulmonary vasculature in each experimental group are shown in figure 3.5.

Furthermore, weight of the right ventricle divided by mass of the left ventricle and ventricular septum (RV/LV+S) (i.e., Fulton's index to assess RV hypertrophy) was significantly increased in SuHx saline mice compared to normoxic saline control (figure 3.6.c). Consistent with above data, bi-weekly intraperitoneal poly(I:C) (2.5mg/kg or 10mg/kg) in SuHx mice did not affect RV hypertrophy when compared to SuHx saline controls (figure 3.6.c).

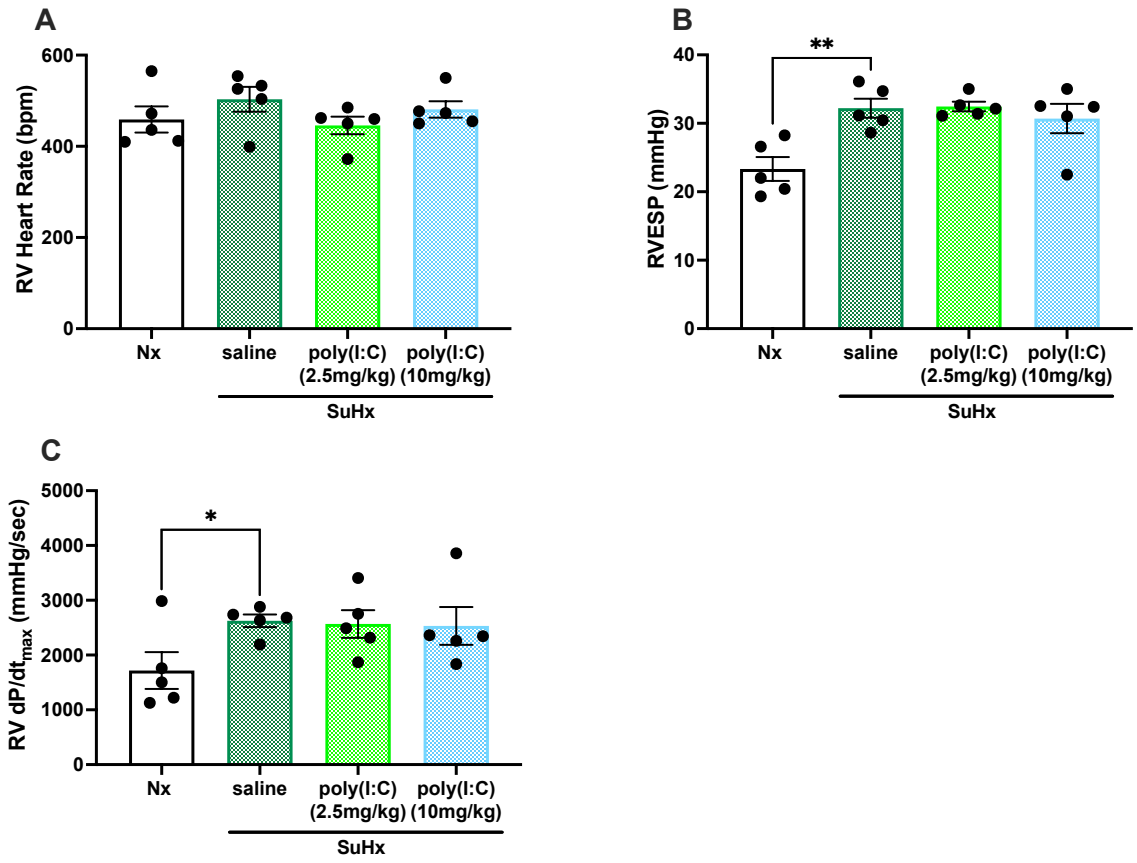

Figure 3.2. Right ventricular pressure measurements in C57BL/6J mice exposed to Sugen-hypoxia and prophylactic bi-weekly intraperitoneal poly(I:C) (Invivogen) or saline.

Heart rate was continuously recorded throughout right ventricular cardiac catheterisation and the average heart rate (bpm) (A) at the point of pressure-volume loop analysis is presented. Graphs present RVESP (mmHg) (B) and RV dP/dt maximum (mmHg/sec) (C) acquired by right ventricular cardiac catheterisation via external jugular vein in anaesthetised mice. Data show mean (top of bar) ± SEM. Normality testing conducted. Unpaired two-tailed t-test to compare saline groups. One-way ANOVA, Tukey's multiple comparisons testing to compare SuHx groups. **, p <0.01; *, p <0.05. n=5. RV; right ventricular. RVESP; right ventricular end systolic pressure. Nx; normoxia. SuHx; Sugen-hypoxia.

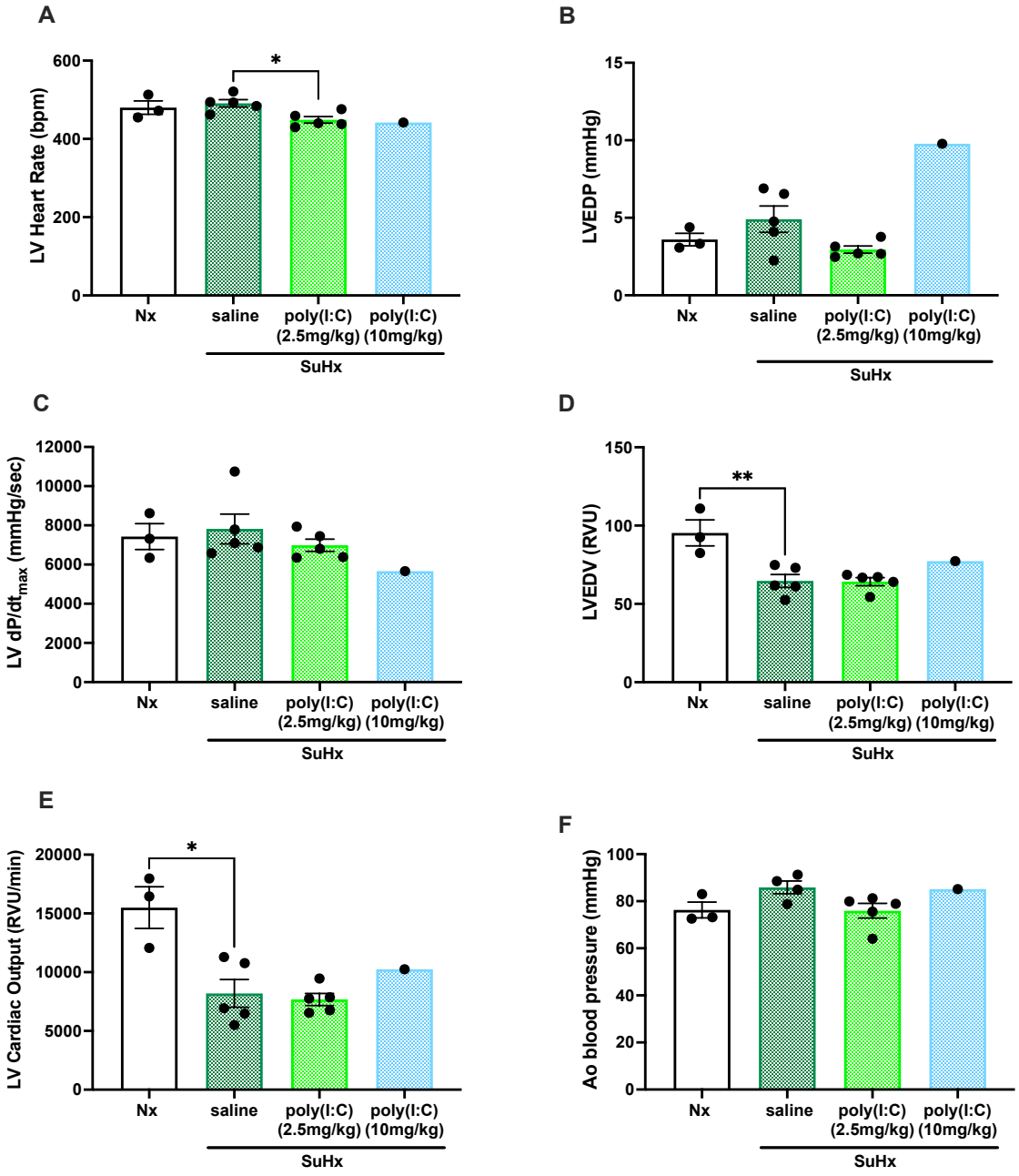

Figure 3.3. Left ventricular haemodynamic measurements and aortic blood pressure in C57BL/6J mice exposed to Sugen-hypoxia and prophylactic bi-weekly intraperitoneal poly(I:C) (Invivogen) or saline.

Heart rate was continuously recorded throughout left ventricular cardiac catheterisation and the average heart rate (bpm) (A) at the point of pressure-volume loop analysis is presented. Haemodynamic pressure measurements of LVEDP (mmHg) (B) and LV dP/dt maximum (mmHg/sec) (C) and volumetric measurements of LVEDV (RVU) (D) and LV cardiac output (RVU/min) (E) and aortic blood pressure (mmHg) (F) were acquired by left ventricular cardiac catheterisation via the left common carotid artery in anaesthetised mice. Data show mean (top of bar) ± SEM. Normality testing and unpaired two-tailed t-test conducted. 'SuHx and poly(I:C) 10mg/kg' group excluded from statistical analysis due to small *n.* **, p <0.01; *, p <0.05. n=1-5; discrepancies in n owed to surgical difficulties. LV; left ventricular. Nx; normoxia. SuHx; Sugen-hypoxia. RVU; relative volume units. Ao; aortic.

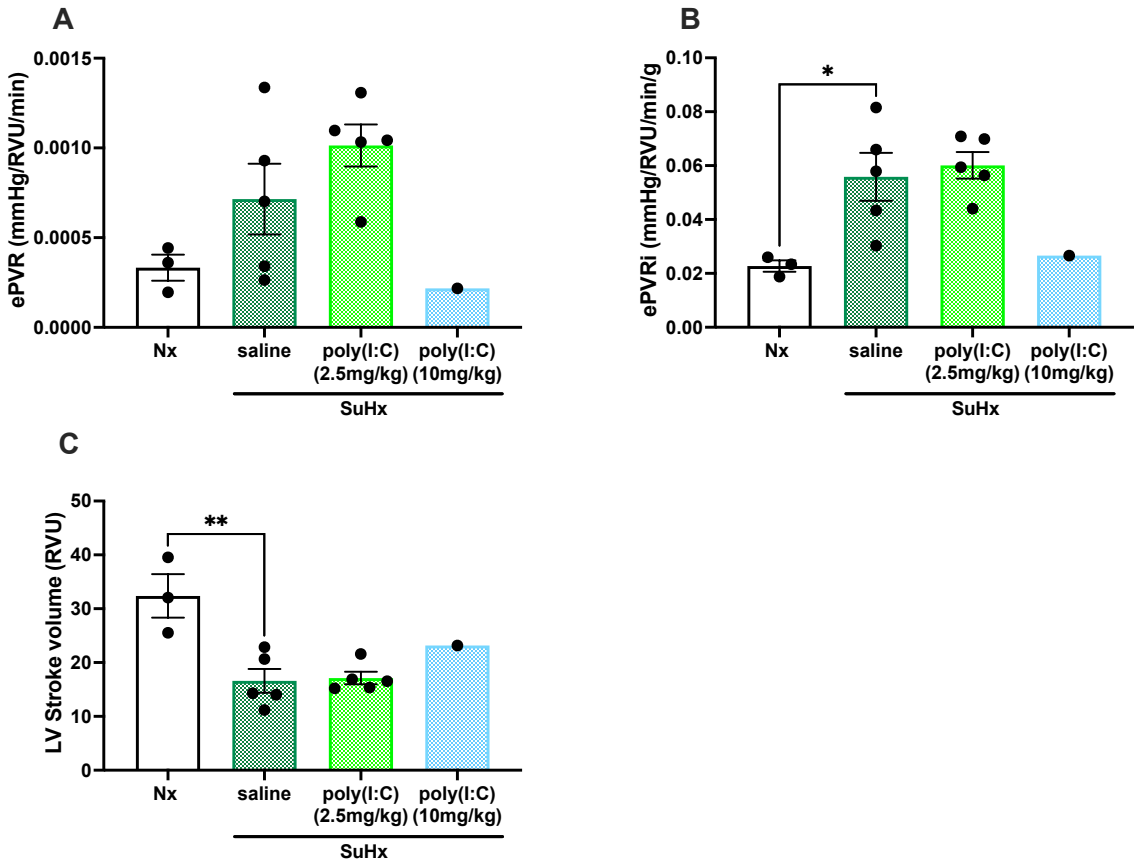

Figure 3.4. Estimated pulmonary vascular resistance and volume measurements in C57BL/6J mice exposed to Sugen-hypoxia and prophylactic bi-weekly intraperitoneal poly(I:C) (Invivogen) or saline.

Graphs present estimated- PVR/i (A/B)) and PVR index acquired by right and left ventricular cardiac catheterisation and calculated using the equation: (estimated mean pulmonary artery pressure (emPAP)- left ventricular end diastolic pressure (LVEDP)/ LV cardiac output or cardiac index). Graph C presents LV stroke volume. Data show mean (top of bar) ± SEM. Normality testing conducted. Unpaired two-tailed t-test to compare saline groups and 'SuHx saline vs SuHx poly(I:C) 2.5mg/kg' for ePVR (A) and ePVRi (B). One-way ANOVA, Tukey's multiple comparisons testing to compare SuHx groups (C-D). **, p <0.01; *, p <0.05. n=1-5; discrepancies in n owed to surgical difficulties. RV; right ventricular. ePVR/i; estimated pulmonary vascular resistance/index. Nx; normoxia. SuHx; Sugen-hypoxia. RVU; relative volume units.

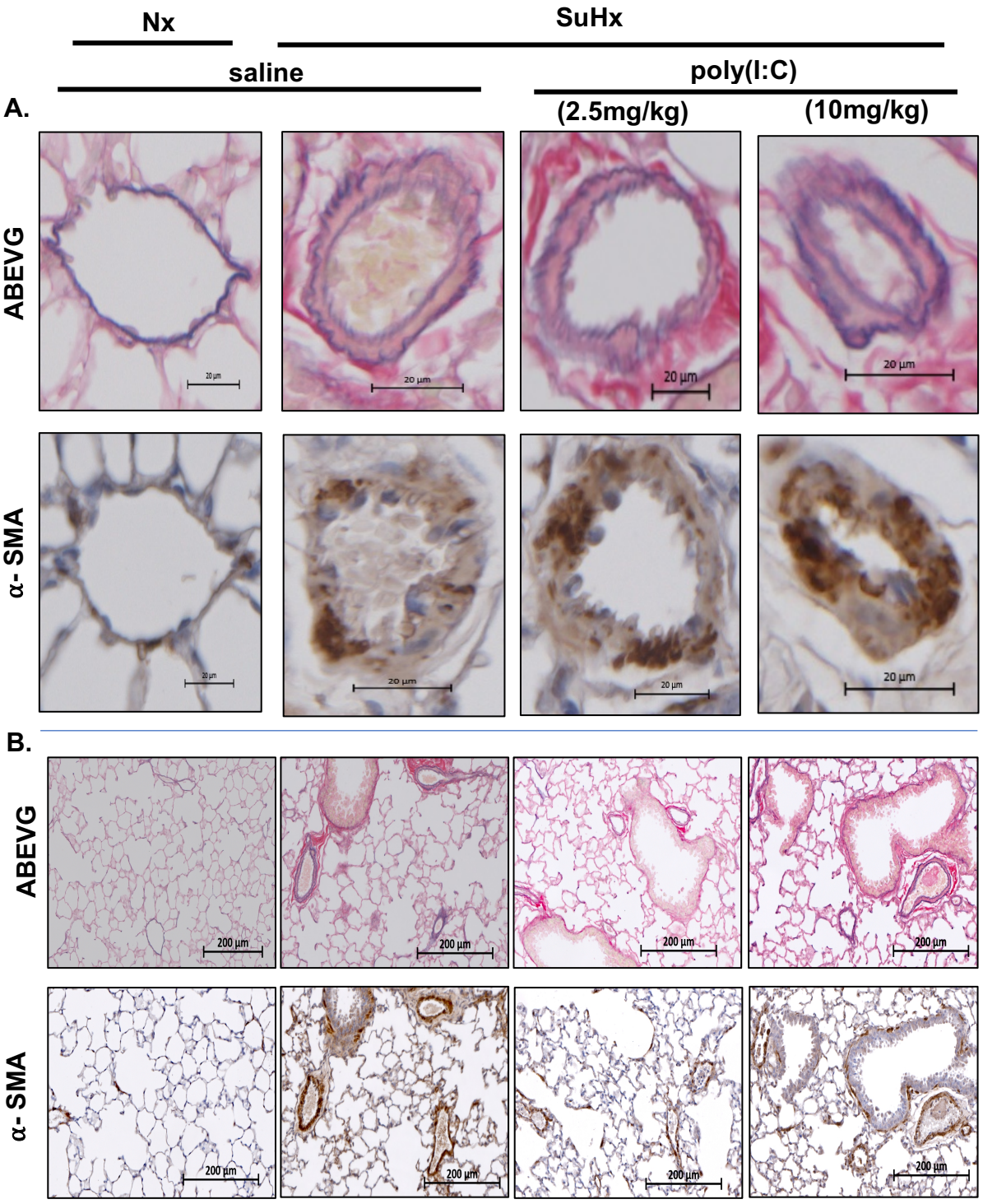

Figure 3.5. Representative images of distal (A) and proximal (B) pulmonary vasculature in FFPE lung sections of C57BL/6J mice injected with bi-weekly intraperitoneal poly(I:C) (Invivogen) or saline control during the 3-week duration of Sugen-hypoxia or normoxic exposure.

FFPE lung sections were tinctorial stained with ABEVG or indirectly immunostained with α-SMA. Morphometry was conducted on arterioles that were <50µm in diameter. Nx; normoxia. SuHx; Sugen-hypoxia. FFPE; formalin fixed paraffin embedded. ABEVG; Miller's elastin stain with alcian blue and Curtis modified van Gieson. α-SMA; Alpha smooth muscle actin. Scale bars as indicated.

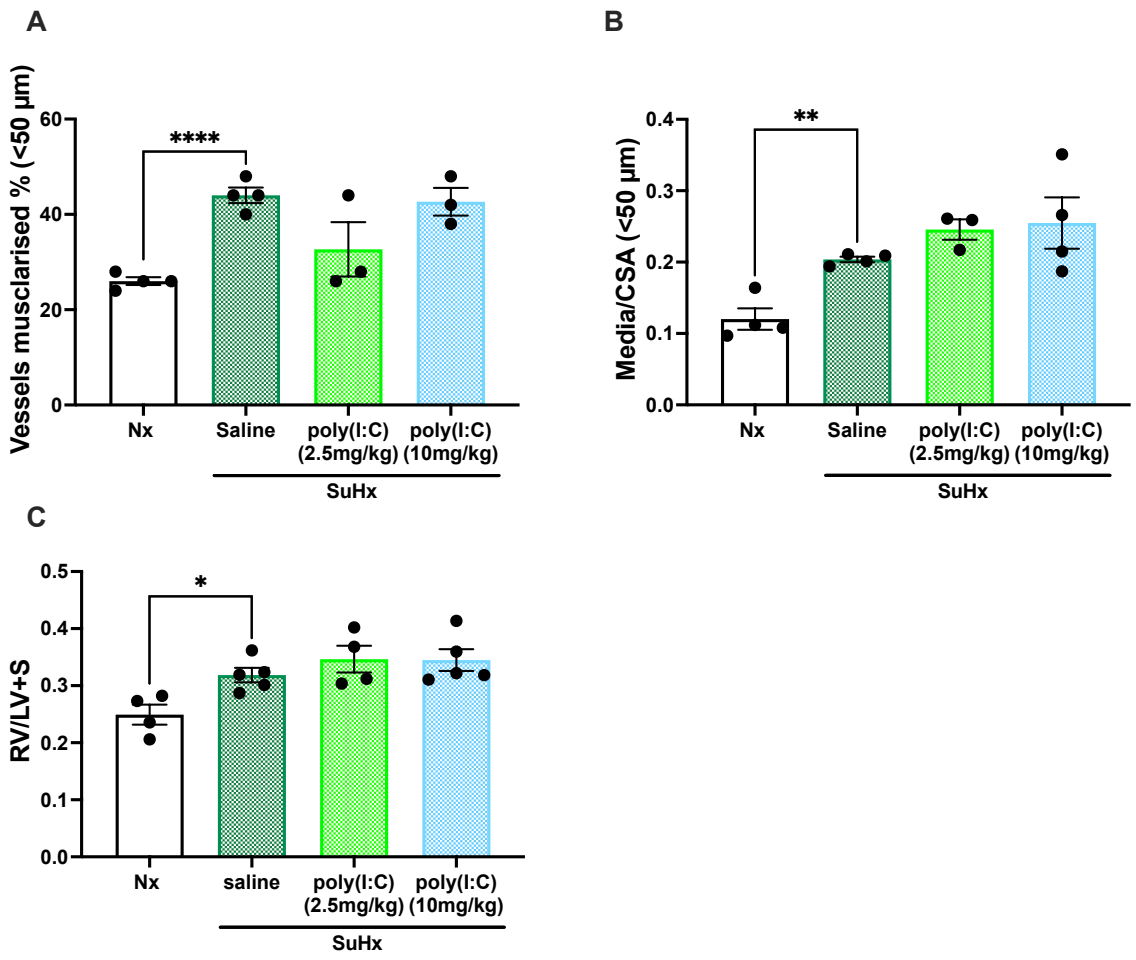

Figure 3.6 Pulmonary vascular morphometric analysis of FFPE lung sections and right ventricular hypertrophy analysis from C57BL/6J mice exposed to Sugen-hypoxia and prophylactic bi-weekly intraperitoneal poly(I:C) (Invivogen) or saline.

Pulmonary vascular remodelling was quantified by the proportion of muscularised arterioles (<50µm diameter) in FFPE lung sections stained with ABEVG (A) and medial area to cross-sectional area (CSA) ratio for arterioles in FFPE lung section immunostained indirectly with α-smooth muscle actin (α-SMA) (B). Hearts were dissected and chambers compartmentalised, and right ventricular free wall weight was normalised to left ventricle plus septum weight (RV/LV+S) to measure ventricular hypertrophy (C). Data show mean (top of bar) ± SEM. Normality testing conducted. Unpaired two-tailed t-test to compare saline groups. One-way ANOVA, Tukey's multiple comparisons testing to compare SuHx groups. ****, *p.* <0.0001; **, *p* <0.01; *, *p* <0.05. *n*=3-5.

3.4 Significant weight loss in C57BL/6J mice exposed to Sugen-hypoxia and treated with thrice-weekly intraperitoneal poly(I:C)

In results section 3.3, a bi-weekly intraperitoneal poly(I:C) dosing regimen was chosen in attempt to mitigate potential sickness behaviour caused by poly(I:C), however, bi-weekly doses of 2.5mg/kg and 10mg/kg (Invivogen) injections did not prevent the development of PH or pulmonary vascular remodelling in SuHx mice. Therefore, this subsequent experiment exactly replicated the dosing, administration frequency and supplier of poly(I:C) (i.e., Tocris) in the experiments by Farkas et al (2019.

Nine-week-old male C57BL/6J mice received thrice-weekly intraperitoneal poly(I:C) (supplied by Tocris) at a dose of 10mg/kg during the three-week exposure to SuHx. Subsequently, 21 days after induction of SuHx exposure, pressure, volume, and contractility parameters were assessed via right and left cardiac catheterisation. Animals were then sacrificed for lung and heart to assess pulmonary vascular remodelling and Fulton's Index, respectively, to further assess pulmonary hypertension phenotype. To control for any effects of poly(I:C) on haemodynamic parameters and pulmonary vascular remodelling, a normoxic group treated with poly(I:C) was added to the experimental design, thus finalising the 4 experimental groups as: normoxia and saline; normoxia and poly(I:C), SuHx and saline; SuHx and poly(I:C) (figure 3.7.a).

The weight of all animals was recorded on day 0 (baseline), prior to induction of SuHx and the first injection of poly(I:C). Nx and SuHx mice injected with poly(I:C) and SuHx mice injected with saline had significant reductions in weight on day 8 compared to their respective baseline weights (figure 3.7.b). Whereas Nx mice injected with saline has a significant weight increase from week 2 of the experiment (i.e., weights recorded day 15 and 21) compared to their respective baseline weights (figure 3.7.b). On day

21, absolute weight (grams) (figure 3.7.b) and percentage weight delta from day 0 (figure 3.7.c) were significantly reduced in SuHx control mice compared to Nx control mice and SuHx mice injected with poly(I:C) compared to Nx mice injected with poly(I:C). In addition, SuHx mice injected with poly(I:C) had a significant reduction in absolute weight compared to SuHx control mice (figure 3.7.b).

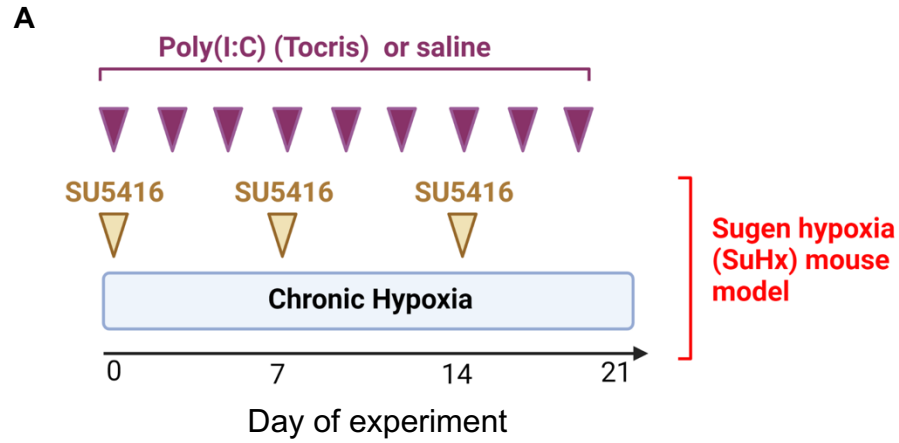
A
Poly(I:C) (Tocris) or saline
SU5416
SU5416
SU5416
Chronic Hypoxia
Sugen hypoxia (SuHx) mouse model
0
7
14
21
Day of experiment

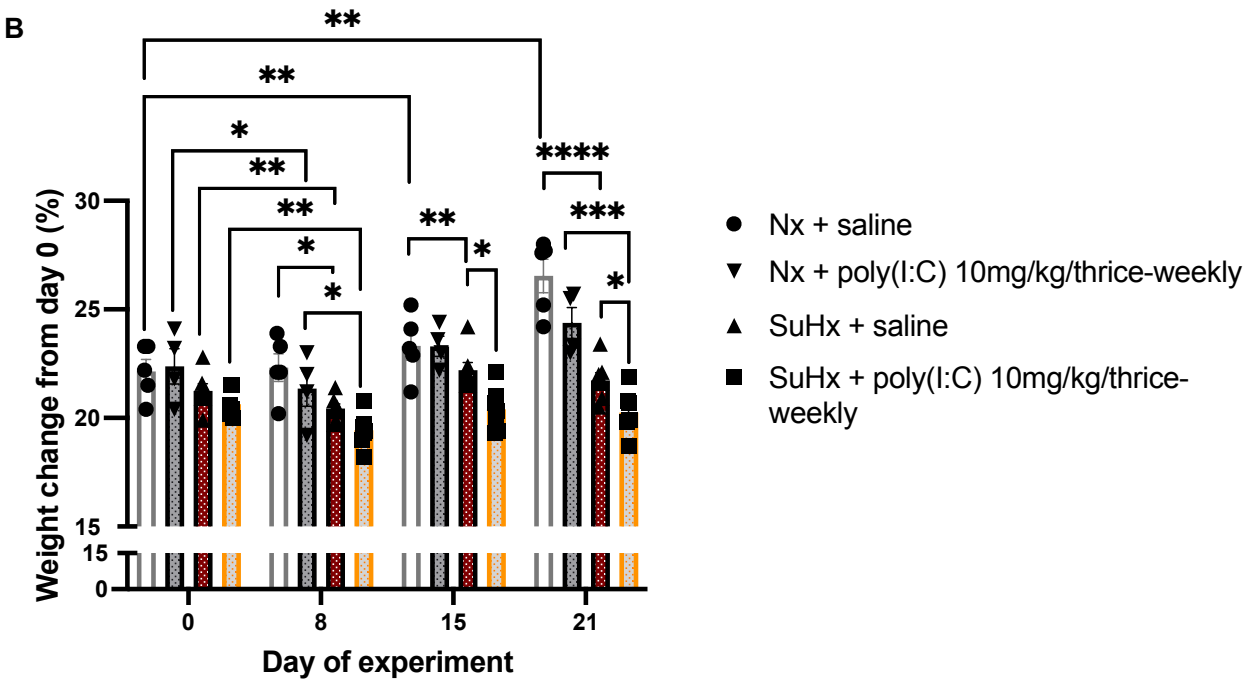
B
Weight change from day 0 (%)
Day of experiment
Nx + saline
Nx + poly(I:C) 10mg/kg/thrice-weekly
SuHx + saline
SuHx + poly(I:C) 10mg/kg/thrice-weekly

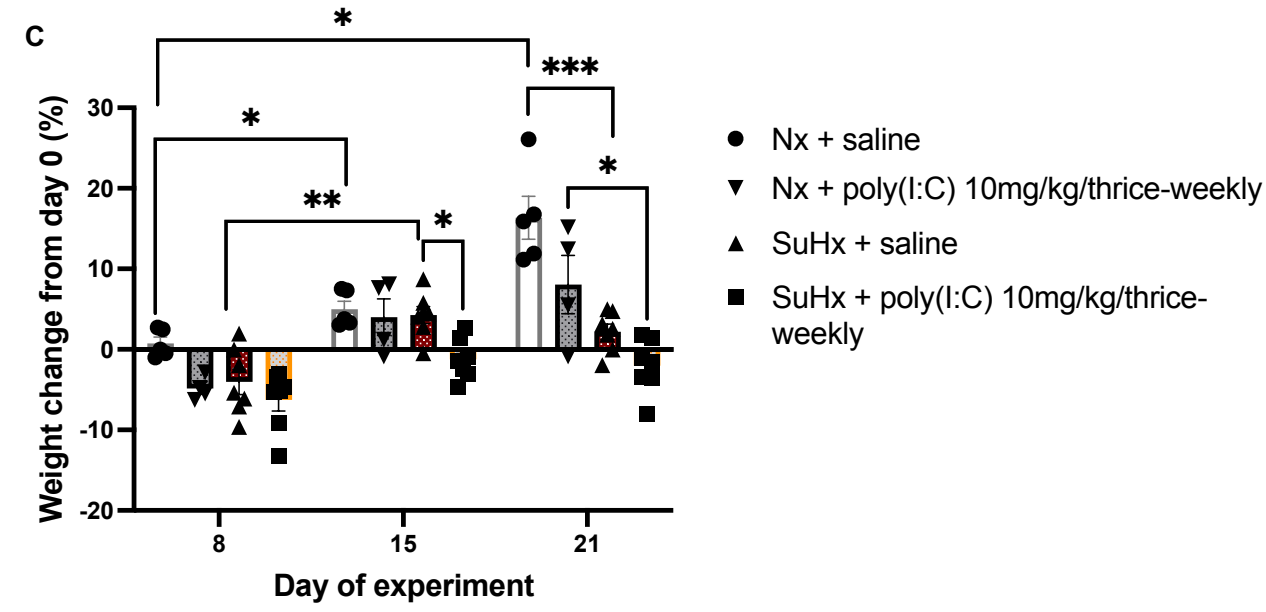
C
Weight change from day 0 (%)
Day of experiment
Nx + saline
Nx + poly(I:C) 10mg/kg/thrice-weekly
SuHx + saline
SuHx + poly(I:C) 10mg/kg/thrice-weekly

Figure 3.7 Experimental design of prophylactic thrice-weekly intraperitoneal poly(I:C) (Tocris) and saline injections in C57BL/6J mice exposed to Sugen-hypoxia and periodic weight recordings throughout the duration of the experiment.

Thrice-weekly intraperitoneal poly(I:C) (supplied by Tocris) (2.5mg/kg or 10mg/kg) and saline control injections were given during a three-week SuHx exposure in male C57BL/6J mice aged 9 weeks at the point of SuHx induction. Original image created in Biorender.com (A). Weights of animals were recorded weekly, and graphs present absolute weight (g) (B) and percentage weight change (delta) from day 0 (C). Data show mean ± SEM. One-way ANOVA, Tukey's multiple comparisons testing. ****, p <0.0001; ***, p<0.001; **, p <0.0; *, p < 0.05. n=4-7. Nx; normoxia. SuHx; Sugen-hypoxia.

3.5 Prophylactic thrice-weekly intraperitoneal poly(I:C) (Tocris) injections did not prevent the development of pulmonary hypertension or pulmonary vascular remodelling in Sugen-hypoxia C57BL/6J mice

Mice exposed to SuHx and injected with thrice-weekly intraperitoneal saline developed significantly increased RVESP compared to normoxic controls (mean increase of 6.34 mmHg) (figure 3.8.b). This increase in RVESP was measured despite the SuHx mice and saline group measuring a decreased mean heart rate (bpm) compared to normoxia controls (mean decrease of 113 beats per minute) (figure 3.8.a). Importantly, no significant differences in heart rate at the time of pressure-volume loop analysis was measured within the SuHx group and therefore haemodynamic parameters were confidently assessed within this experimental arm.

Normoxic mice with thrice-weekly intraperitoneal poly(I:C) developed significantly reduced RV dP/dt_{max} compared with normoxic controls (figure 3.8.c). However, thrice-weekly doses of intraperitoneal poly(I:C) injected during SuHx exposure did not affect any other right ventricular haemodynamic parameter assessed by right heart catheterisation when compared to SuHx control mice (figure 3.8 and 3.10). Rather, LV dP/dt_{max} was significantly reduced in SuHx mice with poly(I:C) compared to SuHx control mice during left cardiac catheterisation (figure 3.9.c). Normoxic mice treated with intraperitoneal poly(I:C) showed a similar trend of reduction in LV dP/dt_{max} when compared to saline controls (figure 3.9 c), however, no statistical significance testing was performed on left ventricular catheterisation parameters of normoxic mice due to insufficient *n*.

Consistent with the cardiac catheterisation data, SuHx mice had a significant percentage increase in pulmonary vessel muscularisation (figure 3.12.a) and cross-sectional area/medial ratio (figure 3.12.b) when compared to normoxic control. In

addition, within the normoxic and SuHx arm of the experiment, thrice-weekly intraperitoneal poly(I:C) did not affect pulmonary vessel muscularisation (figure 3.12.a) and pulmonary cross-sectional area/medial ratio (figure 3.12.b) when compared to their respective saline controls. Representative images of the respective pulmonary vasculature in each experimental group are shown in figure 3.11.

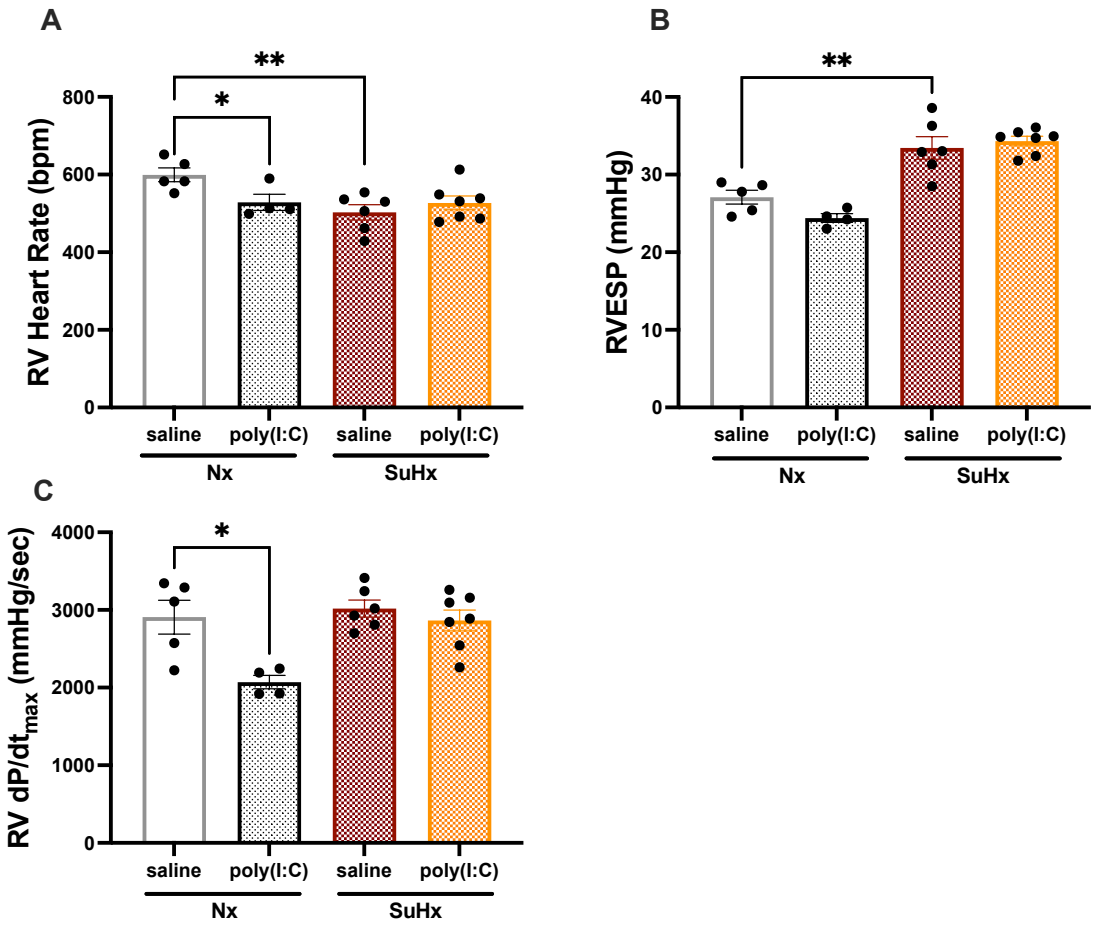

Figure 3.8 Right ventricular pressure measurements in C57BL/6J mice exposed to Sugen-hypoxia and prophylactic thrice-weekly intraperitoneal poly(I:C) (Tocris) or saline.

Heart rate was continuously recorded throughout right ventricular cardiac catheterisation and the average heart rate (bpm) (A) at the point of pressure-volume loop analysis is presented. Graphs present RVESP (mmHg) (B) and RV dP/dt maximum (mmHg/sec) (C) acquired by right ventricular cardiac catheterisation via external jugular vein in anaesthetised mice. Data show mean (top of bar) ± SEM. Normality testing and unpaired two-tailed conducted. **, p <0.01; *, p <0.05. n=4-7. RV; right ventricular. RVESP; right ventricular end systolic pressure. Nx; normoxia. SuHx; Sugen-hypoxia.

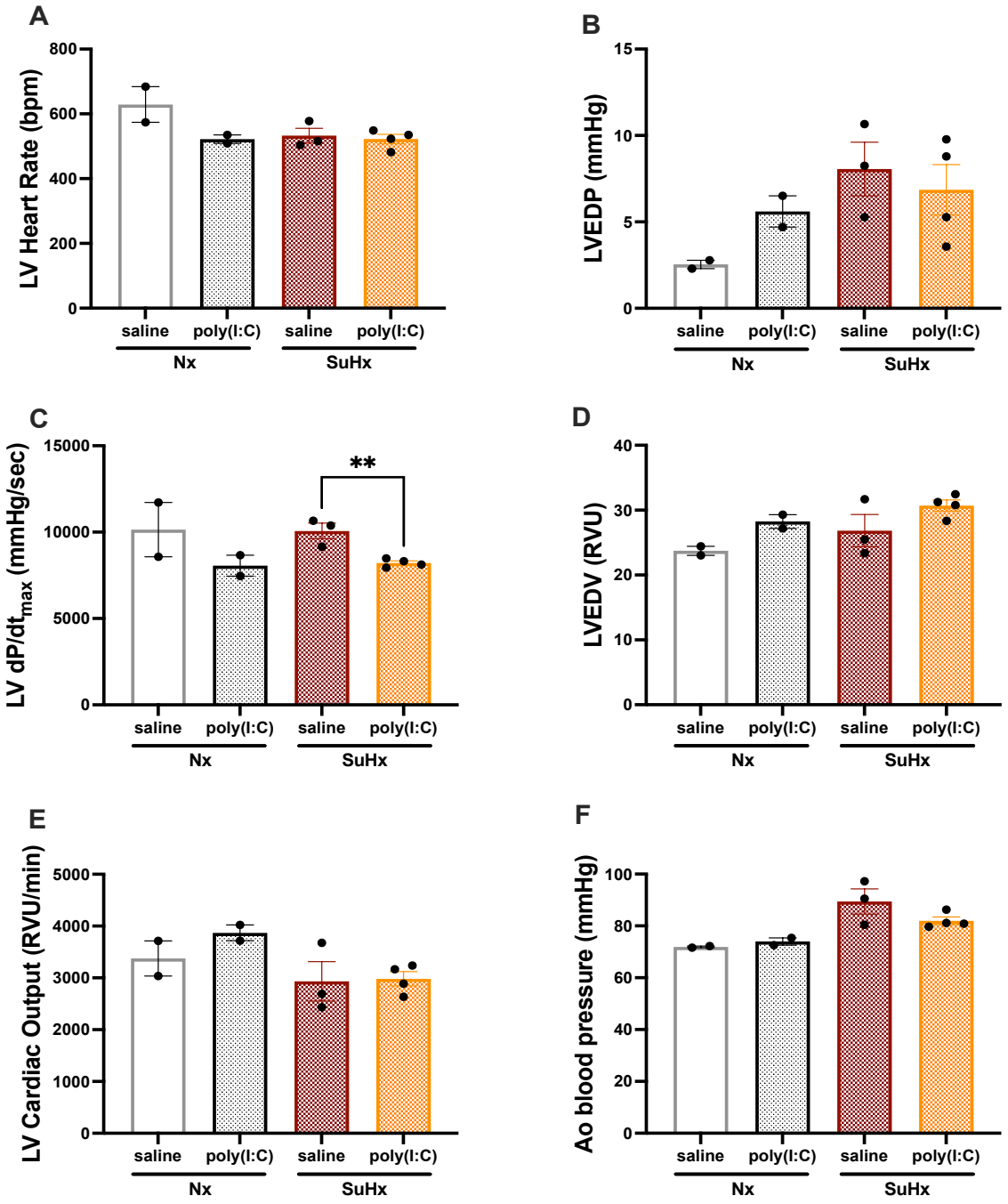

Figure 3.9 Left ventricular haemodynamic measurements and aortic blood pressure in C57BL/6J mice exposed to Sugen-hypoxia and prophylactic thrice-weekly intraperitoneal poly(I:C) (Tocris) or saline. Heart rate was continuously recorded throughout left ventricular cardiac catheterisation and average heart rate (bpm) (A) at the point of pressure-volume loop analysis is presented. Haemodynamic pressure measurements of LVEDP (mmHg) (B) and LV dP/dt maximum (mmHg/sec) (C) and volumetric measurements of LVEDV (RVU) (D) and LV cardiac output (RVU/min) (E) and aortic blood pressure (mmHg) (F) were acquired by left ventricular cardiac catheterisation via the left common carotid artery in anaesthetised mice. Data show mean (top of bar) ± SEM. Data show mean (top of bar) ± SEM. Normality testing and unpaired two-tailed t-test conducted. Nx groups excluded from statistical analysis due to small *n*. **, p <0.01. n=2-4;.discrepancies in n owed to surgical difficulties. LV; Left ventricular. Nx; normoxia. SuHx; Sugen-hypoxia. RVU; relative volume units.

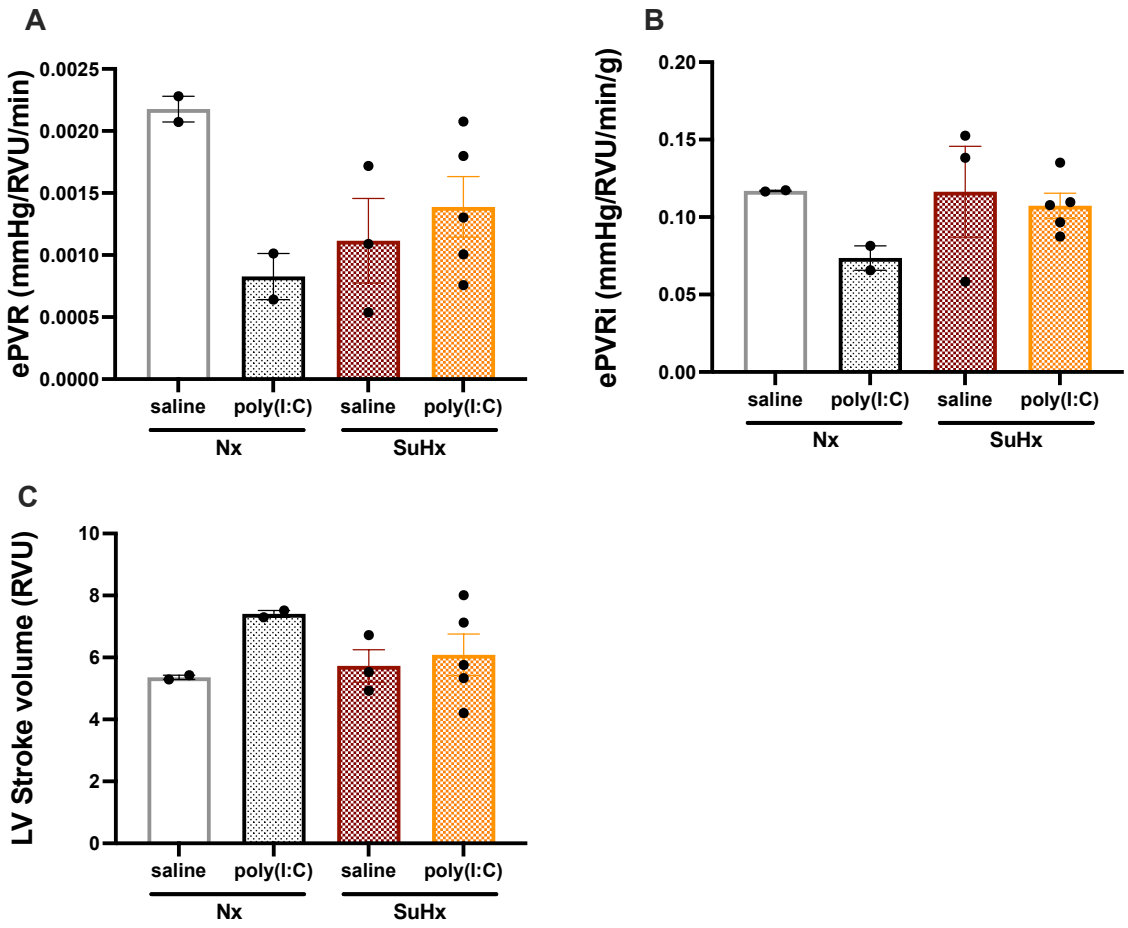

Figure 3.10 Estimated pulmonary vascular resistance and right ventricular contractility and volume measurements in C57BL/6J mice exposed to Sugen-hypoxia and prophylactic thrice-weekly intraperitoneal poly(I:C) (Tocris) or saline.

Graphs present estimated- PVR (A) and PVR index acquired by right and left ventricular cardiac catheterisation and calculated using the equation: (estimated mean pulmonary artery pressure (emPAP) - left ventricular end diastolic pressure (LVEDP)/ LV cardiac output or cardiac index). Graph C presents LV stroke volume Data show mean (top of bar) ± SEM. Normality testing and unpaired two-tailed t-test conducted. *n*=2-5; discrepancies in *n* owed to surgical difficulties RV; right ventricular. ePVR/i; estimated pulmonary vascular resistance/index. Nx; normoxia. SuHx; Sugen-hypoxia. RVU; relative volume units.

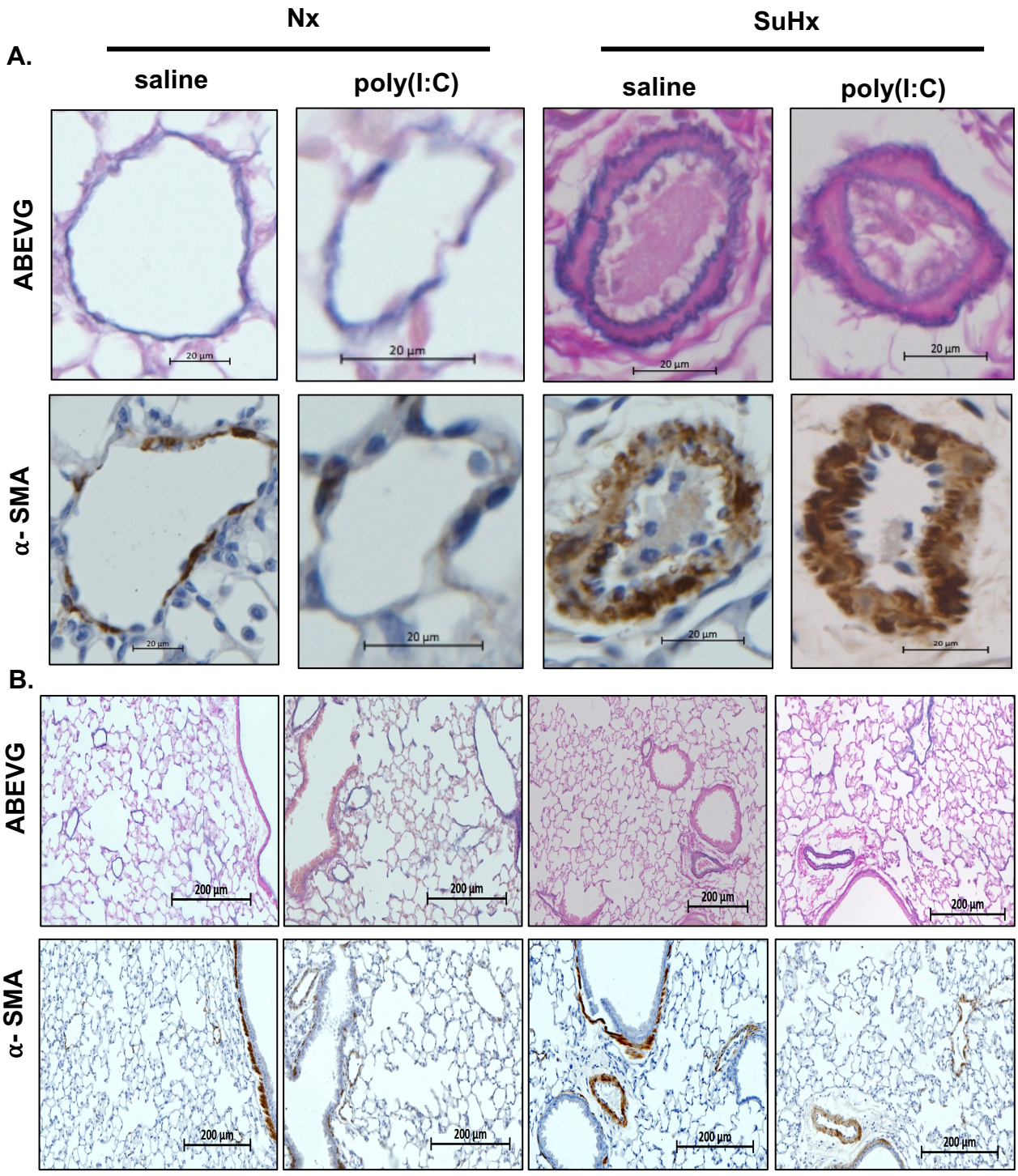

Figure 3.11 Representative images of distal (A) and proximal (B) pulmonary vasculature in FFPE lung sections of C57BL/6J mice injected with thrice weekly intraperitoneal poly(I:C) (Tocris) or saline control during the 3-week duration of Sugen-hypoxia or normoxic exposure.

FFPE lung sections were tinctorial stained with ABEVG or indirectly immunostained with α-SMA. Morphometry was conducted on arterioles that were <50µm in diameter. Nx; normoxia. SuHx; Sugen-hypoxia. FFPE; formalin fixed paraffin embedded. ABEVG; Miller's elastin stain with alcian blue and Curtis modified van Gieson. α-SMA; Alpha smooth muscle actin. Scale bars as indicated.

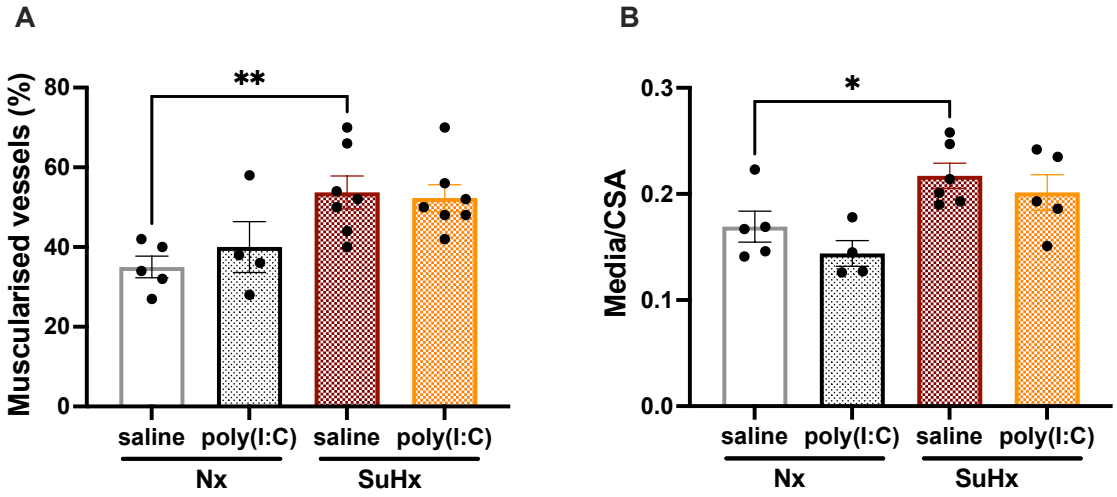

Figure 3.12 Pulmonary vascular morphometric analysis of FFPE lung sections analysis from C57BL/6J mice exposed to Sugen-hypoxia or normoxia and prophylactic thrice-weekly intraperitoneal poly(I:C) (Tocris) or saline.

Pulmonary vascular remodelling was quantified by the proportion of muscularised arterioles (<50μm diameter) in FFPE lung sections stained with ABEVG (A) and medial area to cross-sectional area (CSA) ratio for arterioles in FFPE lung section immunostained indirectly with α-smooth muscle actin (α-SMA) (B). Data show mean (top of bar) ± SEM. Normality testing and unpaired two-tailed t-test conducted. **, p <0.01; *, p <0.05. n=4-7.

3.6 Summary

The aim of this chapter was to investigate the potential of prophylactic intraperitoneal poly(I:C) as a therapeutic in a Sugen-hypoxia mouse model of pulmonary hypertension. In summary:

- Three weeks of chronic hypoxia exposure and weekly Sugen injections consistently produced pulmonary hypertension in male C57BL/6J mice as assessed by cardiac catheterisation and pulmonary vascular remodelling analysis.

- The preventative action of prophylactic intraperitoneal poly(I:C) demonstrated in a SuHx rat model of PH (Farkas et al, 2019) was not conserved in a SuHx mouse model of PH.

- Thrice weekly intraperitoneal poly(I:C) reduced right and left ventricular dP/dt_{max} in normoxic and SuHx mice, respectively, but limitations of this haemodynamic equation and technical artefacts need to be considered.

- All tested dosage regimens of prophylactic intraperitoneal poly(I:C) in SuHx or Nx mice had no effect on pulmonary vascular remodelling.

- Intraperitoneal poly(I:C) temporally induced weight loss in SuHx in a dose dependent manner.

3.7 Discussion

3.7.1 Prophylactic poly(I:C) did not prevent PH in a Sugen-hypoxia mouse model

In this chapter, I investigated the cross-species conservation of beneficial effects of prophylactic intraperitoneal poly(I:C) reported in Farkas et al (2019) in a SuHx mouse model rather than a SuHx rat model. In contrast to Farkas et al (2019), prophylactic intraperitoneal bi-weekly poly(I:C) (supplied by Invivogen; chapter 3.3.) or intraperitoneal thrice-weekly poly(I:C) (supplied by Tocris; section 3.5.) did not prevent PH, pulmonary vascular remodelling or right ventricular hypertrophy as induced by 3-week SuHx exposure. Of note, the choice to use Tocris-supplied poly(I:C) in section 3.5 rather than Invivogen-supplied poly(I:C) in section 3.3 was taken to exactly reproduce Farkas et al (2019) work in mice. Furthermore, I measured a different range of base pair lengths of poly(I:C) between the different manufactured poly(I:C) (see methods: figure 2.2.) and given the literature surrounding base pair length dependent recognition of poly(I:C) sensors, it was important to exactly reproduce the Farkas et al (2019) protocol (Kato et al., 2008; Kell et al., 2015).

Nevertheless, no right or left ventricular pressure, volumetric or contractility, excluding LV dP/dt_{max}, differences were reported in SuHx mice injected with any dosage regimen of intraperitoneal poly(I:C) compared to SuHx control mice. This contrasting result from the work of Farkas et al (2019) occurred despite the consistent production of successful PH model in the SuHx mouse.

A successful PH model was determined by a significant increase in RVESP in SuHx control mice when compared to normoxic mice in both experimental attempts to optimise prophylactic intraperitoneal poly(I:C) in SuHx mice (section 3.3. and 3.5.). Descriptively, LVEDP (mmHg) increased in SuHx mice compared to normoxic controls,

but low *n* number did not allow for meaningful statistical testing between these normoxic and SuHx groups. However, despite this increase trend, all data points for LVEDP (mmHg) in SuHx mice lie in-between the normal range of 4-12mmHg, making the presence of left ventricular failure to be unlikely in these animals (figure 3.9.b). Further, pulmonary vascular remodelling and RV hypertrophy were significantly induced in the SuHx mouse compared to normoxic controls (figure 3.6 and 3.12). Significant mean reductions in LV stroke volume (figure 3.4.c) and LV cardiac output (figure 3.3.e) were recorded in SuHx mice compared to normoxic mice inferring RV decompensation and ventricular interdependence, respectively. To further explain, decreased filling of the LV due to a lowered RV stroke volume has previously been described in a process called ventricular series interaction (Fogel et al., 1995; C. T. J. Gan et al., 2006a). This RV decompensation and ventricular interdependence suggests a strong and progressed PH phenotype, yet the SuHx mouse model is a relatively subtle PH phenotype compared to the SuHx rat. In more detail, the SuHx mouse produced an approximate mean RVESP of 30-35 mmHg compared to an approximate RVESP of 100 mmHg in a SuHx rat, and unlike the SuHx rat, the SuHx mouse does not develop angioproliferative plexiform lesions and is partially reversible (Abe et al., 2010). This phenotypic difference could explain the inconsistencies between the data in this thesis and Farkas et al (2019) regarding prophylactic intraperitoneal poly(I:C). When measuring the prophylactic effects of intraperitoneal poly(I:C) in murine SuHx models, the importance in severity of the PH *in vivo* was alluded to in Farkas et al (2019) paper where poly(I:C) treatment had no effect on the fraction of partially occluded vessels when compared to vehicle, whereas, poly(I:C) reduced the fraction of completely occluded small pulmonary arteries (external diameter >25 and <50μm) when compared to vehicle.

Possible explanations for the difference in results could include differences in dsRNA (or poly(I:C)) sensing capacities. For example, future efforts should compare TLR3 expression and other receptors of poly(I:C) such as RIG-I and MDA5 to explain inconsistencies between different murine models of PH. In support of this speculation, Hoshikawa et al. (2003), via a microarray approach, showed that hypoxia induces distinct gene expression in the lungs of a rat compared to mouse associated with a higher degree of pulmonary vascular remodelling and higher pressures in the rats. Specifically, known poly(I:C)-induced pro-inflammatory mediators of CXCL5 and PI3K were significantly elevated in a hypoxia exposed rat lung but were unchanged in a hypoxia exposed mouse (Hoshikawa et al. 2003).

Likewise, one could speculate the mechanisms governing absorption of intraperitoneal injection from peritoneal cavity may differ between species. As the base pair length, and so, the molecular size of poly(:C), administered in saline, is relatively small, one could speculate that absorption would predominantly occur via diffusion in mesenteric capillaries and portal circulation, rather than, peritoneal lymphatics, yet the quantification of such blood flow in the peritoneum is poorly understood due to the diffuse nature of its tissue and vasculature (Al Shoyaib et al., 2019).

Species related differences in immune response may also provide explanation for differences in mine and Farkas et al (2019) observations. For example, discordant proinflammatory cytokine responses to the TLR3-restricted dsRNA agonist, rintatolimod, have been measured between rats and monkeys (Mitchell et al., 2014). Even though, rats and mice were not compared in this study, other studies have shown mouse strain related immune response differences to a bacterial stimulus (a respiratory pneumococcal infection) where BALB/c mice demonstrated no bacteraemia or death compared to 50% mortality rates in C57BL/6 mice (Gingles et

al., 2001). Given this evidence for different innate immune responses amongst mice strains, it is reasonable to speculate such difference between the murine species (mouse vs rat) as an explanation for differences in mine and Farkas et al (2019) work.

In addition, it is now accepted that the microbiota is fundamental in the regulation of the host immune response and microbiota differences between mice and rats have been documented. Specifically, the mouse gut is dominated by members of *Muribaculaceae*, whereas the rat gut is dominated by *Prevotella* and these microbome may have influenced the different immune responses to poly(I:C) (Nagpal et al., 2018).

Alternatively, differences in mine and Farkas et al (2019) observations could be explained by the imperfect species dose scaling in this experiment. For example, the scaling of poly(I:C) dose (mg/kg) was based on body weight alone and biochemical and functional systems- species differences have the capacity to affect pharmacokinetics. In future, allometric scaling should be the preferred method. Allometric scaling normalises dose to body surface area (Nair et al.,2016). To convert dose in mg/kg to dose in mg/m^2 , the correction factor (K_m) should be used (Nair et al.,2016). As the K_m of rat is 6 and the K_m of mouse is 3,the original rat dose (10mg/kg) should be halved to 5mg/kg, in attempt to optimise this experiment in the future (Nair et al.,2016).

3.7.2 Intraperitoneal poly(I:C) reduced left ventricular dP/dt $_{max}$

Acquired via cardiac catheterisation, dP/dt_{max} is a surrogate of cardiac contractility and can be assessed in either the left or right ventricle. LV dP/dt_{max} was significantly reduced in thrice-weekly poly(I:C)-treated SuHx mice compared to SuHx control mice, indicating a reduction in the maximal rate of rise of left ventricular pressure during a

contraction (figure 3.9.c). The dP/dt_{max} parameter imperfectly predicts contractile reserve as it is limited to its load dependency and in particular is influenced by preload. Reduced ventricular preload can be caused by blood loss (Morimont et al., 2012). Notably, blood loss is common during ventricular cardiac catheterisation and blood loss is particularly prevalent in left ventricular cardiac catheterisation due to high pressures in the arterial system; therefore, an important caveat when interpreting dP/dt_{max} (Zhang et al. 2015). However, an unchanged aortic blood pressure between poly(I:C)- and saline-treated SuHx mice reported in figure 3.9.f refutes speculation of blood loss to influence dP/dt_{max} given reports of $\geq$300µl blood withdrawal to markedly reduce arterial blood pressure in C57BL/6J mice after 15 minute and compensation (i.e., blood pressure increased) not to occur until >30 minutes after blood loss (Pfeifer et al., 2013).

In addition, RV dP/dt_{max} was significantly reduced in thrice-weekly poly(I:C)-treated normoxic mice compared to saline control but interpretation of this data is further limited by the significant reduction in heart rate that was also measured in these animals. I speculate that frequency-dependent inotropy referred to as the Bowditch effect may explain these RV dP/dt_{max} differences. The Bowditch effect describes the phenomenon in which an increased heart rate increases the force of myocardial contraction, yet this is usually absent or reversed in heart failure or cardiomyopathy (Zhang et al. 2015). When considering this notion, it is feasible that the significantly lower heart rate in poly(I:C)-treated mice compared to control mice in normoxic conditions was a cause of anaesthesia and is a confounder when interpreting the significant reduction in RV dP/dt_{max} (Zhang et al. 2015).

Furthermore, a decreased Bowditch effect (i.e., decreased contractility) is a hallmark of many cardiomyopathy models. Myocarditis is a specific cardiomyopathy and

describes inflammation of the myocardium. To the best of my knowledge, intraperitoneal poly(I:C) has not been reported to induce myocarditis, but the inoculation of RNA virus, coxsackievirus B3 (CVB3), via intraperitoneal injection (the same administration route as my experiment) was first modelled to induce acute and chronic myocarditis by Fairweather and Rose (2007) and has been used thereafter (Chen et al. 2021; Wei et al. 2020). Given the known inflammatory effects of poly(I:C), and in attempt to explain dP/dt_{max} difference in these data, in future cardiac muscle will be stained for biomarkers of lymphocytes and neutrophils in reference to endomyocardial biopsy being the gold standard for myocarditis diagnosis (Dominguez et al., 2016).

Of note, RV dP/dt_{max} was significantly increased in the SuHx model of PH compared to normoxic control mice in result section 3.2.c inferring increased contractility. This phenomenon has previously reported in SuHx mouse models of PH, as well as PAH patients, and could be explained as an adaptation of the right ventricle (Rako et al., 2023; Voelkel et al., 2006). Increased contractility in a pressure-overloaded right ventricle is a known phenomenon to preserve the coupling of pulmonary artery and right ventricle in an adapted right ventricle, thus maintaining cardiac output. Therefore, one could speculate that this an appropriate model of milder, less progressed PH phenotype as decreased right ventricular contractility is characteristic of a maladapted, decompensated right ventricular in an individual with progressed PAH (Rako et al., 2023).

However, to assess myocardial contractility more accurately in future I would acquire the preload independent contractility parameter of maximal elastance (Emax), or otherwise referred to end-systolic elastance (Ees), during cardiac catheterisation (Monge Garcia et al., 2018). The acquisition of Ees requires transient occlusions of

the inferior vena cava via application of forceps (Zhang et al. 2015).This generates an end systolic pressure volume relationship graph which is independent of load and the slope of the graph represents Ees (Zhang et al. 2015).

3.7.3 Intraperitoneal poly(I:C) causes significant weight loss in a Sugen-hypoxia mouse model

Sugen-hypoxia exposure in control mice (i.e., thrice-weekly intraperitoneal saline) (section 3.7) caused a small and temporary (day 8 only) reduction in weight loss when compared to baseline weights but this was not observed in SuHx control mice that received bi-weekly intraperitoneal saline (section 3.1). This inconsistent weight loss in SuHx models may be attributed to significant differences in baseline weights (appendix figure 1). This significant weight difference is likely to be reflection of age differences at baseline, where control mice injected with bi-weekly saline (section 3.2) were 3 weeks older than control mice injected with thrice-weekly saline (section 3.4) at the point of SuHx induction. Therefore, one could speculate lighter, younger mice, tolerant SuHx exposure less well than older mice. Age dependent signalling pathways implicated in PAH could provide a mechanistic rationale for inconsistent weight loss in control mice exposed to SuHx (Carman et al, 2019; He et al, 1991).

SuHx mice treated with thrice-weekly poly(I:C) (10mg/kg) had a greater reduction in absolute weight when SuHx control mice on day 15 and day 21 (figure 3.7.b). In addition, thrice-weekly poly(I:C) (10mg/kg) had a greater reduction in percentage weight loss from day 0 when SuHx control mice on day 15 (figure 3.7.c). A further significant weight loss delta was not reported on day 21 in SuHx mice injected with poly(I:C). These significant weight losses were not observed in SuHx mice treated with bi-weekly poly(I:C) (2.5 mg/kg or 10mg'/kg) inferring that the adverse effect of significant weight loss occurred in a dose-dependent manner. These data therefore

raise questions about the feasibility of poly(I:C) as a therapeutic to pulmonary hypertension patients. This would have been especially important to consider had the therapeutic effect of prophylactic poly(I:C) in a SuHx mouse been observed. In attempt to mitigate adverse effects, a clinical grade dsRNA called Rintatolimod (Ampligen®) with specific affinity to TLR3 and other modes of delivery such as osmotic pump would have been investigated (Mitchell, 2016).

Furthermore, to definitively measure sickness behaviour more robustly in future, I would measure temperature, monitor food, and water intake, assess serum inflammatory cytokines and interferon, and assess metabolism.

3.7.4 Future work

As prophylactic intraperitoneal poly(I:C) was not protective in the SuHx mouse model, my research interest turned to assessing the importance of the route of poly(I:C) administration. Given the accepted notion of intranasal poly(I:C) as a pro-inflammatory viral mimic, and existing literature arguing inflammation to be a driver of pulmonary vascular remodelling and PH, I decided to investigate whether intranasal poly(I:C) altered severity of PH in the SuHx mouse model in the next chapter.

To note, if prophylactic thrice-weekly intraperitoneal poly(I:C) had been measured as protective in a SuHx mouse model, future experiments would have included a therapeutic intraperitoneal model. Specifically, the start of intraperitoneal poly(I:C) thrice-weekly treatment would have been administered after a successful PH phenotype was established using a 21 day SuHx mouse model protocol.

4. Investigating the effects of previous exposure to poly(I:C)-induced lung inflammation on the Sugen-hypoxia mouse model of pulmonary hypertension

4.1 Introduction

Primarily based on the work by Farkas et al (2019), the previous results chapter (chapter 3) investigated intraperitoneal poly(I:C) as a potential therapeutic in a Sugen-hypoxia mouse model of pulmonary hypertension (PH). An alternate *in vivo* administration route to intraperitoneal poly(I:C) is intranasal poly(I:C) instillation. Intranasal poly(I:C) instillation is a well-established model of lung inflammation in mice, and some refer to the model as a viral mimic or viral-related lung injury (Aeffner et al., 2011; Gao et al., 2021; Harris et al., 2013; Starkhammar et al., 2012; Stowell et al., 2009; Zhao et al., 2012) As lung inflammation is thought to be a key driver of pulmonary vascular remodelling, it is reasonable to ask whether the route of administration could influence the effects of poly(I:C) on pulmonary vascular remodelling and PAH.

Intranasal instillation in murine models is a non-invasive method of delivering substances to the upper and lower respiratory tract (Southam et al., 2002). Poly(I:C) is a synthetic analogue of dsRNA that induces innate immune responses via signalling through pattern recognition receptors (PRRs). Double stranded (ds)RNA is produced as an intermediate of viral replication and it is because of this that poly(I:C) is referred to as an inducer of antiviral immunity. Notably, intranasal poly(I:C) in mice induced molecular, inflammatory, and anatomical phenotypes similar to respiratory syncytial virus (RSV) (Aeffner et al., 2011; Harris et al., 2013; Tian et al., 2017). Specifically, in

two mouse strains (BALB/c mice and C57BL/6J), intranasal poly(I:C) produced local type I interferon and pro-inflammatory cytokine responses (IL-6, IL-1α, IFNγ, IP-10 (CXCL10), KC (CXCL1), mGCSF, IL-5, IL-12, and TNFα) in mouse lungs (Starkhammar et al., 2012; Stowell et al., 2009). Furthermore, poly(I:C)-induced inflammation has contributed to acute cell injury in lung epithelial cells and *in vivo* (Aeffner et al., 2011; Stowell et al., 2009). For example, three repeated intranasal poly(I:C) instillations induced marked perivascular and peribronchial interstitial infiltrates of neutrophils and mononuclear cells (Stowell et al., 2009). Physiologically, intranasal poly(I:C) impaired lung function as determined by a greater airway hyperresponsiveness to methacholine in whole body plethysmography (Stowell et al., 2009). Intranasal poly(I:C)-induced inhibition of alveolar fluid clearance and pulmonary perivascular oedema has also been reported in mice (Aeffner et al., 2011). Therefore, all aforementioned studies provide evidence that intranasal poly(I:C) is a potent inducer of lung inflammation in mice.

Inflammation and acute lung injury are strongly implicated in the pathogenesis of PAH. In the pathophysiology model by Voelkel et al (2012), an initial pulmonary vascular endothelium injury in combination with a dysregulation of vasoconstrictors and vasodilators result in vasoconstriction in the pulmonary circulation. Thereafter, vasoconstriction-induced abnormal pulmonary blood flow propagates more endothelial cell injury and apoptosis which eventually leads to pulmonary vascular cell proliferation, apoptosis resistance and angio-obliterative pulmonary vascular remodelling as a consequence of a maladaptive response (Voelkel et al., 2012). This progressive pulmonary vascular remodelling is associated with exaggerated perivascular inflammation and immune cell infiltration. Specifically, macrophages,

neutrophils, dendritic cells, T lymphocytes, B lymphocytes and mast cells have all been identified within pulmonary vascular lesions of PAH patients (Huertas et al., 2020). Chronic inflammation in PAH patients is reinforced by studies which show elevated systemic inflammation. Increased serum and/or plasma cytokines of interleukin (IL) -1β, -4, -5, -6, -8, -10 and -13, and TNFα, type I interferon have been measured in PAH patients compared to controls (Cracowski et al., 2014; Humbert et al., 2012; Soon et al., 2010). Specifically, IL-6, -8 and -12 and. TNFα positively correlated with adverse clinical outcomes (Soon et al., 2010). Furthermore, chemokines (CXCL1, CXCL8 CXLC10 and CXCL12) in the serum of PAH patients were increased compared to controls and these in combination could predict PAH patients from controls (Li et al. 2021). Specifically, CXCL1 (KC in mouse), CXCL8 and CXCL10 positively correlated with mean pulmonary artery pressure (mPAP) which is the haemodynamic parameter used to definitively diagnose PH (Li et al. 2021).

The above studies show that local pulmonary vascular and systemic inflammation are characteristics of established PAH. Furthermore, PAH has epidemiological associations with other systemic inflammatory diseases (i.e., systemic sclerosis and systemic lupus erythematosus) and infectious diseases (i.e., HIV) are reflected in the clinical classification of PAH. In addition, interferon therapy has been linked to the development of PAH in some rare cases (Savale et al., 2014).

All the aforementioned studies evidence the importance of inflammation in pulmonary vascular remodelling and PAH pathogenesis. As inflammation has been shown to precede pulmonary vascular remodelling in an experimental PH model (Tamosiuniene et al., 2011), some argue that altered immunity is a cause rather than consequence of

pulmonary vascular disease, but it is also accepted that the presence of local inflammatory cytokines directly controls pulmonary vascular cell proliferation, migration, and differentiation to propagate pulmonary vascular remodelling and contribute to progression of disease. For instance, recombinant IL-6 protein alone can cause mild experimental PH *in vivo,* and IL-6 exaggerates pulmonary vascular remodelling and PH in the chronic hypoxia mouse model (Golembeski et al., 2005). And so, while the exact mechanism by which inflammation contributes to pulmonary vascular remodelling and PAH pathogenesis is still not clear, it is accepted that altered innate immunity is one aspect of PAH pathogenesis (Golembeski et al., 2005; Zawia et al., 2020).

Researchers are now beginning to understand that innate immunity is regulated by the previous activation of the immune system, potentially leading to long-term sequela and altered clinical outcomes. For example, in a prospective study that used data collected from a national representative cohort (England, Scotland and Wales), recruited at birth in 1946, significant associations between lower respiratory tract infections (LRTIs) in early childhood and premature adult death from respiratory disease were reported in The Lancet (Allinson et al., 2023). Specifically, people who had LRTIs by 2 years of age were 93% more likely to die prematurely from respiratory disease compared to those did not have early childhood LTRIs. This exceeded estimated excess deaths, was adjusted for markers of childhood social disadvantages and pollution exposure and was specific to respiratory diseases when also considering LTRIs associations to circulatory-, cancer- and external- caused deaths (Allinson et al., 2023). Others have provided mechanistic explanations for the heterogeneity of innate immune responses that in theory have the capacity to alter disease. Researchers have argued that

genetics cannot solely explain heterogeneity of innate immune response and it is partly regulated by previous exposure history to inflammatory stimuli i.e., virus, bacteria, vaccinations, or environmental factors (Netea et al., 2016). For example, Bacillus Calmette-Guerin (BCG), a live-attenuated vaccine strain of *Mycobacterium bovis* was shown to induce genome-wide epigenetic reprogramming of human monocytes *in vivo* and significantly alter future innate immune responses, specifically enhancing TNFα, IL-6, and IL-1β production (Arts et al., 2018). Similarly, altered methylation in peripheral blood mononuclear cells in COVID-19 patients have been reported (Yang et al., 2022). Specifically, some histone methylation marks correlated to the inflammatory-associated differential expression patterns such as arginase 1 and IL-1 receptor 2 (Yang et al., 2022).

Given the above studies which state that childhood respiratory infections, and therefore respiratory inflammation, are associated with premature respiratory death (Allinson et al., 2023), molecular studies have shown previous inflammatory stimuli to alter future innate immune responses (Netea et al., 2016), and the association of innate immunity in PAH pathogenesis, this results chapter is dedicated to investigating how previous lung inflammation may alter the SuHx model of PH. Notably, a SuHx model has hypoxia- induced stabilisation of HIF1-α and subsequent transcription of pro-inflammatory target genes, lung inflammatory cell infiltration, increased mRNA levels of IL-6 and some reports of inflammation associated angioproliferative lesions, when compared to normoxic control (Ciuclan et al., 2011; Kojima et al., 2019).

Therefore, I hypothesised that previous lung inflammation via intranasal poly(I:C) instillation would alter the severity of PH in the Sugen-hypoxia mouse model. To do this my aims were to:

1. Assess the immunological responses in lung to a single dose of intranasal poly(I:C) in C57BL/6J mice
2. Investigate the effect of previous exposure to a single dose of intranasal poly(I:C) on pulmonary hypertension, pulmonary vascular remodelling, and right ventricular hypertrophy in a Sugen-hypoxic mouse
3. Assess the immunological responses in lung to repeated doses of intranasal poly(I:C) in C57BL/6J mice
4. Investigate the effects of previous exposure to repeated doses of intranasal poly(I:C) on pulmonary haemodynamics, pulmonary vascular remodelling, and right ventricular hypertrophy in a Sugen-hypoxic mouse

Results

4.2 A single instillation of intranasal poly(I:C) induced lung airway inflammation in C57BL/6J mice

To assess immunological responses in C57BL/6J mice instilled with a single dose of intranasal poly(I:C) (100μg/50μl), mice were sacrificed 24 hours and 9 days after instillation using pentobarbitone. Then, bronchoalveolar lavage fluid (BALF) was harvested and cell counts, and cytokine analysis were performed. In other C57BL/6J mice, lungs and heart were resected for immunohistological phenotyping (figure 4.1.a).

Twenty-four hours post intranasal poly(I:C) (100μg/50μl) instillation, total cell number (figure 4.1.b), total macrophages (figure 4.1.d) and total neutrophils (figure 4.1.f) and in BALF were significantly increased compared to 24 hours post intranasal saline control mice. This raised total cell number and total macrophage and neutrophil number returned to baseline levels (saline control) at 9 days post intranasal poly (I:C) instillation in mice (figure 4.1).

The relative proportions of the macrophage and neutrophil population were significantly altered at 24 hours post intranasal poly(I:C) instillation compared to saline control mice. Twenty-four hours post intranasal poly(I:C), neutrophil percentage (figure 4.1.e) was significantly increased, and macrophage percentage (figure 4.1.c) significantly decreased when compared to saline control mice before returning to baseline levels.

Twenty-four hours post intranasal poly(I:C) (100μg/50μl) instillation, KC (CXCL1) (figure 4.2.a), TNFα (figure 4.2.b) and IL-6 (figure 4.2.c) were significantly elevated in

BALF compared to intranasal saline control mice. Nine days post intranasal poly(I:C) (100µg/50µl) instillation KC, (CXCL1), TNFα and IL-6 in BALF were significantly reduced compared to 24 hours post poly(I:C) instillation, returning to baseline levels (figure 4.2.).

Twenty-four hours post intranasal poly(I:C) (100µg/50µl) instillation, the number of cells expressing Ly6G (a neutrophil biomarker), iNOS (a M1 macrophage biomarker), and CD206 (a M2 macrophage biomarker) in formalin fixed paraffin embedded (FFPE) lung sections were significantly increased compared to 24 hours post saline intranasal instillation (figure 4.4.a-c). The representative images for this data is presented in figure 4.3.

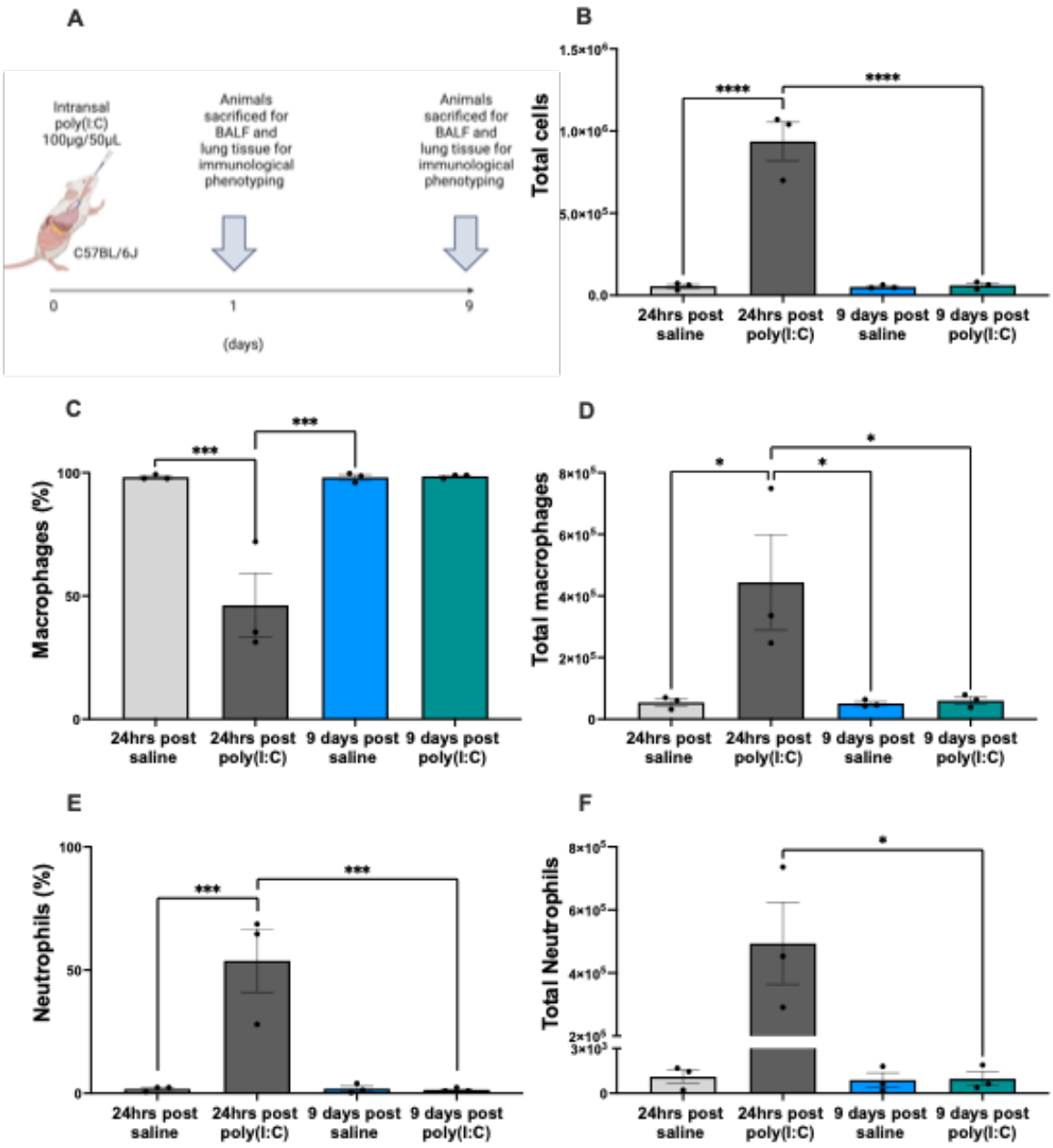

Figure 4.1. Immunological cellular responses measured 24 hours- and 9 days-post intranasal poly(I:C) instillation in bronchoalveolar lavage fluid (BALF) of C57BL/6J mice.

Intranasal poly(I:C) (100µg/50µl) instillation was performed in anaesthetised mice under 1.5–2.0% isoflurane delivered in 100% oxygen with a flow of 2.0 L/min. Animals were sacrificed at 24 hours and 9 days post- intranasal poly(I:C) (or saline) instillation and BALF and lung tissue were harvested at this time (A). Total cell count (B) was measured using a haemocytometer. Total and percentage neutrophil and macrophage (C-F) were measured after cytospin capture and Diff-Quik staining. Three hundred cells (macrophages or neutrophils) were counted per cytospin, and percentage data (C and E) and total cell count (B) were used in combination to extrapolate total macrophages (D) and total neutrophil (F) plots. Data show mean (top of bar) ± SEM. Normality testing, two-way ANOVA and Šídák's multiple comparisons testing conducted. ****, *p.* <0.0001; ***, *p* <0.001; **, *p* <0.01; *, *p* <0.05. *n*=3.

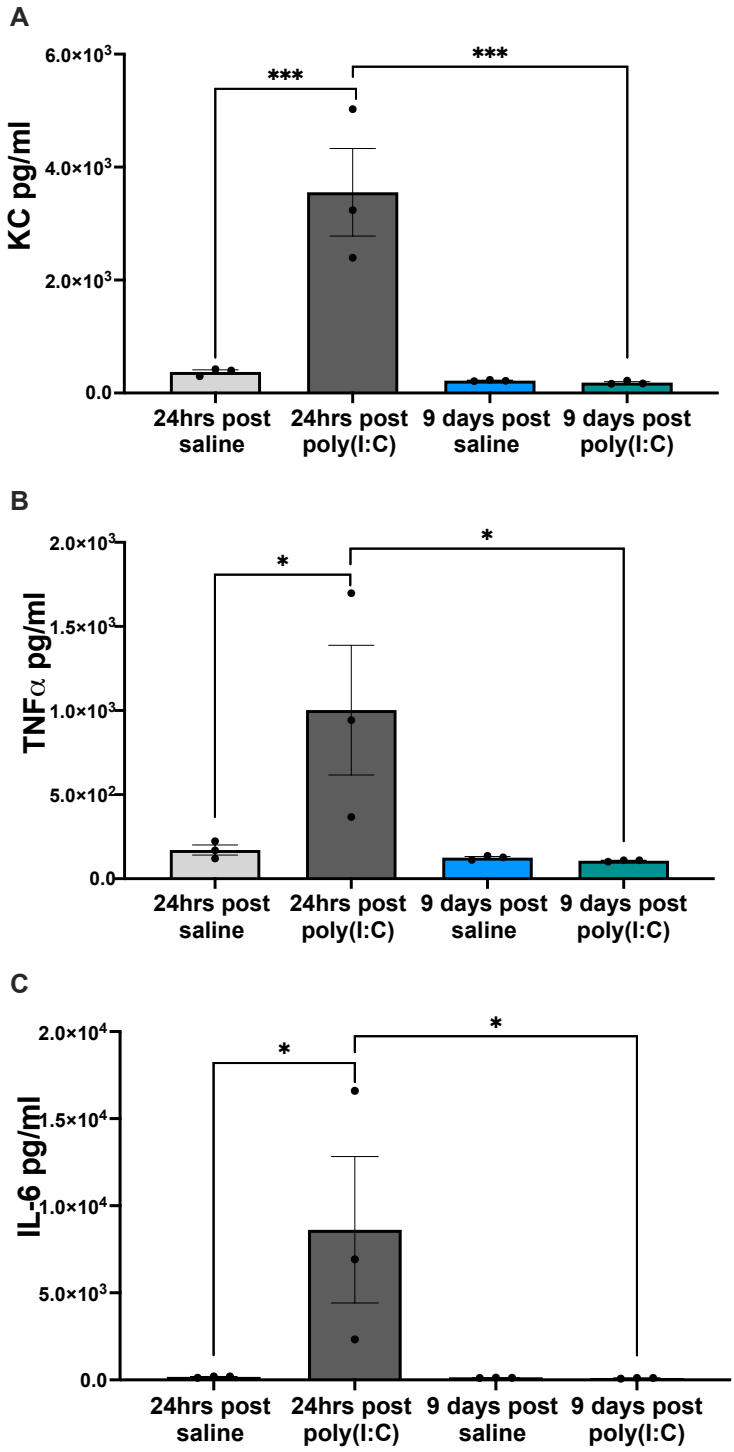

Figure 4.2. Proinflammatory cytokines measured 24 hours- and 9 days- post intranasal poly(I:C) instillation in bronchoalveolar lavage fluid (BALF) of C57BL/6J mice via cytokine bead array using flow cytometer.

Pro-inflammatory cytokines of KC (pg/ml) (A), TNFα (pg/ml) (B) and IL-6 (pg/ml) (C) were measured via flow cytometry technology with a cytometric bead array application, 24 hours- and 9 days- post intranasal instillation of poly(I:C) (100µg/50µl) or saline control (50µl). Data show mean (top of bar) ± SEM. Normality testing, two-way ANOVA and Šídák's multiple comparisons testing conducted ***, p <0.001; *, p <0.05. n=3.

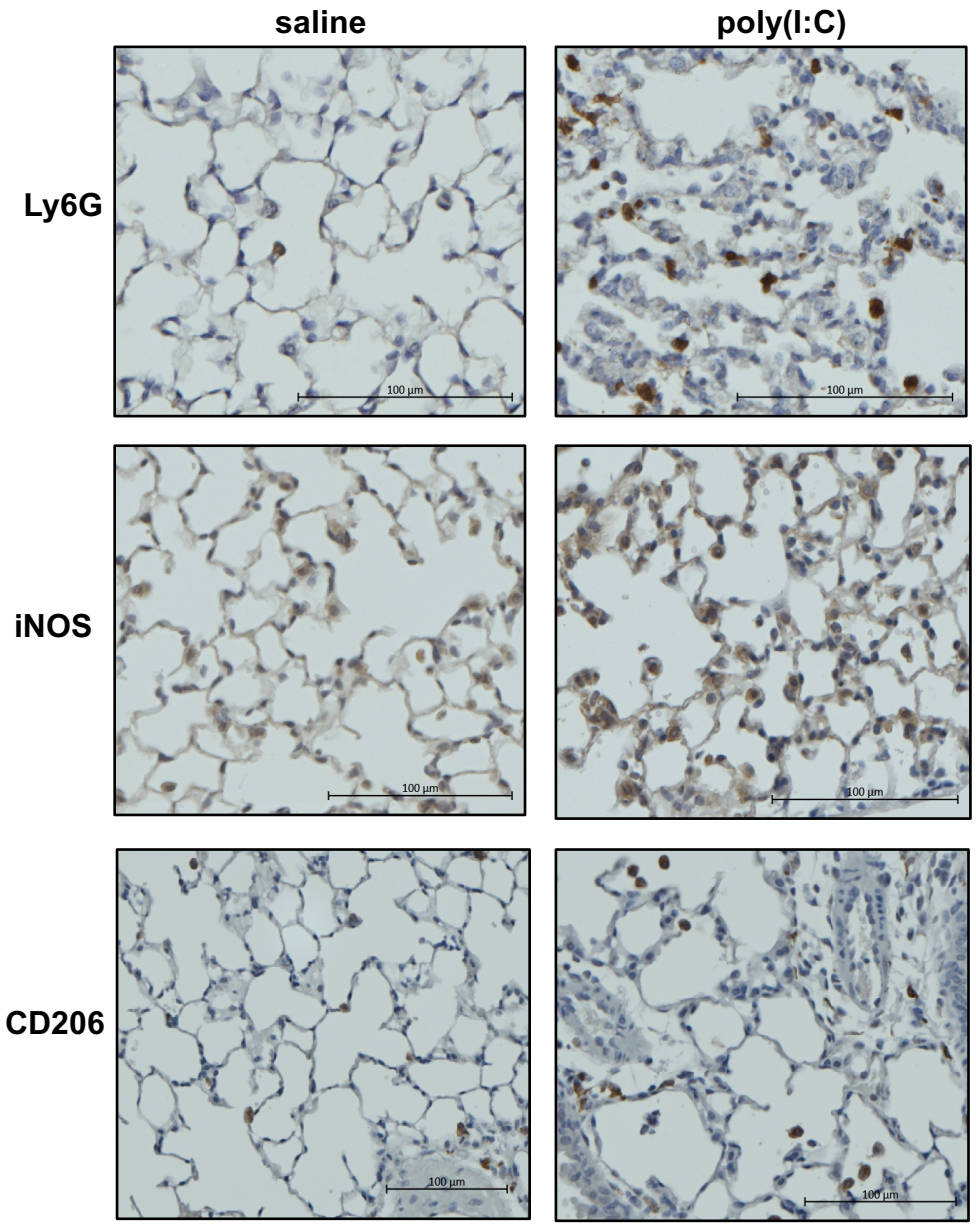

Figure 4.3. Representative images of lung sections stained by indirect immunohistochemistry for Ly6G, iNOS and CD206 from C57BL/6J mice instilled with intranasal poly(I:C) or saline 24 hours prior to lung harvest.

PFFE lung sections from mice that received intranasal poly(I:C) (100µg/50µl) or saline (50µl) instillation, 24 hours prior to lung harvest. Lung sections were stained with Ly6G, iNOS and CD206. Scale bars as indicated.

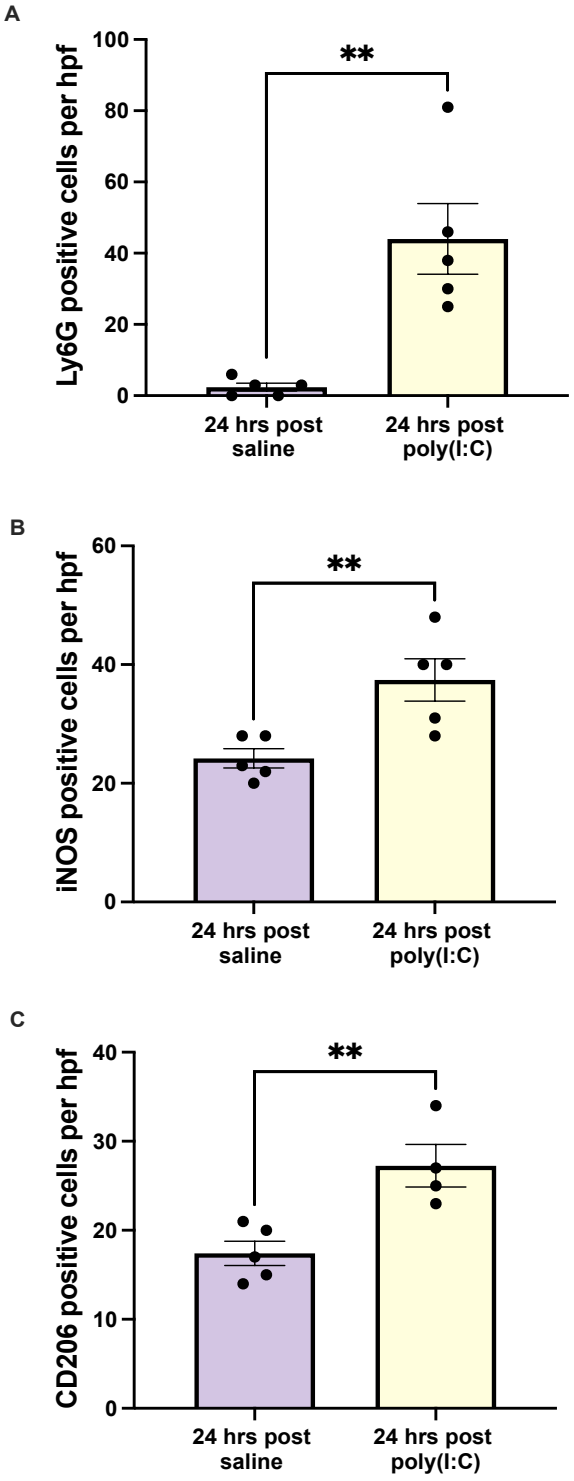

Figure 4.4. Quantification of Ly6G-, iNOS- and CD206- positive cells per high powered field (hpf) in C57BL/6J mice instilled with intranasal poly(I:C) or saline 24 hours prior to lung harvest.

Quantification of Ly6G (A), iNOS (B) and CD206 (C) positive cells per high powered field (hpf) in FFPE lung sections from mice that received intranasal poly(I:C) (100μg/50μl) or saline (50μl) instillation, 24 hours prior to lung harvest. Data show mean (top of bar) ± SEM. Normality testing and unpaired two-tailed t-test conducted. **, p <0.01. Saline, n=5. Poly(I:C), n=4-5.

4.3 Previous exposure to a single intranasal poly(I:C) instillation in a SuHx mouse model of PH exacerbated pulmonary vascular remodelling and resistance but had no effect on PH pressures

In results section 4.2, I established that intranasal poly(I:C) induced biomarkers of innate inflammation in BALF and lung tissue at 24 hours post instillation, before resolving to baseline levels at day 9. Therefore, to investigate how previous poly(I:C)-induced lung inflammation may affect the severity of PH, SuHx was induced 9 days post intranasal poly(I:C) (100μg/50μl) instillation i.e., at the time of known inflammatory resolution. On day 30, PH phenotype was assessed by cardiac catheterisation, pulmonary vascular remodelling, and RV hypertrophy (figure 4.6.a).

SuHx significantly increased right ventricular end-systolic pressure (RVESP) in C57BL/6J mice previously instilled with intranasal saline (mean difference 6.7 mmHg) when compared to normoxic control mice (figure 4.5.c). Aligned with the haemodynamic definition of PAH, LVEDP was unchanged in SuHx control mice compared to normoxic control mice (figure 4.6.b).

In addition, RV dP/dt (figure 4.5.d) was significantly increased and LVEDV (figure 4.6.d), LV cardiac output (figure 4.6.e) and LV stroke volume (RVU) (Figure 4.7.c) were significantly decreased in SuHx control mice compared to normoxic control mice.

Accordingly, SuHx control mice also had significantly more muscularisation of the lung small arterioles (<50μm) as determined by csa/media ratio, quantified from α-SMA staining (figure 4.9.a). The percentage of small arterioles that were fully muscularised (i.e., >50% of the vessel had visible separation of 2 elastic laminae) per 50 discrete

vessels, as identified by ABEVG staining, in SuHx control mice were also significantly increased compared to normoxic control mice (figure 4.9.b). In addition, the RV was significantly muscularised as measured by Fulton Index (i.e., weight ratio of RV /LV+ septum mass) in SuHx control mice compared to normoxic control mice (figure 4.9.c).

Interestingly, SuHx mice previously instilled with intranasal poly(I:C) had significantly increased estimated (e)PVR and ePVRi (index) (figure 4.7.a-b) when compared to SuHx control mice. Furthermore, LV cardiac output (figure 4.6.e) and LV stroke volume (figure 4.7.c) significantly reduced in SuHx mice previously instilled with intranasal poly(I:C) when compared to SuHx control mice.

With the exception of ePVR/i, LV cardiac output and LV stroke volume, all other measured haemodynamic parameters of RV and LV pressures, volume, or contractility measurements (figure 4.5-7) were unchanged in SuHx mice previously instilled with intranasal poly(I:C) compared to SuHx control mice.

In accordance with increased ePVR/i measurements, SuHx mice previously instilled with intranasal poly(I:C) had enhanced muscularisation of lung small arterioles (<50μm), as determined by α-SMA (figure 4.9.a) and ABEVG staining (figure 4.9.b) and enhanced RV hypertrophy (figure 4.9.c) when compared to SuHx control mice.

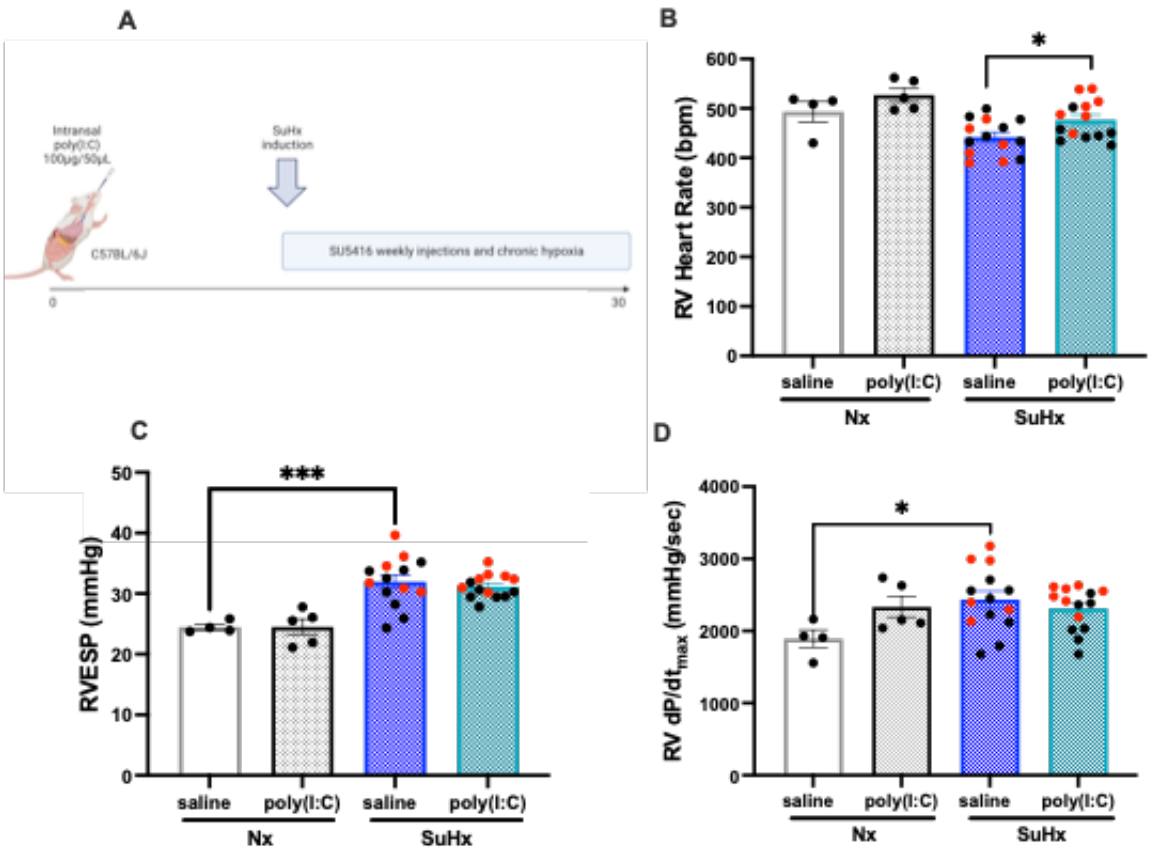

Figure 4.5. Right ventricular pressure measurements in C57BL/6J mice instilled with a single dose of intranasal poly(I:C) (Invivogen) or saline control, 9 days prior to Sugen-hypoxia.

Intranasal poly(:C) (100µg/50µl) instillation was performed in anaesthetised mice under 1.5–2.0% isoflurane delivered in 100% oxygen with a flow of 2.0 L/min, before SuHx was induced 9 days after poly(I:C) instillation. Original image created in Biorender.com (A). Heart rate was continuously recorded throughout right ventricular cardiac catheterisation and the average heart rate (bpm) (B) at the point of pressure-volume loop analysis is presented. Graphs present RVESP (mmHg) (C) and RV dP/dt maximum (mmHg/sec) (D) as acquired by right ventricular cardiac catheterisation via external jugular vein. Data show mean (top of bar) ± SEM. Normality testing, two-way ANOVA and Šídák's multiple comparisons testing conducted. ***, p <0.001; *, p <0.05. n=4-15. Experiment was conducted in 2 batches and experimental batches were grouped by colour (i.e., red, and black). RV; right ventricular. RVESP; right ventricular end systolic pressure. Nx; normoxia. SuHx; Sugen-hypoxia.

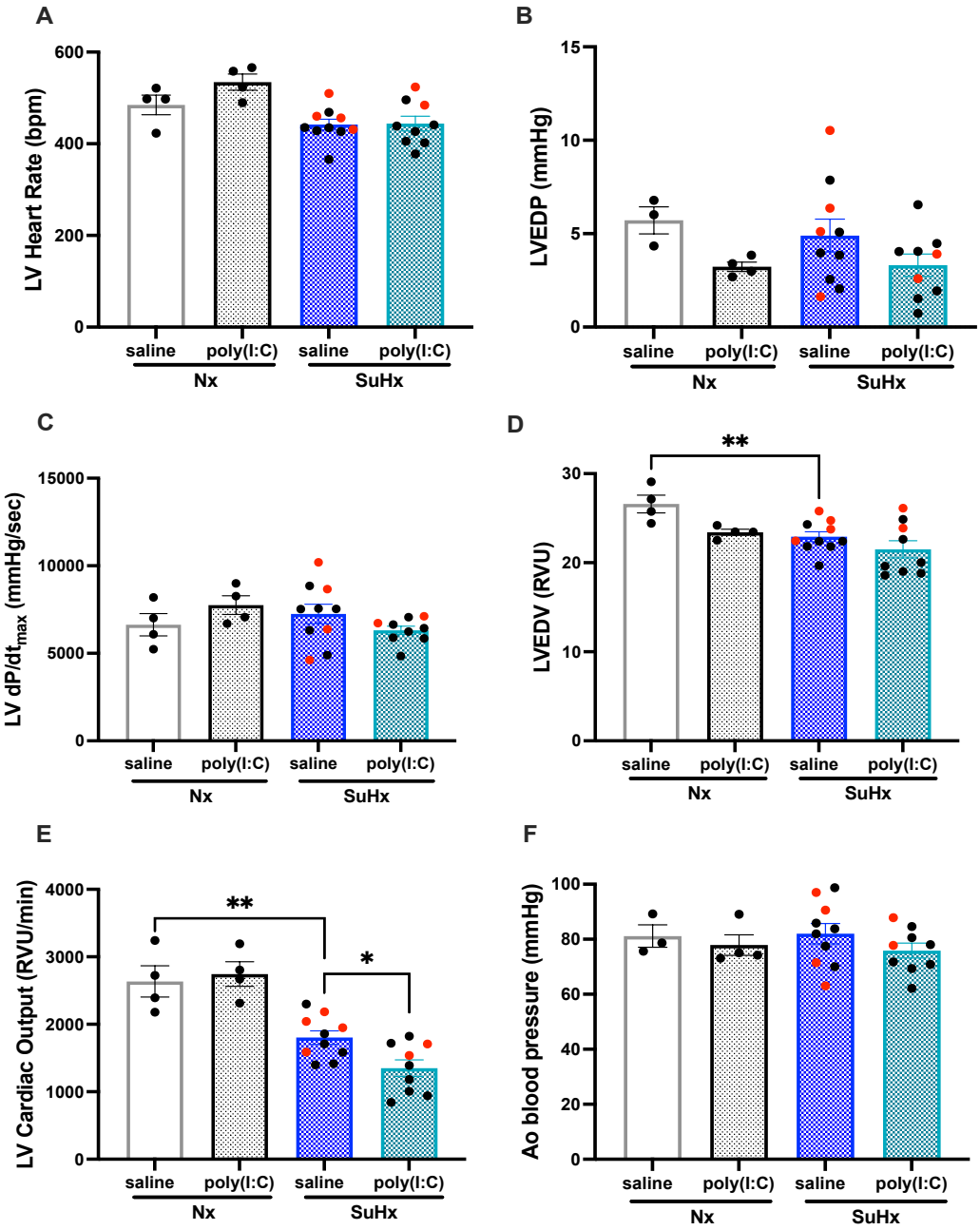

Figure 4.6. Left ventricular haemodynamic measurements and aortic blood pressure in C57BL/6J mice instilled with a single dose of intranasal poly(I:C) (Invivogen) or saline control, 9 days prior to Sugen-hypoxia.

Heart rate was continuously recorded throughout left ventricular cardiac catheterisation and the average heart rate (bpm) (A) at the point of pressure-volume loop analysis is presented. Haemodynamic pressure measurements of LVEDP (mmHg) (B) and LV dP/dt maximum (mmHg/sec) (C) and volumetric measurements of LVEDV (RVU) (D) and LV cardiac output (RVU/min) (E) and aortic blood pressure (mmHg) (F) were acquired by left ventricular cardiac catheterisation via the left common carotid artery. Normality testing, two-way ANOVA and Šídák's multiple comparisons testing conducted. **, p <0.01; *, p <0.05. n=3-9. Experiment was conducted in 2 batches and experimental batches were grouped by colour (i.e., red, and black). LV; left ventricular. RVU; relative volume units. Nx; normoxia. SuHx; Sugen-hypoxia. Ao; Aortic.

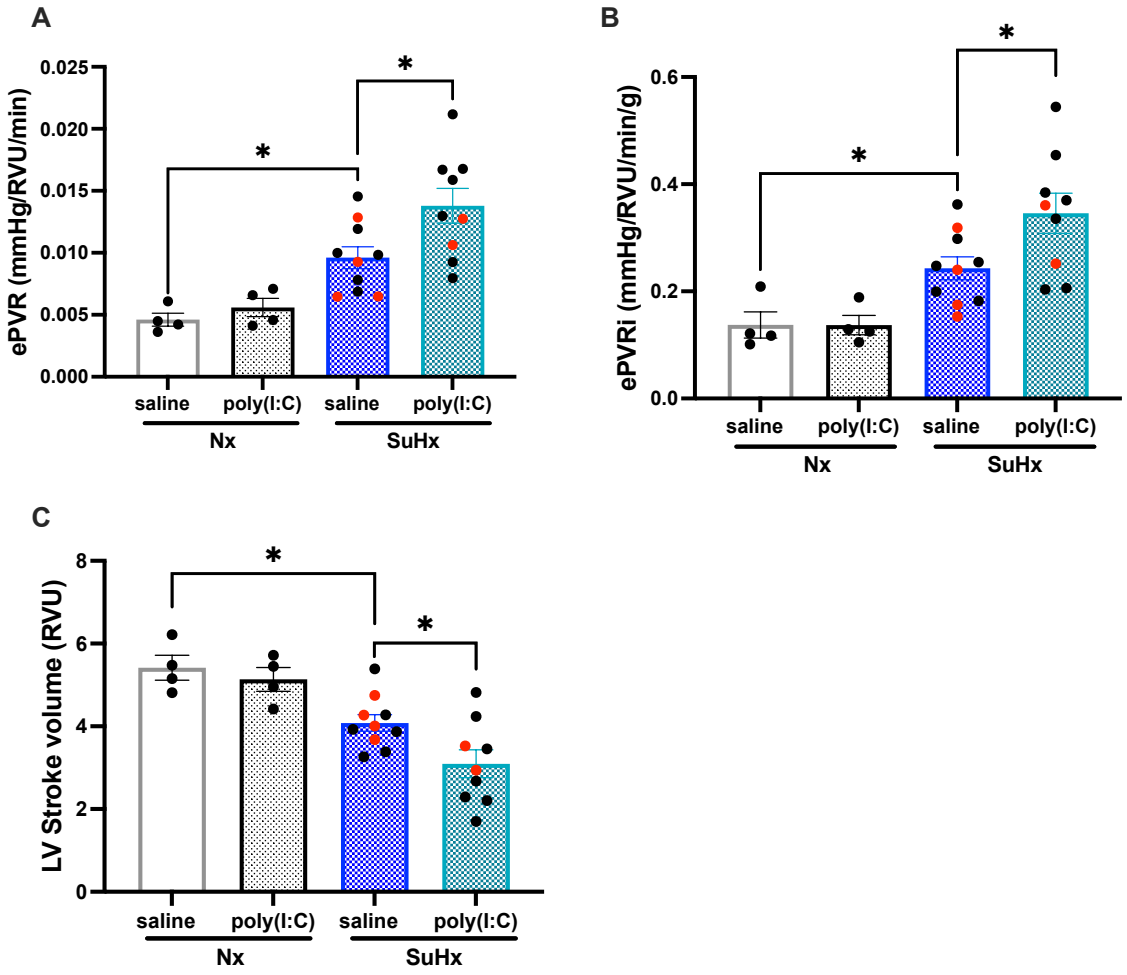

Figure 4.7. Estimated pulmonary vascular resistance and left ventricular stroke volume in C57BL/6J mice instilled with a single dose of intranasal poly(I:C) (Invivogen) or saline control, 9 days prior to Sugen-hypoxia.

Graphs present estimated- PVR (ePVR) (A) and -PVR index (ePVRi) (B) acquired by right and left ventricular cardiac catheterisation and calculated using the equation: (estimated mean pulmonary artery pressure (emPAP)- left ventricular end diastolic pressure (LVEDP)/ LV cardiac output or cardiac index). LV stroke volume (C) presented which is used to calculate LV cardiac output used in ePVR (A) and ePVRi (B) equations i.e., LV cardiac output = heart rate x LV stroke volume. Normality testing, two-way ANOVA and Šídák's multiple comparisons testing conducted. *, p <0.05. n=4-15. Experiment was conducted in 2 batches and experimental batches were grouped by colour (i.e., red, and black). RV; right ventricular. ePVRi; estimated pulmonary vascular resistance/index. RVU; relative volume units. Nx; normoxia. SuHx; Sugen-hypoxia.

.

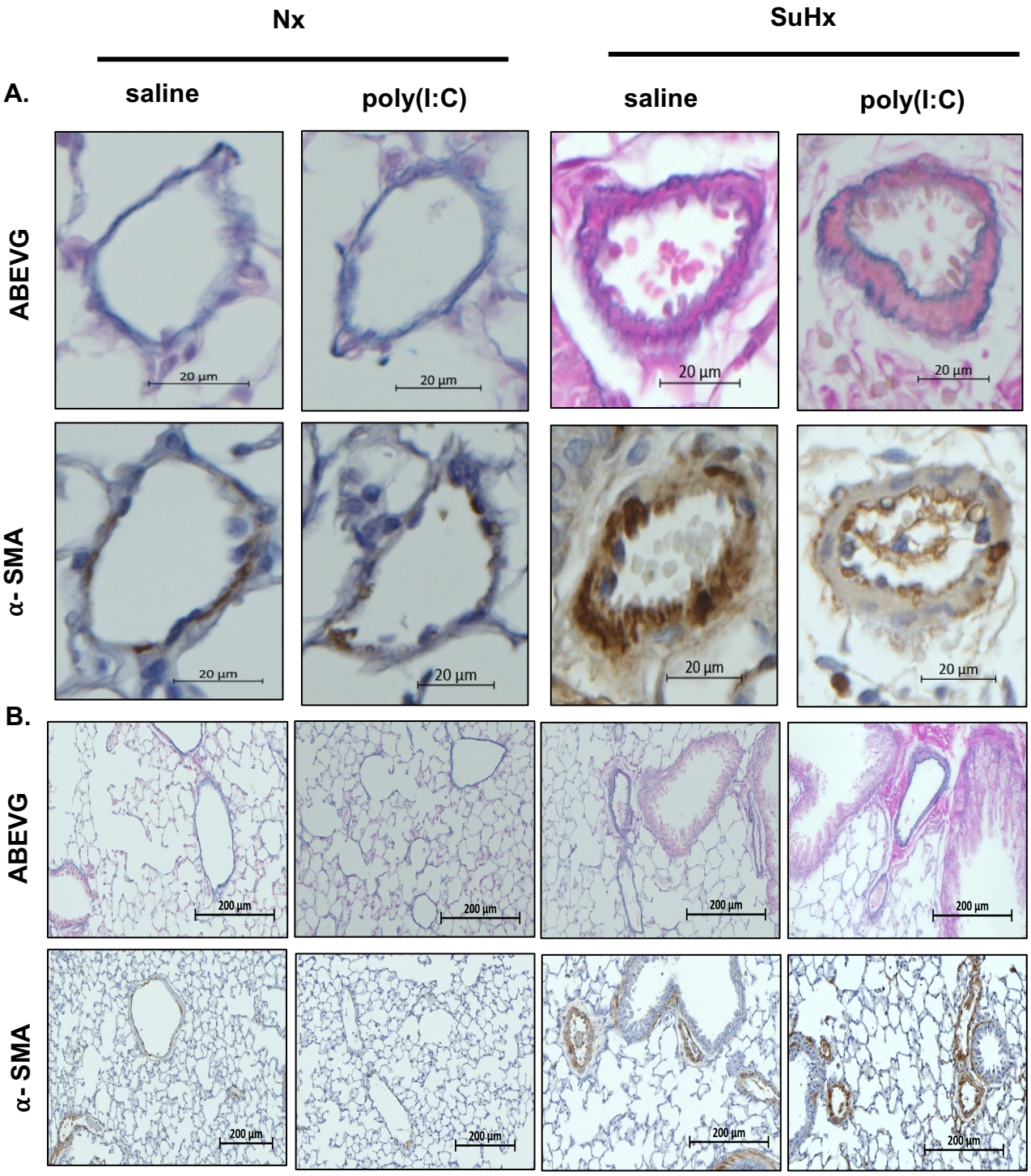

Figure 4.8. Representative images of distal (A) and proximal (B) pulmonary vasculature in FFPE lung sections of C57BL/6J mice treated with a single dose of intranasal poly(I:C) (Invivogen) or saline control, 9 days prior to Sugen-hypoxia.

FFPE lung sections were tinctorial stained with ABEVG or indirectly immunostained with α-SMA. Morphometry was conducted on arterioles that were <50µm in diameter. Nx; normoxia. SuHx; Sugen-hypoxia. FFPE; formalin fixed paraffin embedded. ABEVG; Miller's elastin stain with alcian blue and Curtis modified van Gieson. α-SMA; Alpha smooth muscle actin. Scale bars as indicated.

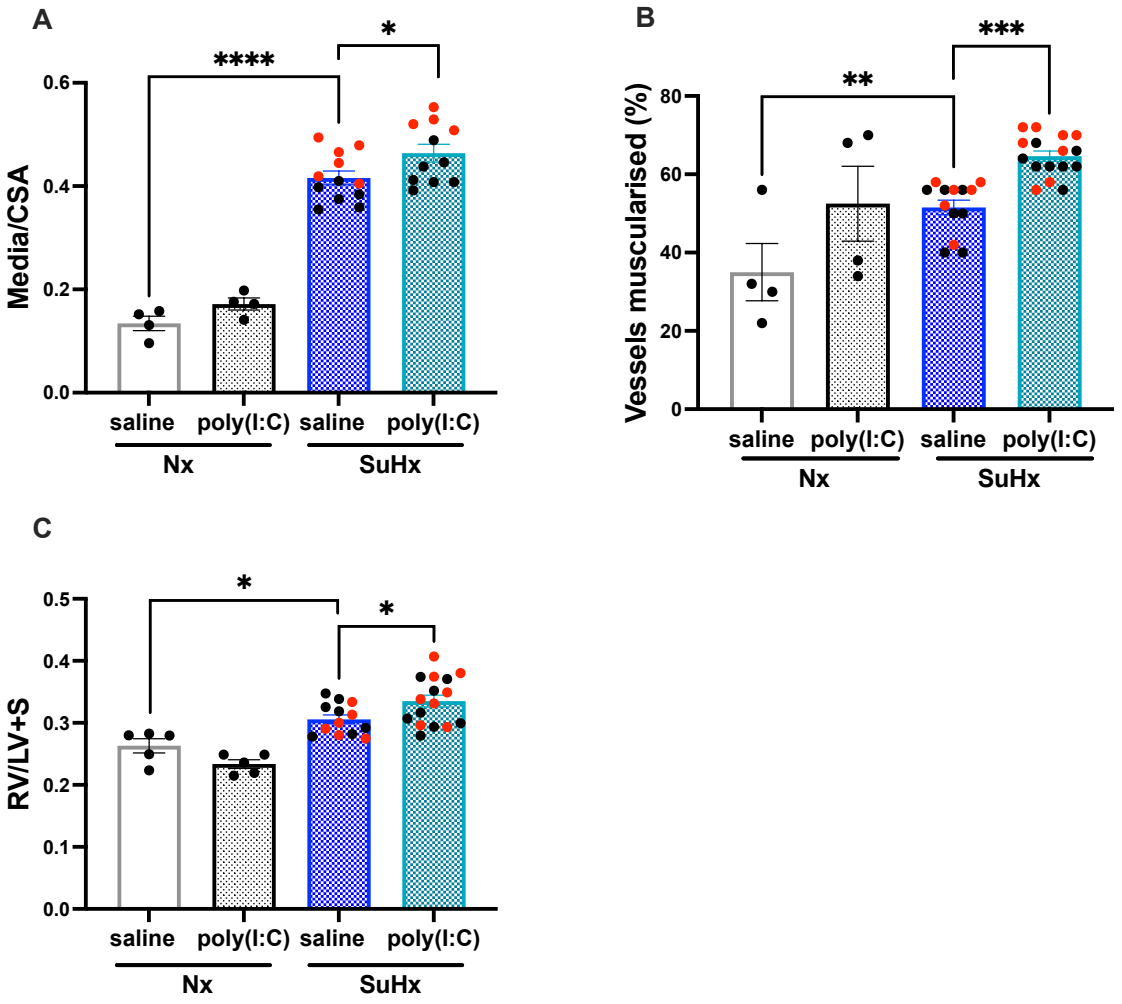

Figure 4.9. Pulmonary vascular morphometric analysis of FFPE lung sections and right ventricular hypertrophy analysis from C57BL/6J mice instilled with a single dose of intranasal poly(I:C) (Invivogen) or saline control, 9 days prior to Sugen-hypoxia.

Pulmonary vascular remodelling was quantified by the proportion of muscularised arterioles (<50μm diameter) in FFPE lung sections stained with medial area to cross-sectional area (CSA) ratio for muscularised arterioles in FFPE lung section immunostained indirectly with α-smooth muscle actin (α-SMA) (A) and ABEVG staining (B). Hearts were dissected and chambers compartmentalised, and right ventricular free wall weight was normalised to left ventricle plus septum weight (RV/LV+S) to measure ventricular hypertrophy (C). Normality testing, two-way ANOVA and Šídák's multiple comparisons testing conducted.****, *p.* <0.0001; ***, *p.* <0.001; **, *p* <0.01; *, *p* <0.05. *n*=4-16. Experiment was conducted in 2 batches and experimental batches were grouped by colour (i.e., red, and black).

4.4 A previous instillation of intranasal poly(I:C) alters lung inflammation in response to a subsequent instillation of poly(I:C) in C57BL/6J mice

To model repeated incidences of lung inflammation, I then assessed immunological responses in lung airways in response to repeated intranasal poly(I:C) (100μg/50μl) instillations and compared these data with immunological responses in lung airways after one intranasal poly(I:C) instillation. Specifically, intranasal poly(I:C) was instilled on day 0 and 9 (two doses i.e., repeated instillation), or day 9 only (one dose), and mice were sacrificed on day 10 (i.e., 24 hours after poly(I:C) instillation) or day 18 (i.e., 9 days after poly(I:C) instillation), before BALF or lung tissue was harvested for immunological phenotyping (figure 4.10.a).

Total cell count in BALF was not altered at 24 hours after two doses of intranasal poly(I:C) instillations compared to 24 hours post one dose of intranasal poly(I:C) (figure 4.10.b). Neutrophil percentage was significantly reduced at 24 hours post two doses of intranasal poly(I:C) instillations compared to 24 hours post one dose of intranasal poly(I:C) (figure 4.10.e). Macrophage percentage and total macrophage count was significantly increased at 24 hours post two doses of intranasal poly(I:C) instillations compared to 24 hours post one dose of intranasal poly(I:C) (figure 4.10.c-d). Total cell count, total macrophages and neutrophils and percentage macrophages and neutrophils in BALF were significantly different at 9 days post 2 doses of intranasal poly(I:C) compared to 24 hours post 2 doses of poly(I:C) (figure 4.10 b-f).

Via a flow cytometry approach, IL-6 pg/ml (figure 4.11.b) and TNFα pg/ml (figure 4.11.c) measured in BALF were significantly reduced at 24 hours post two doses of intranasal poly(I:C) instillations compared to 24 hours post one dose of intranasal

poly(I:C). A trend towards KC pg/ml (figure 4.11.a) reduction in BALF at 24 hours post two doses of intranasal poly(I:C) instillations compared to 24 hours post one dose of intranasal poly(I:C) was measured but statistical significance at a 95% confidence interval was not reached, possibly owed to large variability in data points of KC pg/ml at 24 hours post one dose of intranasal poly(I:C).

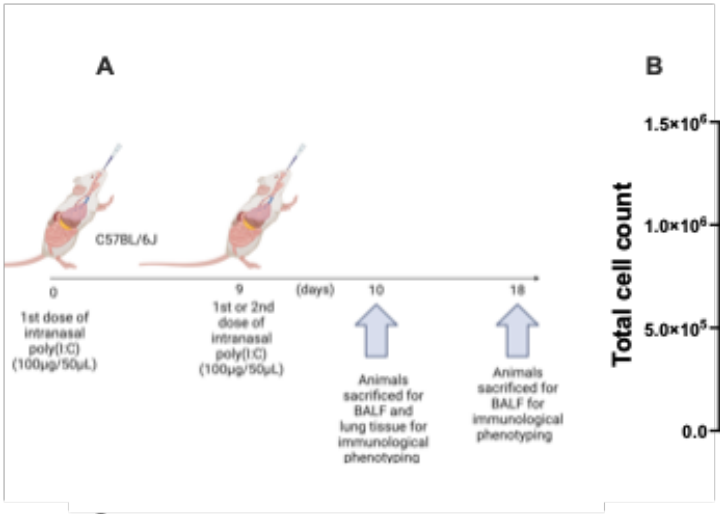
A
C57BL/6J
0
1st dose of intranasal poly(I:C) (100µg/50µL)
9
1st or 2nd dose of intranasal poly(I:C) (100µg/50µL)
(days)
10
Animals sacrificed for BALF and lung tissue for immunological phenotyping
18
Animals sacrificed for BALF for immunological phenotyping

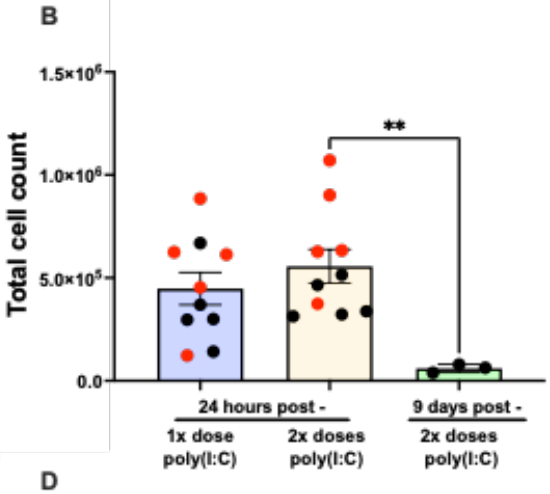
B
Total cell count
1.5×10⁶
1.0×10⁶
5.0×10⁵
0.0
**
24 hours post -
1x dose poly(I:C)
2x doses poly(I:C)
9 days post -
2x doses poly(I:C)

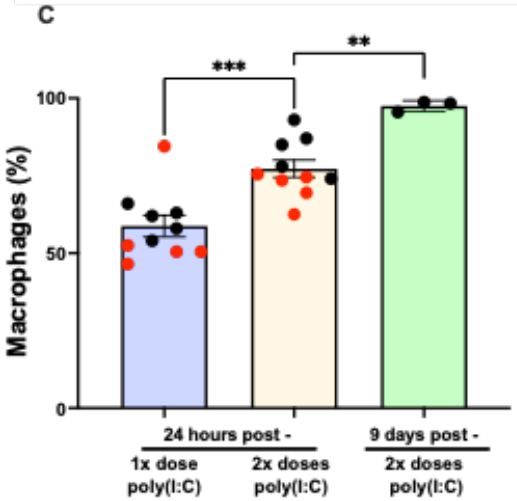
C
Macrophages (%)
100
50
0
***
**
24 hours post -
1x dose poly(I:C)
2x doses poly(I:C)
9 days post -
2x doses poly(I:C)

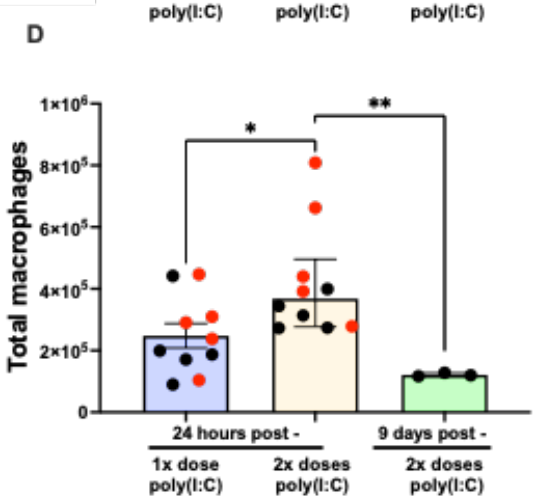
D
Total macrophages
1×10⁶
8×10⁵
6×10⁵
4×10⁵
2×10⁵
0
*
**
24 hours post -
1x dose poly(I:C)
2x doses poly(I:C)
9 days post -
2x doses poly(I:C)

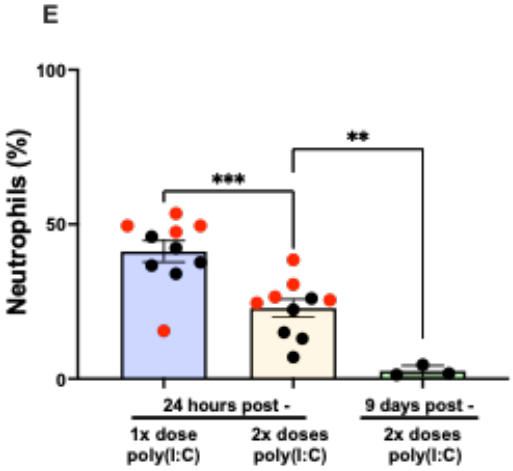
E
Neutrophils (%)
100
50
0
***
**
24 hours post -
1x dose poly(I:C)
2x doses poly(I:C)
9 days post -
2x doses poly(I:C)

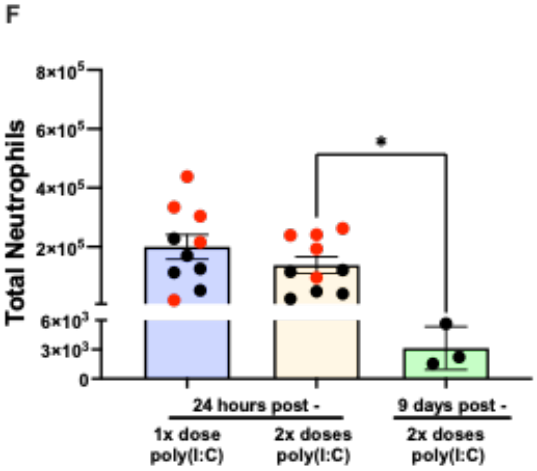
F
Total Neutrophils
8×10⁵
6×10⁵
4×10⁵
2×10⁵
6×10³
3×10³
0
*
24 hours post -
1x dose poly(I:C)
2x doses poly(I:C)
9 days post -
2x doses poly(I:C)

Figure. 4.10 Comparison of bronchoalveolar lavage fluid (BALF) cellular responses measured at 24 hours or 9 days after one dose or two doses (9 days apart) of intranasal poly(I:C).

Intranasal poly(I:C) (100μg/50μl) was instilled on day 0 and 9, or day 9 only, in anaesthetised C57BL/6J mice. All mice were sacrificed on day 10 or day 18 (i.e., 24 hours or 9 days after poly(I:C) instillation), before BALF or lung tissue was harvested for immunological phenotyping (A). Total cell count (B) was measured using a haemocytometer. Total and percentage neutrophil and macrophage (C-F) were measured after cytospin capture and Diff-Quik staining. Three hundred cells (macrophages or neutrophils) were counted per cytospin, and percentage data (C and E) and total cell count (B) were used in combination to extrapolate total macrophages (C) and total neutrophil (E) plots. Normality testing conducted. Unpaired two-tailed t-test and mean (top of bar) ± SEM recorded in B-C, E-F. Unpaired two-tailed Mann-Whitney test and median (top of bar) with interquartile range recorded in D. ***, *p.* <0.001; **, *p* <0.01. *n*=3-10. Experiment was conducted in 2 batches and experimental batches are grouped by colour (i.e., red, and black).

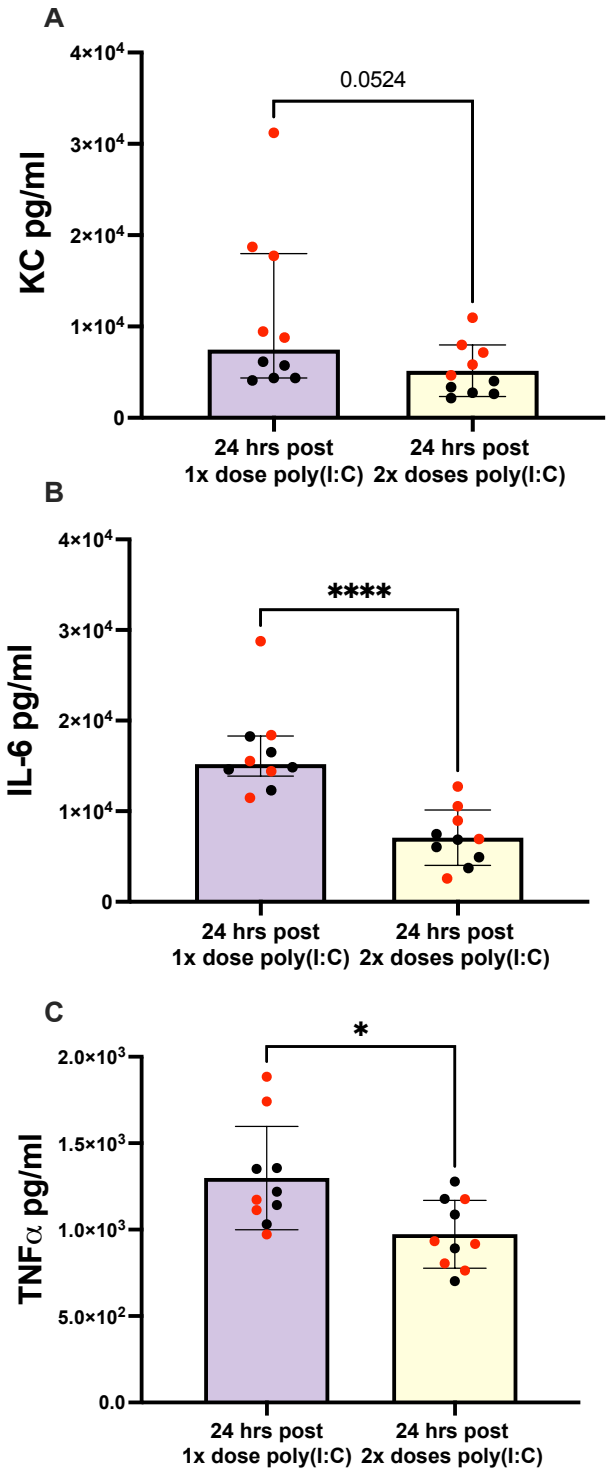

Figure 4.11 Comparison of cytokine responses measured 24 hours- post one or two doses of intranasal poly(I:C) (9 days apart) instillation in bronchoalveolar lavage fluid (BALF) of C57BL/6J mice.

Pro-inflammatory cytokines of KC (pg/ml) (A), IL-6 (pg/ml) (B) and TNFα (pg/ml) (C) were measured via flow cytometry technology with a cytometric bead array application. Normality testing and unpaired two-tailed t-test (A) or Mann-Whitney tests (B-C) were conducted. Data show mean (top of bar) ± SEM (A) and median (top of bar) with IQR (B-C). ****, p <0.0001; *, p <0.05. n=10. Experiment was conducted in 2 batches and experimental batches are grouped by colour (i.e., red, and black).

4.5 Previous repeated exposure of intranasal poly(I:C), with unresolved inflammation, does not alter severity of PH or pulmonary vascular remodelling in the SuHx mouse model

In section 4.4, I showed that previous exposure to intranasal poly(I:C) altered the lung airway innate inflammatory response to a second dose of intranasal poly(I:C). Considering a reduction in macrophages and an altered M1/M2 ratio is associated with the development of PH in male mice (Zawia et al., 2020), I aimed to investigate whether previous repeated exposure of intranasal poly(I:C) affects the SuHx mouse model of PH. To do this, C57BL/6J mice were instilled with intranasal poly(I:C) on day 0 and 9 and SuHx was induced on day 10. The PH phenotype was assessed by cardiac catheterisation, pulmonary vascular remodelling, and RV hypertrophy. Intranasal saline instillations were completed as a control (figure 4.12.a).

Previous repeated doses of poly(I:C), with unresolved airway inflammation at the point of SuHx induction, did not affect RV and LV haemodynamic measurements of pressure, contractility, estimated resistance, or volume (figure 4.12-14). Average heart rate at the time of RV pressure-volume loop analysis was higher (figure 4.12.b) in SuHx mice previously instilled with repeated doses of intranasal poly(I:C) compared to SuHx control mice, thus a confounder when interpreting these haemodynamic data. Of note, LV heart rate (figure 4.13.a) was unchanged in SuHx mice that were previously instilled with repeated doses of intranasal poly(I:C) when compared to SuHx control mice providing more robust data interpretation of LV haemodynamics than RV haemodynamics. Consistent with haemodynamic data, pulmonary arteriole muscularisation assessed by ABEVG staining (figure 4.16.a) and α-SMA staining (figure 4.16.b) and RV hypertrophy (figure 4.16.c) were also unchanged in SuHx mice

previously instilled with repeated dose of intranasal poly(I:C) compared to SuHx control mice.

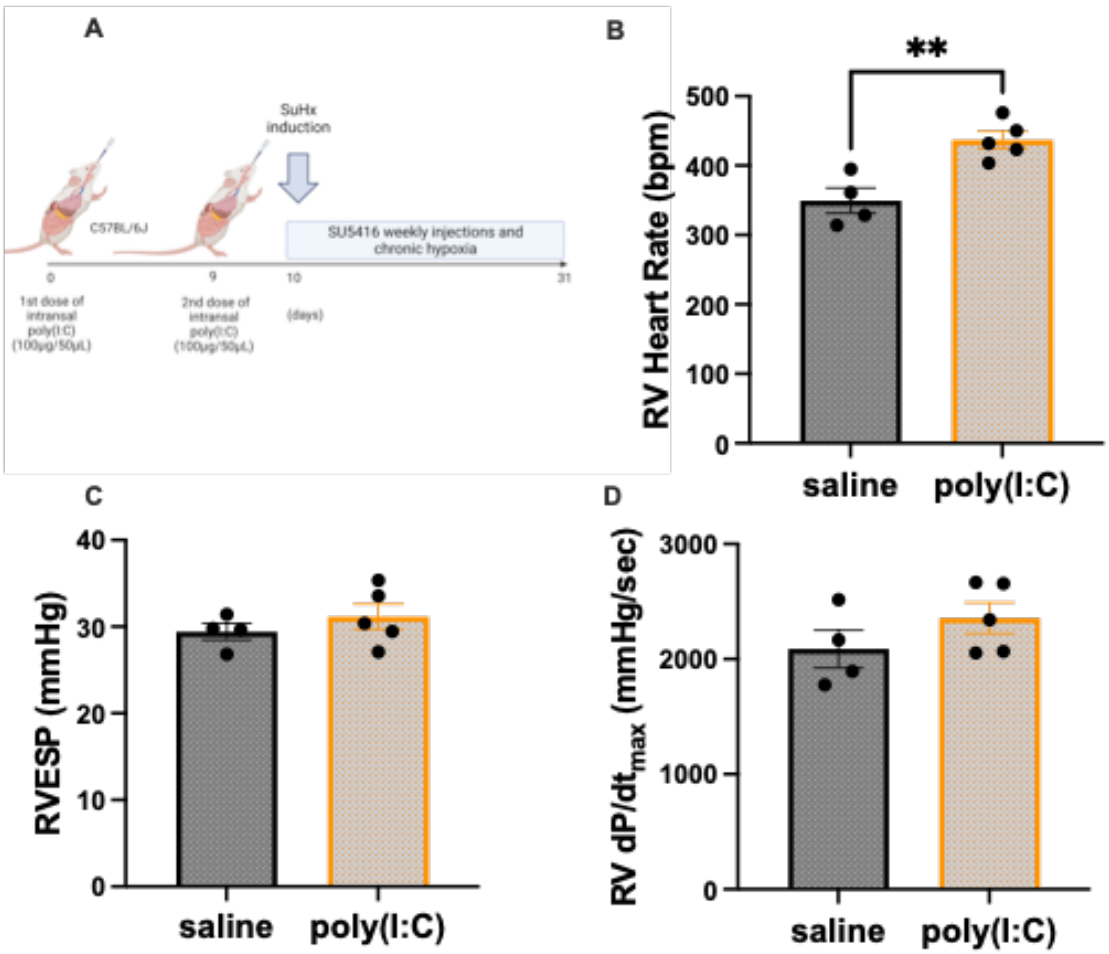

Figure 4.12 Right ventricular pressure measurements in C57BL/6J mice instilled with repeated doses of intranasal poly(I:C) (Invivogen) or saline, 24 hours prior to Sugen-hypoxia.

Intranasal poly(:C) (100µg/50µl) instillations were performed in anaesthetised mice under 1.5–2.0% isoflurane delivered in 100% oxygen with a flow of 2.0 L/min on day 0 and 9, before SuHx was induced on day 10. Original image created in Biorender.com (A). Heart rate was continuously recorded throughout right cardiac catheterisation and the average heart rate (bpm) (B) at the time of pressure-volume loop analysis are presented. Graphs presents parameters of RVESP (C), and RV dP/dt maximum (mmHg/sec) (D) as acquired by right ventricular cardiac catheterisation via external jugular vein. Data show mean (top of bar) ± SEM. Normality testing and unpaired two-tailed t-test conducted. **, p <0.01. n=4-5. RV; right ventricular. RVESP; right ventricular end systolic pressure. SuHx; Sugen-hypoxia.

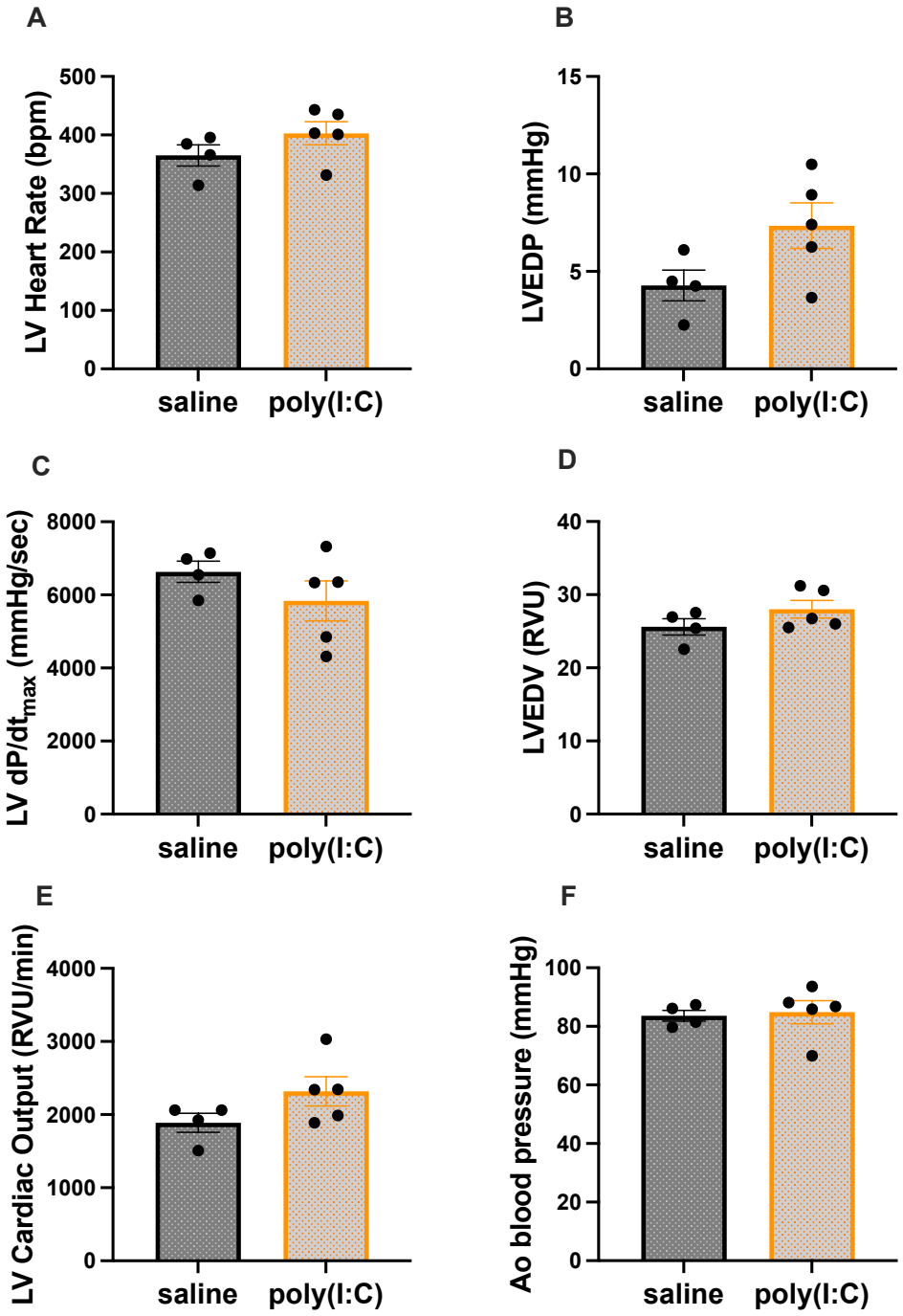

Figure 4.13 Left ventricular haemodynamic measurements and aortic blood pressure in C57BL/6J mice instilled with repeated doses of intranasal poly(I:C) (Invivogen) or saline, 24 hours prior to Sugen-hypoxia.

Heart rate was continuously recorded throughout left cardiac catheterisation and the average heart rate (bpm) (A) at the time of pressure-volume loop analysis are represented. Graphs present LVEDP (mmHg) (B), LV dP/dt maximum (mmHg/sec) LVEDV (RVU) (D), LV cardiac output (RVU/min) (E) and aortic blood pressure (mmHg) (F) were measured by left ventricular cardiac catheterisation via the left common carotid artery Data show mean (top of bar) ± SEM. Normality testing and unpaired two-tailed t-test conducted. *n*=4-5 LV; left ventricular. RVU; relative volume units. Ao; Aortic.

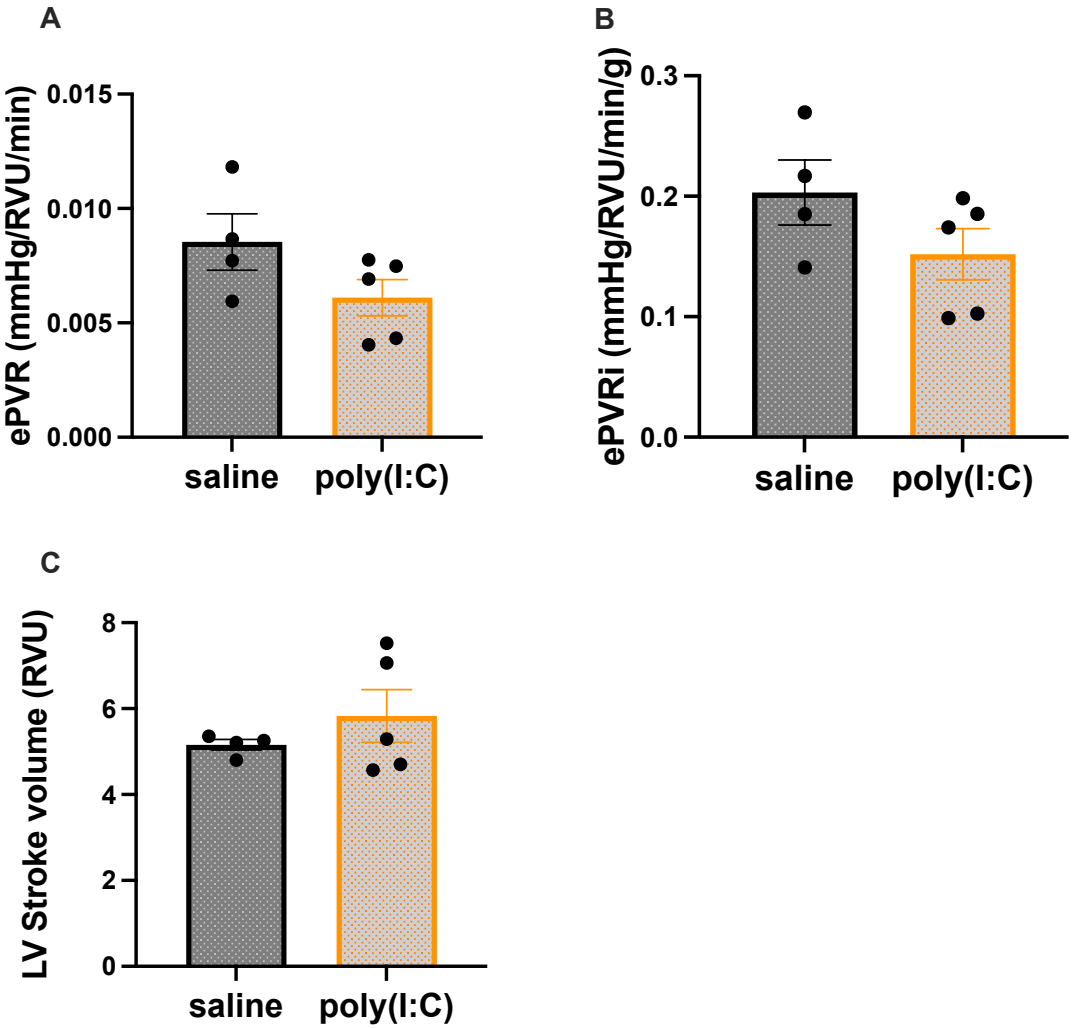

Figure 4.14. Estimated pulmonary vascular resistance and right ventricular contractility and volume measurements in C57BL/6J mice instilled with repeated doses of intranasal poly(I:C) (Invivogen) or saline, 24 hours prior to Sugen-hypoxia.

As previous experimental design, graphs present estimated(e)- PVR (A) and PVR index acquired by right and left ventricular cardiac catheterisation and calculated using the equation: (estimated mean pulmonary artery pressure (emPAP)- left ventricular end diastolic pressure (LVEDP)/ LV cardiac output or cardiac index). Graph presents LV stroke volume (RVU) (C). Data show mean (top of bar) ± SEM. Normality testing and unpaired two-tailed t-test conducted. *n*=4-5 LV; left ventricular. RVU; relative volume units. PVR; pulmonary vascular resistance.

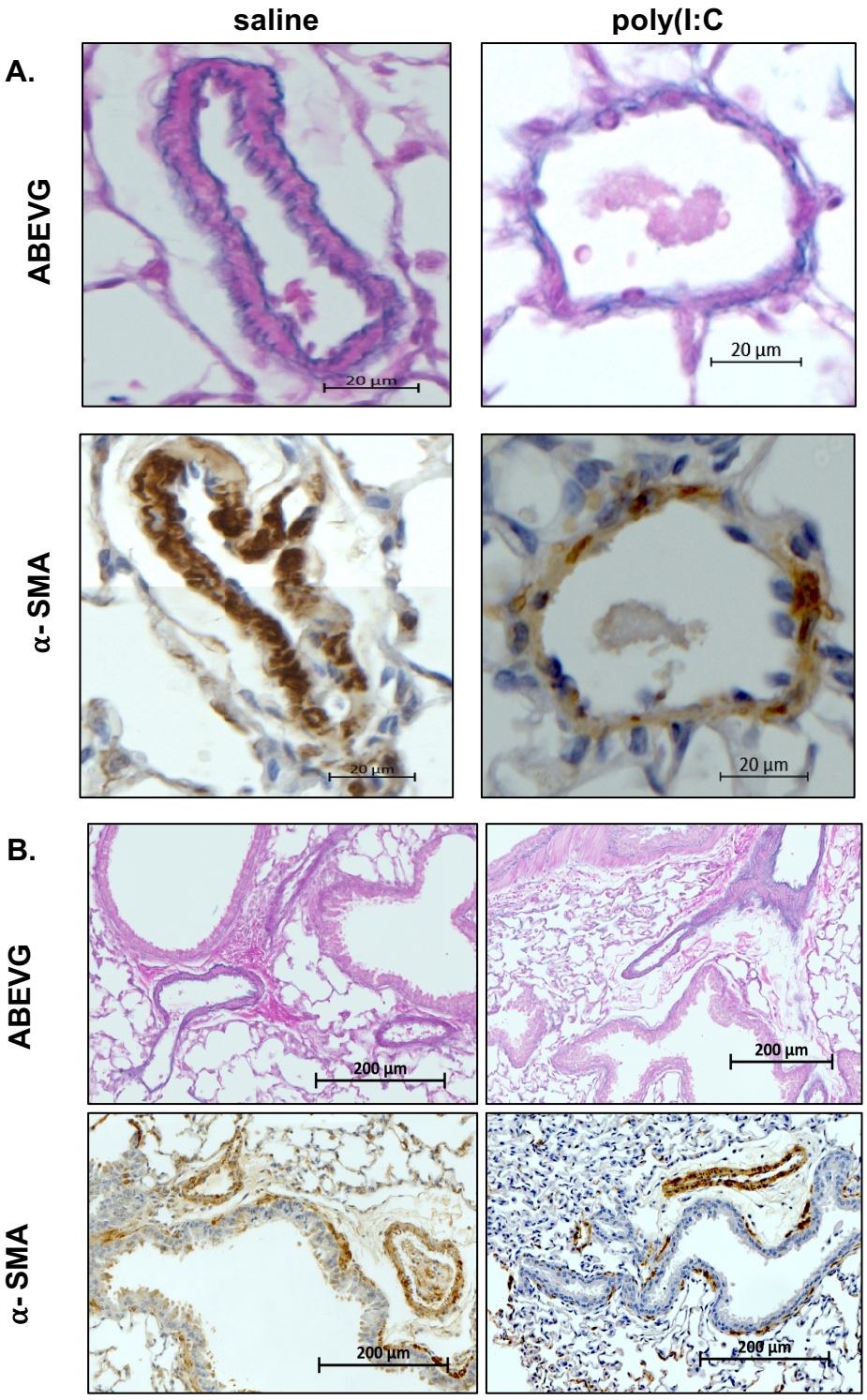

Figure 4.15 Representative images of distal (A) and proximal (B) pulmonary vasculature in FFPE lung sections of C57BL/6J mice instilled with repeated doses of intranasal poly(I:C) (Invivogen) or saline, 24 hours prior to Sugen-hypoxia.

FFPE lung sections were stained with ABEVG or indirectly immunostained with α-SMA. Morphometry was conducted on arterioles that were <50µm in diameter. Nx; normoxia. SuHx; Sugen-hypoxia. FFPE; formalin fixed paraffin embedded. ABEVG; Miller's elastin stain with alcian blue and Curtis' modified van Gieson. α-SMA; Alpha smooth muscle actin. Scale bars as indicated.

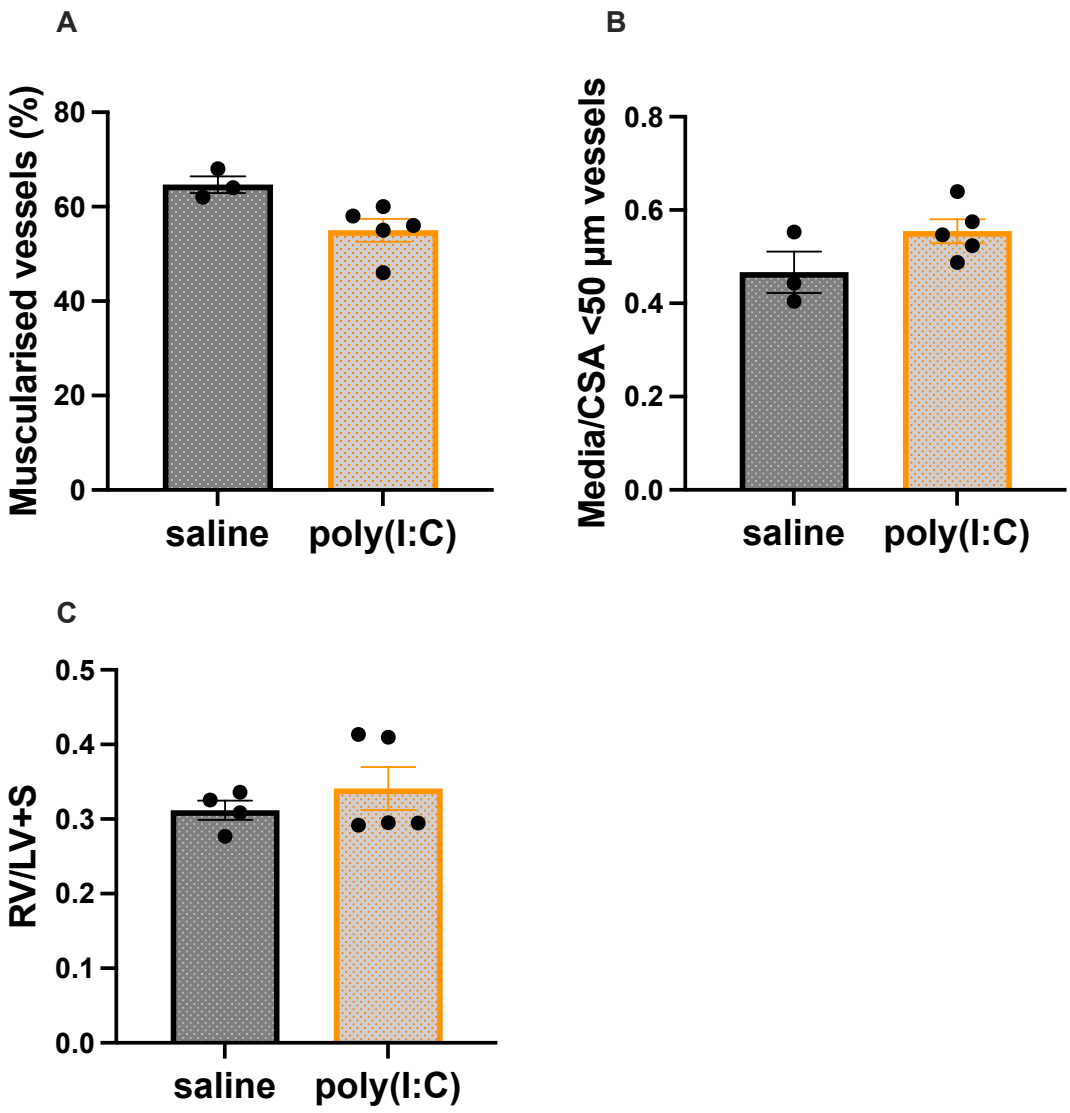

Figure 4.16 Pulmonary vascular morphometric analysis of FFPE lung sections and right ventricular hypertrophy analysis from C57BL/6J mice instilled with repeated doses of intranasal poly(I:C) (Invivogen) or saline, 24 hours prior to Sugen-hypoxia.

Pulmonary vascular remodelling was quantified by the proportion of muscularised arterioles (<50μm diameter) in FFPE lung sections stained with ABEVG (A) and medial area to cross-sectional area (CSA) ratio for muscularised arterioles in FFPE lung sections immunostained indirectly with α-smooth muscle actin (α-SMA) (B). Hearts were dissected and chambers compartmentalised, and right ventricular free wall weight was normalised to left ventricle plus septum weight (RV/LV+S) to measure ventricular hypertrophy (C). Data show mean (top of bar) ± SEM. Normality testing and unpaired two-tailed t-test (A-B) or Mann-Whitney test (C) conducted. *n*=3-5.

4.6 Previous repeated exposure of intranasal poly(I:C) with resolved inflammation does not alter severity of PH or pulmonary vascular remodelling in the SuHx mouse model

To investigate the effect of previous repeated intranasal poly(I:C) instillations, with resolved airway inflammation at the time of SuHx induction, C57BL/6J mice were instilled with intranasal poly(I:C) (100μg/50μl) on day 0 and 9 and SuHx was induced on day 18 i.e., 9 days after the latter instillation; the time of known lung inflammatory cell resolution. The PH phenotype was assessed by cardiac catheterisation, pulmonary vascular remodelling, and RV hypertrophy. Intranasal saline instillations were completed as a control (figure 4.17.a).

Previous repeated instillations of intranasal poly(I:C), with resolved airway inflammation at the time of SuHx induction, did not affect RV and LV haemodynamic measurements of pressure, contractility, estimated resistance, or volume (figure 4.17-19). Haemodynamic data was consistent with pulmonary vascular remodelling as assessed by ABEVG staining (figure 4.21.a) and α-SMA staining (figure 4.21.b) and RV hypertrophy (figure 4.21.c). All of which were unaffected by previous repeated instillations of intranasal poly(I:C) compared to saline control in SuHx mice.

Like in section 4.3 and 4.5, the average heart rate at the point of RV pressure-volume loop analysis was significantly raised in SuHx mice previously instilled with repeated doses of intranasal poly(I:C) compared to SuHx control mice. As stated previously this is a confounder when interpreting RV haemodynamic data (figure 4.17.a).

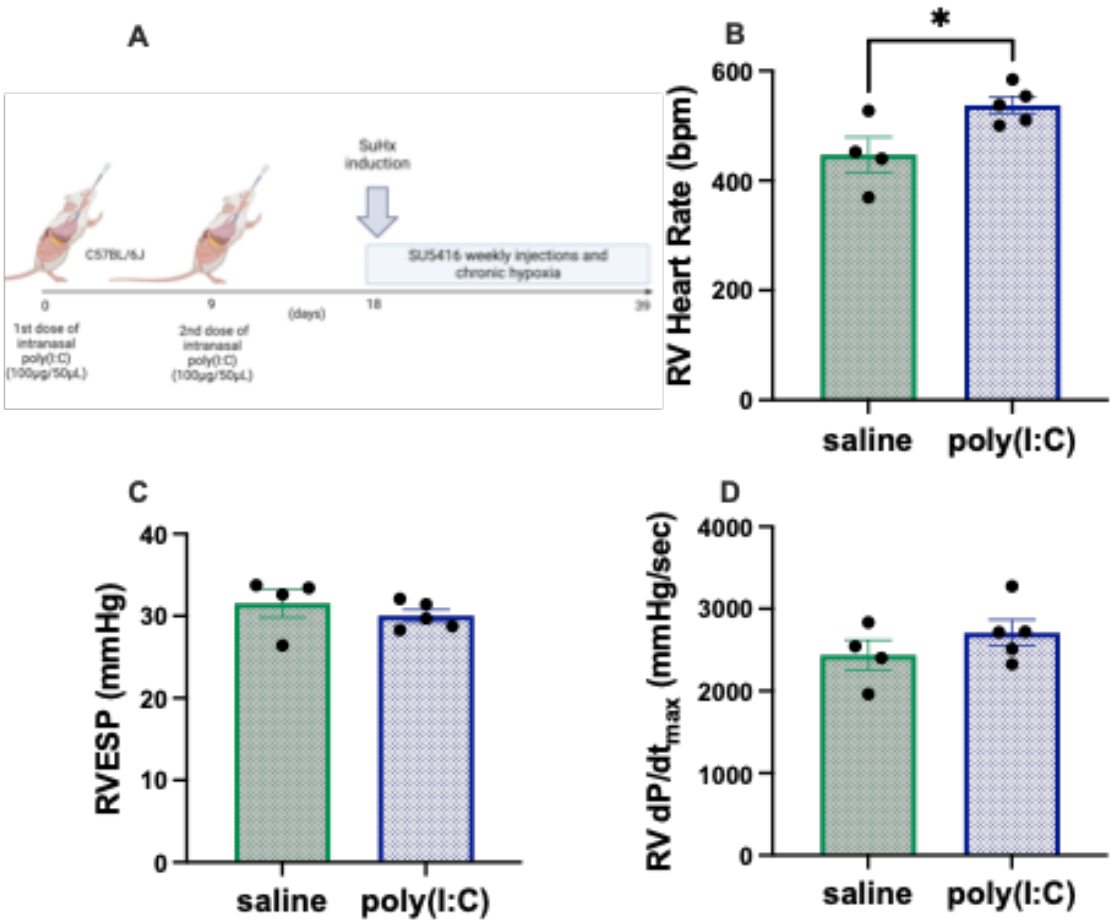

Figure 4.17 Right ventricular haemodynamic and contractility measurements in C57BL/6J mice instilled with repeated doses of intranasal poly(I:C) (Invivogen) or saline, 9 days prior to Sugen-hypoxia.

Intranasal poly(:C) (100µg/50µl) instillations were performed in anaesthetised mice under 1.5–2.0% isoflurane delivered in 100% oxygen with a flow of 2.0 L/min on day 0 and 9, before SuHx was induced on day 18. Original image created in Biorender.com (A). Heart rate was continuously recorded throughout right cardiac catheterisation and the average heart rate (bpm) (B) at the time of pressure-volume loop analysis are presented. Graphs show RVESP (C), and RV dP/dt maximum (mmHg/sec) (D) as acquired by right ventricular cardiac catheterisation via external jugular vein. Data show mean (top of bar) ± SEM. Normality testing and unpaired two-tailed t-test conducted. *, p <0.05. n=4-5. RV; right ventricular. RVESP; right ventricular end systolic pressure. SuHx; Sugen-hypoxia.

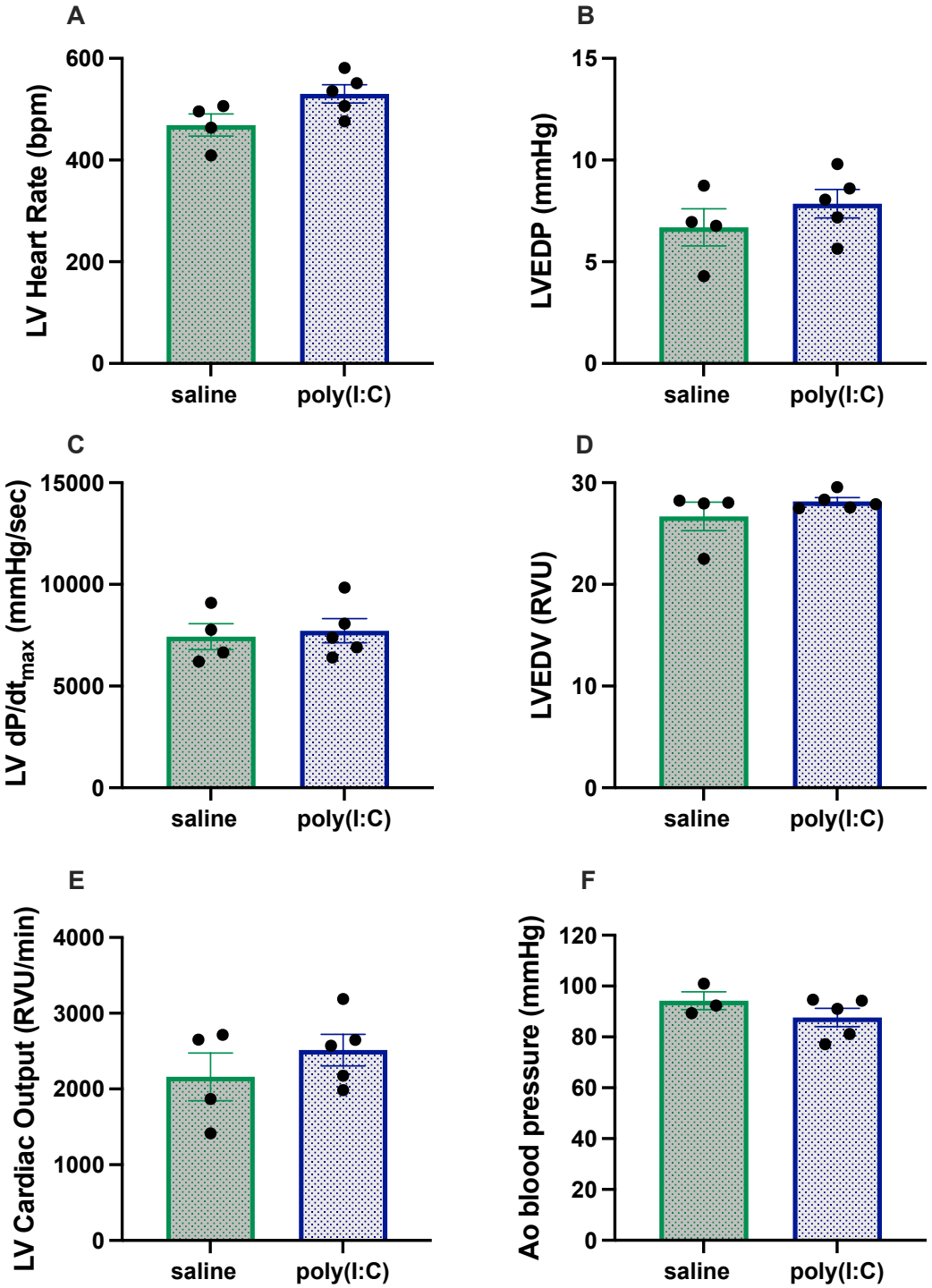

Figure 4.18. Left ventricular haemodynamic measurements and aortic blood pressure in C57BL/6J mice previously instilled with repeated doses of intranasal poly(I:C) (Invivogen) saline, 9 days prior to Sugen-hypoxia.

Heart rate was continuously recorded throughout left cardiac catheterisation and the average heart rate (bpm) (A) at the time of pressure-volume loop analysis are represented. Graphs present LVEDP (mmHg) (B), LV dP/dt maximum (mmHg/sec) LVEDV (RVU) (D), LV cardiac output (RVU/min) (E) and aortic blood pressure (mmHg) (F) were measured by left ventricular cardiac catheterisation via the left common carotid artery. Data show mean (top of bar) ± SEM. Normality testing and unpaired two-tailed t-test or Mann-Whitney tests were conducted accordingly. *n*=3-5. LV; left ventricular. RVU; relative volume units. Ao; aortic.

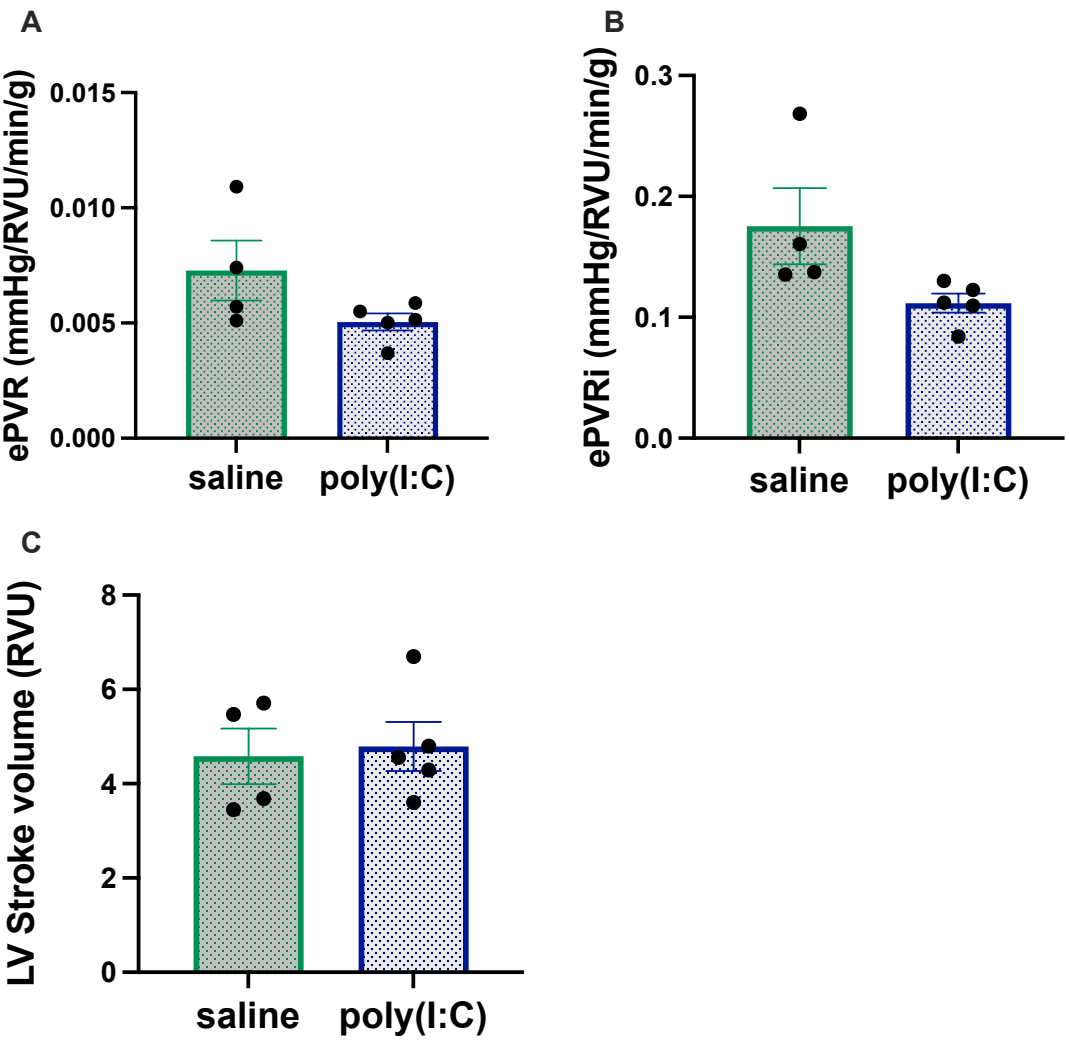

Figure 4.19. Estimated pulmonary vascular resistance and left ventricular stroke volume measurements in C57BL/6J mice previously instilled with repeated doses of intranasal poly(I:C) (Invivogen) or saline, 9 days prior to Sugen-hypoxia.

As previous experimental design, graphs present estimated(e)- PVR (A) and PVR index acquired by right and left ventricular cardiac catheterisation and calculated using the equation: (estimated mean pulmonary artery pressure (emPAP)- left ventricular end diastolic pressure (LVEDP)/ LV cardiac output or cardiac index). Graph presents LV stroke volume (RVU) (C). Data show mean (top of bar) ± SEM. Normality testing and unpaired two-tailed t-test conducted. *n*=4-5 LV; left ventricular. RVU; relative volume units. PVR; pulmonary vascular resistance.

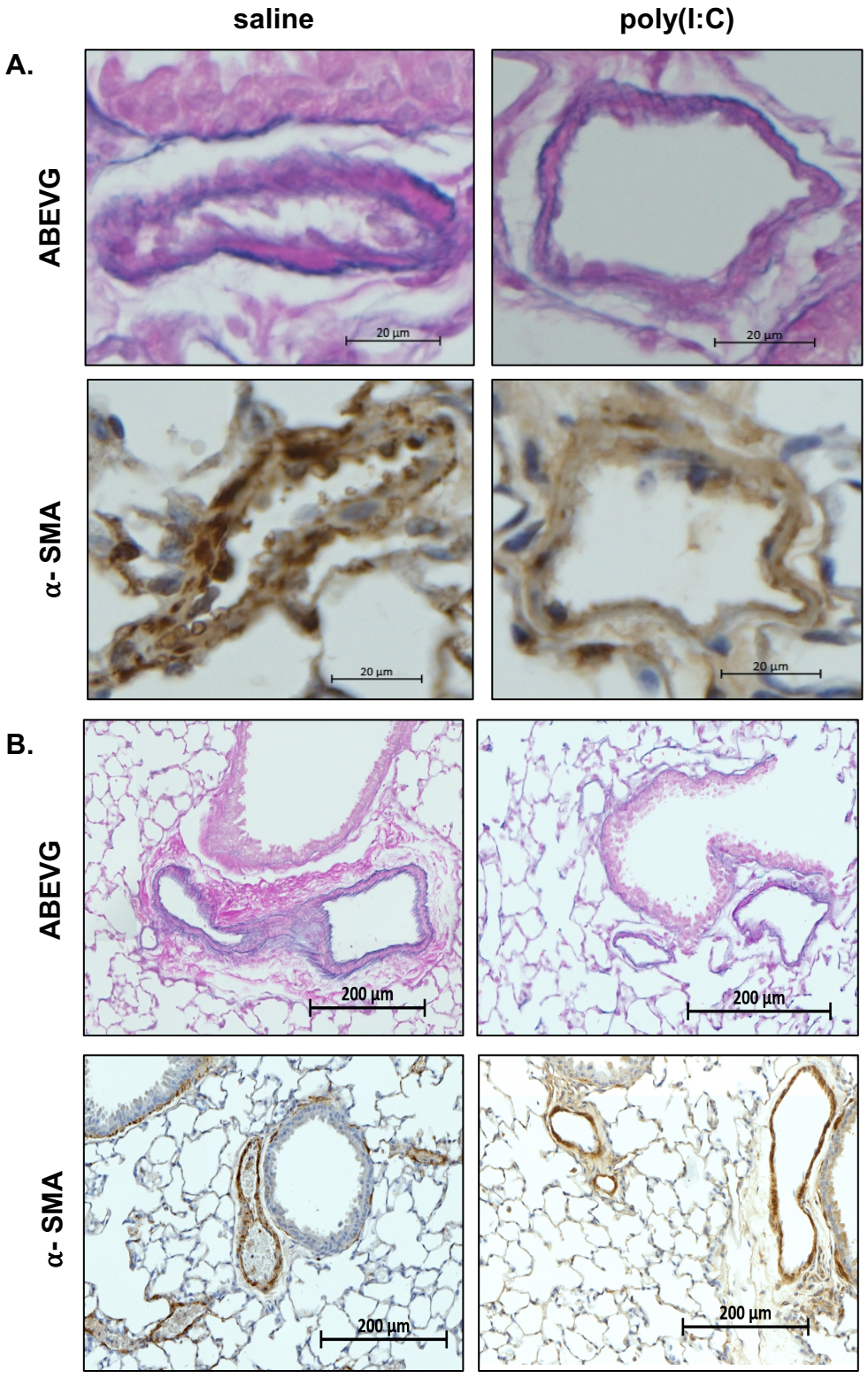

Figure 4.20. Representative images of distal (A) and proximal (B) pulmonary vasculature in FFPE lung sections of C57BL/6J mice instilled with repeated doses of intranasal poly(I:C) (Invivogen) or saline, 9 days prior to Sugen-hypoxia.

FFPE lung sections were stained with ABEVG or indirectly immunostained with α-SMA. Morphometry was conducted on arterioles that were <50µm in diameter. Nx; normoxia. SuHx; Sugen-hypoxia. FFPE; formalin fixed paraffin embedded. ABEVG; Miller's elastin stain with alcian blue and Curtis' modified van Gieson. α-SMA; Alpha smooth muscle actin. Scale bars as indicated.

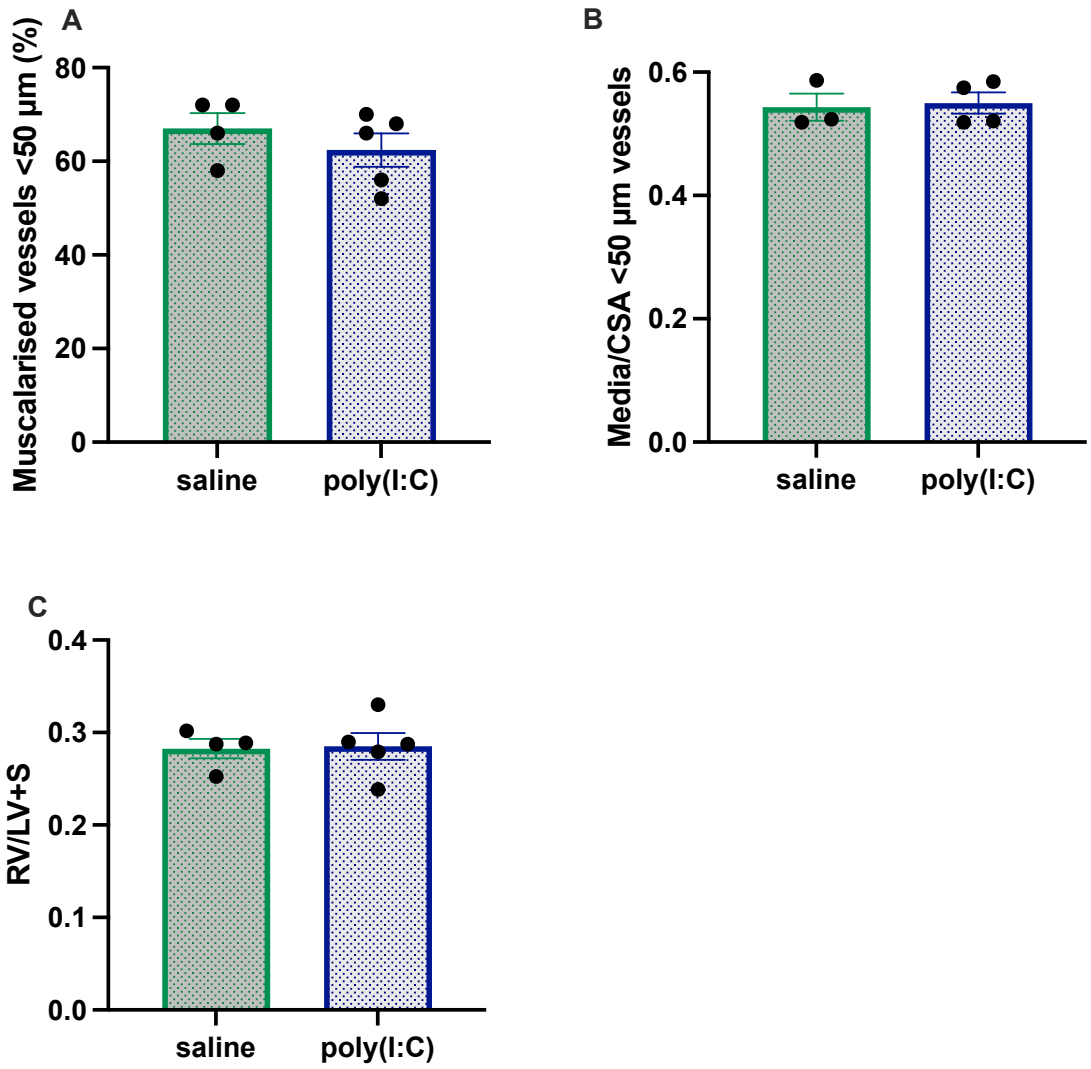

Figure 4.21 Pulmonary vascular morphometric analysis of FFPE lung sections and right ventricular hypertrophy analysis from C57BL/6J mice instilled with repeated doses of intranasal poly(I:C) (Invivogen) or saline, 9 days prior to Sugen-hypoxia.

Pulmonary vascular remodelling was quantified by the proportion of muscularised arterioles (<50µm diameter) in FFPE lung sections stained with ABEVG (A) and medial area to cross-sectional area (CSA) ratio for muscularised arterioles in FFPE lung section immunostained indirectly with α-smooth muscle actin (α-SMA) (B). Hearts were dissected and chambers compartmentalised, and right ventricular free wall weight was normalised to left ventricle plus septum weight (RV/LV+S) to measure ventricular hypertrophy (C). Data show mean (top of bar) ± SEM. Normality testing and unpaired two-tailed t-test conducted. *n*=3-5.

4.7 Summary

The aim of this chapter was to investigate how previous exposure to poly(I:C)-induced lung inflammation may affect the Sugen-hypoxia mouse model of PH. In summary:

- A single dose of intranasal poly(I:C) (100μg/50μl) induced inflammation in BALF 24 hours after instillation as assessed by increased total cell count, percentage of and total number of neutrophils, and proinflammatory cytokine concentration. These biomarkers of lung airway inflammation returned to baseline levels 9 days post intranasal poly(I:C) instillation in C57/BL6J mice.

- A single dose of intranasal poly(I:C) (100μg/50μl) increased the number of cells positive for Ly6G, iNOS and CD206 in lung tissue 24 hours after instillation in C57/BL6J mice.

- Exposure to a single instillation of intranasal poly(I:C) (100μg/50μl), 9 days prior to SuHx induction and subsequent 3-week SuHx exposure in C57/BL6J mice significantly:
  a) Increased pulmonary vascular muscularisation,
  b) Increased estimated pulmonary vascular resistance (ePVR) and ePVR(i) index,
  c) Decreased left ventricular cardiac output and stroke volume,
  d) Increased right ventricular hypertrophy,

  when compared to SuHx control mice.

- In the 2-dose intranasal poly(I:C) model, twenty-four hours after a second instillation of intranasal poly(I:C) (100μg/50μl) (9 days apart), the distribution of neutrophils and macrophages were altered in BALF and IL-6 pg/ml and TNFα pg/ml were significantly lower than 24 hours after a single dose of intranasal poly(I:C) in C57/BL6J mice.

- Instillation of 2 doses of intranasal poly (I:C) (9 days apart), 24 hours or 9 days prior to SuHx induction, and subsequent 3-week SuHx exposure in C57/BL6J mice did not alter any RV or LV haemodynamic parameters, pulmonary vascular remodelling, or right ventricular hypertrophy.

4.8 Discussion

4.8.1 Intranasal poly(I:C) induced airway inflammation in C57BL/6J mice

Firstly, bronchoalveolar lavage fluid (BALF) and lung tissue were assessed for biomarkers of inflammation at 24 hours and then 9 days post a single instillation of intranasal poly(I:C) (100μg/50μl). The 9-day time point post poly(I:C) instillation was informed by work by Harris et al (2013) who measured a tri-phasic inflammatory response in male BALB/cJ mice over several time points from 2 hours to 168 hours; early, middle, and late associated acute inflammatory responses, and both cellular and molecular signatures had resolved at 168 hours post intranasal poly(I:C).

Consistent with the innate immune responses to intranasal poly(I:C) previously reported in literature, intranasal poly(I:C) significantly induced neutrophil and macrophage tissue infiltration and in BALF, 24 hours after instillation, before inflammation resolution at 9 days after poly(I:C) instillation (Aeffner et al., 2011; Gao et al., 2021; Harris et al., 2013; Starkhammar et al., 2012; Stowell et al., 2009; Zhao et al., 2012). The well characterised downstream cytokines effectors of poly(I:C) stimulation, IL-6, KC, and TNFα in BALF, were significantly increased at 24-hour post poly(I:C) instillation. These data evidences a successful model of lung inflammation and also implies a degree of acute lung injury. To definitively model acute lung injury, it has been proposed that a pre-clinical study should include three out of the four domains of lung injury, which are as follows: histological evidence of tissue injury, presence of an inflammatory response, and the following two domains which I did not study, alterations of alveolar-capillary barrier and evidence of physiological dysfunction (Kulkarni et al., 2022; Matute-Bello et al., 2012). However, the consensus in literature

is that intranasal poly(I:C) is a potent inducer of the remaining two domains of acute lung injury. With regard to physiological dysfunction, a whole-body plethysmography approach measured significantly impaired lung function and airway hyperresponsiveness 24 hours after intranasal poly(I:C) instillation at the same dose (100μg/50μl) that was used in my experiments (Stowell et al., 2009). Moreover, intranasal poly(I:C)-induced impaired the alveolar-capillary barrier have been demonstrated previously with elevated BALF albumin and total protein and increased lung wet-dry weight ratio observed in several studies (Gao et al., 2021; Vintiñi et al., 2022). Therefore, my data supports existing knowledge of intranasal poly(I:C) as a potent inducer of lung inflammation.

4.8.2 Previous exposure to a single dose of intranasal poly(I:C) in a Sugen-hypoxia mouse model enhanced estimated pulmonary vascular resistance (ePVR)/ ePVR (index) and reduced cardiac output

To investigate the effect of previous poly(I:C)-induced lung inflammation on the haemodynamic parameters of the SuHx mouse model of PH, the gold standard diagnostic tool for PAH, cardiac catheterisation, was conducted at the end of 3-week SuHx exposure.

Firstly, the success of the SuHx mouse model of PH was confirmed by significant an increase in RVESP (figure 4.5.c). In addition, increases in RV dP/dt_{max} and decreases in LVEDV, LV stroke volume and LV cardiac output in SuHx control mice compared to normoxic control mice were recorded (figure 4.5-7). The significant reductions of LV cardiac output (figure 4.6.e) and LV stroke volume (figure 4.7.c) implied a severe PH phenotype. Severe or progressed PAH is characterised by a maladapted right ventricle that is typically dilated, leading to a reduced RV stroke volume, and in turn, reduced

cardiac output. As the main consequence of PAH is right heart failure, traditionally PAH researchers have compartmentalised the two (left and right) cardiac ventricles and predominantly focused on studying the RV in PAH. However, the concept of 'ventricular interdependence' has recently been cited more in literature and a novel left ventricular mechanical index of PAH was even proposed by Ichimura et al. (2023). Ventricular interdependence refers to the interaction between left and right ventricles and a study by Yamaguchi et al. (1991) showed that 20-40% of RVESP and RV volume output results from left ventricular contraction, thus signifying the importance of considering both RV and LV haemodynamic parameters. Specifically, RV decompensation may influence the LV performance via the following biomechanical processes: interventricular bowing that disturbs LV geometry and impacts filling (direct interaction; detectable by echocardiogram or cardiac MRI) or reduced LV cardiac output due to reduced LV preload leading to reduced LV unloading and atrophy thus reducing force generating capacity (indirect interaction) (Gan et al., 2006; Santamore et al., 1976). Therefore, I speculate that ventricular interdependence, likely in the process of indirect interaction, could explain why LV cardiac output was reduced in this SuHx mouse model. In future, echocardiography and/or cardiac MRI should be used to image the heart and investigate direct interaction (Méndez et al., 2011).

In this thesis, LV cardiac output and LV stroke volume are reported rather than the traditionally PAH-associated RV cardiac output and RV stroke volume due to technical artefacts that are mostly associated when acquiring volumes in the right side of a mouse heart rather than left side of the heart when using a conductance approach in mice. Specifically, the dimensions of the right ventricle are smaller than the left ventricle, making it difficult to centre the catheter along the longitudinal axis of the right

ventricle. Centring the catheter within the RV chamber is paramount to equally spreading out the electric field inside the heart. The voltage generated by high frequency current from the outer electrodes is sensed by the inner electrodes on the catheter. The electric field spreads outs through the blood as well as surrounding myocardium and the voltage that is sensed increases with the resistance of surrounding blood, where resistance is inversely proportional to conductance to equate relative volume units (Danton et al. 2003; Pacher et al. 2008).

After establishing a successful SuHx mouse model in relation to the normoxic control, previous intranasal poly(I:C) instillation in a SuHx mouse significantly enhanced estimated pulmonary vascular resistance (ePVR) and ePVRi and further reduced LV cardiac output and LV stroke volume, without influencing pulmonary pressures. To postulate, enhanced ePVR likely mediated further reduction in LV CO via indirect interaction in the notion of ventricular interdependence. Specifically, increased pulmonary resistance may have caused RV decompensation and subsequent reductions in RV stroke volume/ RV cardiac output. And so, LV cardiac output was reduced in the setting of the closed double circulatory system, which like humans, mice also possess. As previously stated, RV volume data are not shown due to technical artefacts of the conductance catheterisation in mice. Moreover, significant differences in RV heart rate in SuHx mice previously instilled with intranasal poly(I:C) or saline (figure 4.5), at the time of pressure-loop analysis further confounds the RV cardiac output measurements when considering the equation: cardiac output = heart rate x stroke volume. Therefore, this could provide an explanation to why no differences in RV cardiac output in SuHx mice previously instilled with intranasal poly(I:C) or saline control were measured (data not shown), conversely to LV cardiac

output. An alternate explanation for a reduction in LV cardiac output and enhanced ePVR, without an effect in pressure, could be poly(I:C)-induced impairment of LV systolic function. As stated in the previous chapter, poly(I:C) could have a direct effect on the LV myocardium, however, the lack of difference in LV cardiac output in normoxic mice previously instilled with intranasal poly(I:C) or saline makes this an unlikely event. Another reason for discrepancies in RV and LV cardiac output is ventricular shunting but is unlikely in this model.

An alternative explanation for the significant reduction in LV cardiac output and ventricular discrepancies is blood loss. Furthermore, LV cardiac output also influences estimated PVR when considering the equation i.e., ePVR = (emPAP-LVEDP)/ LV cardiac output, whereby LV cardiac output is the denominator of the equation. Of note, in PAH patient definitive diagnosis by cardiac catheterisation, only right cardiac catheterisation is performed, and so, PVR is calculated using RV cardiac output. As stated previously, RV cardiac output is not shown or used in this thesis due to technical artefacts associated with RV catheterisation in a mouse and confounding heart rate differences. And so, during pressure-volume loop acquisition for LV haemodynamic parameters including LV cardiac output in my mice experiments, LV catheterisation and RV catheterisation occurs separately, and LV catheterisation occurs after RV catheterisation. Therefore, LV cardiac output measurements are subject to cumulative blood loss (from RV and LV catheterisation) compared to RV catheterisation alone. Physiologically, blood loss reduces cardiac output by decreasing preload to the heart. In other words, blood loss causes reduced cardiac filling and cardiac pressure which potentially leads to a condition called hypovolemia. More than 10% blood loss is not well tolerated in mice and compensatory mechanisms that attempt to increase cardiac

output such as increased heart rate, arterial and venous contractions and hormonal changes are insufficient in maintaining cardiac output (Pfeifer et al., 2013). Furthermore, the PVR equation itself is caveated by the fact is it based on the unmet assumptions of blood being a Newtonian fluid, rather it is pulsatile and turbulent, and blood vessels being cylindrical, rather they expand and reduce to accommodate flow, all of which are particularly dysregulated in PAH patients or *in vivo* models of PAH (Chemla et al., 2004).

PVR can also be influenced by hypoxia-induced increases in blood viscosity that is caused by raised haematocrit levels (De Raaf et al., 2014; Vanderpool & Naeije, 2018). Likewise, decreasing haematocrit from 40% to 20% in an experimental hypoxic dog model decreased PVR from 2-3-1.8 to 1.4-1.2 wood units (WU) (Kerbaul et al., 2004) I propose that SuHx-induced haematocrit could be exacerbated in SuHx mice previously instilled with intranasal poly(I:C) and therefore should be tested in future.

4.8.3 Previous exposure to a single dose of intranasal poly(I:C) in the Sugen-hypoxia mouse model enhanced pulmonary vascular remodelling and right ventricular hypertrophy

Despite the above discussed caveats to the observed changes in ePVR and LV cardiac output, their plausibility as true biological effects are supported by histopathological analysis of pulmonary vessels. For example, SuHx mice previously instilled with intranasal poly(I:C) had significantly enhanced pulmonary vascular muscularisation and RV hypertrophy when compared to SuHx control mice. Pulmonary vascular remodelling which obliterates and/or obstructs pulmonary vascular beds contribute to increased PVR. Other hallmarks of PAH pathogenesis

including vasoconstriction and thrombi formation are also known contributors to increased PVR and could be quantified in future (Humbert et al., 2019)

Yet, if the significant increase in ePVR in SuHx mice previously instilled with intranasal poly(I:C) is validated in future experiments, this could be extrapolated to hold significant clinical relevance. PVR is an independent predictor and is used in combination with other parameters in the REVEAL risk calculator to predict patient outcomes in PAH patients (Benza et al., 2019, 2021; Maron et al., 2020; Suzuki et al., 2022). To clarify ePVR in future, I would increase mice per experimental group to decrease the noise in data that may have occurred due to heart rate differences and potential blood loss. Furthermore, I would test for increased plasma troponin levels, of which has been previously correlated to increased PVR (Hojda et al., 2022).

Significantly enhanced RV hypertrophy in SuHx mice previously instilled with intranasal poly(I:C) compared to SuHx also supports the presence of increased ePVR. Chronic RV afterload (i.e., PVR) stimulated RV hypertrophy in PAH patients as mechanically cardiomyocytes work more to overcome resistance in the pulmonary resistance and maintain blood flow (Ryan & Archer, 2014).The finding of no difference in RV hypertrophy in normoxic mice instilled with intranasal poly(I:C) compared to saline suggests that there are no direct effects of intranasal poly(I:C) on RV hypertrophy.

4.8.4 Previous intranasal poly(I:C) alters the immune response to a subsequent exposure of intranasal poly(I:C) in C57BL/6J mice

To model repeated exposures to lung inflammation, I produced a repeated poly(I:C) model which included two doses of intranasal poly(I:C), instilled 9 days apart i.e., at the point of known inflammatory resolution. C57BL/6J mice previously instilled with intranasal poly(I:C) had reduced neutrophil numbers and reduced IL-6 and TNFα concentrations in BALF 24 hours after a subsequent intranasal poly(I:C) instillation. This implies the presence of poly(I:C) tolerization where poly(I:C), and ultimately activation of anti-viral immunity, drives mechanisms to suppress or dampen airway inflammation in response to a second instillation of poly(I:C). This poly(I:C) tolerance was somewhat unexpected as published literature describes poly(I:C) as an adjuvant for other inflammatory-inducing stimuli such as vaccines and anti-cancer immunotherapies, albeit poly(I:C) was administered simultaneously and via subcutaneous injection in these studies (Di et al., 2019; Tewari et al., 2010). In addition, these data evidence that poly(I:C) enhanced adaptative immune responses i.e., humoral, and cell-mediated immunity, and I measured innate immune responses i.e., acute cytokine production and neutrophil infiltration. However, simultaneous intratracheal administration of poly(I:C) and SARS-Cov-2 recombinant protein in mouse model of ARDS induced significant increases in BAL innate inflammatory cytokines (IL-6, IL-1α, TNFα) compared to SARS-Cov-2 recombinant protein alone (Gu et al., 2021). In another previous inflammation exposure mouse model, previous exposure to other inflammatory stimuli such as cigarette smoke exacerbated poly(I:C)-induced airway inflammation, remodelling, and apoptotic responses in mice, suggesting the exact type of previous intranasal inflammatory stimulus influences the innate immune response to a secondary hit of intranasal poly(I:C) (Kang et al., 2008).

And so, all of the above studies and an elegant review by Owen et al. (2021) suggest that poly(I:C) prior or administrated simultaneously with infections or vaccination enhanced immune responses and in turn provide protection to subsequent infection.

Conversely, Dyck et al. (1987) showed that repeated poly(I:C) injections, at a 7-day interval, reduced splenic natural killer cell activity 18 hours after the last poly(I:C) injection compared to a single dose of poly(I:C). Yet, immune tolerance to repeated exposures of intranasal poly(I:C) has largely been uninvestigated. The paucity of investigation in this area contrasts with the well characterised phenomenon of 'LPS tolerance' which involves a sublethal LPS (i.e., bacterial mimic) injection to alter subsequent immune responses to LPS and other inflammatory stimuli. LPS-induced receptor desensitisation and suppression of downstream signalling, tolerizeable gene expression (i.e., genes not inducible in tolerant macrophages) and loss of H3K4 trimethylation at the promoters of tolerizeable genes explain mechanisms of LPS tolerance (Foster et al., 2007; Medvedev et al., 2002; Nomura et al., 2000). To the best of my knowledge, this is the first-time immune tolerance in BAL and lung tissue to repeat doses of intranasal poly(I:C) has been shown, thus offering a different facet of poly(I:C)-induced trained immunity.

4.8.5. Previous repeated intranasal poly(I:C) does not alter the SuHx mouse model of PH

Given that altered innate immunity is associated with pathogenesis of PAH (Ormiston et al., 2012; Perros et al., 2012; Zawia et al., 2020) and previously in this chapter I showed evidence that repeat intranasal poly(I:C) instillation leads to immune tolerance

of cytokine production and innate immune cell in BALF, I chose to study repeated intranasal poly(I:C) prior to induction of the SuHx mouse model of PH.

Irrespective of this altered immune response to a repeat dose of poly(I:C), and the time after the last poly(I:C) instillation to the point of SuHx induction (i.e., 24 hours; inflammation present- or 9 days; inflammation resolved- at the point of SuHx induction), the PH phenotype was not altered when compared to saline control mice (section 4.5 and 4.6). I postulate that potential of molecular immune reprogramming or a lesser degree of acute lung injury after two instillations of poly(I:C) may explain why the SuHx model of PH was not exacerbated, unlike how a previous single dose of intranasal enhanced ePVR, RV hypertrophy and pulmonary vascular muscularisation (section 4.3). This potentially highlights the importance of the specific history of respiratory inflammation stimuli, where it is plausible that differing innate immune landscapes after 2 doses of intranasal poly(I:C) compared to one dose of intranasal poly(I:C) influences the severity of pulmonary vascular remodelling in a subsequent SuHx model of PH.

The repeated intranasal poly(I:C) experiments were powered to detect a larger difference in RVESP. For example, by using *n* of ≥ 3, this study was sensitive enough to detect pressure differences of >5mmHg (methods section 2.13.1). Due to the lack of signals in both haemodynamic and remodelling (section 4.5 and 4.6), I did not use additional animals to detect subtle differences.

4.8.6. Future work

This chapter shows that previous instillation of a single dose of intranasal poly(I:C) provoked subtle changes in PH phenotype, where the main effect was enhanced pulmonary vascular remodelling with some subtle haemodynamic effects. Blood loss associated with the technicalities of LV cardiac output acquisition using a conductance catheterisation, and the subsequent use of LV cardiac output measurement as the denominator in the ePVR/i equations, hinder my conclusions but would merit further investigation in future. As I refer to above, the noise of technical artefacts could be minimised by increasing animal per groups and assessing haemodynamics by a combination of modalities (i.e., echocardiography or cardiac MRI) in future.

In future, I would investigate the mechanism of action of enhanced pulmonary vascular remodelling in SuHx mice previously instilled with one dose of intranasal poly(I:C) by a multi-approach of assessing: poly(I:C)-induced anatomical, immunological memory, bystander sensitisation and molecular changes. I would take inspiration from recent work which showed poly(I:C) induced epigenetic changes via BRD4-dependent histone acetyltransferase activation and this work could provide an explanation for long term innate immune effects (Tian et al., 2019).

If the differences on the effects of pulmonary vascular remodelling in SuHx mice between the models of one and two instillations of intranasal poly(I:C) still uphold after increasing power of experiments in future, this would suggest that the previous type or levels of background inflammation may alter pulmonary vascular remodelling. I speculate that age-dependent innate immune responses to intranasal poly(I:C), the time period between each lung inflammatory stimuli and the length of time from prior

lung inflammatory stimuli to onset of disease also have the capacity to influence subsequent diseases and are illustrated by several papers (Allinson et al., 2023; McGarry et al., 2021).These factors should be considered in experimental design when using the SuHx mouse model of PH in future.

Arguably, this previous intranasal poly(I:C) exposure to SuHx model of PH is oversimplified as it is accepted that PAH pathogenesis is multifactorial. But if further investigations could elicit the complexities in the type of lung inflammation and combinations of other environmental and genetic variations that one may be exposed prior to disease onset, this could be helpful in stratifying patients who are more likely to have aggressive pulmonary vascular remodelling and guide earlier accelerations of therapies.

To address the multi-factorial nature of PAH pathogenesis, the next chapter will focus on the effects of poly(I:C), specifically in the context of GCN2 deficiency, due to the recent discovery of causative mutations in *EIF2AK4* (encoding for GCN2) in pulmonary veno-occlusive disease (PVOD) (a subclassification of PAH) (Eyries et al., 2014). In addition, links between GCN2 and sensing of dsRNA (poly(I:C)) by another component of the integrated stress response, PKR, add weight to the exploration of this pathway (Pakos-Zebrucka et al., 2016).

5. The effects of GCN2 deficiency on poly(I:C)-induced inflammation in endothelial cells

5.1 Introduction

The pathogenesis of PAH is considered multifactorial with no single aetiology leading to the development and/or progression of disease. Rather, it is thought that a combination of genetic and environmental factors contribute to disease. Researchers have identified PAH-associated gene mutations predominantly in the BMP signalling pathway. Mutations in *BMPR2* are the most common mutation found in heritable (H)PAH patients. In a subclassification of PAH, pulmonary veno-occlusive disease (PVOD), the most common gene mutation is Eukaryotic Translation Initiation Factor 2 Alpha Kinase 4 (*EIF2AK4*) (Eyries et al., 2014). Biallelic mutations of the *EIF2AK4* gene are considered the major genetic cause of PVOD, as *EIF2AK4* mutations were present in 100% of familial and 25% of sporadic PVOD cases (Eyries et al., 2014). The penetrance of disease in carriers of *EIF2AK4* mutations is unknown but age and severity at PVOD onset differ dramatically in this patient population. This suggests that other genetic factors and/or environmental factors are influential in PVOD pathogenesis. Investigating how *EIF2AK4* loss-of-function mutations contribute to PVOD and identifying potential targets for therapeutic intervention is vital as a PVOD diagnosis carries a worse prognosis than PAH. The one-year mortality has been reported to be approximately 70% (Karakurt, 2010). Moreover, there are no effective treatments apart from lung transplantation.

A wildtype *EIF2AK4* gene encodes for the protein GCN2 (general control nonderepressible 2). GCN2 is an integrated stress response (ISR) kinase that upon activation leads to global translational suppression in response to uncharged transfer RNA (i.e., amino acid deprivation). More specifically, GCN2 phosphorylates eIF2 (eukaryotic translation initiation factor 2) at serine 51 of its alpha subunit (eIF2α) globally suppressing translation initiation whilst simultaneously favouring the selective translation of some mRNA, such as activating transcription factor 4 (ATF4) (Pakos-Zebrucka et al., 2016). Though the function of GCN2 to respond to amino acid deprivation under cellular stress is well established in the literature, the role of *EIF2AK4*-encoding GCN2 loss-of-function mutations in pulmonary vascular remodelling and PVOD pathogenesis is largely uninvestigated.

A small number of studies have shown potential mechanisms by which GCN2 loss-of-function contributes to PVOD pathogenesis. In experimental and human PVOD, eIF2α-independent pulmonary protein overexpression of downstream effectors of GCN2, HO-1 (heme oxygenase 1) and CHOP (CCAAT-enhancer-binding protein (C/EBP) homologous protein) have been reported in which HO-1 has been previously implicated in angiogenesis and endothelial cell proliferation (Manaud et al., 2020). Aberrant MAPK, SMAD1/5/8 and SMAD2/3 signalling pathways, previously implicated in pulmonary vascular remodelling and PAH pathogenesis, have also been associated with GCN2 deficiency *in vivo* and *in vitro* (Chen et al. 2021; Manaud et al. 2020)

In a mitomycin-C (MMC) rat model of PVOD, other ISR kinases including PKR and PERK, protein had significantly higher expression in lung, thus implying biological compensation from other kinases in the ISR (Manaud et al., 2020). However, the report

by Manaud et al (2020) showed that phosphorylation of eIF2α was unaffected in GCN2-deficient PASMCs from PVOD donors. Whether there could be compensation of canonical GCN2 signalling via other ISR kinases therefore remains uncertain. PKR is of particular interest in the context of the work in this thesis, as it is an intracellular ISR kinase activated by the presence of dsRNA, in turn inducing the transcription of pro-inflammatory mediators and type I interferon.

Very little is understood about how GCN2 deficiency contributes to pulmonary vascular remodelling and PVOD pathogenesis. In the original research articles exploring mechanisms downstream of GCN2 deficiency, all have investigated GCN2 deficiency as a discrete entity and not in combination with other factors which may trigger or drive the pulmonary vascular remodelling. Arguably, investigating GCN2 deficiency in combination with other potential triggers and drivers is a more appropriate model given the accepted notion that PAH and PVOD pathogenesis is multifactorial. Given the compensatory interaction between ISR kinases in models of PVOD (Manaud et al, 2020), the known role of PKR in dsRNA signalling and the evidence of dsRNA signalling in pulmonary vascular remodelling, it is therefore reasonable to question if GCN2 deficiency could alter dsRNA signalling and thus contribute to PVOD pathogenesis. I hypothesised that GCN2 deficiency enhances poly(I:C)-induced inflammation and promotes pulmonary vascular remodelling.

As endothelial vascular injury is believed to be a key step in the initiation of vascular remodelling, this work prioritised the investigation of dsRNA signalling in the context of GCN2 deficiency in endothelial cells.

Therefore, in this chapter I aimed to create a ‘2-hit’ model of dsRNA signalling in the context of GCN2 deficiency in endothelial cells.

To do this, the work in this chapter aimed to:

1. Investigate poly(I:C)-mediated induction of inflammatory cytokines in GCN2-deficient endothelial cells
2. Investigate cellular phenotypes associated with pulmonary vascular remodelling in GCN2-deficient endothelial cells stimulated with poly(I:C)
3. Investigate poly(I:C)-induced transcriptomic effects in GCN2-deficient endothelial cells

Results

5.2 Successful knockdown of *GCN2 (EIF2AK4)* mRNA expression and GCN2 protein in BOECs from healthy volunteers

To investigate the effects of GCN2 in poly(I:C)-treated endothelial cells, a siRNA approach (section 2.4) was used to reduce transcripts of *GCN2 (EIF2AK4)* in human blood outgrowth endothelial cells (BOECs) from healthy volunteers. Quantitative reverse-transcription PCR (qRT-PCR) was used to assess the knockdown of *GCN2 (EIF2AK4)* transcripts. Western blotting measuring GCN2 protein expression was used to validate knockdown.

GCN2 (EIF2AK4) mRNA was significantly reduced in si*GCN2*-treated BOECs with and without poly(I:C) stimulation (figure 5.1.a). Poly(I:C) (25μg/ml) treatment for 24 hours did not affect *GCN2 (EIF2AK4)* mRNA expression in BOECs (figure 5.1.a).

GCN2 protein was also reduced in si*GCN2*-treated BOECs with and without poly(I:C) stimulation (figure 5.1.b).

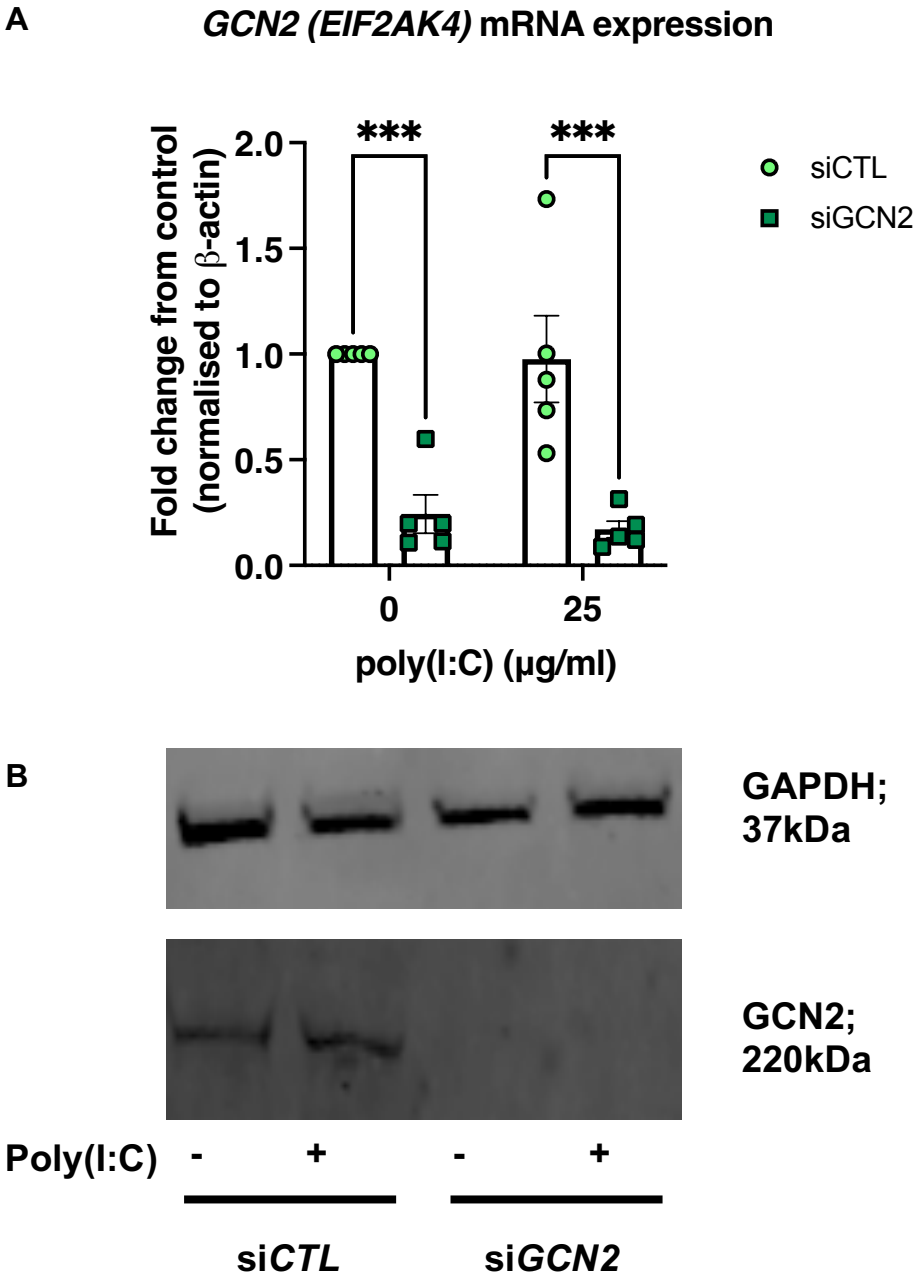

Figure 5.1. The knockdown of *GCN2 (EIF2AK4)* mRNA expression and GCN2 protein in si*GCN2*-treated BOECs, with and without poly(I:C) (25μg/ml) stimulation for 24 hours.

Via qRT-PCR analysis, *GCN2 (EIF2AK4)* mRNA expression was significantly reduced in si*GCN2*-treated BOECs with and without poly(I:C) (25μg/ml) stimulation for 24 hours when compared to respective controls (A). Data show mean (top of bar) ± SEM. Two-way ANOVA, Šídák's multiple comparison testing. ***, p <0.001. n=5 experimental repeats from 3 donors. Western blot analysis shows GCN2 protein was reduced in si*GCN2*-treated BOECs, with and without poly(I:C) stimulation for 24 hours, when compared to control (B). n=1. This experiment was repeated in n=3 donors and successful protein reduction of GCN2 was achieved in.all n.

5.3 GCN2 deficiency enhanced pro-inflammatory cytokine release in response to poly(I:C) in BOECs

To investigate GCN2 deficiency effects on poly(I:C)-induced proinflammatory cytokine release, the cell supernatants of si*GCN2*-treated BOECs with and without poly(I:C) (25μg/ml) stimulation for 24 hours were investigated for the presence of TNFα, IL-6 and IP-10 using Luminex technology (section. 2.6). Poly(I:C) concentration was firstly optimised ahead of the subsequent experiments.

Poly(I:C) concentrations of 0.25μg/ml and 25μg/ml were initially used on s*iGCN2* or si*CTL*-treated BOECs and levels of TNFα, IL-6 and IP-10 protein in supernatant were determined (appendix figure 2). Due to lack of significant stimulation of pro-inflammatory cytokine release with poly(I:C) stimulation of 0.25μg/ml, the decision was taken to complete all subsequent experiments with 25μg/ml of poly(I:C).

GCN2-deficient BOECs had significantly increased IP-10 (figure 5.2.c) and TNFα (figure 5.2.a) release in response to poly(I:C), when compared to poly(I:C)-stimulated control BOECs.

Poly(I:C) significantly induced the release of IL-6 and IP-10 in siCTL-treated BOECs compared to the unstimulated siCTL-treated BOECs (figure 5.2.b-c). Likewise, poly(I:C) significantly induced the release of TNFα in si*GCN2*-treated BOECs compared to the unstimulated si*GCN2*-treated BOECs (figure 5.2.a).

GCN2 deficiency in unstimulated BOECs did not affect cytokine release when compared to unstimulated control BOECs (figure 5.2).

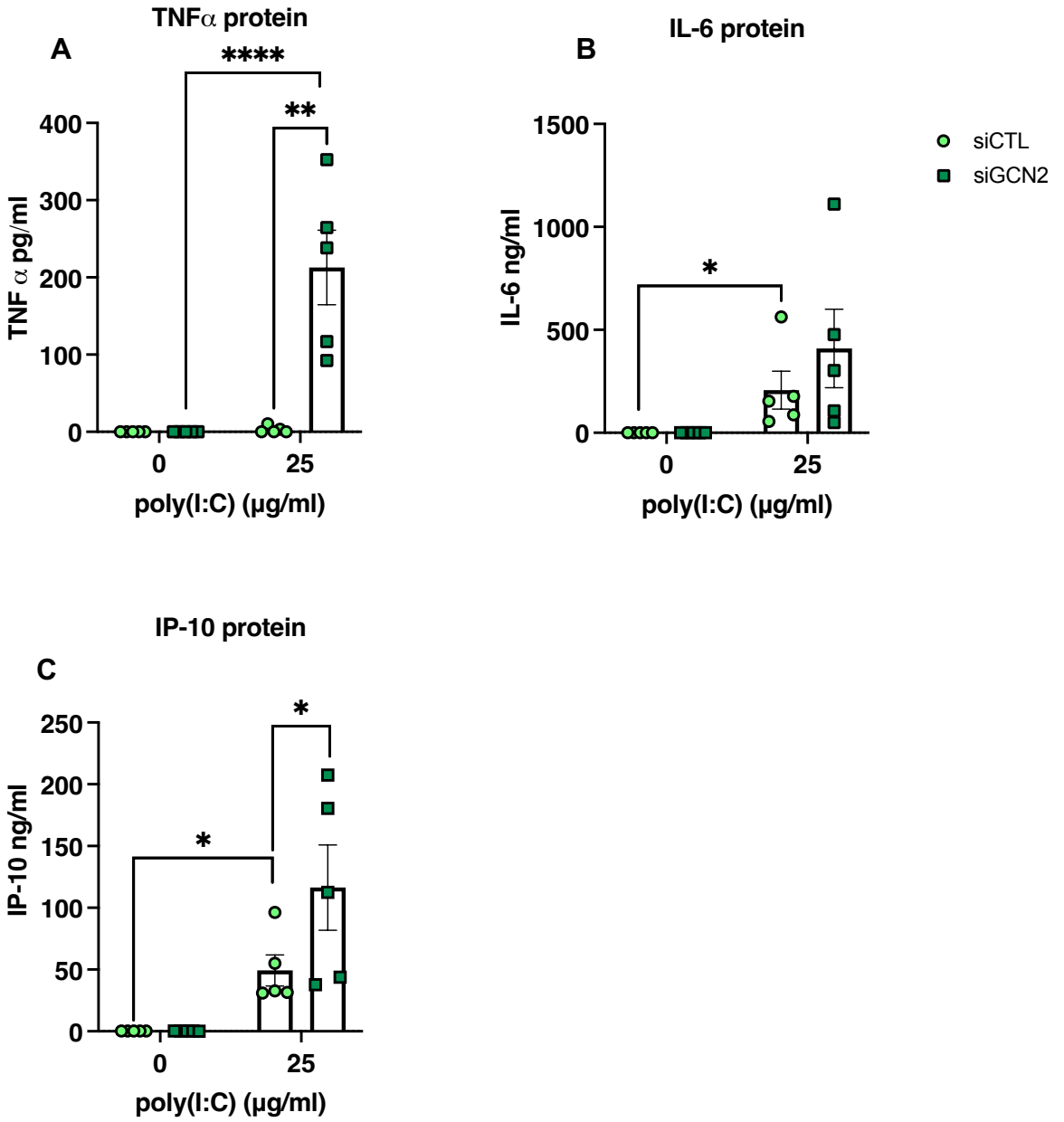

Figure 5.2. The protein levels of proinflammatory cytokines in supernatant of GCN2-deficient BOECs with and without 24 hours of poly(I:C) stimulation.

Luminex technology assessed pro-inflammatory cytokine release of TNFα (A), IL-6 (B) and IP-10 (C), in the cell supernatants of si*GCN2*-treated BOECs with and without poly(I:C) (25μg/ml) stimulation for 24 hours. Data show mean (top of bar) ± SEM. Two-way ANOVA, Šídák's multiple comparisons test. ****, p <0.0001; **, p <0.01: *, p < 0.05. n=5 experimental repeats from 3 donors.

5.4 GCN2 deficiency enhanced pro-inflammatory cytokine transcription in response to poly(I:C) in BOECs

To investigate if the enhanced pro-inflammatory cytokine (TNFα and IP-10) release in GCN2-deficient BOECs was associated with increased transcription, *IP-10*, *IL-6,* and *TNFA* mRNA expression was assessed in GCN2-deficient BOECs with and without poly(I:C) stimulation for 24 hours via qRT-qPCR.

GCN2-deficient BOECs had significantly increased *TNFA* (figure 5.3.a) and *IP-10* (figure 5.3.c) mRNA expression in response to poly(I:C), when compared to siCTL-treated poly(I:C)-stimulated BOECs.

In addition, the mRNA expression of *TNFA,* IP-*10* and *IL-6* increased in siCTL-treated BOECs stimulated with poly(I:C) when compared to unstimulated siCTL-treated BOECs but did not reach a 5% level of significance (figure 5.3.a-c). In si*GCN2*-treated BOECs, poly(I:C) stimulation significantly increased *IP-10* (figure 5.3.c) and *IL-6* (figure 5.3.b) compared to unstimulated si*GCN2*-treated BOECs.

GCN2 deficiency in unstimulated BOECs did not affect cytokine mRNA expression when compared to unstimulated control BOECs (figure 5.3).

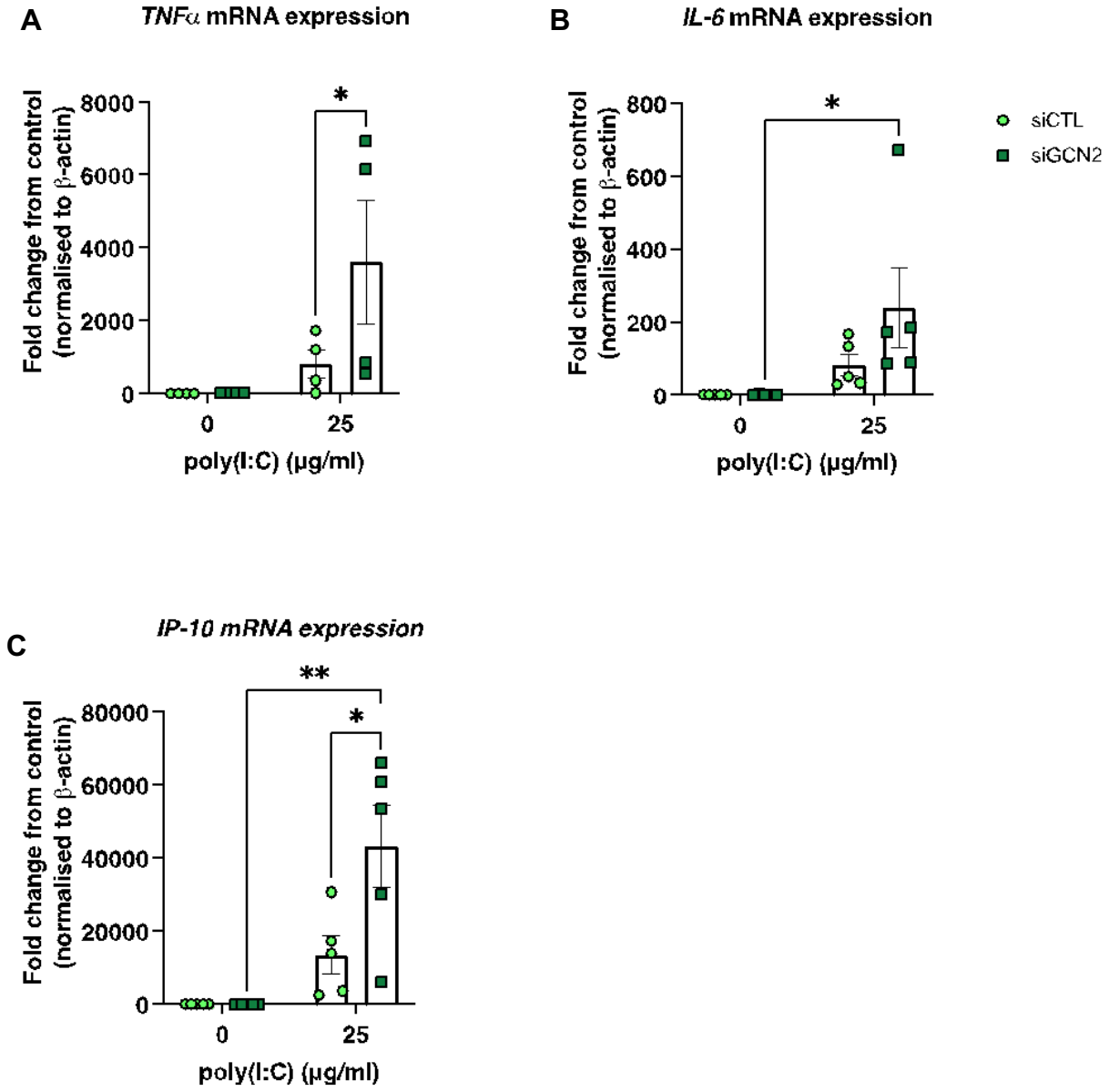

Figure 5.3. The relative mRNA expression of proinflammatory cytokines in GCN2 deficient BOECs with and without 24 hours of poly(I:C) stimulation.

Quantitative RT-PCR measured proinflammatory cytokines *TNFA* (A), *IL-6* (B) and *IP-10* (C) mRNA expression in GCN2-deficient BOECs, with and without, poly(I:C) (25µg/ml) for 24 hours. All data are presented as fold change where delta-delta Ct values are normalized to siCTL and unstimulated group. Delta Ct values were normalized to housekeeper gene *ACTB* and then to a reference sample (delta-delta Ct). A no transfection, unstimulated was not conducted in this specific experiment, however, appendix III (table 3 and figure 3) shows no transcriptomic effect of proinflammatory cytokines in siCTL-lipofectamine transfection hPAECs when compared to untransfected, unstimulated hPAECs. Data show mean (top of bar) ± SEM. Two-way ANOVA, Šídák's multiple comparisons test. **, p <0.01; *, p < 0.05. n=5 experimental repeats from 3 donors.

5.5 GCN2 deficiency did not alter dsRNA sensor expression in response to poly(I:C) in BOECs

To investigate if enhanced pro-inflammatory cytokine (TNFα and IP-10) release and transcription in GCN2-deficient BOECs stimulated with poly(I:C), were associated with altered mRNA expression of receptors in dsRNA signalling, *TLR3*, *MDA5* and *PKR* (*EIF2AK2*) mRNA expression levels were assessed by qRT-PCR.

The mRNA expression of *MDA5* and *PKR* (*EIF2AK2*) increased in siCTL-treated BOECs stimulated with poly(I:C) when compared to unstimulated siCTL-treated BOECs (figure 5.4.b-c).

GCN2 deficiency did not affect mRNA expression of any dsRNA sensor when compared to control, with or without poly(I:C) (figure 5.4. a-c).

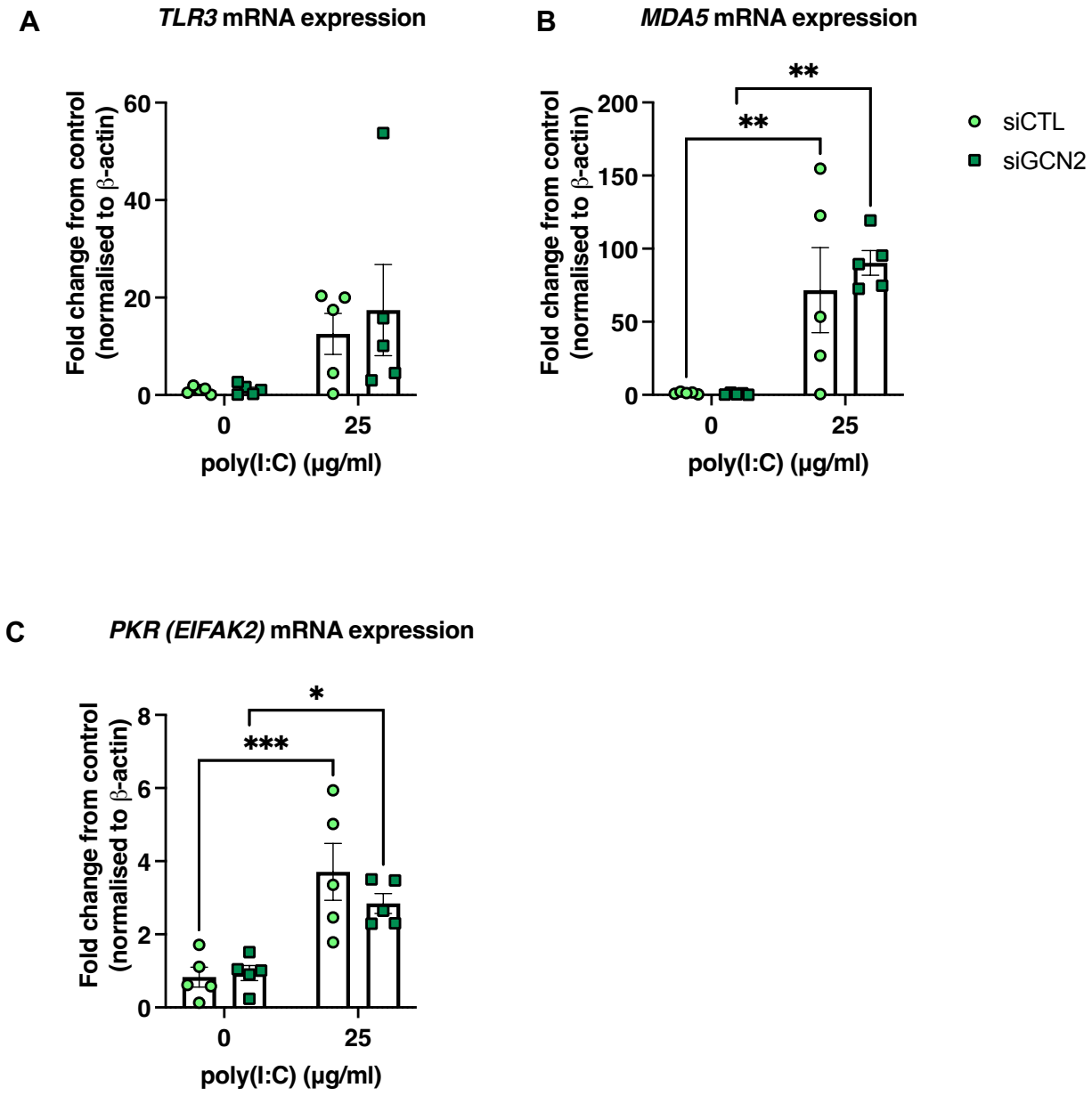

Figure 5.4 The relative mRNA expression of dsRNA sensors in GCN2-deficient BOECs with and without 24 hours of poly(I:C) stimulation.

Quantitative RT-PCR measured known sensors of poly(I:C), *TLR3 (*A), *MDA5* (B) and *PKR* (C) mRNA expression in GCN2-deficient BOECs, with and without, poly(I:C) (25μg/ml) for 24 hours. All data are presented as fold change where delta-delta Ct values are normalized to siCTL and unstimulated group. Delta Ct values were normalized to housekeeper gene *ACTB* and then to a reference sample (delta-delta Ct). A no transfection, unstimulated was not conducted in this specific experiment, however, appendix III (table 3 and figure 3) shows no transcriptomic effect of dsRNA sensors in siCTL-lipofectamine transfection hPAECs when compared to untransfected, unstimulated hPAECs. Data show mean (top of bar) ± SEM. Two-way ANOVA, Šídák's multiple comparisons test. ***, p <0.01; **, p <0.01; *, p < 0.05. n=5 experimental repeats from 3 donors.

5.6 Knockdown of *GCN2 (EIF2AK4)* and/or *PKR* (*EIF2AK2*) in hPAECs stimulated with poly(I:C)

To extend the findings from healthy donor BOECs and validate the initial observation of enhanced pro-inflammatory cytokine (i.e., TNFα and IP-10) release and transcription in GCN2 deficient cells stimulated with poly(I:C), all subsequent *in vitro* experiments were completed using human pulmonary artery endothelial cells (hPAECs) purchased from Lonza. Alongside the experiment of si*GCN2*-treated hPAECs with and without poly(I:C) stimulation, simultaneous si*GCN2* and si*PKR* knockdown in hPAECs with and without poly(I:C) stimulation (and an si*PKR*-treated control) were completed in hPAECs as a way to investigate if enhanced pro-inflammatory cytokine release and transcription from GCN2-deficient ECs stimulated with poly(I:C) was via altered PKR signalling.

Firstly, RNA was extracted from siCTL-, si*GCN2*-, si*PKR*-, and si*GCN2* and si*PKR*-treated hPAECs, with and without poly(I:C) stimulation (24 hours; 25μg/ml), and knockdown efficacy by quantification of *GCN2 (EIF2AK4*) and/or *PKR* (*EIF2AK2*) mRNA transcripts via qRT-PCR analysis was carried out, .

In unstimulated conditions (i.e., no poly(I:C)), *GCN2 (EIF2AK4*) mRNA expression was significantly reduced in si*GCN2*- and si*GCN2*- and si*PKR*-treated hPAECs when compared to siCTL-treated hPAECs (figure 5.5.a). In addition, *GCN2 (EIF2AK4*) mRNA expression was significantly reduced in si*GCN2*-treated hPAECs stimulated with poly(I:C) when compared to siCTL-treated hPAECs stimulated with poly(I:C) (figure 5.5.a). *GCN2 (EIF2AK4*) mRNA expression in si*GCN2* and si*PKR*-treated hPAECs stimulated with poly(I:C) was reduced by 67% relative to siCTL-treated

hPAECs stimulated with poly(I:C) but a 5% significance level was not reached (figure 5.5.a). *GCN2 (EIF2AK4*) mRNA expression was unaffected in si*PKR*-treated hPAECs, in poly(I:C) stimulated and unstimulated conditions (figure 5.5.a).

In unstimulated conditions (i.e., no poly(I:C)), *PKR (EIF2AK2*) mRNA expression was significantly reduced in si*PKR*-treated hPAECs when compared to siCTL-treated hPAECs. Yet in simultaneous si*GCN2*- and si*PKR*-treated hPAECs with no poly(I:C) stimulation, *PKR (EIF2AK2*) mRNA expression was unaffected when compared to siCTL-treated hPAECs (figure 5.5.b).

PKR (EIF2AK2) mRNA expression was significantly induced by poly(I:C) in siCTL-treated hPAECs compared to unstimulated control (figure 5.5.b).

Relative to siCTL-treated hPAECs with poly(I:C) stimulation, *PKR (EIF2AK2*) mRNA expression was reduced by a negative fold change of 6.8- and 7.3-fold in si*PKR*- and combined si*GCN2*- and si*PKR*-treated hPAECs, respectively, but a 5% significance level was not reached (figure 5.5.b).

To validate knockdown of GCN2 and PKR at the mRNA level, GCN2 and PKR protein expression was also assessed. GCN2 protein was substantially reduced in si*GCN2*- and si*PKR* and si*GCN2*- treated hPAECs with and without poly(I:C) stimulation (figure 5.6). PKR protein was reduced in si*PKR*- and si*PKR* and si*GCN2*- treated hPAECs with and without poly(I:C) stimulation compared to control hPAECs, though, some protein PKR expression still remained (figure 5.6).

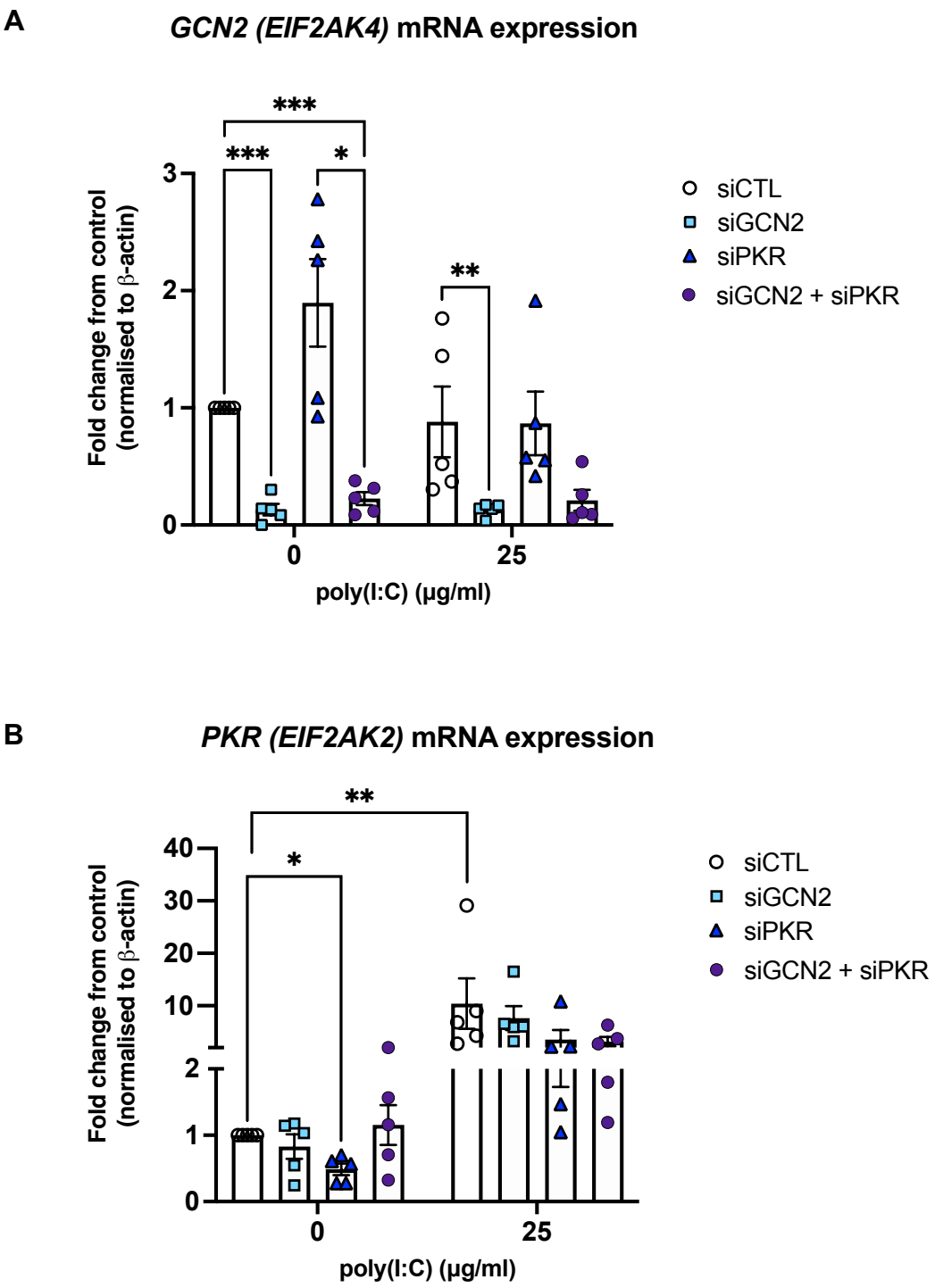

Figure 5.5 The knockdown of *GCN2 (EIF2AK4)* (A) and *PKR* (*EIF2AK2*) mRNA expression in si*GCN2*- and/or si*PKR* treated hPAECs, with and without poly(I:C) (25µg/ml) stimulation for 24 hours.

GCN2 (EIF2AK4) (A) and *PKR* (*EIF2AK2*) (B) mRNA expression was quantified by qRT-PCR. All data are presented as fold change where delta-delta Ct values are normalized to siCTL and unstimulated group. Delta Ct values were normalized to housekeeper gene *ACTB* and then to a reference sample (delta-delta Ct). Data show mean (top of bar) ± SEM. Two-way ANOVA, Šídák's multiple comparisons test. ***, p <0.001: **, p <0.01; *, p < 0.05. n=5 experimental repeats from 3 donors.

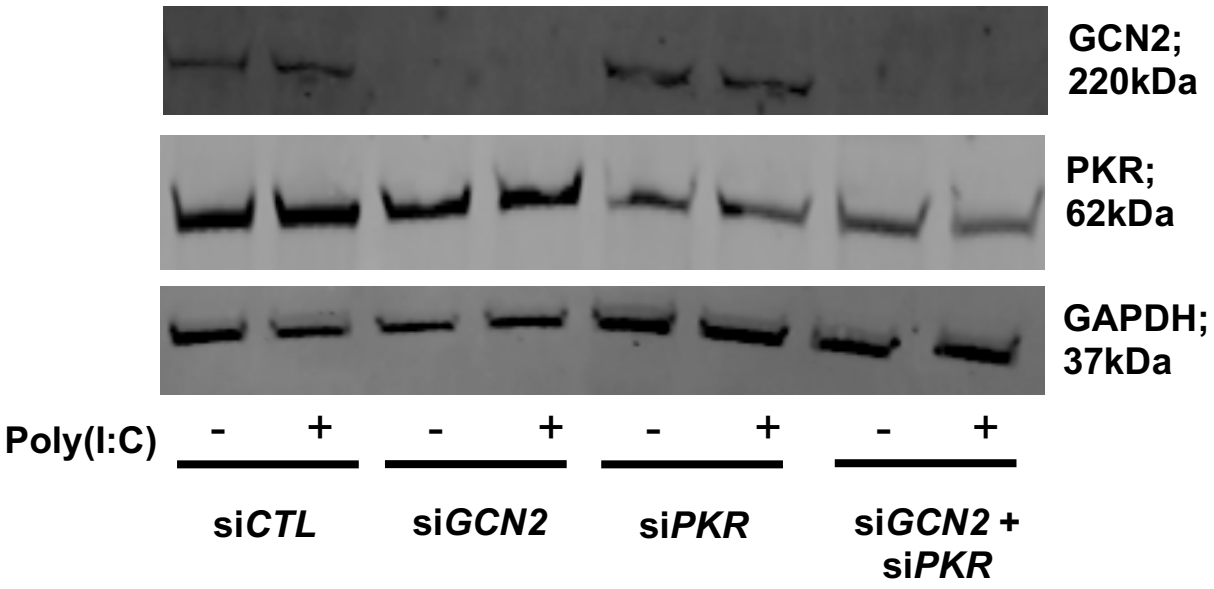

Figure 5.6 The knockdown of GCN2 and PKR protein in si*GCN2*- and/or si*PKR* treated hPAECs, with and without poly(I:C) (25µg/ml) stimulation for 24 hours.

Western blot analysis showing GCN2, and PKR protein to further validate knockdown in si*GCN2*- and/or si*PKR* treated hPAECs, with and without poly(I:C) stimulation for 24 hours. GADPH used as loading control. *n*=1.

5.7 GCN2 deficiency selectively enhanced poly(I:C)-induced TNFα release in hPAECs and simultaneous si*GCN2* and si*PKR* treatment attenuated TNFα release

In the attempt to validate initial observations of enhanced pro-inflammatory cytokine (i.e., TNFα and IP-10) release from GCN2-deficient BOECs stimulated with poly(I:C) (figure 5.2), pro-inflammatory cytokines in the supernatant of si*GCN2*-treated hPAECs stimulated with poly(I:C) (24 hours; 25μg/ml) were measured. To investigate mechanism, pro-inflammatory cytokines in the supernatant of si*PKR*- and double s*iGCN2*- and si*PKR*-treated hPAECs stimulated with poly(I:C) were also assessed by Luminex technology. At the same time, ATP activity as a surrogate of cell number was determined by CellTitre-Glo technology and data are shown in figure 5.8. The cytokines measured were normalised by cell number.

TNFα, IL-6 and IP-10 protein release were significantly induced by poly(I:C) in siCTL-treated hPAECs compared to unstimulated control (figure 5.7a-c).

GCN2 deficiency significantly enhanced poly(I:C)-induced TNFα release compared to control hPAECs stimulated with poly(I:C) (figure 5.7.a). Simultaneous GCN2 deficiency with partial PKR deficiency attenuated TNFα release compared to GCN2-deficient cells stimulated with poly(I:C) (figure 5.7.a).

GCN2 and/or deficiency did not affect poly(I:C)-induced IL-6 and IP-10 release compared to control hPAECs stimulated with poly(I:C) (figure 5.7.b-c).

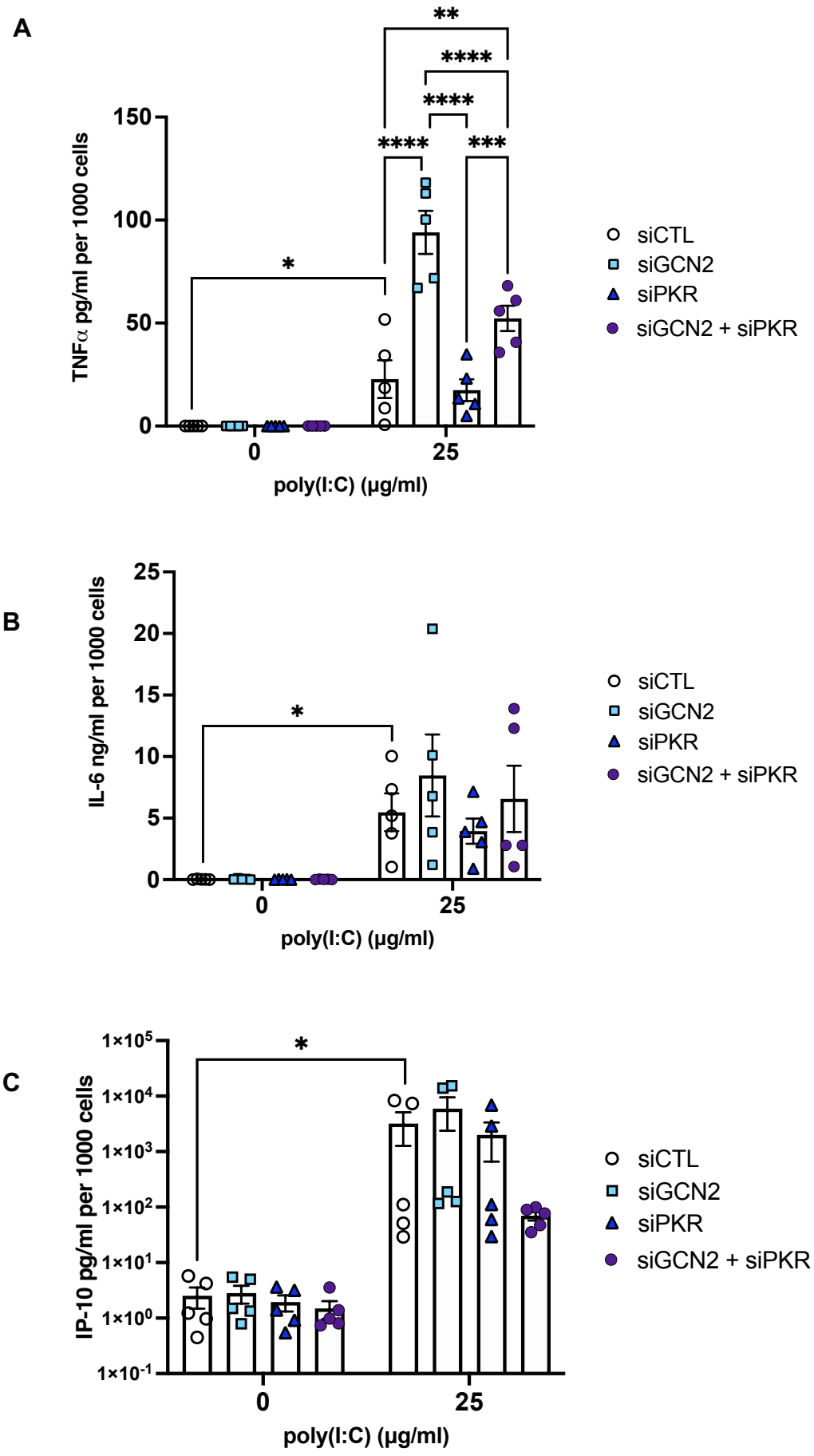
A
**
****
****
****
***
*
150
100
50
0
TNFα pg/ml per 1000 cells
0
25
poly(I:C) (μg/ml)
siCTL
siGCN2
siPKR
siGCN2 + siPKR
B
25
20
15
10
5
0
IL-6 ng/ml per 1000 cells
*
0
25
poly(I:C) (μg/ml)
siCTL
siGCN2
siPKR
siGCN2 + siPKR
C
1×10^5
1×10^4
1×10^3
1×10^2
1×10^1
1×10^0
1×10^-1
IP-10 pg/ml per 1000 cells
*
0
25
poly(I:C) (μg/ml)
siCTL
siGCN2
siPKR
siGCN2 + siPKR

Figure 5.7 The protein levels of TNFα, IL-6 and IP-10 in supernatant of GCN2- and/or PKR- deficient hPAECs with and without 24 hours of poly(I:C) stimulation.

Via Luminex technology, proinflammatory cytokine protein levels were quantified in cell supernatants of si*GCN2*- and/or si*PKR*- treated hPAECs with and without poly(I:C) stimulation (24 hours; 25μg/ml). To normalize, cytokine concentration was calculated per 1000 cells, in which the cell number was determined by CellTitre-Glo assay (figure 5.8). Data show mean (top of bar) ± SEM. Two-way ANOVA, Šídák's multiple comparisons test. ****, $p<0.0001$; ***, $p<0.001$; **, $p<0.01$; *, $p < 0.05$. $n=5$ experimental repeats from 3 donors.

5.8. GCN2 deficiency reduced ATP activity (surrogate marker of cell number) in poly(I:C) stimulated hPAECs in a caspase 3/7 activity independent manner

To investigate GCN2-deficient pulmonary endothelial cell phenotypes in response to poly(I:C) stimulation, cell number and apoptosis were assessed. ATP activity (i.e., cell viability) was utilised as a surrogate marker of cell number and caspase 3/7 activity as a surrogate marker of apoptosis. Assays were performed in si*GCN2*- and/or si*PKR*-treated hPAECs with and without poly(I:C) (24 hours; 25μg/ml) via CellTitre-Glo and caspase 3/7 assays, respectively.

ATP activity was significantly reduced in GCN2-deficient hPAECs with poly(I:C) stimulation when compared to poly(I:C)-stimulated control hPAECs (figure 5.8.a.). Simultaneous GCN2 deficiency with partial PKR deficiency in hPAECs stimulated with poly(I:C) had increased ATP activity levels compared to GCN2-deficient hPAECs stimulated with poly(I:C) (figure 5.8.a.).

Caspase 3/7 activity was significantly induced by poly(I:C) stimulation in siCTL-treated hPAECs compared to unstimulated control (figure 5.8.b). The treatment of. si*GCN2*- and/or si*PKR*- treated in hPAECs with and without poly(I:C)-stimulated hPAECs had no effect on caspase 3/7 activity when compared to respective control (figure 5.8.b).

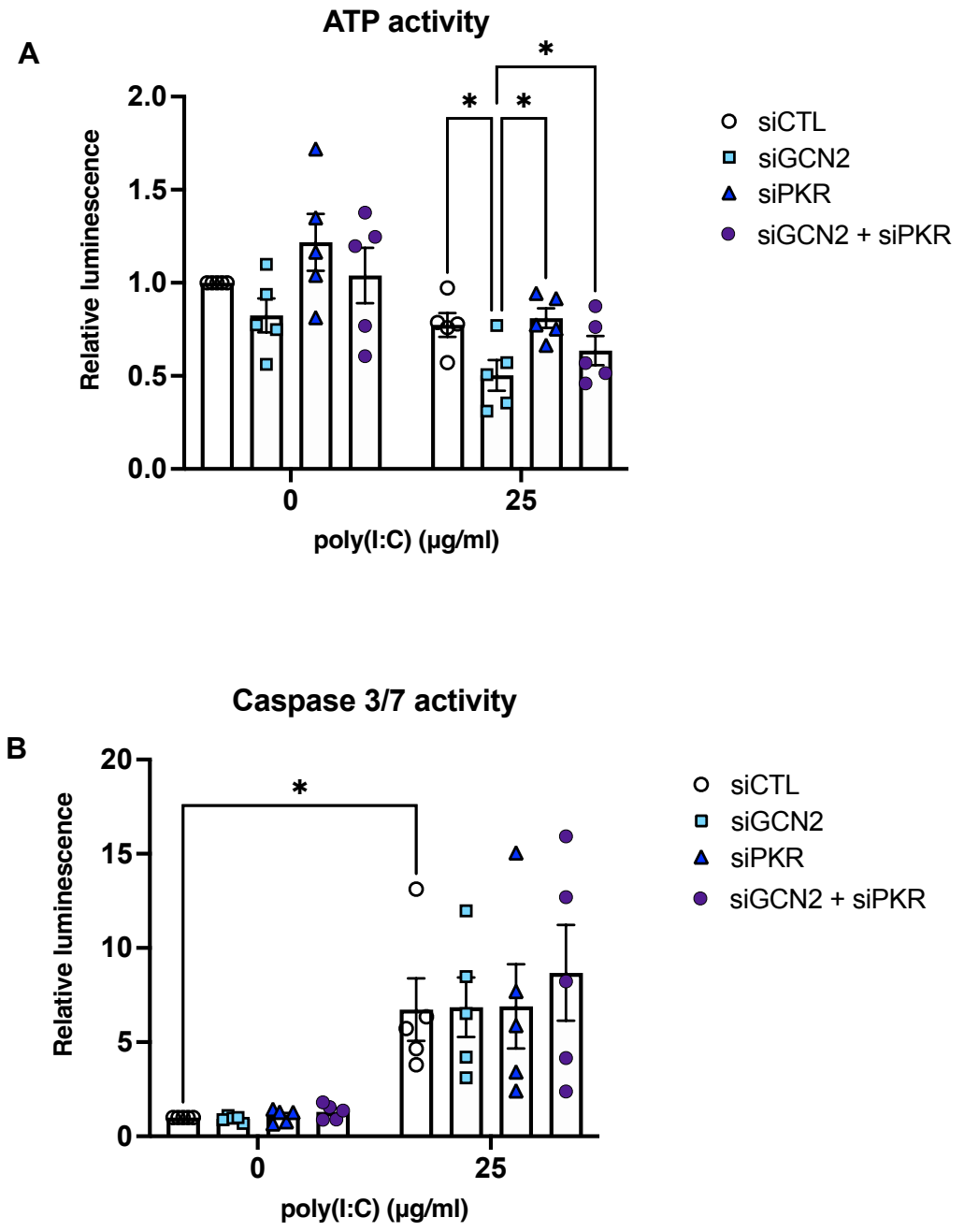

Figure 5.8 The relative luminescence as an indirect measurement of cell number and apoptosis in GCN2- and/or PKR- deficient hPAECs with and without 24 hours of poly(I:C) stimulation.

ATP activity and caspase 3/7 activity was quantified by indirect luminescence in si*GCN2* and/or si*PKR* treated hPAECs with and without poly(I:C) (24 hours; 25µg/ml). All data are presented as fold change relative to siCTL unstimulated hPAECs. Data show mean (top of bar) ± SEM. Two-way ANOVA, Šídák's multiple comparisons test. ***, $p < 0.001$; *, $p < 0.05$. n=5 experimental repeats from 3 donors.

5.9. Pro-inflammatory cytokines and *PKR* (*EIF2AK2*) mRNA expression in si*GCN2*-treated hPAECs were unaffected in response to 4 hours of poly(I:C)

To extend the findings from healthy donor BOECs and to investigate if the selective enhancement of poly(I:C)-induced TNFα release in GCN2-deficient hPAECs was associated with increased transcription, *TNFA, IL-6* and *IP-10 mRNA* expression was assessed in GCN2-deficient hPAECs with and without 4 hour poly(I:C) stimulation via qRT-qPCR. An earlier time point of 4 hour poly(I:C) stimulation in this hPAECs was chosen as transcriptional effects of poly(I:C) have previously been observed after 4 hours in previous studies (Conniff *et al*, 2022; Wang et al, 2016). Given that simultaneous si*GCN2*- and si*PKR*-treated hPAECs attenuated poly(I:C)-induced TNFα release compared to si*GCN2*-treated hPAECs poly(I:C) stimulated (24 hours), *PKR (EIF2AK2)* mRNA expression was also assessed in attempt to investigate mechanism.

Poly(I:C) stimulation for 4 hours in siCTL-treated hPAECs significantly induced *TNFA, IL-6, IP-10,* and *PKR (EIF2AK2)* mRNA expression when compared to unstimulated control (figure 5.9.a).

However, GCN2 deficiency did not affect the poly(I:C)-induced mRNA expression of *TNFA, IL-6, IP-10,* and *PKR (EIF2AK2)* (figure 5.9.a).

GCN2 deficiency in unstimulated hPAECs did not affect *TNFA, IL-6, IP-10,* and *PKR (EIF2AK2)* mRNA expression also (figure 5.9.a).

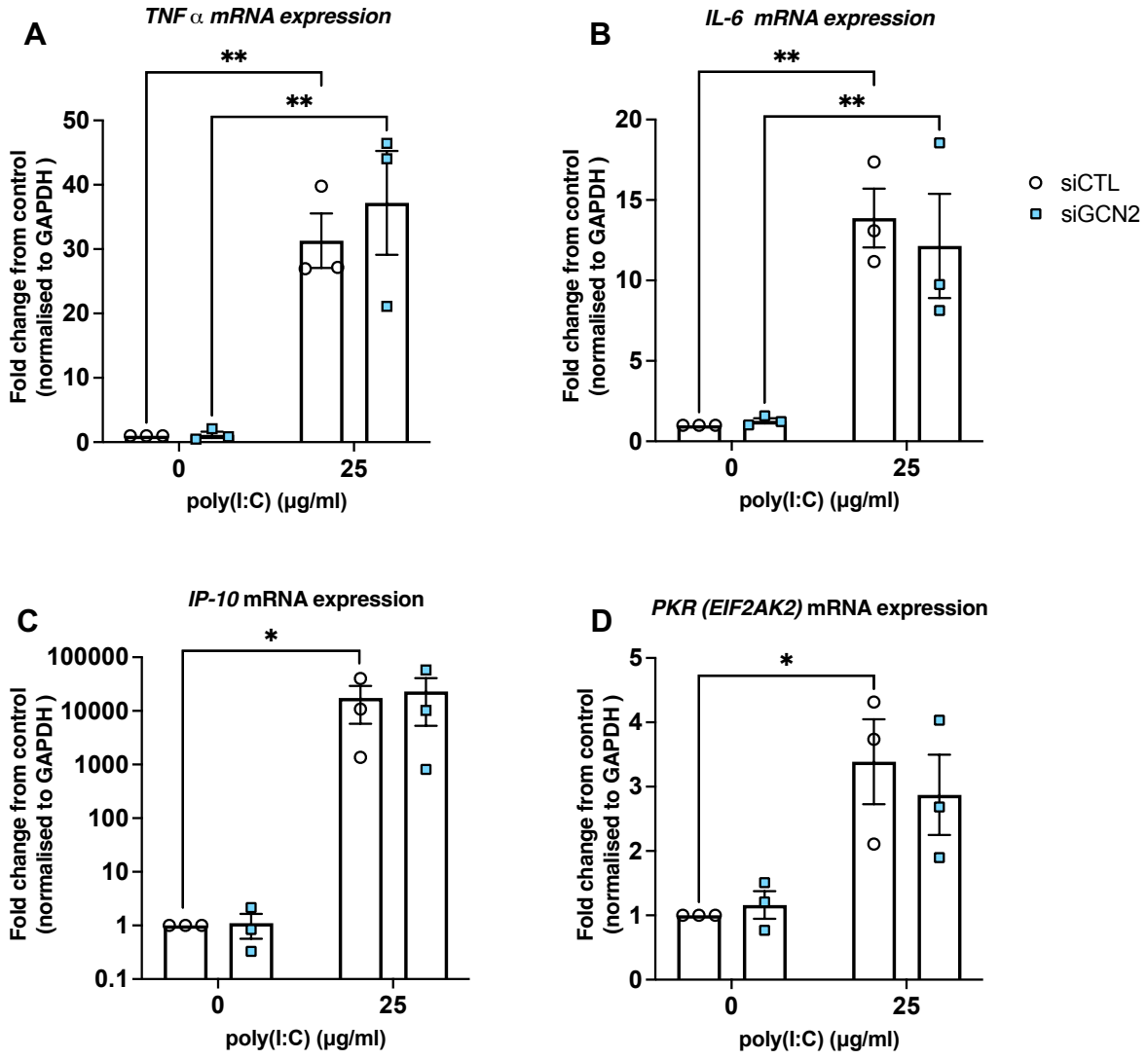

Figure 5.9 The relative mRNA expression of proinflammatory cytokines and *PKR (EIF2AK2)* in GCN2-deficient hPAECs with and without 4 hours of poly(I:C) stimulation.

Quantitative RT-PCR measured proinflammatory cytokines *TNFA* (A), *IL-6* (B) and *IP-10* (C) and interferon-stimulated gene *PKR* (*EIF2AK2*) mRNA expression in si*GCN2*- treated hPAECs with and without, poly(I:C) (4 hours; 25µg/ml). All data are presented as fold change where delta-delta Ct values are normalized to siCTL and unstimulated group. Delta Ct values were normalized to housekeeper gene *GAPDH* and then to a reference sample (delta-delta Ct). Data show mean (top of bar) ± SEM. Two-way ANOVA, Šídák's multiple comparisons test. **, p <0.01; *, p < 0.05. n=3.

5.10. Enhancement of *TNFA* mRNA expression in si*GCN2*-hPAECs in response to 24 hours of poly(I:C)

To investigate if the attenuation of TNFα release in simultaneous GCN2- and PKR-deficient hPAECs was associated with altered mRNA expression (at the later time point used in initial experiments with BOECs), RNA was extracted from si*GCN2*-and/or si*PKR*-treated hPAECs with and without poly(I:C) stimulation (24 hours; 25μg/ml). Subsequently qRT-PCR analysis measured *TNFA* mRNA expression, as well as *IL-6* and *IP-10.*

TNFA mRNA expression was significantly induced by poly(I:C) stimulation in siCTL-treated hPAECs compared to unstimulated control (figure 5.10.a). GCN2 deficiency significantly enhanced poly(I:C)-induced *TNFA* mRNA expression compared to siCTL hPAECs stimulated with poly(I:C) (figure 5.10.a). Whilst the trend of the mean *TNFA* mRNA expression in si*PKR*- and double si*GCN2*- and si*PKR*-treated hPAECs stimulated with poly(I:C) aligns with TNFα protein levels in section 5.7, such differences did not reach statistical significance at 95% confidence interval when compared to poly(I:C) stimulated controls (figure 5.10.a).

In addition, GCN2 deficiency did not affect the poly(I:C)-induced mRNA expression of *IL-6* and *IP-10* (figure 5.10.b-c).

A

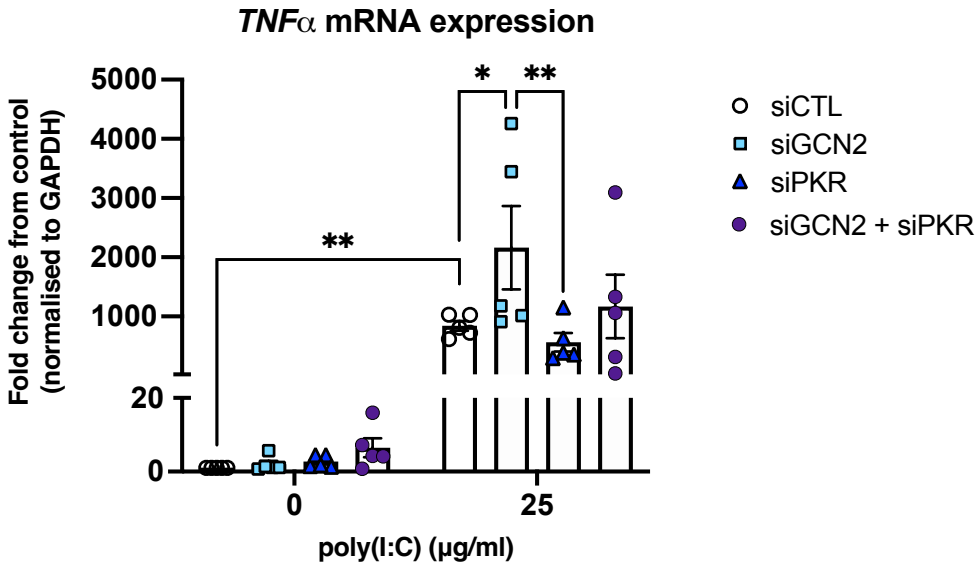
TNFα mRNA expression
Fold change from control (normalised to GAPDH)
5000
4000
3000
2000
1000
20
0
*
**
**
0
25
poly(I:C) (µg/ml)
siCTL
siGCN2
siPKR
siGCN2 + siPKR

B

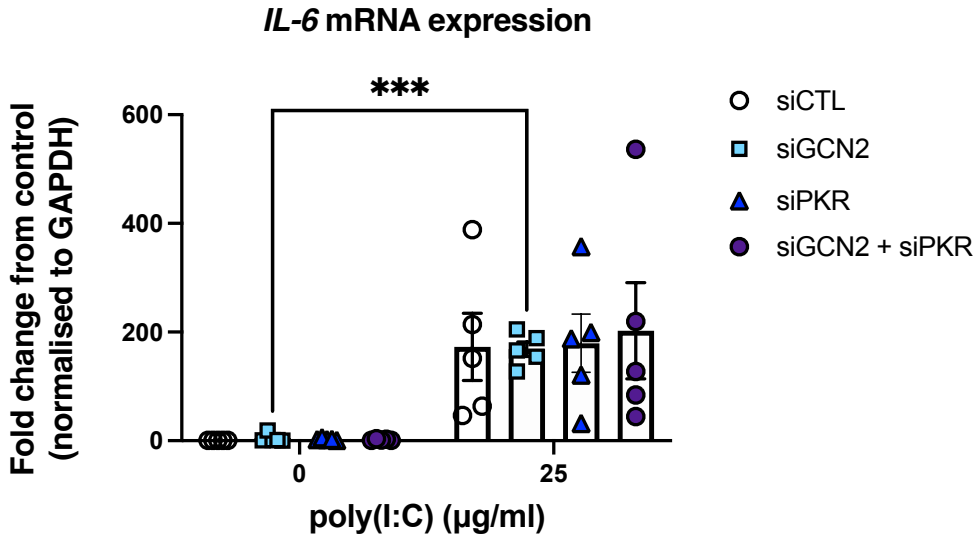
IL-6 mRNA expression
Fold change from control (normalised to GAPDH)
600
400
200
0
***
0
25
poly(I:C) (µg/ml)
siCTL
siGCN2
siPKR
siGCN2 + siPKR

C

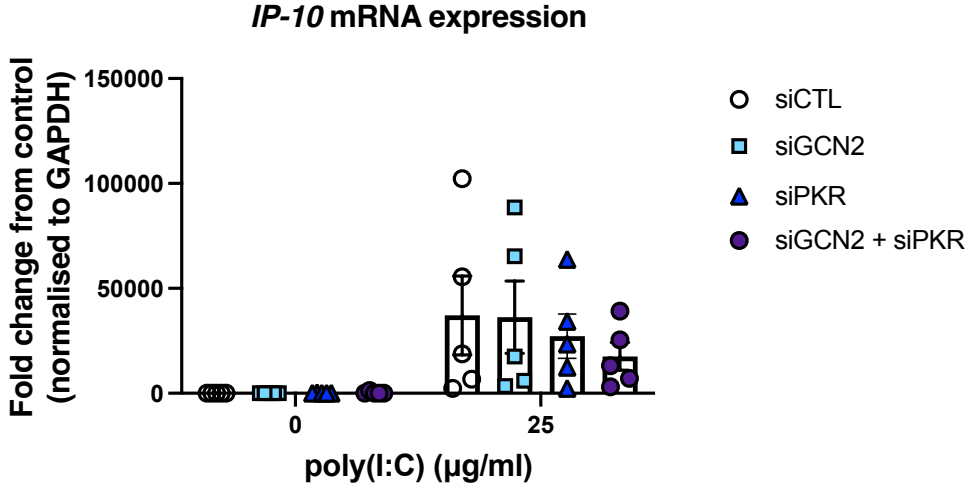
IP-10 mRNA expression
Fold change from control (normalised to GAPDH)
150000
100000
50000
0
0
25
poly(I:C) (µg/ml)
siCTL
siGCN2
siPKR
siGCN2 + siPKR

Figure 5.10 The relative mRNA expression of proinflammatory cytokines in GCN2 and/or PKR deficient hPAECs with and without 24 hours poly(I:C) stimulation.

Quantitative RT-PCR measured proinflammatory cytokines *TNFA* (A), *IL-6* (B) and *IP-10* (C) mRNA expression in si*GCN2*- and/or si*PKR*- treated hPAECs with and without, poly(I:C) (24 hours; 25μg/ml). All data are presented as fold change where delta-delta Ct values are normalized to siCTL and unstimulated group. Delta Ct values were normalized to housekeeper gene *GAPDH* and then to a reference sample (delta-delta Ct). Data show mean (top of bar) ± SEM. Two-way ANOVA, Šídák's multiple comparisons test. ***, $p<0.001$, **, $p<0.01$; *, $p < 0.05$. $n=5$ experimental repeats from 3 donors.

5.11 mRNA sequencing in GCN2 deficient hPAECs stimulated with poly(I:C)

RNA-sequencing of GCN2-deficient hPAECs stimulated with poly(I:C) (4 hours; 25μg/ml) was performed to investigate the phenotype of enhanced TNFα release and to explore possible mechanisms for the enhanced *TNFA* transcription previously observed after 24 hours of stimulation.

Poly(A)-enriched RNA from si*GCN2*-treated hPAECs (and siCTL-treated hPAECs) with and without poly(I:C) (25μg/ml) stimulation for 4 hours (*n*=3, clinical data in appendix table 1) were subjected to Illumina sequencing technology of sequencing by synthesis and software identified each nucleotide in a process called base calling to produce FASTQ files. The bioinformatic pipeline of 'nf-core/rnaseq' allowed the input of FASTQ files and performed quality control, adapter trimming, genome alignment using STAR and read quantification using Salmon (Patel et al., 2023). All experimental groups subjected to RNA-sequencing are presented in table 5.1.

The following RNA-sequencing analysis makes two different comparisons:

1. 'Poly(I:C)-stimulated' versus 'unstimulated' in siCTL; assessing the transcriptomic effects of poly(I:C) stimulation in control hPAECs
2. 'si*GCN2*-treated poly(I:C)-stimulated' versus 'siCTL poly(I:C)-stimulated'; assessing the transcriptomic effects of GCN2 deficiency in poly(I:C) stimulated hPAECs

In addition, to control for the effects of lipofectamine-transfection on hPAECs, an untransfected and unstimulated (i.e., no poly(I:C)) control was produced for each

biological repeat and this was compared to transfected (i.e., siCTL-treated), unstimulated hPAECs (appendix table 3 and figure 3). Via DESeq2 analysis, it was determined that the method of lipofectamine-transfection had no significant effect on the unstimulated transcriptome of hPAECs (appendix table 3 and figure 3).

Table 5.1 Experimental groups subjected to RNA-sequencing in hPAECs

ID	*Transfection*	*poly(I:C)*	*N=3 (batch no)*
HT1	no	no	(*n*1) 5513
HT2	yes (siCTL)	no	(*n*1) 5513
HT3	yes (siCTL)	yes (4 hrs)	(*n*1) 5513
HT4	yes (siGCN2)	no	(*n*1) 5513
HT5	yes (siGCN2)	yes (4hrs)	(*n*1) 5513
HT11	no	no	(*n*2) 8987
HT12	yes (siCTL)	no	(*n*2) 8987
HT13	yes (siCTL)	yes (4 hrs)	(*n*2) 8987
HT14	yes (siGCN2)	no	(*n*2) 8987
HT15	yes (siGCN2)	yes (4hrs)	(*n*2) 8987
HT16	no	no	(*n*3) 8096
HT17	yes (siCTL)	no	(*n*3) 8096
HT18	yes (siCTL)	yes (4 hrs)	(*n*3) 8096
HT19	yes (siGCN2)	no	(*n*3) 8096
HT20	yes (siGCN2)	yes (4hrs)	(*n*3) 8096

Firstly, all FASTQ files were assessed for quality control and data are presented in the next section.

5.11.1 Quality control of FASTQ files

MultiQC v1.11 aggregated quality control results from several bioinformatic analyses (i.e., Salmon, FastQC and cutadapt). This generated a general statistic table

containing mapped aligned (%), mapped aligned (millions), duplicate reads (%), average GC content (%), average sequence length (bp), total sequences (millions) before and after trimming and the total base pairs (trimmed) (appendix table 2).

As assessed by FastQC, 41.6-54.5 million sequences were generated per sample (*n*=15) (figure 5.11.a). All reads (base pair length 150) had median Phred quality score of more than 30, inferring an error rate less than 0.1% (i.e., accuracy of more than 99.99%) when base calling (figure 5.11.b). The percentage GC content in all 15 samples was normally distributed (figure 5.11.c).

Using the DESeq2 bioinformatic package in R (Love *et al*, 2014), principal component analysis (PCA) and heat map of sample-to-sample distances reduced dimensionality of the data to aid with data visualisation. Both plots showed clustering of data points in unstimulated hPAECs compared to poly(I:C) stimulated hPAECs, irrespective of siRNA treatment (figure 5.12).

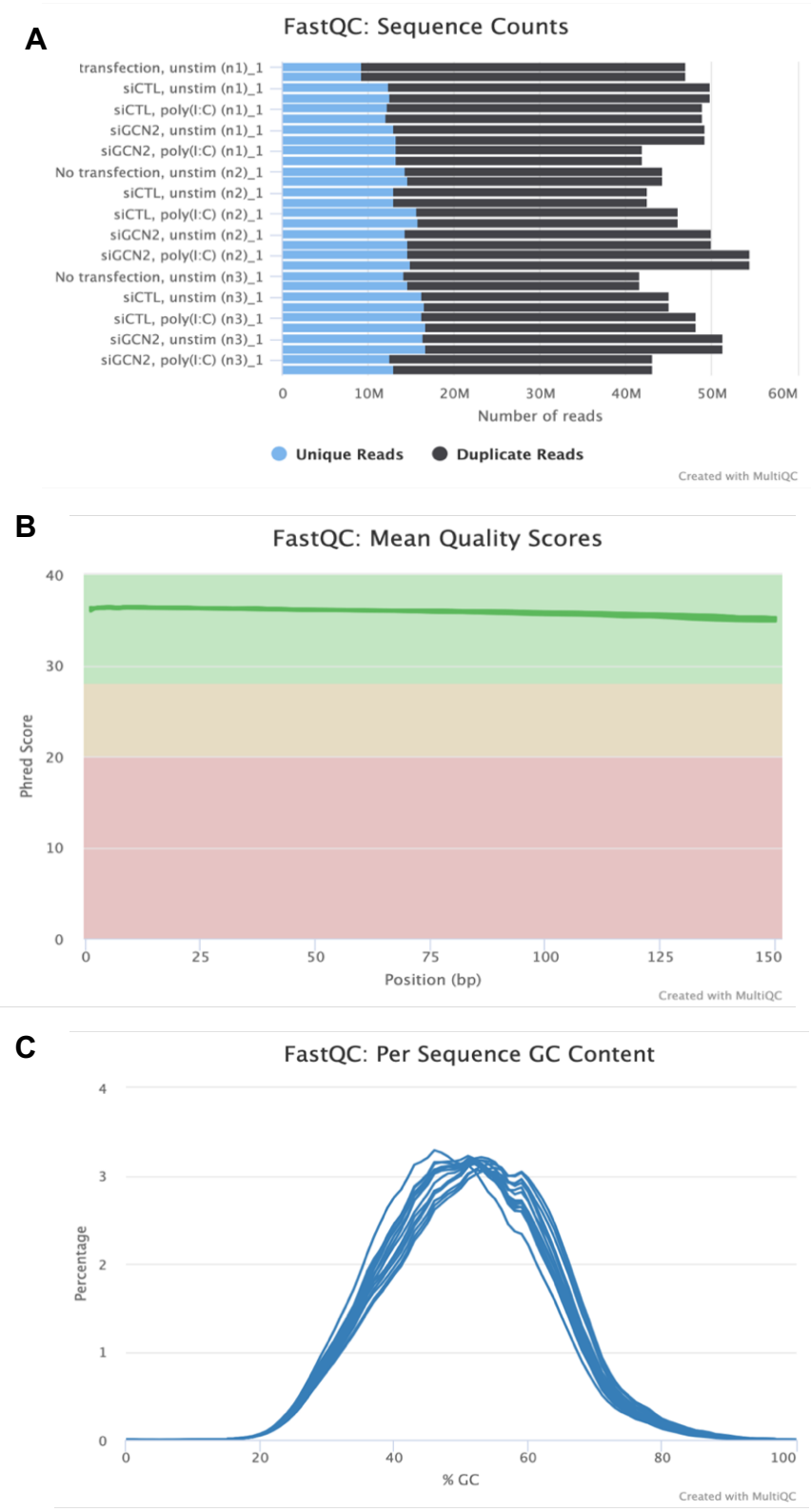

Figure 5.11. Quality control analysis of FASTQ files using FASTQC bioinformatic package.

Plots of sequence counts (millions) (A), Phred score (B) and GC content (%) (C) for all 15 samples after adapter trimming as generated with FASTQC bioinformatic analysis and presented in MultiQC report.

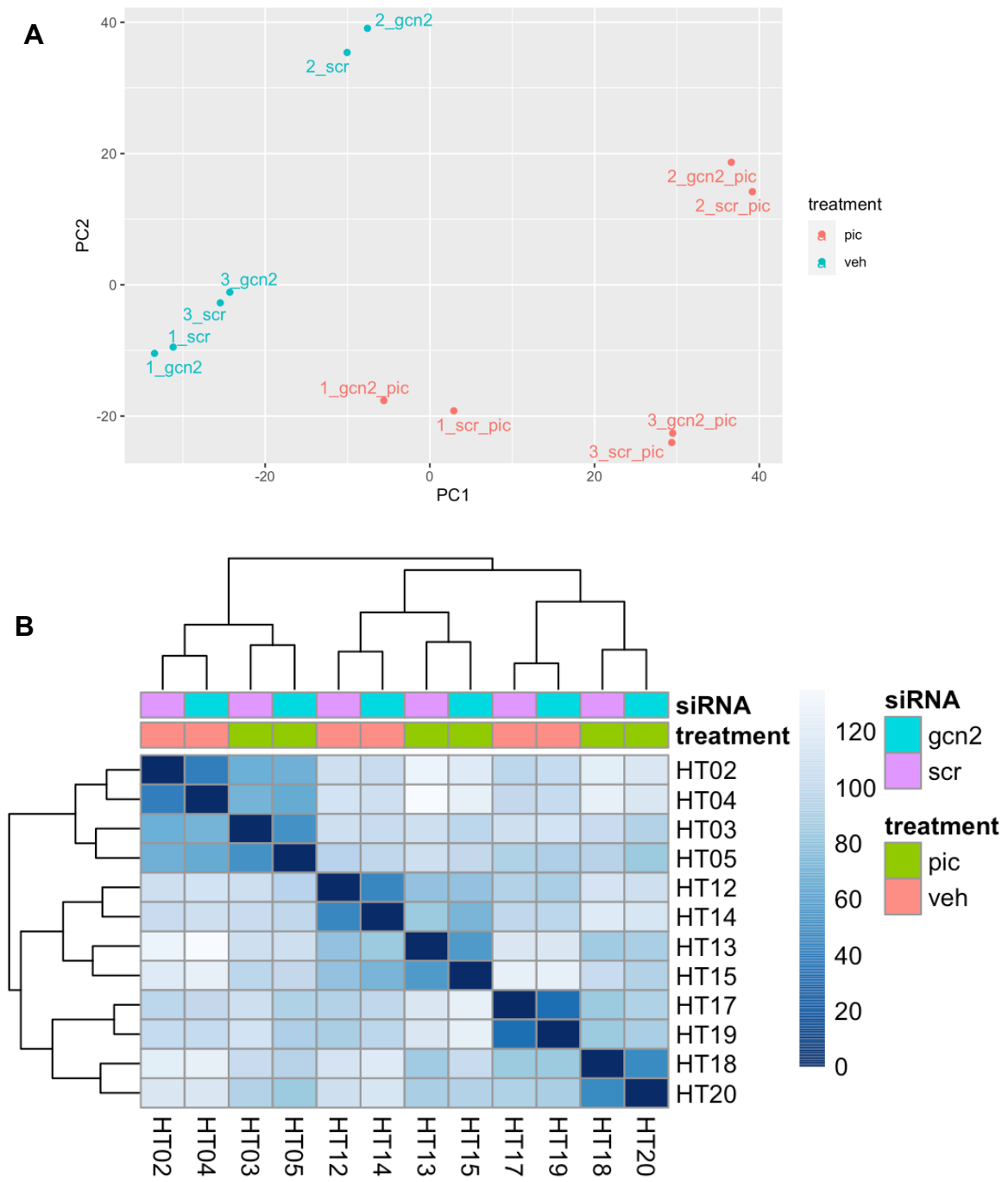

Figure 5.12 PCA plot and heat map to visual the relationship between all samples in a 2D representation of the data.

PCA plot (A) and heat map (B) for all 15 samples after adapter trimming as generated with Salmon DESeq2 bioinformatic packages in R studio.

5.11.2 Poly(I:C)-induced differentially expressed genes in hPAECs

DESeq2 quantified 1199 differentially expressed genes (DEGs) (adj. *p*>0.05) in poly(I:C) stimulated versus unstimulated in siCTL-treated hPAECs. All significant DEGs are presented as a volcano plot (figure 5.13) and in a list (appendix table 4). Of all the statistically significant DEGs, 477 genes had a log2 fold change ≥1 and 127 genes had a log2 fold change ≤ -1 (i.e., 2-fold absolute difference). The top 50 DEGs ranked by adjusted *p* value are shown in table 5.2. The most significant (i.e., smallest adjusted *p* value) DEG was *IFIT5* and its log2 fold change was determined as 4.221 (3.dp) (table 5.2; figure 5.13).

Notably, the largest log2 fold change in poly(I:C)-stimulated versus unstimulated hPAECs was *CXCL10* (*IP-10*) (14.29 log2 fold change, adjusted *p*-value: $9.754e\text{-}^{14}$) (appendix table 4; figure 5.13). As previously shown by qRT-PCR analysis in section 5.9, *IL-6, TNFA,* and *PKR (EIF2AK2)* had significant (adjusted *p*-value <0.05) positive log2 fold changes in poly(I:C)-stimulated versus unstimulated in siCTL hPAECs (appendix table 4; figure 5.13).

PKR (EIF2AK2) was the only gene transcript of all integrated stress response kinases to be differentially expressed with poly(I:C) stimulation in siCTL-treated hPAECs. *GCN2* (*EIF2AK4*), *HRI* (*EIF2AK1)* and *PERK (EIF2AK3)* were not differentially expressed at a threshold of adjusted *p*-value <0.05.

In addition, the dsRNA pattern recognition receptors *TLR3*, *IFIH1* (*MDA5), DDX58 (RIG-I), OASL,* and transcription factors subunits of NF-KB (i.e., *NFKB1* and *NFKB2*)

and subunits of AP1 (i.e., *JUNB* and *FOSL2*) had significant (adjusted *p*-value <0.05) positive log2 fold changes in poly(I:C)-stimulated versus unstimulated in siCTL-treated hPAECs (appendix table 4; figure 5.13).

Table 5.2. Top 50 DEGs ranked on adjusted *p*-values in poly(I:C)-stimulated versus unstimulated in siCTL-treated hPAECs

Gene Symbol	*Gene Name*	*Log2 (Fold Change)*	*SE of Log2*	*Adj. p-value*
IFIT5	interferon induced protein with tetratricopeptide repeats 5	4.22101024	0.196	2.08E-98
RND1	Rho family GTPase 1	4.71431914	0.236	4.51E-85
ATF3	activating transcription factor 3	4.70333476	0.242	2.05E-80
USP18	ubiquitin specific peptidase 18	3.17181062	0.174	2.21E-70
IRF1	interferon regulatory factor 1	4.33022539	0.250	1.05E-63
FAM46A	terminal nucleotidyltransferase 5A	2.82216256	0.164	2.54E-63
IL6	interleukin 6	3.77065823	0.232	3.13E-56
CCRN4L	nocturnin	3.0923222	0.201	6.29E-50
CEBPD	CCAAT enhancer binding protein delta	3.80173138	0.252	2.84E-48
ZFP36	ZFP36 ring finger protein	2.42819653	0.164	2.51E-46
GCH1	GTP cyclohydrolase 1	3.93157766	0.289	6.76E-39
NCOA7	nuclear receptor coactivator 7	2.9702001	0.219	1.18E-38
SAMD9	sterile alpha motif domain containing 9	3.91765273	0.297	1.31E-36
PPM1K	protein phosphatase, Mg2+/Mn2+ dependent 1K	3.10571771	0.238	6.93E-36
DHX58	DExH-box helicase 58	3.74252654	0.294	4.33E-34
MYD88	MYD88 innate immune signal transduction adaptor	1.97595063	0.157	2.19E-33
PMAIP1	phorbol-12-myristate-13-acetate-induced protein 1	3.42317937	0.273	3.19E-33
LOC101929758	Gene Locus	4.27409788	0.345	2.63E-32
DDX60	DExD/H-box helicase 60	3.48787407	0.283	5.12E-32
TRIM21	tripartite motif containing 21	2.46707524	0.203	5.76E-31
ARID5A	AT-rich interaction domain 5A	2.6003312	0.217	3.34E-30
MSX1	msh homeobox 1	4.53554216	0.181	7.15E-30
IL7R	interleukin 7 receptor	2.15830219	0.381	7.15E-30
PPAP2B	phospholipid phosphatase 3	1.82404622	0.154	1.54E-29
SLC7A2	solute carrier family 7 member 2	2.65458334	0.226	5.17E-29
IFI44	interferon induced protein 44	3.67614218	0.315	1.22E-28
TXNIP	thioredoxin interacting protein	2.03689649	0.176	2.96E-28
SOX18	SRY-box transcription factor 18	-2.5374931	0.222	1.60E-27
RCAN1	regulator of calcineurin 1	1.76652359	0.160	1.43E-25
JUNB	JunB proto-oncogene, AP-1 transcription factor subunit	2.33406037	0.212	2.16E-25
SP110	SP110 nuclear body protein	2.78219258	0.253	2.28E-25
CSRNP1	cysteine and serine rich nuclear protein 1	1.9889961	0.183	8.07E-25
HLA-F	major histocompatibility complex, class I, F	3.63013166	0.335	1.05E-24

TRAFD1	TRAF-type zinc finger domain containing 1	2.22451658	0.208	5.21E-24
RIPK2	receptor interacting serine/threonine kinase 2	3.07765793	0.289	8.42E-24
LIF	LIF interleukin 6 family cytokine	2.74712986	0.262	4.96E-23
SLC25A28	solute carrier family 25 member 28	2.71833903	0.260	6.05E-23
IFI35	interferon induced protein 35	3.36203622	0.323	1.01E-22
SLFN5	schlafen family member 5	2.51578543	0.243	1.90E-22
CCL5	C-C motif chemokine ligand 5	8.66114137	0.839	2.13E-22
OASL	2'-5'-oligoadenylate synthetase like	11.5431187	1.123	3.09E-22
IL18R1	interleukin 18 receptor 1	2.39448108	0.234	4.03E-22
C2CD4B	C2 calcium dependent domain containing 4B	2.58891491	0.254	7.20E-22
FGF5	fibroblast growth factor 5	2.18584278	0.220	9.47E-21
PLSCR1	phospholipid scramblase 1	2.55546831	0.259	2.09E-20
RHOB	ras homolog family member B	1.55562561	0.159	3.37E-20
SOCS1	suppressor of cytokine signaling 1	2.80416121	0.286	3.45E-20
IFIT3	interferon induced protein with tetratricopeptide repeats 3	8.26547093	0.844	3.89E-20
CXCL11	C-X-C motif chemokine ligand 11	9.56707306	0.978	3.98E-20

Log2 fold change between poly(I:C)-stimulated versus unstimulated in siCTL-treated hPAECs as calculated using DESeq2 analysis. SE; standard error of Log2 fold change. A positive log2 fold change implies relatively more gene expression in poly(I:C)-stimulated hPAECs compared to unstimulated siCTL-treated hPAECs. The *p*-value (not shown in this table) calculated using Wald test was adjusted for multiple hypothesis testing using the Benjamini-Hochberg procedure (adjusted (adj.) *p*-value). The table is ranked by adj. *p* value. Log2 fold change and SE of Log2 presented as 3 decimal places.

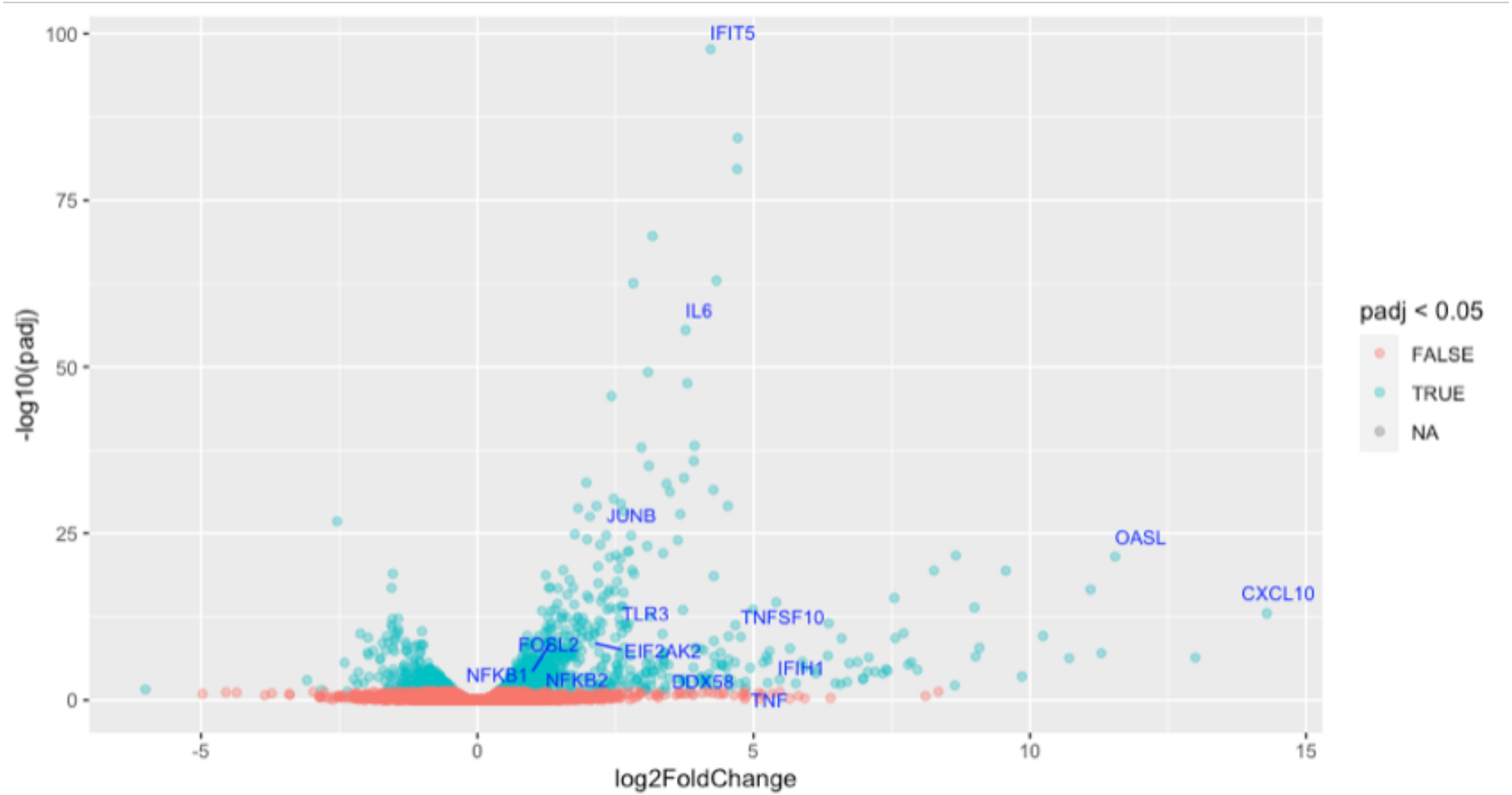

Figure 5.13. Volcano plot showing differentially expressed genes (DEGs) upon 4 hours of poly(I:C) stimulation in siCTL-treated hPAECs.

DESeq2 bioinformatic package identified 1199 DEGs in poly(I:C)-stimulated versus unstimulated in siCTL-treated hPAECs (4 hours; 25 μg/ml) at a 5% level of significance (i.e., adj p<0.05). Adjusted p value is presented as -log^{10}(adj p value) on y axis i.e., -log^{10}(adj p value) >1.3 are significantly different at a 5% significance level.

5.11.3. Over representation analysis of poly(I:C)-induced DEGs in siCTL-treated hPAECs

All (1199) DEGs were subjected to over-representation analysis (ORA) to identify molecular functions, biological processes and KEGG pathway analysis using WEB-based GEne SeT AnaLysis Toolkit (WebGestalt) (Liao et al., 2019).

The most enriched molecular function (Gene Ontology) was identified as 'cytokine receptor binding' (enrichment ratio: 3.4793, FDR: $3.2720e^{-12}$, *p*-value: 1.7764e-^{15}) (figure 5.14).

The most enriched KEGG pathway was identified as TNF signalling pathway (enrichment ratio: 5.8728, FDR: $<2.2e^{-16}$, *p*-value: $<2.2e^{-16}$) (figure 5.14).

The most enriched biological process (Gene Ontology) was identified as innate immune response (enrichment ratio: 2.3271, FDR: $<2.2e^{-16}$, *p*-value: $<2.2e^{-16}$) (figure 5.14).

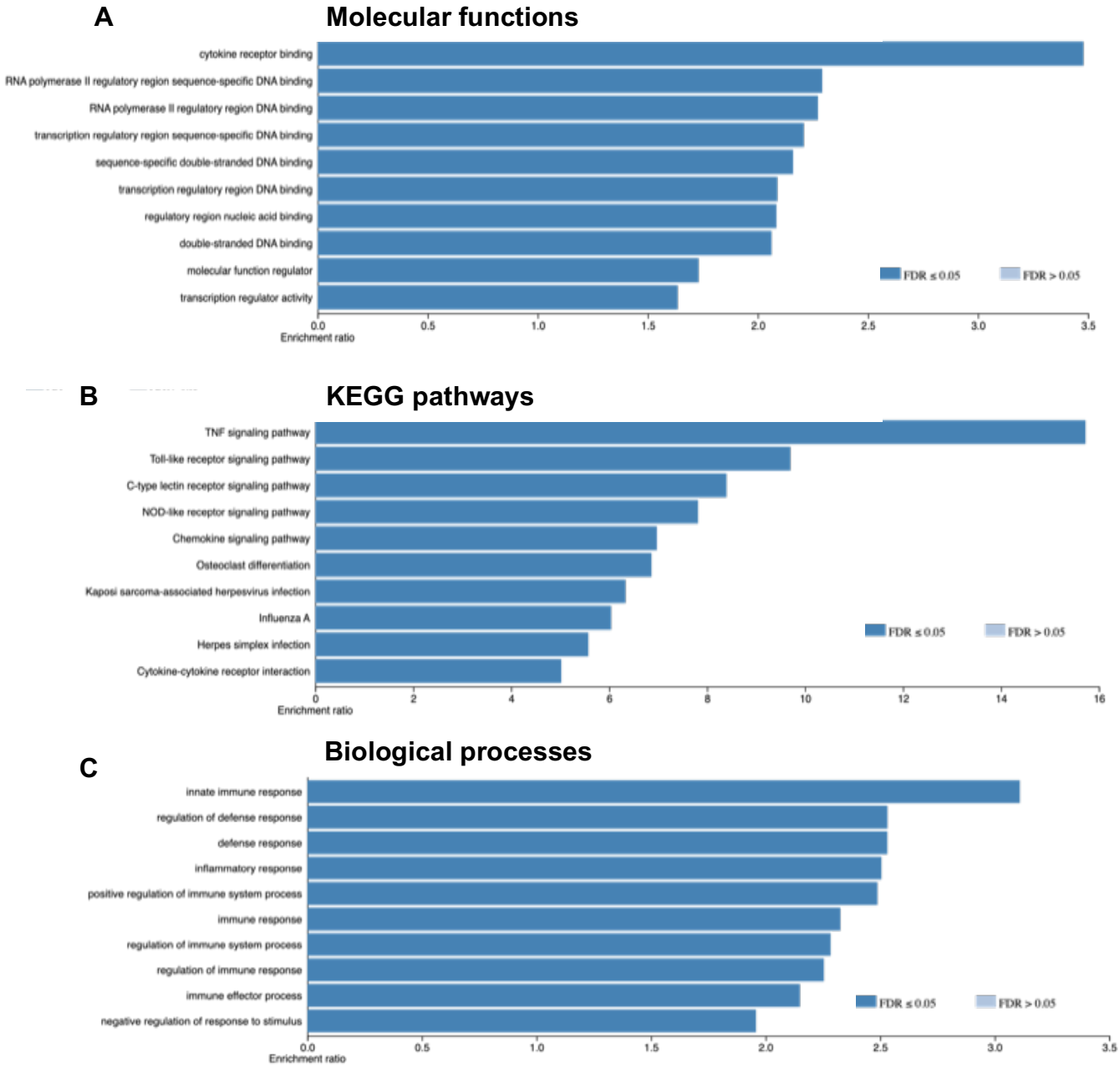

Figure 5.14 In ORA analysis of DEGs, molecular functions (A), KEGG pathways (B) and biological processes (C) were significantly enriched in poly(I:C) (4 hours;25μg/ml) stimulated siCTL-treated hPAECs

All (1199) DEGs (i.e., adjusted *p*-value of ≤ 0.05) as calculated by DESeq2 were inputted into WebGestalt and subjected to over-representation analysis (ORA). Enrichment ratios are ranked and respective false discovery rate (FDR) at a threshold of $p<0.05$ are reported. The false discovery rate (FDR) method of Benjamini-Hochberg method was used.

5.11.4. Differentially expressed genes of si*GCN2*-treated poly(I:C)-stimulated versus siCTL poly(I:C)-stimulated hPAECs

To identify the transcriptional impact of GCN2 deficiency on poly(I:C)-stimulated hPAECs (4 hours; 25μg/ml), DESeq2 was used to compare gene expression between si*GCN2*-treated poly(I:C)-stimulated versus siCTL poly(I:C)-stimulated hPAECs.

DESeq2 quantified 48 DEGs (adjusted p>0.05) in si*GCN2*-treated poly(I:C)-stimulated versus siCTL poly(I:C)-stimulated hPAECs. The threshold of adjusted p value was then expanded to $p \geq 0.1$. DESeq2 quantified 66 DEGs (adjusted $p < 0.1$) (table 5.3) and these are presented in a volcano plot (figure 5.15.). Subsequent ORA was conducted on the 66 DEGs (adjusted $p < 0.1$) (section 5.11.5).

Of all the statistically significant 66 DEGs (adjusted $p < 0.1$), 14 genes had a positive log2 fold change of which 10 out of 14 genes had log2 fold change >1 and 52 genes had a negative log2 fold change of which 17 out of 52 genes had a log2 fold change < -1 (i.e., 2-fold absolute difference) (table 5.3).

The most significant (i.e., smallest adjusted p value) DEGs was *EIF2AK4 (GCN2)* and its log2 fold change was determined as -2.213 (3.dp) (table 5.3; figure 5.13). *EIF2AK4 (GCN2)* was identified as a significant DEG in si*GCN2*-treated unstimulated versus siCTL unstimulated hPAECs (-2.063 log2 fold change, adjusted p-value: 0.0197) (appendix table 5). This successful knockdown of si*GCN2*-treated hPAECs with and without poly(I:C) (4 hours; 25μg/ml), was validated by qRT-PCR analysis and significant reductions in *EIF2AK4 (GCN2)* were measured (figure 5.16).

In an attempt to identify DEGs in poly(I:C)-stimulated siCTL (i.e., no PVOD model) hPAECs which respond differential to poly(I:C)-stimulation in the context of GCN2 deficiency (i.e. si*GCN2*; PVOD *in vitro* model) in hPAECs, gene lists of DEGs in poly(I:C)-stimulated control hPAECs (table 5.2) and DEGs in GCN2 deficient poly(I:C)-stimulated hPAECs (table 5.3) were compared and 21 duplicate gene IDs between list were identified and are highlighted in red in table 5.3.

TNFA mRNA transcripts were not differentially expressed in si*GCN2*-treated hPAECs stimulated with poly(I:C) compared to siCTL poly(I:C)-stimulated hPAECs (4 hours; 25μg/ml) as assessed by DESeq2. The normalised counts of *TNFA* in siGCN2-treated hPAECs stimulated with poly(I:C) and controls are plotted in figure 5.17 to easily visualise this. These data are consistent with the previous qRT-PCR analysis presented in figure 5.9.a.

Table 5.3 All DEGs in si*GCN2*-treated poly(I:C)-stimulated versus siCTL poly(I:C)-stimulated hPAECs

Gene symbol	*Gene Name*	*Log2 (Fold Change)*	*SE of Log2*	*Adj. p-value*
EIF2AK4	eukaryotic translation initiation factor 2 alpha kinase 4 (encodes GCN2)	-2.213	0.293	5.90E-10
FABP4	fatty acid binding protein 4	1.338	0.218	5.82E-06
LOC102723726		-1.476	0.258	5.25E-05
TBX20	T-box transcription factor 20	-2.476	0.462	3.07E-04
EEF1E1-BLOC1S5	EEF1E1-BLOC1S5 readthrough (NMD candidate)	-3.453	0.685	*1.33E-03*
RAD51L3-RFFL		3.672	0.752	*2.53E-03*
RNF103-CHMP3	RNF103-CHMP3 readthrough	-7.226	1.509	*2.75E-03*
LOC102724705		-3.893	0.809	*2.75E-03*
TMED8	transmembrane p24 trafficking protein family member 8	-1.610	0.338	*2.75E-03*
RN7SL2	RNA component of signal recognition particle 7SL2	-1.317	0.275	*2.75E-03*
LOC100506603		1.410	0.299	*3.10E-03*
SLMO2-ATP5E		-3.960	0.842	*3.12E-03*
ZBED6	zinc finger BED-type containing 6	-1.941	0.418	*3.73E-03*
TRIM56	tripartite motif containing 56	-0.995	0.216	*3.73E-03*
PVRL3	nectin cell adhesion molecule 3	-0.950	0.207	*3.73E-03*
APOL6	apolipoprotein L6	-0.842	0.182	*3.73E-03*
C7orf55-LUC7L2	FMC1-LUC7L2 readthrough	1.540	0.334	*3.73E-03*
COL4A6	Collagen type IV alpha 6 chain	-0.994	0.222	*6.13E-03*
PIEZO2	piezo type mechanosensitive ion channel component 2	-0.994	0.227	*8.93E-03*
LAMA5	laminin subunit alpha 5	-0.803	0.185	*1.03E-02*
LOC101929758		-1.210	0.281	*1.11E-02*
SOD2	superoxide dismutase 2	-0.857	0.203	*1.65E-02*
IRF6	interferon regulatory factor 6	1.001	0.238	*1.69E-02*
CSF2RB	colony stimulating factor 2 receptor subunit beta	-0.852	0.204	*1.73E-02*
PCDH7	protocadherin 7	-1.018	0.245	*1.79E-02*
ARMCX5-GPRASP2	ARMCX5-GPRASP2 readthrough	3.287	0.790	*1.79E-02*
EVC	EvC ciliary complex subunit 1	-0.831	0.201	*1.92E-02*
SLFN5	schlafen family member 5	-1.023	0.249	*2.06E-02*
GALNT4	polypeptide N-acetylgalactosaminyltransferase 4	-0.997	0.247	*2.73E-02*
COL4A5	Collagen type IV alpha 5 chain	-0.898	0.226	*3.11E-02*
OTUD4	OTU deubiquitinase 4	-0.799	0.200	*3.11E-02*
MGP	matrix Gla protein	0.796	0.200	*3.11E-02*
BDNF	brain derived neurotrophic factor	1.391	0.350	*3.11E-02*
PLBD2	phospholipase B domain containing 2	-0.941	0.238	*3.27E-02*
CLEC2B	C-type lectin domain family 2 member B	0.749	0.190	*3.27E-02*
LOC102723728		1.183	0.300	*3.27E-02*
GBP4	guanylate binding protein 4	-0.793	0.202	*3.47E-02*
GABBR2	gamma-aminobutyric acid type B receptor subunit 2	-0.817	0.210	*3.55E-02*
COL8A1	Collagen type VIII alpha 1 chain	-0.797	0.204	*3.55E-02*
GNB4	G protein subunit beta 4	-0.714	0.184	*3.55E-02*
TGM2	transglutaminase 2	-0.699	0.180	*3.55E-02*
CPA3	carboxypeptidase A3	1.246	0.319	*3.55E-02*

ARL10	ADP ribosylation factor like GTPase 10	-1.449	0.374	*3.58E-02*
P2RX7	purinergic receptor P2X 7	-0.998	0.261	*4.42E-02*
DHH	desert hedgehog signaling molecule	-1.354	0.356	*4.49E-02*
SEMA3F	semaphorin 3F	-0.701	0.184	*4.49E-02*
NPIPA8	nuclear pore complex interacting protein family member A8	1.121	0.295	*4.49E-02*
RBM43	RNA binding motif protein 43	-0.784	0.208	*4.97E-02*
FAM46A	terminal nucleotidyltransferase 5A	-0.708	0.189	*5.10E-02*
HIVEP2	HIVEP zinc finger 2	-0.763	0.205	*5.60E-02*
SNX29	sorting nexin 29	-0.841	0.226	*5.60E-02*
DDX60	DExD/H-box helicase 60	-0.747	0.202	*5.97E-02*
RN7SL1	RNA component of signal recognition particle 7SL1	-0.890	0.243	*6.88E-02*
FNIP2	folliculin interacting protein 2	-0.826	0.226	*6.95E-02*
PFKFB3	6-phosphofructo-2-kinase/fructose-2,6-biphosphatase 3	-0.706	0.195	*7.25E-02*
RGP1	RGP1 homolog, RAB6A GEF complex partner 1	-0.883	0.243	*7.25E-02*
THSD7A	thrombospondin type 1 domain containing 7A	-1.040	0.286	*7.25E-02*
MTDH	metadherin	-0.719	0.199	*7.51E-02*
ADIRF	adipogenesis regulatory factor	-0.764	0.214	*8.29E-02*
FUT11	fucosyltransferase 11	-0.755	0.211	*8.29E-02*
PTX3	pentraxin 3	-0.773	0.216	*8.29E-02*
MIR4435-1HG	MIR4435-2 host gene	0.742	0.208	*8.37E-02*
GTF2H3	general transcription factor IIH subunit 3	-0.695	0.198	*9.82E-02*
PAPD5	terminal nucleotidyltransferase 4B	-0.817	0.232	*9.82E-02*
SMG1P1	SMG1 pseudogene 1	-1.078	0.307	*9.82E-02*
SNHG16	small nucleolar RNA host gene 16	0.654	0.186	*9.82E-02*

Log2 fold change differences in transcript expression si*GCN2*-treated poly(I:C)-stimulated versus si*CTL* poly(I:C)-stimulated hPAECs as calculated using DESeq2. A negative log2 fold change implies relatively less gene expression in si*GCN2* poly(I:C)-stimulated hPAECs compared to si*CTL* poly(I:C)-stimulated hPAECs. Conversely, a positive log2 fold change implies relatively more gene expression in si*GCN2* poly(I:C)-stimulated hPAECs compared to si*CTL* poly(I:C)-stimulated hPAECs. SE; standard error of Log2 fold change. The *p*-value (not shown in this table) calculated using Wald test and adjusted for multiple hypothesis testing using the Benjamini-Hochberg procedure (adjusted (adj.) *p*-value). The table is ordered by adj. *p* value. Log2 fold change and SE of Log2 presented as 3 decimal places.

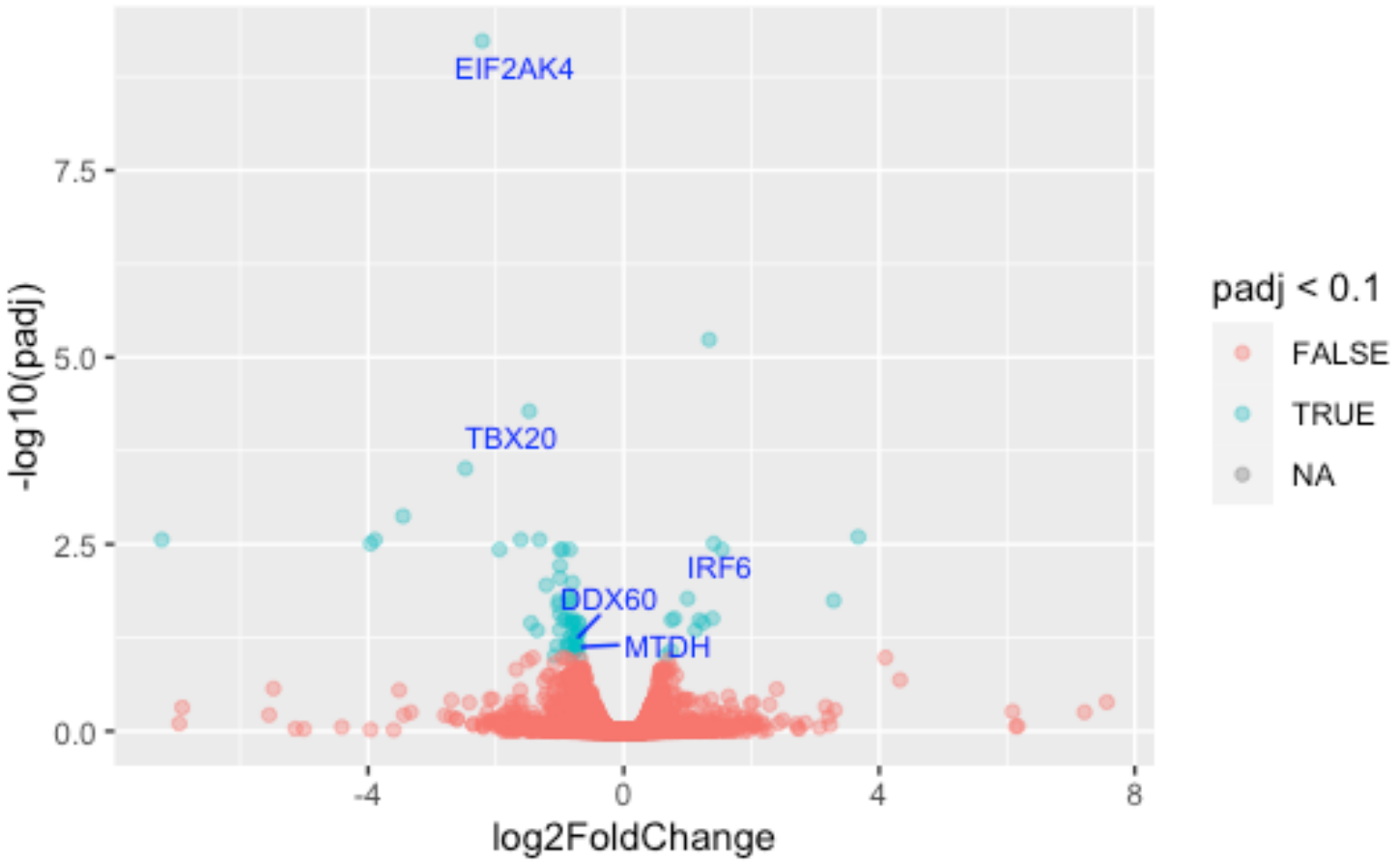

Figure 5.15 Volcano plot showing differentially expressed genes (DEGs) in si*GCN2*-treated poly(I:C)-stimulated versus siCTL poly(I:C)-stimulated hPAECs

DESeq2 bioinformatic package identified 66 DEGs in siGCN2-treated hPAECs stimulated with poly(I:C) (4 hours; 25µg/ml) at a 10% confidence level (i.e., adj p<0.1). Adjusted p value is represented as -log^{10}(adj p value) on y axis i.e., -log^{10}(adj p value) >1 are significantly different at a 10% confidence level. Poly(I:C) stimulation was for 4 hours.

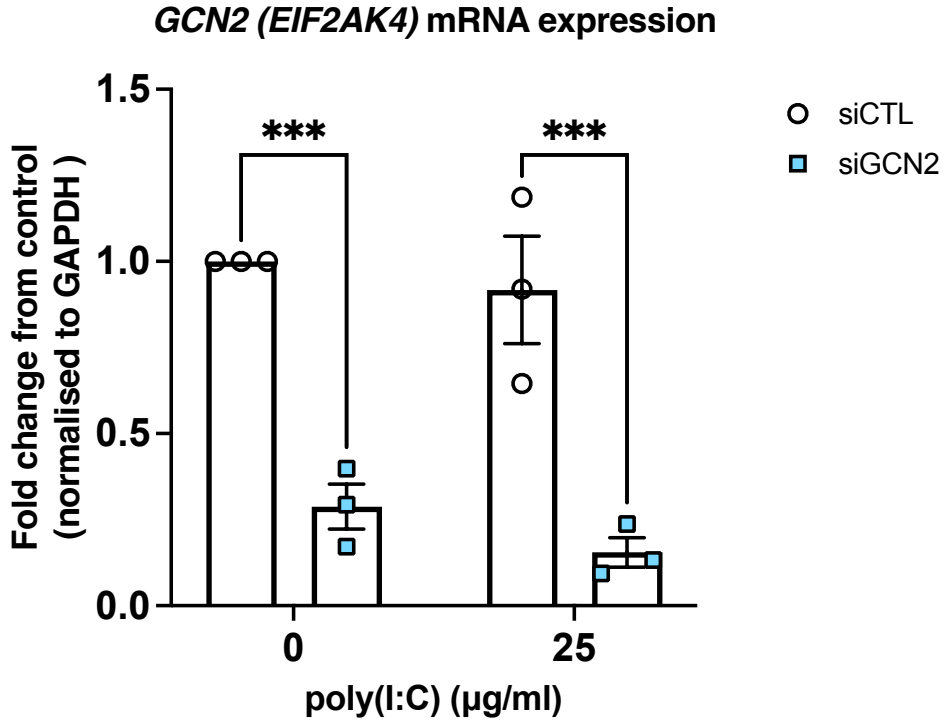

Figure 5.16 The relative mRNA expression of *GCN2 (EIF2AK4)* in GCN2-deficient hPAECs with and without 4 hours of poly(I:C) stimulation.

Quantitative RT-PCR measured *GCN2* (*EIF2AK4*) mRNA expression in si*GCN2*-treated hPAECs with and without, poly(I:C) (4 hours; 25μg/ml). Data are presented as fold change where delta-delta Ct values are normalized to siCTL and unstimulated group. Delta Ct values were normalized to housekeeper gene *GAPDH* and then to a reference sample (delta-delta Ct). Data show mean (top of bar) ± SEM. Two-way ANOVA, Šídák's multiple comparisons test. ***, p <0.001.n=3.

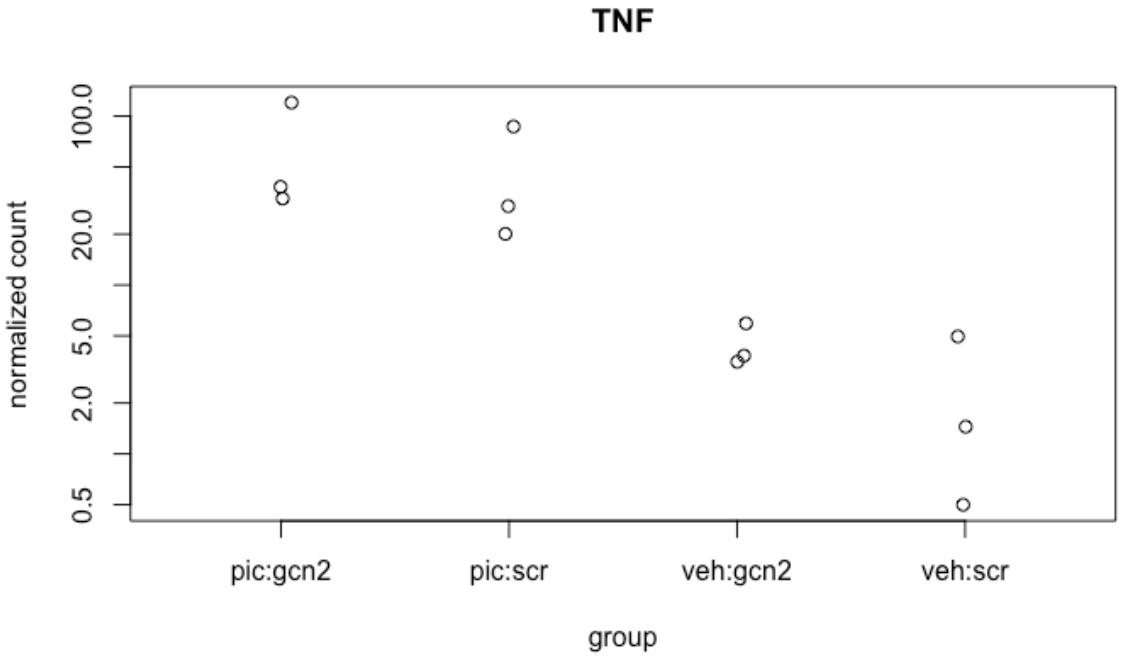

Figure 5.17 Normalised counts of *TNFA* expression in GCN2 deficient hPAECs with and without 4 hours of poly(I:C) stimulation.

Normalised counts by estimated size factors in groups: 'pic:gcn2' (siGCN2 + poly(I:C), 'pic:scr' (siCTL + poly(I:C), 'veh:gcn2" (siGCN2 + no poly(I:C) and 'veh:scr' (siCTL + no poly(I:C). Normalised counts were quantified using plotCounts function via input of count matrix constructed by DESeqDataSet. n=3.

5.11.5 Over representation analysis of DEGs between si*GCN2*-treated poly(I:C)-stimulated versus siCTL poly(I:C)-stimulated hPAECs

All 66 DEGS identified at an adjusted $p<0.1$ were used in over representation analysis. No Gene Ontology (GO) biological processes or pathways provided by KEGG, Panther, Reactome or Wikipathway were enriched above a 5% false discovery rate threshold. However, one of the top ten ranked molecular function data bases provided by Gene Ontology (GO) had a significant FDR ≤ 0.05. Molecular function was ranked by enrichment ratio.

The enriched molecular function included 'extracellular matrix structural constituent' gene set (enrichment ratio: 11.903; FDR: 0.015; *p*-value: 5.56e-^{5}; overlapped 5 genes to the gene set: *COL4A5*, *COL4A6*, *COL8A1, LAMA5* and *MGP*) (figure 5.18).

Though not enriched with an FDR ≤ 0.05, functional analysis of DEGs highlighted the molecular function of dsRNA binding to have an enrichment ratio of 9.9137 and significant *p*-value of 0.017. The overlapped genes to the gene set 'dsRNA binding' according to GO include *DDX60* and *MTDH.*

To further investigate pathways associated with DEGs identified at a (adjusted $p<0.1$) (i.e., 66 genes) were next subjected to gene set enrichment analysis (GSEA) using ranks of Log2 fold change. No enrichment analysis identified enriched gene sets in the gene list of DEGs according to GO molecular function, cellular components, and biological function or pathways according to KEGG, Panther, Reactome and Wikipathway at a FDR ≤ 0.05 (data not shown).

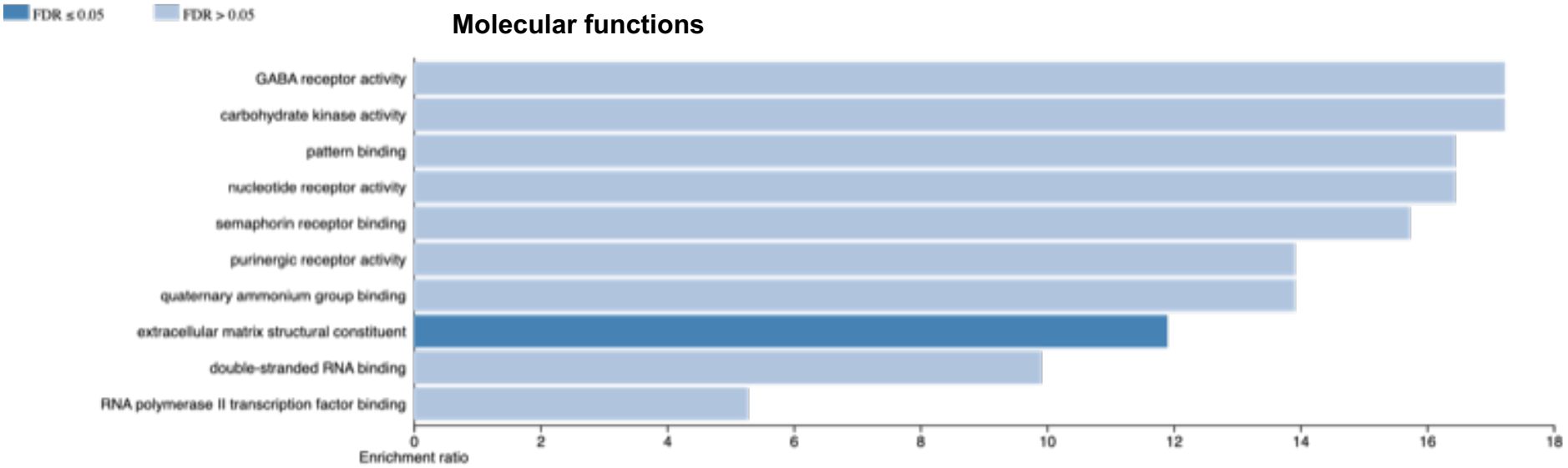

Figure 5.18. Over representation analysis of DEGs identified from si*GCN2*-treated poly(I:C)-stimulated versus siCTL poly(I:C)-stimulated hPAECs

All (66) DEGs (i.e., an adjusted *p*-value of $\leq$ 0.1) as calculated by DESeq2 were subjected to over representation analysis (ORA) using WebGestalt. The enriched genes set were provided by GO molecular function database within WebGestalt. Ranked by enrichment ratio and respective false discovery rate (FDR) at a threshold of $p<0.05$ are reported. The FDR method of Benjamini-Hochberg method was used.

5.12 Summary

The aim of this chapter was to investigate how GCN2 deficiency may alter poly(I:C)-induced inflammation in endothelial cells. In summary:

- In two endothelial cell models (i.e., healthy donor BOECs and hPAECs), GCN2-deficient endothelial cells had significantly enhanced TNFα release in response to 24 hours of poly(I:C)
    - Significantly enhanced IP-10 release was exclusively observed in GCN2-deficient BOECs in response to 24 hours of poly(I:C) but not in hPAECs
- In two endothelial cell models (i.e., healthy donor BOECs and hPAECs), GCN2-deficient endothelial cells had significantly enhanced *TNFA* transcription (assessed by qRT-PCR) in response to 24 hours of poly(I:C)
    - Significantly enhanced *IP-10* transcription was exclusively observed in GCN2-deficient BOECs in response to 24 hours of poly(I:C) but not in hPAECs
- RNA-sequencing of GCN2-deficient hPAECs stimulated with poly(I:C) for 4 hours was performed to investigate the phenotype of enhanced TNFα release. Via DESeq2 analysis, 66 DEGs (adjusted *p*-value < 0.1) were identified

- Unlike the response to 24 hours of poly(I:C) in GCN2-deficient hPAECs, DESeq2 and qRT-PCR measured that *TNFA* transcription was unaffected in GCN2-deficient hPAECs in response to 4 hours of poly(I:C)

- The genes *DDX60* and *MTDH* were included in the 66 DEGs identified in GCN2 deficient hPAECs stimulated with 4 hours of poly(I:C). As highlighted by ORA, the protein products of *DDX60* and *MTDH* have previously been identified to have dsRNA binding activity

- GCN2-deficient hPAECs had reduced cell number, independent of caspase 3/7 activity, in response to 24 hours of poly(I:C)

- In control hPAECs, poly(I:C) stimulation for 4 hours and 24 hours significantly induced the release and/or transcription of pro-inflammatory cytokines, including TNFα , IL-6 and IP-10

- In control hPAECs, poly(I:C) stimulation for 4 hours induced differential expression of 1199 genes. Notably ORA of these DEGs identified TNF signalling pathway (KEGG pathway) to have the highest enrichment ratio.

5.13. Discussion

In this chapter, a '2-hit' *in vitro* model was produced by activating dsRNA signalling (via poly(I:C) stimulation), whilst simultaneously establishing GCN2 deficiency in endothelial cells. Specifically, GCN2 deficiency in hPAECs and BOECs was achieved using an siRNA approach to model PVOD-associated loss-of-function mutations in *GCN2 (EIF2AK4)* (Eyries et al., 2014). Whilst GCN2's role during amino acid deprivation in the integrated stress response (ISR) is well established in the literature, very little is understood about how GCN2 loss-of-function contributes to the pathogenesis of PVOD (Pakos-Zebrucka et al., 2016). It is widely accepted that PVOD (and PAH) pathogenesis is multifactorial. As a process of innate immunity, dsRNA signalling including dsRNA sensors such as TLR3 and another ISR kinase, PKR, and their downstream effectors of pro-inflammatory cytokines and type I interferon have all been previously implicated in pulmonary vascular remodelling. And so, how GCN2 deficiency alters or regulates dsRNA signalling was the subject of this thesis chapter.

5.13.1 GCN2 deficiency enhanced TNFα release in response to 24 hours of poly(I:C) in endothelial cells

The major finding of this chapter was that GCN2 deficiency significantly enhanced TNFα release in response to synthetic dsRNA, poly(I:C), (25μg/ml for 24 hours) in healthy donor BOECs and hPAECs. Notably, GCN2 deficiency significantly enhanced IP-10 release in response to poly(I:C) (25μg/ml for 24 hours) from BOECs but was not observed in hPAECs. Poly(:C)-induced IL-6 release was not significantly affected by GCN2-deficiency in both healthy donor BOECs and hPAECs after 24 hours of stimulation. This implies selective enhancement of poly(I:C)-induced proinflammatory

cytokines in GCN2-deficient ECs, and this may be different between types of endothelial cells. From these findings, I inferred that GCN2 in hPAECs may regulate a specific signaling cascade within the complex dsRNA signaling pathway that is associated with TNFα release and not IL-6 or IP-10. I postulate that this selective enhancement of TNFα may be driven by specific activation of transcription factors in the context of GCN2 deficiency. For example, canonical NF-κB target genes include TNFα, IL-6 and IP-10, but dsRNA also activates IRF3 targeted transcription. IRF3 is not classically associated with TNFα but its target genes do include IP-10 and other interferon-stimulated genes (Yanai et al., 2018). Yet, there is an extensive list of transcription factors implicated in dsRNA signalling, and so, this notion is considered in mechanistic experiments discussed below.

Possibly due to the rarity of PVOD, there is no conclusive literature linking TNFα to PVOD pathogenesis, however, TNFα is a proinflammatory cytokine that has been linked to PAH pathogenesis, in which PVOD is a sub-classification (i.e., group 1.6 PH). Evidence implicating TNFα in PAH pathogenesis includes studies that have demonstrated significantly higher circulating levels of plasma and serum TNFα in PAH patients when compared to healthy controls (Itoh et al. 2006; Soon et al. 2010). Serum TNFα negatively correlated with the haemodynamic parameter of cardiac index and exercise tolerance parameter of 6-minute walk distance test in PAH patients (Soon et al, 2010). Thus, highlighting the importance of TNFα in adverse outcomes in PAH patients. No other cytokines measured in this study (i.e., IL-1β, IL-2, IL-6, IL-8, IL-10, and IL-12) significantly correlated with 6-minute walk distance (Soon et al., 2010). In addition, increased TNFα expression has also been observed locally in the pulmonary vasculature of PAH patients compared to healthy controls (Hurst et al., 2017).

In an experimental model of PH, overexpression of TNFα correlated with adverse outcomes. Specifically, TNFα over-expression in alveolar type II cells enhanced right ventricular mean and systolic pressures and RV hypertrophy in an altitude-exposed mouse model of PH, when compared to altitude-exposed control mice (Fujita et al., 2001). In accordance, the TNF inhibitor of Etanercept prevented and reversed monocrotaline-induced PH in rats and reserved endotoxin-induced PH in pigs (Mutschler et al., 2006; Zhang et al., 2016). To date, no clinical trials have used TNFα inhibitors in PAH patients.

Mechanistically, Hurst et al (2017) reported TNFα-mediated reduction of BMPR2 protein and transcription via the NF-κB subunit, RELA, in PASMCs and PAECs. Reduced BMPR2 signalling predominantly underpins pulmonary vascular remodelling in PAH and Hurst et al (2017) further supports this by evidencing TNFα-mediated reduction of BMPR2 to subvert BMP signalling, leading to BMP6-mediated PASMC proliferation. The majority of TNFα-mediated phenotypes evidenced in literature have been completed in PASMCs rather than endothelial cells. However, overexpressing TNFα transgenic mice exhibited phenotypes of both pulmonary vascular endothelial loss cell and smooth muscle cell proliferation at 3 months of age (Bell et al., 2020). EC dysfunction is considered to be early event in pulmonary vascular remodelling and contributes to the subsequent sustained and progressive proliferation of endothelial and smooth muscle cells (Rafikova et al., 2019).

The experimental design in this thesis of si*GCN2*-treated ECs with acute (4 and 24 hour) poly(I:C) stimulation is therefore more representative of early events in pulmonary vascular remodelling. My results showed that GCN2-deficency reduced

ATP activity (as a surrogate for cell number) of hPAECs, in response to 24 hours of poly(I:C). This implies that GCN2-deficency may increase endothelial cell susceptibility to poly(I:C)-induced damage. Caspase 3/7-mediated apoptosis as a mechanism of cell death was determined to be unaffected by GCN2-deficiency in poly(I:C)-stimulated hPAECs. Therefore, mechanisms of reduced cell number that are independent of caspase 3/7-mediated apoptosis such as necroptosis or cell cycle regulation should be considered in future mechanistic experiments. Indeed, at present, one can only postulate that the reduction in cell number is dependent on GCN2-deficent enhanced poly(I:C)-induced TNFα, and so further experiments using a TNFα blockade could be used to investigate this.

To the best of my knowledge, this is the first-time GCN2 deficiency has been linked to enhanced inflammation in response to poly(I:C) in ECs. Importantly, GCN2 deficiency alone (i.e., devoid of poly(I:C) stimulation) did not provoke changes in the proinflammatory cytokine transcription and release, suggesting that GCN2 has a specific regulatory role in the dsRNA signalling pathway. As TNFα release, unlike IP-10 and IL-6, was consistently enhanced in GCN2-deficent hPAECs and BOECs in response to poly(I:C) stimulation for 24 hours, subsequent experiments were performed to investigate the phenotype of enhanced TNFα release in hPAECs and are discussed below.

5.13.2 Potential mechanisms of enhanced TNFα release in GCN2-deficient hPAECs in response to poly(I:C)

TNFα release from GCN2-deficient hPAECs in response to poly(I:C) could be explained by enhanced *TNFA* transcription in GCN2-deficent hPAECs. Interestingly, enhanced *TNFA* transcription in GCN2-deficent was not observed after 4 hours of poly(I:C) stimulation, but enhanced *TNFA* transcription after 24 hours of poly(I:C) stimulation in GCN2-deficient hPAECs. Though discrete experiments, these observations imply that in the context of GCN2 deficiency, poly(I:C)-induced *TNFA* transcription may be sustained for longer than in control cells, but a formal time course experiment would be required to validate this (discussed section 5.13.3).

Other experiments in this chapter using siRNA simultaneously targeting *GCN2* and *PKR* transcripts implied that TNFα release from GCN2-deficient hPAECs in response to 24 hours of poly(I:C) was associated with PKR signalling activity, independent of differences in *PKR* mRNA expression. This is in contrast to findings by Manaud et al (2020) which showed that in parallel to the loss of GCN2 expression in MMC-exposed rats, PKR protein was increased in lungs. Albeit the significant and progressive increase of PKR was firstly observed at 3-weeks of MMC-exposure whilst GCN2 protein was significantly reduced after 2 weeks of MMC-exposure (Manaud et al. 2020). Though other canonical dsRNA sensors such as *TLR3* and *MDA5* were not altered in GCN2-deficient hPAECs in response to poly(I:C), ORA of DEGs identified in GCN2-deficient hPAECs with 4 hours of poly(I:C) stimulation highlighted *DDX60* and *MTDH* to have dsRNA binding activity.

DDX60 is the gene symbol for DEAD (Asp-Glu-Ala-Asp) Box Polypeptide 60 or otherwise referred to as DExD/H-Box Helicase 60. DDX60 has shown to function as a ligand-specific sentinel to positively regulate RIG-I/MDA5-dependent-type I interferon (Oshiumi et al., 2015). Specifically, in HEK293 cells, DDX60 knockdown significantly attenuated viral- induced *IFN-*β mRNA expression and interferon-stimulated genes, *IP-10* and *IFIT1* (Oshiumi et al., 2015). Though these data are contrary to data in this chapter where a negative log2 fold change in *DDX60* was associated with an enhanced pro-inflammatory phenotype in the context of GCN2 deficiency with poly(I:C). *DDX60* is also essential for nuclease-mediated viral RNA degradation (Oshiumi et al., 2015). Thus, I postulated that less *DDX60* expression in GCN2-deficient poly(I:C)- stimulated hPAECs may mediate less dsRNA degradation, promoting enhanced TNFα. Future experiments could be constructed around this notion.

The other gene to have dsRNA binding activity as identified in ORA of DEGs was *MTDH* (metadherin). MTDH expression is predominately associated with solid tumours and is an oncogene. It is associated with activation of NF-κB (Emdad et al., 2006).Yet, the dsRNA binding activity of MTDH refers to 2 reports of *MTDH* binding to RNA-induced silencing complex (RISC) in yeast models rather than the dsRNA binding in the context of innate immunity (Ying et al., 2011).

To reduce bias introduced by previously collated gene sets used in ORA, all 66 DEGs in GCN2-deficient hPAECs stimulated with poly(I:C) were subjected to extensive literature searches. When delving further into the literature some DEGs were already known to be involved in dsRNA signalling. For example, the protein product of *GBP4*,

Guanylate Binding Protein 4, has shown to regulate an aspect of dsRNA signalling including disrupting the interaction between TNF receptor-associated factor 6 (TRAF6) and IRF7, leading to reduced TRAF6-mediated ubiquitination and transactivation of IRF7 (Hu et al., 2011). Notably, the DEGs list contains *TBX20*, *IRF6,* and *HIVEP2* genes encoding for transcription factors. IRF6 has recently been revealed to play a role in TLR3 signalling in keratinocytes. Specifically, IRF6 was determined to promote TLR3-inducuble *IL-23p19* expression, but TNFα was not quantified (Ramnath et al., 2015). Notably, *IRF6* was positively differentially expressed in GCN2-deficent ECs in response to poly(I:C). To the best of my knowledge, TBX20 and HIVEP2 have not been previously implicated in dsRNA signalling pathways.

5.13.3. Conclusions and future work

This chapter highlights a novel role for GCN2 deficiency in the regulation of dsRNA signalling in endothelial cells. Unlike, IP-10 and IL-6, TNFα release was consistently enhanced in GCN2 deficient ECs stimulated with poly(I:C) leading to subsequent mechanistic experiments to explore this phenotype in hPAECs. These highlighted that enhanced TNFα is likely to be via an aspect of PKR signalling activity, as well as being associated with differential *TNFA* expression at the later time point of 24 hours of poly(I:C) stimulation and not at 4 hours of poly(I:C) stimulation. Other differentially expressed genes in GCN2-deficient hPAECs in response to 4 hours of poly(I:C) were identified, of which some have known associations with dsRNA signalling.

At present, technical caveats limit conclusions about the above mechanisms of enhanced TNFα release in GCN2-deficient hPAECs stimulated with poly(I:C). Therefore, future work should firstly focus on completing a time course experiment for

TNFα transcription and release in GCN2-deficient hPAECs stimulated with different durations of poly(I:C) (i.e., 1, 4, 8, 12 and 24 hours stimulations). If differences in *TNFA* transcription are validated in this time course, this could provide mechanistic insight into enhanced TNFα release. Subsequently, experiments could explore how GCN2 regulates feedback loops that may result in sustained *TNFA* transcription (Kagoya et al., 2014).

To further investigate the contribution of PKR signalling to enhanced TNFα in GCN2-deficient hPAECs stimulated with poly(I:C), an alternative approach to inhibit PKR signalling could be used to circumvent the induction of *PKR* transcription with poly(I:C) stimulation. CRISPR/Cas9 experiments knocking down *PKR* alongside *GCN2* could be designed or a pharmacological inhibitor, C16, could be used. C16 inhibits the phosphorylation of PKR and in turn inhibits the nuclear translocation of NF-κB and IRF3 (Czerkies et al., 2018).

Arguably a more disease relevant cell model of ECs could come in the form of PVOD patient derived BOECs. PVOD patients with confirmed loss-of-function mutations in *GCN2 (EIF2AK4)* could be subjected to poly(I:C) stimulation and proinflammatory cytokine levels in cell supernatants could be quantified.

The RNA-sequencing of GCN2 deficient PAECs provided some alternative potential candidates that could be involved in mediating enhanced TNFα. *DDX60*, *GBP4* and *IRF6* are arguably the most plausible differentially expressed genes to potentially explain enhanced TNFα in GCN2-deficient hPAECs stimulated with poly(I:C). Firstly, these genes should be validated via qPCR and western blot analysis.

It is also important to consider that GCN2's canonical function is a kinase as part of the ISR, where GCN2 activation mediates phosphorylation of eIF2α to globally suppress translation. Therefore, it would be somewhat unintuitive that GCN2 deficiency would directly affect transcription. However, one could hypothesize that altered kinase activity in GCN2-deficient ECs may influence transcriptional regulation as part of the dsRNA signalling pathway. Future experiments could use high throughput kinomic profiling via PamGene technology to assess novel proteins associated with altered phosphorylation, as well as, investigating the canonical GCN2 signalling pathway of eIF2α phosphorylation. Although phosphorylation of eIF2α has been previously reported to be unaffected in the lung of MMC-exposed rat with reduced GCN2 protein expression (Manaud et al. 2020), these efforts should be extended to GCN2-deficient hPAECs stimulated with poly(I:C).

To conclude, this chapter begins to elicit the interplay between GCN2 deficiency and dsRNA signalling in endothelial cells to induce a specific pro-inflammatory phenotype of enhanced TNFα release. Conclusions explaining mechanisms of enhanced TNFα release are currently limited by technical caveats. In future, the importance of TNFα specifically in the pathogenesis of PVOD should be investigated as data are currently lacking. Due to the rarity of PVOD, a multiple centre approach to collecting blood samples to measure TNFα serum levels should be made and compared to healthy and IPAH controls. Likewise, TNFα inhibitors such as Etanercept could be tested with *in vivo* models of MMC-induced PVOD and/or GCN2 knockdown mice in SuHx model of PH. Endpoints of *in vivo* experiments could be pulmonary vascular remodelling by lung histology assessment and cardiac haemodynamics via cardiac catheterisation.

6. Investigating the effects of GCN2 knockout in a chronic hypoxic mouse model of pulmonary hypertension with previous exposure to intranasal poly(I:C)

6.1. Introduction

Loss-of-function mutations in *EIF2AK4* (encoding for GCN2) have been identified as causative in familial pulmonary veno-occlusive disease (PVOD), a subclassification of pulmonary arterial hypertension (PAH) (Eyries et al., 2014). Sporadic *EIF2AK4* mutations (i.e., mutations existing with no known familial disease) in idiopathic PAH and PVOD patients have also been identified (Eichstaedt et al., 2016; Eyries et al., 2014). GCN2 is an integrated stress response kinase that globally suppresses translation under amino acid deprivation, but how GCN2 loss of function contributes to PVOD pathogenesis is largely unknown. PAH pathogenesis is considered to be multifactorial, therefore in chapter 5 of this thesis, a '2-hit model' was produced *in vitro* by transfecting endothelial cells (ECs) with siGCN2 and stimulating with poly(I:C), before measuring the acute inflammatory and transcriptomic effects. Significantly enhanced TNFα release and transcription was consistently measured in GCN2-deficient human ECs (blood outgrowth endothelial cells (BOECs) and pulmonary artery endothelial cells (PAECSs)) in response to poly(I:C) (chapter 5). Notably, several *in vitro*, *in vivo,* and human studies suggest a role for TNF signalling in PAH pathogenesis (Bell et al., 2020; Hurst et al., 2017; Soon et al., 2010).

Data in this thesis also shows that previous exposure to a single dose of intranasal poly(I:C) in the SuHx mouse model of PH subtly enhanced haemodynamic parameters

and pulmonary vascular remodelling when compared to SuHx control mice (chapter 4). Given that PAH pathogenesis is considered multifactorial, an *in vivo* multi-hit model with a combination of inflammatory exposure and genetic predisposition was designed.

In more detail, I hypothesised that GCN2 knockout (KO; GCN2 -/-) mice previously instilled with intranasal poly(I:C) 9 days prior to chronic hypoxia (Hx) would produce a more severe PH phenotype than GCN2 wildtype (GCN2 +/+) littermates. I chose to implement a Hx-induced mouse model of PH rather than SuHx-induced mouse model of PH in an attempt to mitigate potential adverse effects and/or maximal effects that could occur in a mouse model of PH with multiple 'hits' i.e., genetic mutation (GCN2 KO) in combination with intranasal poly(I:C). I chose to implement the three-week Hx (10% oxygen) method as it is an established mouse model of PH (Hoshikawa *et al*, 2003). To also investigate the effects of previous intranasal poly(I:C) instillation 9 days prior to induction of chronic Hx (a SuHx model was exclusively investigated in chapter 4), an intranasal saline control was added to this experiment. Cardiac catheterisation to measure ventricular haemodynamics and lung harvest for pulmonary vascular histology analysis were conducted 21 days after Hx induction with the aim of investigating:

- The effect of GCN2 deficiency (GCN2 KO) on haemodynamic parameters in a hypoxia-induced mouse model of PH, previously exposed to intranasal poly(I:C).

- The effect of GCN2 deficiency (GCN2 KO) on pulmonary vascular remodelling in a hypoxia-induced mouse model of PH, previously exposed to intranasal poly(I:C).

Results

6.2 GCN2 knockout in a chronic hypoxia mouse model of PH, previously instilled with intranasal poly(I:C), had no effect on the PH phenotype

GCN2 KO (GCN2 -/-) mice and their littermate controls (GCN2 +/+) were exposed to intranasal poly(I:C) 9 days prior to 3 weeks of chronic Hx (10% oxygen tension). After 21 days of Hx, PH phenotyping was conducted by right heart catheterisation and lungs were harvested for histological analysis of pulmonary vessels (figure 6.1. and 6.2).

The global deletion of GCN2 (GCN2 KO; GCN2 -/-) mice exposed to a Hx model of PH, previously instilled with intranasal poly(I:C) had no effect on right ventricular haemodynamic parameters, including pressure and contractility (figure 6.1), when compared to wildtype mice (GCN2 +/+). GCN2 KO mice in this model also displayed no differences in pulmonary vascular remodelling (figure 6.2.a-b) or right ventricular hypertrophy (figure 6.2.c), when compared to wildtype mice (GCN2 +/+).

When considering the control arm of this experiment, in wildtype mice (GCN2 +/+) instilled with intranasal poly(I:C) prior to the induction of chronic Hx, right ventricular haemodynamic parameters (figure 6.1), pulmonary vascular remodelling (figure 6.2.a-b) and right ventricular hypertrophy (figure 6.2.c) were not affected when compared to wildtype mice (GCN2 +/+) instilled with intranasal saline prior to induction of Hx mouse model of PH.

Discrepancies between *n* numbers between haemodynamic analysis and pulmonary vascular remodelling morphometry are present due to technical difficulties during cardiac catheterisation.

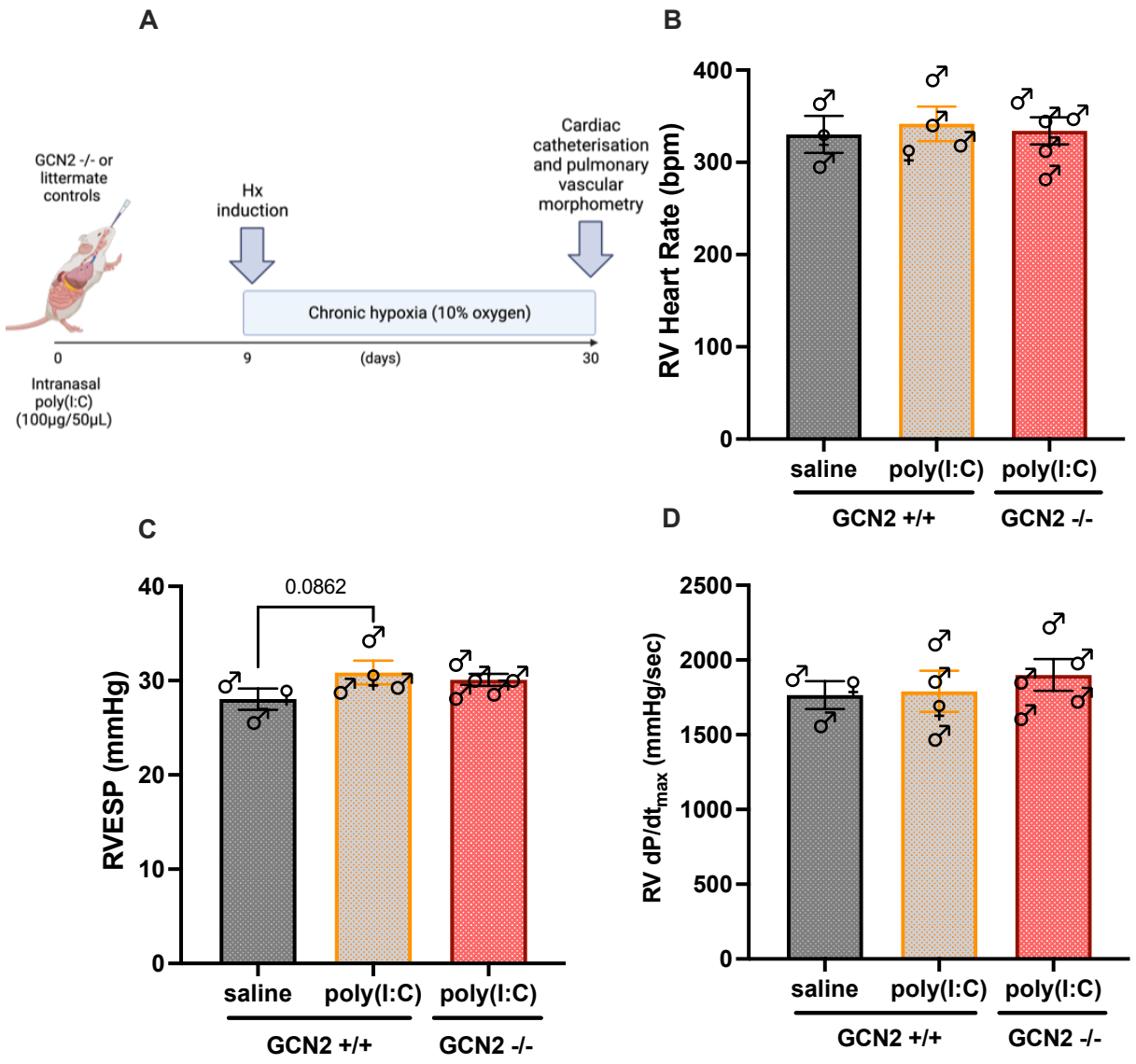

Figure 6.1. Right ventricular pressure and contractility measurements in GCN2 knockout mice, previously instilled with a single dose of intranasal poly(I:C), 9 days prior to hypoxia.

In GCN2 KO (GCN2 -/-) mice and/or wildtype littermate controls (GCN2 +/+), intranasal poly(I:C) (100µg/50µl) (or saline control) instillation was performed in anaesthetised mice under 1.5–2.0% isoflurane delivered in 100% oxygen with a flow of 2.0 L/min, before Hx was induced 9 days after poly(I:C) instillation. Original image created in Biorender.com (A). Heart rate was continuously recorded throughout right ventricular cardiac catheterisation and the average heart rate (bpm) (B) at the point of pressure-volume loop analysis is presented. Graphs present RVESP (mmHg) (C) and RV dP/dt maximum (mmHg/sec) (D) as acquired by right ventricular cardiac catheterisation via external jugular vein. Unpaired two-tailed t-test conducted to compare 'intranasal saline versus poly(I:C) in GCN2+/+ mice' and 'GCN2 +/+ versus GCN2 -/- mice with intranasal poly(I:C)'. Data show mean (top of bar) ± SEM. *n*=3-5. Males and females were used and is denoted as symbols. RV; right ventricular. RVESP; right ventricular end systolic pressure.

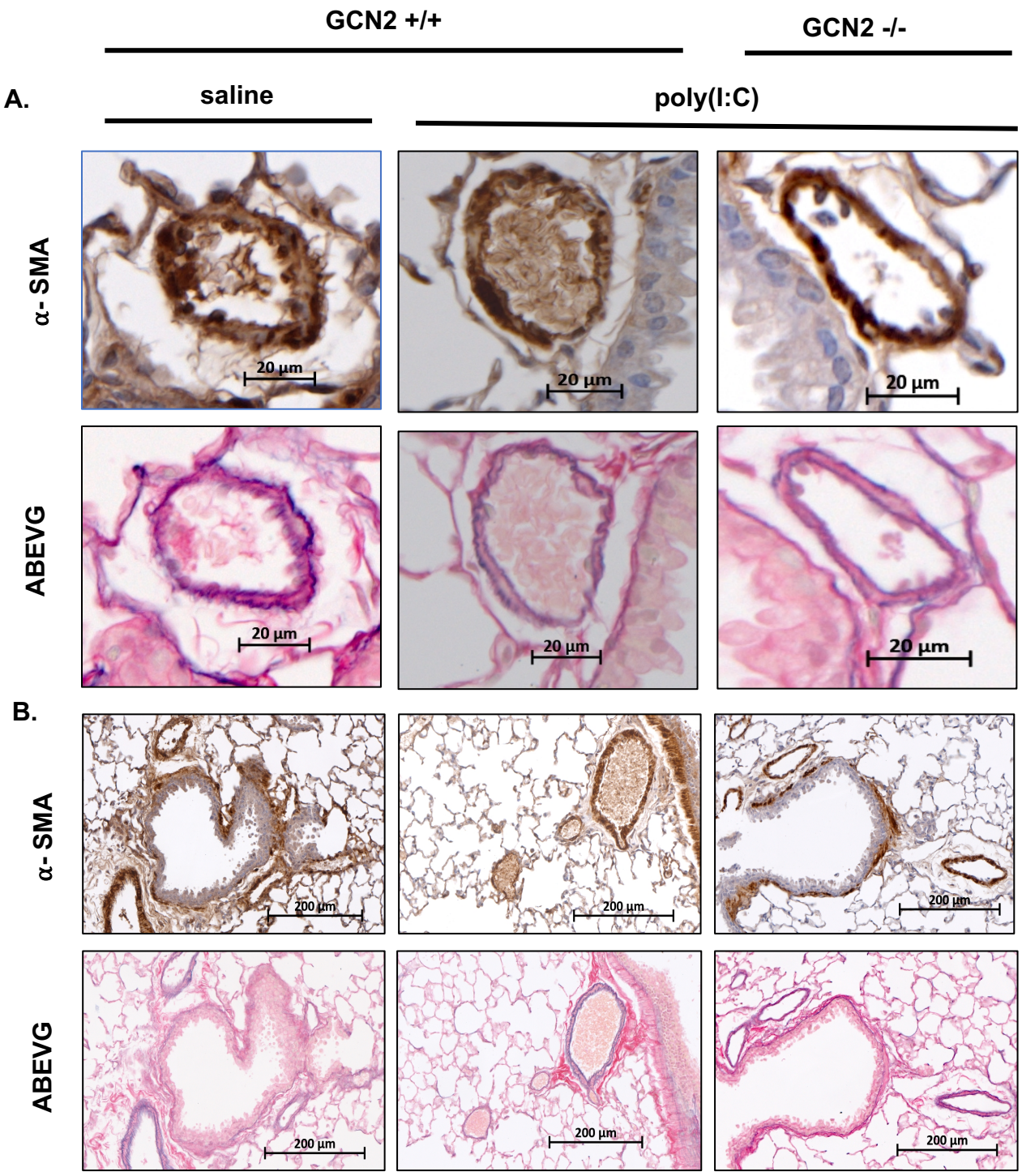

Figure 6.2 Representative images of distal (A) and proximal (B) pulmonary vasculature in FFPE lung sections of GCN2 knockout mice, previously instilled with a single dose of intranasal poly(I:C), 9 days prior to hypoxia.

FFPE lung sections were stained with ABEVG or indirectly immunostained with α-SMA. Morphometry was conducted on arterioles that were <50µm in diameter. Nx; normoxia. SuHx; Sugen-hypoxia. FFPE; formalin fixed paraffin embedded. ABEVG; Miller's elastin stain with alcian blue and Curtis' modified van Gieson. α-SMA; Alpha smooth muscle actin. Scale bars as indicated.

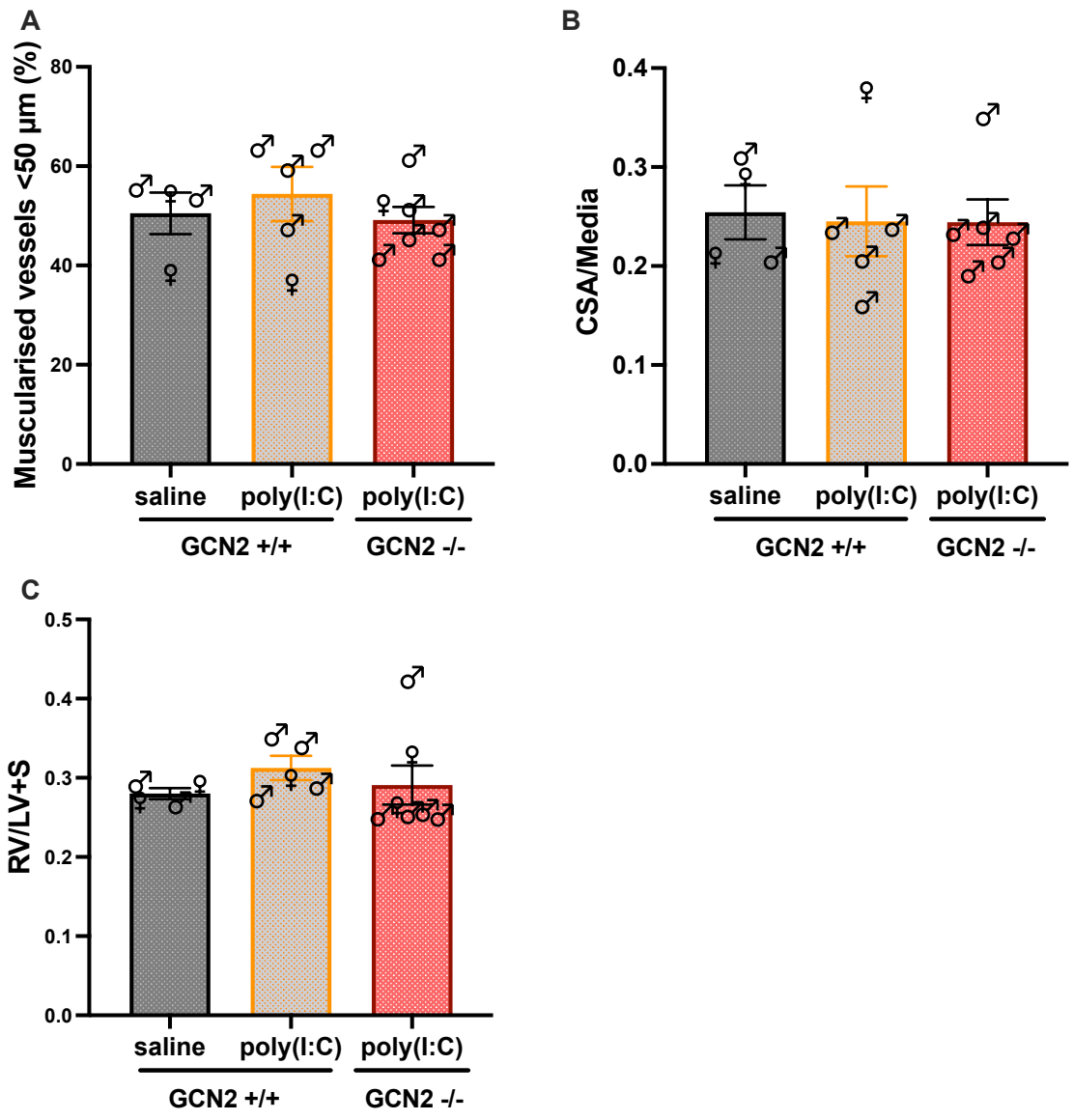

Figure 6.3 Pulmonary vascular morphometric analysis of FFPE lung sections and right ventricular hypertrophy analysis in GCN2 knockout mice, previously instilled with a single dose of intranasal poly(I:C), 9 days prior to hypoxia.

Pulmonary vascular remodelling was quantified by the proportion of muscularised arterioles (<50µm diameter) in FFPE lung sections stained with ABEVG (A) and medial area to cross-sectional area (CSA) ratio for muscularised arterioles in FFPE lung section immunostained indirectly with α-smooth muscle actin (α-SMA) (B). Hearts were dissected and chambers compartmentalised, and right ventricular free wall weight was normalised to left ventricle plus septum weight (RV/LV+S) to measure right ventricular hypertrophy (C). Unpaired two-tailed t-test conducted to compare 'intranasal saline versus poly(I:C) in GCN2+/+ mice' and 'GCN2 +/+ versus GCN2 -/- mice with intranasal poly(I:C)'. Data show mean (top of bar) ± SEM *n*=4-7. Males and females were used in both groups and is denoted as symbols.

6.3 Summary

The aim of this chapter was to investigate how GCN2 KO affects a Hx mouse model of PH, previously instilled with intranasal poly(I:C). In summary:

- The deletion of GCN2 (GCN2 KO) in a Hx mouse model of PH, previously instilled with intranasal poly(I:C) (100μg/50μl), 9 days prior to Hx-induction had no effect on right ventricular haemodynamics, pulmonary vascular remodelling or right ventricular hypertrophy.

- A single instillation of intranasal poly(I:C) (100μg/50μl), 9 days prior to Hx induction in wildtype (GCN2 +/+) mice had no effect on right ventricular haemodynamics, pulmonary vascular remodelling and right ventricular hypertrophy compared to control mice (intranasal saline followed by Hx exposure).

6.4 Discussion

6.4.1 Previous intranasal poly(I:C) did not affect the chronic hypoxia mouse model of PH

In contrast to results section 4.3 that showed previous instillation of intranasal poly(I:C) to enhance haemodynamic and pulmonary vascular remodelling in the SuHx mouse model of PH, data in this results chapter did not show any significant differences in PH phenotype when wild-type mice were exposed to intranasal poly(I:C) prior to chronic hypoxia (Hx) exposure. Specifically, figure 6.1 shows that wild-type Hx mice previously instilled with intranasal poly(I:C) had no significant differences in RVESP (surrogate for pulmonary artery systolic pressure) or RV dP/dt_{max} (surrogate of contractility) when compared to Hx saline control. Supporting these data, wild-type Hx mice previously instilled with intranasal poly(I:C) also had no significant differences in pulmonary vascular remodelling or right ventricular hypertrophy when compared to Hx saline control (figure 6.2).

The disparity between these data and previous data in chapter 4 may be due to the more severe phenotype induced by the combination of Sugen and hypoxia (SuHx) when compared to Hx alone. The decision to use a Hx mouse model of PH rather than the SuHx mouse model of PH was to mitigate the potential of adverse effects and/or maximal effects presumed of a multi-hit model. In my setting, I did not directly compare the severity of the PH phenotype in the SuHx mouse versus the Hx only mouse, however, as informed by Ciuclan et al (2011) and Vitali et al (2015), the consensus is that the SuHx mouse model leads to higher RV systolic pressures and enhanced RV hypertrophy. Therefore, I postulate that the magnitude of the PH model is influential

when investigating the effect of previous intranasal poly(I:C)-induced lung inflammation on subsequent PH mouse models. It is plausible that a more severe PH phenotype, like that of a SuHx model, may be required to elicit small changes in haemodynamic parameters and pulmonary vascular remodelling. In an attempt to compare PH mouse models in my thesis, the mean (± SEM) RVESP for Hx control mice was 28.04 ± 1.13 mmHg (figure 6.1.c) and in SuHx control mice was 31.95 ± 1.09 mmHg (figure 4.5.c), albeit the magnitude in both PH models is not directly comparable as the experiments were in different mouse strains (see below) and subject to batch effects. Moreover, the parameter of ePVR/i that was notably enhanced in the SuHx mouse model of PH when previously instilled with intranasal poly(I:C) (figure 4.7.a-b) was not calculated in this experiment due to surgical difficulties that did not allow for successful left ventricular cardiac catheterisation.

The magnitude of the PH response and the comparisons to earlier work presented in this thesis, is also confounded by strain and sex differences between experimental designs. For example, C57BL/6J male mice were subjected to SuHx whereas GCN2 KO female and male mice of mixed background (B6.129S6-Eif2ak4$^{tm1.2Dron}$/J) were subjected to Hx. Furthermore, GCN2 KO mice were generated by using 129-derived embryonic stem cells positive for the transgenic mutation, injected into C57BL/6 blastocysts, before backcrossing onto C57BL/6J mice for at least 10 generations (Ledermann, 2000). Therefore, the background of the GCN2 transgenic mouse line is a sub-strain of the C57BL/6J mouse, most likely harbouring a different genetic profile to the C57BL/6J mice used in results section 4.2 and therefore providing a potential explanation for differences in results in section 4.2 and 6.2, irrespective of PH model differences.

Due to surgical difficulties that caused experimental animal drop out, experimental groups were not sex matched. This is a limitation of this study design and may contribute to greater variation in results. Furthermore, it is largely accepted that given an experimental mouse model of PH, sex significantly modifies the PH phenotype producing heterogeneity. For instance, female mice present with lower haematocrit levels in response to chronic hypoxia compared to male mice (Vanderpool & Naeije, 2018). This is notable as haematocrit levels influence blood viscosity and therefore has the potential to influence blood flow and resistance further confounding haemodynamic results. Likewise, it has been reported that female mice have improved right ventricular adaptation compared to male mice after four weeks of chronic hypoxia as attributed to significant reductions in pro-angiogenetic factors such as VEGF in the right ventricular myocardium that are exclusively observed in male mice (Bohuslavová et al., 2010). Similarly, female-dependent protection was reported in Zawia et al (2020) where male macrophage-low mice spontaneously developed PH and female counterparts did not.

Mouse strain, sex, and PH model differences are likely to produce heterogeneity in results in this experiment via reasons stated above, making subtle haemodynamic and pulmonary vascular remodelling differences hard to detect. This is further compounded by animal dropout due to surgical difficulties, resulting in a low *n* in each experimental group. By using *n* of ≥ 3, this study was sensitive enough to detect differences of $\geq$5mmHg in RVESP (methods section 2.13.1). Supporting this, the mean RVESP mmHg was increased by 2.82mmHg in wild-type Hx mice previously instilled with intranasal poly(I:C) when compared to wild-type Hx mice previously instilled with

intranasal saline but a significance level of 5% was not reached (i.e., p=0.0862) (figure 6.1.c).

6.4.2. GCN2 KO did not affect a Hx mouse model of PH previously instilled with intranasal poly(I:C)

Given that GCN2-defiency enhanced poly(I:C)-induced TNFα *in vitro* (chapter 5) and considering that the effects of previous intranasal poly(I:C)-lung inflammation enhanced the severity of a SuHx model of PH in C57BL/6J mice (section 4.2), a multi-hit model using a GCN2 KO mouse line (i.e., 1st hit) instilled with intranasal poly(I:C) (i.e., 2nd hit), 9 days prior to the induction of the Hx mouse model of PH (i.e., 3rd hit) was established. As assessed by right ventricular haemodynamics and pulmonary vascular morphometry, GCN2 KO did not alter the PH phenotype in a Hx mouse model of PH, previously instilled with intranasal poly(I:C). This suggests that the impact of GCN2 deficiency on enhanced poly(I:C)- induced cytokine production in airway was not sufficient to alter vascular remodelling in a subsequent mouse model of PH. Albeit, GCN2 deficiency to enhanced poly(I:C)-induced TNFα was measured *in vitro* (chapter 5) and the presence of cytokines in this *in vivo* model using a GCN2 KO mouse and intranasal poly(I:C) is yet to measured.

No effect of GCN2 KO on the PH phenotype of a Hx mouse model with previous intranasal poly(I:C) instillation was arguably surprising when genomic linkage analysis and immunohistochemical analysis of pulmonary vascular remodelling have shown *EIF2AK4* (encoding GCN2) loss-of-function mutations to be a cause of PVOD. Indeed, a more severe and earlier onset of PVOD is associated with *EIF2AK4* mutations when

compared to non-mutated (absence of *EIF2AK4* mutations) PVOD (Eyries et al., 2014; Montani et al., 2015). Eyries et al (2014) highlights the importance of the loss of functions mutations in *EIF2AK4* to cause PVOD. Moreover, patients specifically with biallelic mutations in *EIF2AK4* presented with disease earlier than those without mutation (Montani et al., 2015). Unlike my data, the dysregulation of *EIF2AK4* (GCN2) via EIF2AK4-mutated rats caused additive effects to the bleomycin model of parenchymal fibrosis (Santos-Ribeiro et al., 2023). Specifically, *EIF2AK4*-mutated rats treated with bleomycin showed increased parenchymal fibrosis and pulmonary vascular remodelling as well as increased right ventricular systolic pressure compared to wildtype mice subjected to bleomycin (Santos-Ribeiro et al., 2023).

6.4.3 Future work

This chapter included an *in vivo* pilot study to bring together findings from results chapter 4 and 5. Specifically, a multi-hit model was produced to study the effects of a PAH-associated genetic mutation (GCN2 KO) and prior lung inflammation (intranasal poly(I:C)) to a Hx mouse model of PH. As a pilot study, and to avoid the potential of significant animal numbers experiencing adverse effects, I chose to use a small *n* in each group. However, animal numbers were further reduced by surgical difficulties owing to reduced power during statistical analysis. To make more meaningful conclusions in this chapter the *n* of groups should be increased, and groups should be sex-matched in future. When planning to repeat this experiment, I would reconsider the choice of PH mouse model and use SuHx to produce a more severe PH phenotype. By doing so, results chapter 4 data could be reproduced increasing robustness of data, as well as acting as an appropriate control to test the effects of

GCN2 KO in the setting of previous intranasal poly(I:C) in a mouse model of PH. In addition, particular effort should be made to acquire left ventricular haemodynamics to compare parameters of ePVR/i and LV cardiac output in the context of GCN2 KO with previous significant data in results chapter 4. Taking inspiration from Santos-Ribeiro et al (2023) work, instillation of intranasal poly(I:C) in GCN2 KO mice could occur prior to the induction of bleomycin model of PH, though potentially producing a more appropriate model of group 3 PH i.e., PH due to lung disease. Equally, the intranasal poly(I:C) dosing regimen and duration of time between the events of intranasal poly(I:C) instillation/s and PH model induction could be optimised in future. For example, enhanced TNFα release and transcription was observed after 24 hours of poly(I:C) stimulation in GCN2-deficent ECs *in vitro,* therefore PH model induction could occur 24 hours after intranasal poly(I:C) instillation in GCN2 KO mice in future experiments.

To understand this multi-hit model in more detail, immunological phenotyping of intranasal poly(I:C) in GCN2 KO should also be performed and compared to control mice. Specifically, immunological phenotyping should be carried out as previous (section 4.2) via analysis of bronchoalveolar lavage fluid (BALF) and lung tissue immune cells and BALF cytokines at time points of 24 hours and 9 days after poly(I:C) instillation. To align with previous *in vitro* data (chapter 5), measuring TNFα levels in BALF as well as whole lung and serum should be prioritised in future. Furthermore, pulmonary vascular morphometry in this chapter measured the specific feature of pulmonary arterial medial thickening of pulmonary vascular remodelling. As PVOD is pathologically defined as pulmonary arterial remodelling with venous involvement, particular considerations to measure pulmonary vascular remodelling in the venous

system should occur in future. Historically, small pulmonary arteries and pulmonary venules in histological analysis have been difficult to discriminate but methodology including vessel-specific perfusion using microbead- or barium agarose solutions have been developed to label pulmonary arteries and veins before subsequent immunohistochemical staining is conducted to measure medial muscularisation and/or fibrosis (Fayyaz et al., 2023).

To summarise, no effects on PH phenotype were observed in the multi-hit model (i.e., GCN2 KO, intranasal poly(I:C), Hx-induced PH), but conclusions are limited by small number of animals in each experimental group and the effectiveness of the PH model itself.

7. General discussion

Sensing of double-stranded (ds)RNA is a well-established innate immune process. Activation of dsRNA downstream signalling pathways is associated with pro-inflammatory cytokine and type I interferon production, and these effectors have known roles in vascular disease. Conversely, dsRNA signalling has also been implicated in disease protection and tissue repair. This thesis extends knowledge of the homeostatic role of dsRNA signalling, specifically in the context of pulmonary vascular remodelling and PAH pathogenesis.

7.1 Summary of key findings

The first section of this thesis investigated the protective role of dsRNA signalling in pulmonary vascular remodelling previously described by Farkas et al (2019) in rats. Whilst thrice-weekly prophylactic intraperitoneal injections of synthetic dsRNA, poly(I:C), was previously shown to prevent PH in a SuHx rat model (Farkas et al. 2019), data in this thesis suggest that this is species specific as thrice-weekly prophylactic intraperitoneal poly(I:C) was not therapeutic in a SuHx mouse model of PH (section 3.5). The absence of cross species conservation when giving prophylactic intraperitoneal injections in SuHx murine (i.e., mouse and rat) models of PH decreases the plausibility of poly(I:C) as a potential therapeutic for PAH patients. Ultimately the findings in chapter 3 resulted in a change of research focus for this thesis, where all subsequent investigations explored the canonical signalling pathway of dsRNA which is associated with a highly pro-inflammatory and anti-viral phenotype. Specifically, intranasal poly(I:C) was used to model mouse lung inflammation in chapter 4 and 6.

To investigate how previous lung inflammation may affect a mouse model of PH, poly(I:C) was instilled intranasally to induce lung inflammation prior to induction of the SuHx mouse model of PH. In this experiment, lung inflammation 9 days prior to induction of PH, enhanced the PH phenotype. Specifically, significant increases in pulmonary vascular remodelling, ePVR/i, and right ventricular hypertrophy and a significant decrease in left ventricular stroke volume and cardiac output (section 4.3). These data imply that previous dsRNA signalling activation in the lung airways is a potential driver of PAH pathogenesis. However, repeated doses of intranasal poly(I:C) prior to the induction of SuHx had no apparent effect on the PH phenotype. This finding is caveated by low animal numbers in experimental groups. Notably, with repeated intranasal poly(I:C) instillations in mice, I found evidence consistent with innate immune cell (i.e., neutrophil and macrophage) and cytokine tolerance (section 4.4), which may have altered subsequent vascular responses.

In accordance with the notion of multifactorial PAH pathogenesis, a '2-hit' model of GCN2 deficiency and poly(I:C)-induced inflammation was established in endothelial cells (ECs) *in vitro* (chapter 5). Consistently, GCN2 deficiency enhanced TNFα release, in response to poly(I:C) in two cell models i.e., hPAECs and BOECs. Multiple approaches were taken in an attempt to understand the mechanism by which GCN2 deficiency enhanced poly(I:C)-induced TNFα release. These investigations identified enhanced *TNFA* transcription and PKR signalling as potential mechanisms. Further, differential gene transcripts from DESeq2 analysis highlighted *DDX60*, *GBP4* and *IRF6* as candidates for future investigation. Therefore, these findings begin to elicit an interplay between GCN2 deficiency and the dsRNA signalling pathway in endothelial cells. At present, conclusions regarding mechanism are limited as further

validation is required. Lastly, chapter 5 showed robust evidence of enhanced inflammation in GCN2 -deficient ECs in response to poly(I:C). However, GCN2 knockout mice, in a chronic hypoxia model of PH, provided no evidence of enhanced PH phenotype following an episode of intranasal poly(I:C)-induced lung inflammation (chapter 6). Conclusions from this experiment are caveated by the choice of animal model and low animal numbers caused by cardiac catheterisation technical difficulties.

7.2 Future work

The finding that prophylactic intraperitoneal poly(I:C) is ineffective in the prevention of PH in a SuHx mouse (chapter 3) is contrary to a recent report by Farkas' group which measured thrice-weekly prophylactic intraperitoneal injections of poly(I:C) to reduce RVESP and pulmonary vascular remodelling in a SuHx mouse model of PH (Bhagwani *et al*, 2023). Of note, the data of Bhagwani et al (2023) was published after the completion of the experiment shown in section 3.5. Providing a possible explanation for inconsistencies, the Bhagwani et al (2023) study includes minimal variation of data points within an experimental group in comparison to data in this thesis. Increasing animal number in groups could increase the power to detect differences between such groups with large variability (section 3.5). Differing methodology to this thesis, such as use of different anaesthesia, use of ventilation via tracheostomy, and open-chest approach during right heart catheterisation by Bhagwani et al (2023) could provide possible explanations for differences also. Nevertheless, the lack of reproducibility between data in this thesis and Bhagwani et al (2023), ultimately decreases the plausibility of poly(I:C) as a successful therapy in PAH patients in future. Importantly, measuring clinically relevant endpoints such as PVR and RV cardiac function in the SuHx rat or mouse model of PH with prophylactic poly(I:C) should be prioritised

(Sitbon & Morrell, 2012). This is in light of reports which show MRI indices of RV dysfunction to predict clinical worsening in PAH patients, independently of mPAP (Freed et al., 2012). Likewise, RV intrinsic molecular mechanisms may drive RV deterioration independent of pulmonary vascular remodelling (Ryan & Archer, 2014). Favourably, ePVR/i was reported in this thesis but not in the work by Bhagwani *et al* (2023), but cardiac MRI as the gold standard to measure cardiac function was not completed in either study. Furthermore, qualities of a good PAH therapeutic includes the specific targeting of the pulmonary circulation and/ or right ventricular maladaptive response, but importantly, the therapy should not target the systemic vasculature. With this in mind, future efforts should be put into determining the effects of intraperitoneal poly(I:C) on the systemic vasculature. Specifically, investigating how intraperitoneal poly(I:C) is metabolised (i.e., pharmacokinetic and pharmacodynamic testing) and identifying the cell tropism of intraperitoneal poly(I:C) by fluorescent or isotope tracing *in vivo* in future would be useful to investigate.

Regarding the intranasal poly(I:C)-induced lung inflammation model in C57BL/6J mice, significant increases in BALF proinflammatory cytokines and immune cell infiltration were measured, but the cellular tropism of intranasal poly(I:C) (i.e., poly(I:C) binding to receptors in alveolar epithelium and/or blood vessel endothelium) should also be investigated by fluorescent or isotope tracing in future. Likewise, other hallmarks of poly(I:C)-induced acute lung injury such as alveolar-capillary barrier permeability should be assessed by measuring BALF albumin levels to understand the intranasal poly(I:C)-induced lung inflammation model in more detail (Vassiliou et al., 2020). Likewise, BALF innate immune cells, cytokines, and alveolar-capillary

barrier permeability in GCN2 KO mouse with intranasal poly(I:C) should be measured in future to understand the multi-hit model in more detail (chapter 6).

Once intranasal poly(I:C) cell tropism is confirmed, more specific hypotheses could be subsequently generated in regard to how specifically previous poly(I:C)-induced lung inflammation enhanced the PH phenotype in a SuHx model of PH. As the scientific community begins to elicit how previous activation of the immune response regulates future innate immune responses leading to long term sequalae (Allinson et al. 2023). Future hypotheses aimed at investigating the mechanism by which previous lung inflammation enhances a subsequent SuHx mouse model of PH could be inspired by this work. Multi-method approaches may be required, assessing factors that could lead to innate immune memory, such as poly(I:C)-induced molecular changes, bystander sensitisation, and epigenetic reprogramming (Allinson et al. 2023).

Though the mouse lung inflammation model via a single dose of intranasal poly(I:C) is clearly oversimplified, it provides preliminary evidence that dsRNA signalling activation in lung may drive subsequent vascular remodelling. Undoubtedly, a person will be exposed to multiple incidences of lung inflammation caused by infection (viral or bacterial), other respiratory conditions such as asthma and autoimmune diseases, environmental exposure such as atmospheric pollution and tobacco, as well as vaccinations. Therefore, eliciting how complex histories of lung inflammation regulate future innate immune responses and long-term sequelae for diseases such as PAH will be particularly challenging. The administration of repeated intranasal poly(I:C) instillations prior to the induction of SuHx mouse model begins to highlight the intricacies of previous immune activation to influence future disease, as this

experiment provoked no changes in PH phenotype, but study power could be improved by increasing animal numbers in experimental groups. Furthermore, the clinical relevance of the repeat model of intranasal poly(I:C) (2 doses, 9 days apart) is questionable given that repeated lung inflammation may occur months or years apart in humans. Alterations in the timings of instillations in the repeated poly(I:C) model could be explored in future studies. Other future experiments could focus on using a more clinically relevant model of lung inflammation, especially considering the context of an intranasal instillation model. Live viruses such as influenza, rhinovirus, SARS-CoV-2 (i.e., COVID-19) could be used to model the effect of viral-derived dsRNA-induced previous lung inflammation on a subsequent SuHx mouse model of PH. In combination, association studies of patient's clinical history including viral infections with severity of PAH and patient outcomes could be completed.

Finally, data in this thesis begins to elucidate a role for GCN2 deficiency in dsRNA signalling pathways, but further work is required to fully elicit the mechanism by which GCN2 deficiency enhances poly(I:C)-induced TNFα release (chapter 5). A formal time course for TNFα transcription and release in GCN2-deficient hPAECs stimulated with varying durations of poly(I:C) (time points between 1 and 24 hours) is required to validate the phenotype of sustained *TNFA* transcription. Differentially expressed genes identified by DESeq2 analysis, and specifically those genes that have already been implicated in dsRNA signalling, should be prioritised for confirmation of differential gene expression by qRT-PCR. As GCN2 is a kinase, it is reasonable to suggest that the loss of function in GCN2 could impact phosphorylation activity, indirectly or directly affecting dsRNA signalling. Therefore, a high throughput kinomic profiling approach via PamGene technology could be used in future to measure altered kinomic

responses and predict associated proteins. The differential gene expression data and kinomic profiling data could be integrated in the attempt to explain a mechanism for poly(I:C)-induced enhanced TNFα in the context of GCN2 deficiency. In addition, CRISPR/Cas9 or a pharmacological approach via compound c16 to knockout or inhibit the activity of PKR associated with enhanced TNFα release could be investigated in the context of GCN2 deficiency and poly(I:C) stimulation in ECs (Watanabe et al., 2020). Likewise, the methodology of gene knockdown and pharmacological approaches could be used to validate transcription factors identified via DESeq2 analysis and from ChIP-sequencing data it may be possible to infer direct or indirect mechanisms of action for GCN2 deficiency to enhance poly(I:C)-induced *TNFA* transcription. In addition, the potential of NF-κB/TNFα positive feedback loop in GCN2-deficient ECs stimulated with poly(I:C) needs to be considered in future (Kagoya et al., 2014). For instance, post-transcriptional regulation could lead to enhanced TNFα release, and in an autocrine manner, enhanced TNFα protein could initiate enhanced T*NFA* transcription, rather than the other way around i.e., enhanced *TNFA* transcription to precede enhanced TNFα translation.

7.3. Limitations

In this thesis, the experimental design heavily relies on animal models. Whilst animal models of PH possess complex organ systems that inherently resemble the pathophysiology of disease in ways which *in vitro* cell models cannot, conclusions drawn from animal models of PH must be carefully considered in context. An advantage is that animal models of PH allow the investigation of molecular pathways using transgenic mice as in the case of the GCN2 knockout mouse in this thesis.

However, all currently available animal models of PH do not fully replicate human disease. Therefore, extrapolating my findings from animal models to the clinic remains particularly challenging.

In more detail, any given animal model of PH does not fully replicate the progressive chronic nature of PH. After the onset of disease, patients report progressive symptoms which variably escalate from patient to patient in the months or years after initial diagnosis. This contrasts with the SuHx and Hx mouse models which take a total of 3-weeks to be established with end points usually taken at this time. In addition, in PAH patients there is a predilection towards women, and conversely, in mice there are reports of female-associated protection in PH experimental models (Zawia et al., 2020). Moreover, the specific pathophysiology of SuHx and Hx mouse models of PH does not fully recapitulate human PAH disease. SuHx and Hx mouse models exhibit mild PH that is reversible on re-exposure to normoxia, and unlike the SuHx rat, does not consistently induce pulmonary plexiform lesions (Abe et al., 2010). Arguably, a SuHx rat model is a more relevant model of PH human disease, but restricted availability of transgenic rats dictated the experimental choices in this thesis. The choice of animal model discounts developmental, physiological, and gross anatomical differences in a mouse lung compared to human lung. For instance, mouse and human lung development are different in each three stages of: pseudo- glandular, saccular, and alveolar maturation. Specifically, full maturation of the alveolar sacs occurs from birth until 2 weeks postnatal in mice but in humans alveolarisation begins in the third trimester and persists for up to 3 years postnatally (Miller & Spence, 2017). Bronchioalveolar stem cells giving rise to multiple cell types upon injury has been evidenced in mice but not in humans, and grossly, the mouse lung has one lobe on

the left and four lobes on the right whilst the human lung has 2 lobes on the left and 3 lobes on the right (Pan et al., 2019). Additionally, the human lung has extensive interlobular and segmental connective tissue dividing each lobe into individual lobules whereas mice lungs do not (Pan et al., 2019). As lung airway structure is inextricably linked to the structure of pulmonary circulation (i.e., pulmonary blood vessels) to facilitate gas exchange, mouse and human lungs have inherent anatomical pulmonary circulation differences as well. These species-related pulmonary circulation differences are therefore particularly relevant when considering the translational capabilities of the mouse models of PH data in this thesis.

There is an unmet need for human lung model systems that can complement animal models to improve our understanding of human lung pathophysiology in pulmonary vascular diseases like PAH and in turn increase translational capabilities of pre-clinical PH research to humans. This may arise from bioengineered scaffolds and niches such as ‘lung-on-a-chip’ and ‘PAH-on-a-chip’ (Ainscough et al., 2022; Zamprogno et al., 2021). Whilst these are promising novel models regarding the pathobiology, cell-cell interactions and microfluidics, cardiac catheterisation for acquisition of haemodynamic parameters which are used to definitively diagnose PAH are not applicable in this model, unlike animal models. Yet, ‘organ-on-a-chip’ models are advantageous when modelling genetic abnormalities, detecting potential drug targets, and testing the effects of potential therapies on the pulmonary vascular (Ainscough et al., 2022). *In vitro* models of BOECs derived from healthy donors, and commercially bought hPAECs from non-PAH patients were used in chapter 5. To more accurately model processes unique to the patient pulmonary vasculature, *in vitro* models in future could include BOECs derived from PAH and PVOD patients, patient-specific induced

pluripotent stem cells (iPSCs) differentiated into ECs and SMCs or ECs and SMCs derived from explanted lung.

Based on previous literature, a model of lung inflammation was produced by instillation of intranasal poly(I:C) prior to the induction of a SuHx mouse model of PH. A poly(I:C) model of lung inflammation was chosen as a way to discretely investigate dsRNA signalling. In addition, poly(I:C) is relatively easy to use and available compared to a live virus. Intranasal poly(I:C) has commonly been documented as a 'viral mimic'. In this thesis I refer to intranasal poly(I:C) as an inducer of lung inflammation rather than a 'viral mimic', where others have not been so specific (Harris et al. 2013; Stowell et al. 2009). Indeed, poly(I:C) induces anti-viral innate immune responses in the form of upregulation of type I IFN and IFN-stimulated genes as well as augmenting dendritic cell maturation to complement antigen presenting cells and activate T helper cells (Fučíková et al., 2011; Hänel et al., 2022). However, the synthetic form of dsRNA, poly(I:C), does not have all the features of an obligate intracellular parasite (i.e., a virus by definition). Mechanisms for viral and synthetic dsRNA cell invasion are likely to be different, potentially affecting the affinities for cytosolic versus endosomal dsRNA receptors and in turn the effectors of dsRNA signalling. In addition, viruses can replicate within cells, but dsRNA alone cannot. I postulate that viruses may produce a higher degree of inflammation and/or cell injury. For instance, dsRNA derived from exogenous sources (i.e., virus) is likely to be present in a biological system for a longer duration when compared to endogenous dsRNA and synthetic dsRNA which does not possess such replicating capacity and is subjected to rapid degradation by nucleases in the cell (Schlee & Hartmann, 2016). Therefore, poly(I:C) is arguably a more appropriate model of endogenous dsRNA rather than exogenous dsRNA.

7.4 Concluding remarks

The dsRNA signalling pathway is mostly associated with a proinflammatory phenotype, but recent literature has argued for non-canonical roles of dsRNA signalling in vascular protection. This thesis started with the novel prospect of investigating poly(I:C) as a therapeutic in PAH but the lack of cross-species conservation and reproducibility of prophylactic intraperitoneal poly(I:C) in a SuHx mouse model of PH compared to a SuHx rat model of PH decreased the plausibility of poly(I:C) as a potential therapy in PAH. Thereafter, by using intranasal poly(I:C) as a model of previous lung inflammation in a SuHx mouse model of PH mice, an enhanced PH phenotype was measured. *In vitro*, PAH-associated proinflammatory cytokines were enhanced in response to poly(I:C) in control ECs. Importantly, in ECs with GCN2-deficiency, the genetic abnormality associated with predisposition to PVOD (PH group 1.6), TNFα release was enhanced in response to poly(I:C). The phenotype of enhanced TNFα release is clinically relevant and mechanistic studies to explain this need further validation but do hold promise as drug targets. This thesis therefore largely supports the idea of canonical pathways where dsRNA signalling is associated with a pro-inflammatory phenotype, typically associated with the deleterious effects on pulmonary vascular remodelling. This opposes the rationale for the investigation of prophylactic intraperitoneal poly(I:C) as a potential PAH therapy (chapter 3). Overall, this thesis extends our knowledge of the regulation of dsRNA signalling in pulmonary vascular remodelling.

8. Bibliography

Abe, K., Toba, M., Alzoubi, A., Ito, M., Fagan, K. A., Cool, C. D., Voelkel, N. F., McMurtry, I. F., & Oka, M. (2010). Formation of plexiform lesions in experimental severe pulmonary arterial hypertension. *Circulation*, *121*(25), 2747–2754.

Abston, E. D., Coronado, M. J., Bucek, A., Onyimba, J. A., Brandt, J. E., Augusto Frisancho, J., Kim, E., Bedja, D., Sung, Y. K., Radtke, A. J., Gabrielson, K. L., Mitzner, W., & Fairweather, D. L. (2013). TLR3 deficiency induces chronic inflammatory cardiomyopathy in resistant mice following coxsackievirus B3 infection: Role for IL-4. *American Journal of Physiology - Regulatory Integrative and Comparative Physiology*, *304*(4).

Aeffner, F., Traylor, Z. P., Yu, E. N. Z., & Davis, I. C. (2011). Double-stranded RNA induces similar pulmonary dysfunction to respiratory syncytial virus in BALB/c mice. *American Journal of Physiology. Lung Cellular and Molecular Physiology*, *301*(1), 99–109.

Ainscough, A. J., Smith, T. J., Haensel, M., Rhodes, C. J., Fellows, A., Whitwell, H. J., Vasilaki, E., Gray, K., Freeman, A., Howard, L. S., Wharton, J., Dunmore, B., Upton, P. D., Wilkins, M. R., Edel, J. B., & Wojciak-Stothard, B. (2022). An organ-on-chip model of pulmonary arterial hypertension identifies a BMPR2-SOX17-prostacyclin signalling axis. *Communications Biology*, *5*(1).

Al Shoyaib, A., Archie, S. R., & Karamyan, V. T. (2019). Intraperitoneal Route of Drug Administration: Should it Be Used in Experimental Animal Studies? *Pharmaceutical Research*, *37*(1), 12.

Alexopoulou, L., Holt, A. C., Medzhitov, R., & Flavell, R. A. (2001). Recognition of double-stranded RNA and activation of NF-κB by Toll-like receptor 3. *Nature*, *413*(6857), 732–738.

Allinson, J. P., Chaturvedi, N., Wong, A., Shah, I., Donaldson, G. C., Wedzicha, J. A., & Hardy, R. (2023). Early childhood lower respiratory tract infection and premature adult death from respiratory disease in Great Britain: a national birth cohort study. *The Lancet*, *401*(10383), 1183–1193.

Arnold, N. D., Pickworth, J. A., West, L. E., Dawson, S., Carvalho, J. A., Casbolt, H., Braithwaite, A. T., Iremonger, J., Renshall, L., Germaschewski, V., McCourt, M., Bland-Ward, P., Kowash, H., Hameed, A. G., Rothman, A. M. K., Frid, M. G., Roger Thompson, A. A., Evans, H. R., Southwood, M., … Lawrie, A. (2019). A therapeutic antibody targeting osteoprotegerin attenuates severe experimental pulmonary arterial hypertension. *Nature Communications*, *10*(1).

Arts, R. J. W., Moorlag, S. J. C. F. M., Novakovic, B., Li, Y., Wang, S. Y., Oosting, M., Kumar, V., Xavier, R. J., Wijmenga, C., Joosten, L. A. B., Reusken, C. B. E. M., Benn, C. S., Aaby, P., Koopmans, M. P., Stunnenberg, H. G., van Crevel, R., & Netea, M. G. (2018). BCG Vaccination Protects against Experimental Viral Infection in Humans through the Induction of Cytokines Associated with Trained Immunity. *Cell Host & Microbe*, *23*(1), 89-100.e5.

Badiger, R., Manigold, T., Gashaw, H., Hinton, H. J., Singer, T., George, P. M., Hansel, T. T., & Mitchell, J. A. (2011). Effect of interferon α preparations on IP10 and ET-1 release from human pulmonary artery smooth muscle cells. *European Respiratory Journal*, *38*(55).

Bakshi, S., Taylor, J., Strickson, S., McCartney, T., & Cohen, P. (2017). Identification of TBK1 complexes required for the phosphorylation of IRF3 and the production of interferon β. *Biochemical Journal*, *474*(7), 1163–1174.

Balachandran, S., Kim, C. N., Yeh, W. C., Mak, T. W., Bhalla, K., & Barber, G. N. (1998). Activation of the dsRNA-dependent protein kinase, PKR, induces apoptosis through FADD-mediated death signaling. *EMBO Journal*, *17*(23), 6888–6902.

Bauer, E. M., Zheng, H., Lotze, M. T., & Bauer, P. M. (2014). Recombinant human interferon alpha 2b prevents and reverses experimental pulmonary hypertension. *PLoS ONE*, *9*(5).

Bell, R. D., White, R. J., Garcia-Hernandez, M. L., Wu, E., Rahimi, H., Marangoni, R. G., Slattery, P., Duemmel, S., Nuzzo, M., Huertas, N., Yee, M., O'Reilly, M. A., Morrell, C., Ritchlin, C. T., Schwarz, E. M., & Korman, B. D. (2020). TNF Induces Obliterative Pulmonary Vascular Disease in a Novel Model of Connective Tissue Disease Associated Pulmonary Arterial Hypertension (CTD-PAH). *Arthritis & Rheumatology (Hoboken, N.J.)*, *72*(10), 1759.

Benza, R. L., Gomberg-Maitland, M., Elliott, C. G., Farber, H. W., Foreman, A. J., Frost, A. E., McGoon, M. D., Pasta, D. J., Selej, M., Burger, C. D., & Frantz, R. P. (2019). Predicting Survival in Patients With Pulmonary Arterial Hypertension: The REVEAL Risk Score Calculator 2.0 and Comparison With ESC/ERS-Based Risk Assessment Strategies. *Chest*, *156*(2), 323–337.

Benza, R. L., Kanwar, M. K., Raina, A., Scott, J. V., Zhao, C. L., Selej, M., Elliott, C. G., & Farber, H. W. (2021). Development and Validation of an Abridged Version of the REVEAL 2.0 Risk Score Calculator, REVEAL Lite 2, for Use in Patients With Pulmonary Arterial Hypertension. *Chest*, *159*(1), 337–346.

Beshay, S., Sahay, S., & Humbert, M. (2020). Evaluation and management of pulmonary arterial hypertension. *Respiratory Medicine*, *171*, 106099.

Bhagwani, A. R., Ali, M., Piper, B., Liu, M., Hudson, J., Kelly, N., Bogamuwa, S., Yang, H., Londino, J. D., Bednash, J. S., Farkas, D., Mallampalli, R. K., Nicolls, M. R., Ryan, J. J., Thompson, A. A. R., Chan, S. Y., Gomez, D., Goncharova, E. A., & Farkas, L. (2023). A p53-TLR3 axis ameliorates pulmonary hypertension by inducing BMPR2 via IRF3. *IScience*, *26*(2), 105935.

Bohuslavová, R., Kolář, F., Kuthanová, L., Neckář, J., Tichopád, A., & Pavlinkova, G. (2010). Gene expression profiling of sex differences in HIF1-dependent adaptive cardiac responses to chronic hypoxia. *Journal of Applied Physiology*, *109*(4), 1195–1202.

Caliez, J., Riou, M., Manaud, G., Nakhleh, M. K., Quatredeniers, M., Rucker-Martin, C., Dorfmüller, P., Lecerf, F., Vinhas, M. C., Khatib, S., Haick, H., Cohen-Kaminsky, S., Humbert, M., Montani, D., & Perros, F. (2020). Trichloroethylene increases pulmonary endothelial permeability: implication for pulmonary veno-occlusive disease. *Pulmonary Circulation*, *10*(4).

Callegari, E., Domenicali, M., Shankaraiah, R. C., D'Abundo, L., Guerriero, P., Giannone, F., Baldassarre, M., Bassi, C., Elamin, B. K., Zagatti, B., Ferracin, M., Fornari, F., Altavilla, G., Blandamura, S., Silini, E. M., Gramantieri, L., Sabbioni, S., & Negrini, M. (2019). MicroRNA-Based Prophylaxis in a Mouse Model of Cirrhosis and Liver Cancer. *Molecular Therapy - Nucleic Acids*, *14*, 239–250.

Chaturvedi, A., & Pierce, S. K. (2009). How Location Governs Toll-Like Receptor Signaling. *Traffic*, *10*(6), 621–628.

Chemla, D., Castelain, V., Humbert, M., Hébert, J. L., Simonneau, G., Lecarpentier, Y., & Hervé, P. (2004). New Formula for Predicting Mean Pulmonary Artery Pressure Using Systolic Pulmonary Artery Pressure. *Chest*, *126*(4), 1313–1317.

Chen, A., Diaz-Soto, M. P., Sanmamed, M. F., Adams, T., Schupp, J. C., Gupta, A., Britto, C., Sauler, M., Yan, X., Liu, Q., Nino, G., Cruz, C. S. D., Chupp, G. L., & Gomez, J. L. (2021). Single-cell characterization of a model of poly I:C-stimulated peripheral blood mononuclear cells in severe asthma. *Respiratory Research*, *22*(1), 1–15.

Chen, C., Feng, Y., Zou, L., Wang, L., Chen, H. H., Cai, J. Y., Xu, J. M., Sosnovik, D. E., & Chao, W. (2014). Role of extracellular RNA and TLR3-Trif signaling in myocardial ischemia-reperfusion injury. *Journal of the American Heart Association*, *3*(1).

Chen, E., Chen, C., Niu, Z., Gan, L., Wang, Q., Li, M., Cai, X. W., Gao, R., Katakam, S., Chen, H., Zhang, S., Zhou, R., Cheng, X., Qiu, Y., Yu, H., Zhu, T., & Liu, J. (2020). Poly(I:C) preconditioning protects the heart against myocardial ischemia/reperfusion injury through TLR3/PI3K/Akt-dependent pathway. *Signal Transduction and Targeted Therapy 2020 5:1*, *5*(1), 1–15.

Chen, J., Yang, F., Shi, S., Liu, X., Qin, F., Wei, X., Huang, Y., Liang, W., & Miao, L. (2021). The Severity of CVB3-Induced Myocarditis Can Be Improved by Blocking the Orchestration of NLRP3 and Th17 in Balb/c Mice. *Mediators of Inflammation*, *2021*.

Chen, Z., Zhang, J., Wei, D., Chen, J., & Yang, J. (2021b). GCN2 Regulates ATF3-p38 MAPK Signaling Transduction in Pulmonary Veno-Occlusive Disease. *Journal of Cardiovascular Pharmacology and Therapeutics*, *26*(6), 677–689.

Chester, A. H., & Yacoub, M. H. (2014). The role of endothelin-1 in pulmonary arterial hypertension. *Global Cardiology Science and Practice*, *2014*(2), 29.

Ciuclan, L., Bonneau, O., Hussey, M., Duggan, N., Holmes, A. M., Good, R., Stringer, R., Jones, P., Morrell, N. W., Jarai, G., Walker, C., Westwick, J., & Thomas, M. (2011). A novel murine model of severe pulmonary arterial hypertension. *American Journal of Respiratory and Critical Care Medicine*, *184*(10), 1171–1182.

Clavarino, G., Claúdio, N., Dalet, A., Terawaki, S., Couderc, T., Chasson, L., Ceppi, M., Schmidt, E. K., Wenger, T., Lecuit, M., Gatti, E., & Pierre, P. (2012). Protein phosphatase 1 subunit Ppp1r15a/GADD34 regulates cytokine production in polyinosinic: Polycytidylic acid-stimulated dendritic cells. *Proceedings of the National Academy of Sciences of the United States of America*, *109*(8), 3006–3011.

Cole, J. E., Navin, T. J., Cross, A. J., Goddard, M. E., Alexopoulou, L., Mitra, A. T., Davies, A. H., Flavell, R. A., Feldmann, M., & Monaco, C. (2011). Unexpected protective role for Toll-like receptor 3 in the arterial wall. *Proceedings of the National Academy of Sciences of the United States of America*, *108*(6), 2372–2377.

Cracowski, J. L., Chabot, F., Labarère, J., Faure, P., Degano, B., Schwebel, C., Chaouat, A., Reynaud-Gaubert, M., Cracowski, C., Sitbon, O., Yaici, A., Simonneau, G., & Humbert, M. (2014). Proinflammatory cytokine levels are linked to death in pulmonary arterial hypertension. In *European Respiratory Journal* . 43(3), 915–917.

Crowley, M. A., Delgado, O., Will-Orrego, A., Buchanan, N. M., Anderson, K., Jaffee, B. D., Dryja, T. P., & Liao, S. M. (2018). Induction of Ocular Complement Activation by Inflammatory Stimuli and Intraocular Inhibition of Complement Factor D in Animal Models. *Investigative Ophthalmology & Visual Science*, *59*(2), 940–951.

Czerkies, M., Korwek, Z., Prus, W., Kochańczyk, M., Jaruszewicz-Błońska, J., Tudelska, K., Błoński, S., Kimmel, M., Brasier, A. R., & Lipniacki, T. (2018). Cell fate in antiviral response arises in the crosstalk of IRF, NF-κB and JAK/STAT pathways. *Nature Communications*, *9*(1).

Danton, M. H. D., Greil, G. F., Byrne, J. G., Hsin, M., Cohn, L., & Maier, S. E. (2003). Right ventricular volume measurement by conductance catheter. *American Journal of Physiology. Heart and Circulatory Physiology*, *285*(4).

De Raaf, M. A., Schalij, I., Gomez-Arroyo, J., Rol, N., Happé, C., De Man, F. S., Vonk-Noordegraaf, A., Westerhof, N., Voelkel, N. F., & Bogaard, H. J. (2014). SuHx rat model: partly reversible pulmonary hypertension and progressive intima obstruction. *European Respiratory Journal*, *44*(1), 160–168.

Di, S., Zhou, M., Pan, Z., Sun, R., Chen, M., Jiang, H., Shi, B., Luo, H., & Li, Z. (2019). Combined Adjuvant of Poly I:C Improves Antitumor Effects of CAR-T Cells. *Frontiers in Oncology*, *9*(1).

Dieudonné, A., Torres, D., Blanchard, S., Taront, S., Jeannin, P., Delneste, Y., Pichavant, M., Trottein, F., & Gosset, P. (2012). Scavenger Receptors in Human Airway Epithelial Cells: Role in Response to Double-Stranded RNA. *PLoS ONE*, *7*(8).

Doherty, G. J., & McMahon, H. T. (2009). Mechanisms of Endocytosis. *Annual Review of Biochemistry*, *78*(1), 857–902.

Dominguez, F., Kühl, U., Pieske, B., Garcia-Pavia, P., & Tschöpe, C. (2016). Update on Myocarditis and Inflammatory Cardiomyopathy: Reemergence of Endomyocardial Biopsy. *Revista Espanola de Cardiologia (English Ed.)*, *69*(2), 178–187.

Donnelly, N., Gorman, A. M., Gupta, S., & Samali, A. (2013). The eIF2α kinases: Their structures and functions. In *Cellular and Molecular Life Sciences*. 70(19) 3493–3511.

Dorfmüller, P., Montani, D., & Humbert, M. (2010). Beyond arterial remodelling: Pulmonary venous and cardiac involvement in patients with systemic sclerosisassociated pulmonary arterial hypertension. In *European Respiratory Journal*. 35(18), 6–8.

Douschan, P., Kovacs, G., Avian, A., Foris, V., Gruber, F., Olschewski, A., & Olschewski, H. (2018). Mild Elevation of Pulmonary Arterial Pressure as a Predictor of Mortality. *American Journal of Respiratory and Critical Care Medicine*, *197*(4), 509–516.

Dunlay, S. M., Weston, S. A., Redfield, M. M., Killian, J. M., & Roger, V. L. (2008). Tumor necrosis factor-alpha and mortality in heart failure: a community study. *Circulation*, *118*(6), 625–631.

Dyck, D. G., Driedger, S. M., Nemeth, R., Osachuk, T. A. G., & Greenberg, A. H. (1987). Conditioned tolerance to drug-induced (poly I:C) natural killer cell activation: effects of drug-dosage and context-specificity parameters. *Brain, Behavior, and Immunity*, *1*(3), 251–266.

Eichstaedt, C. A., Song, J., Benjamin, N., Harutyunova, S., Fischer, C., Grünig, E., & Hinderhofer, K. (2016). EIF2AK4 mutation as “second hit” in hereditary pulmonary arterial hypertension. *Respiratory Research*, *17*(1).

El Haddaoui, H., Brood, R., Latifi, D., Oostvogels, A. A., Klaver, Y., Moskie, M., Mustafa, D. A., Debets, R., & van Eijck, C. H. J. (2022). Rintatolimod (Ampligen®) Enhances Numbers of Peripheral B Cells and Is Associated with Longer Survival in Patients with Locally Advanced and Metastasized Pancreatic Cancer Pre-Treated with FOLFIRINOX: A Single-Center Named Patient Program. *Cancers*, *14*(6), 1377.

Eloranta, M. L., Franck-Larsson, K., L??vgren, T., Kalamajski, S., R??nnblom, A., Rubin, K., Alm, L. (2010). Type I interferon system activation and association with disease manifestations in systemic sclerosis. *Annals of the Rheumatic Diseases*, *69*(7), 1396–1402.

Emdad, L., Sarkar, D., Su, Z. Z., Randolph, A., Boukerche, H., Valerie, K., & Fisher, P. B. (2006). Activation of the nuclear factor kappaB pathway by astrocyte elevated gene-1: implications for tumor progression and metastasis. *Cancer Research*, *66*(3), 1509–1516.

Ewald, S. E., Engel, A., Lee, J., Wang, M., Bogyo, M., & Barton, G. M. (2011). Nucleic acid recognition by Toll-like receptors is coupled to stepwise processing by cathepsins and asparagine endopeptidase. *Journal of Experimental Medicine*, *208*(4), 643–651.

Eyries, M., Montani, D., Girerd, B., Perret, C., Leroy, A., Lonjou, C., Chelghoum, N., Coulet, F., Bonnet, D., Dorfmüller, P., Fadel, E., Sitbon, O., Simonneau, G., Tregouët, D. A., Humbert, M., & Soubrier, F. (2014). EIF2AK4 mutations cause pulmonary veno-occlusive disease, a recessive form of pulmonary hypertension. *Nature Genetics*, *46*(1), 65–69.

Fairweather, D. L., & Rose, N. R. (2007). Coxsackievirus-induced myocarditis in mice: a model of autoimmune disease for studying immunotoxicity. *Methods (San Diego, Calif.)*, *41*(1), 118–122.

Farkas, D., Roger Thompson, A. A., Bhagwani, A. R., Hultman, S., Ji, H., Kotha, N., Farr, G., Arnold, N. D., Braithwaite, A., Casbolt, H., Cole, J. E., Sabroe, I., Monaco, C., Cool, C. D., Goncharova, E. A., Lawrie, A., & Farkas, L. (2019). Toll-like receptor 3 is a therapeutic target for pulmonary hypertension. *American Journal of Respiratory and Critical Care Medicine*, *199*(2), 199–210.

Fayyaz, A. U., Sabbah, M. S., Dasari, S., Griffiths, L. G., DuBrock, H. M., Wang, Y., Charlesworth, M. C., Borlaug, B. A., Jenkins, S. M., Edwards, W. D., & Redfield, M. M. (2023). Histologic and proteomic remodeling of the pulmonary veins and arteries in a porcine model of chronic pulmonary venous hypertension. *Cardiovascular Research*, *119*(1), 268.

Fogel, M. A., Weinberg, P. M., Fellows, K. E., & Huffman, E. A. (1995). A Study in Ventricular–Ventricular Interaction. *Circulation*, *92*(2), 219–230.

Foster, G. R., Zeuzem, S., Pianko, S., Sarin, S. K., Piratvisuth, T., Shah, S., Andreone, P., Sood, A., Chuang, W. L., Lee, C. M., George, J., Gould, M., Flisiak, R., Jacobson, I. M., Komolmit, P., Thongsawat, S., Tanwandee, T., Rasenack, J., Sola, R., … Brown, K. K. (2013). Decline in pulmonary function during chronic hepatitis C virus therapy with modified interferon alfa and ribavirin. *Journal of Viral Hepatitis*, *20*(4).

Foster, S. L., Hargreaves, D. C., & Medzhitov, R. (2007). Gene-specific control of inflammation by TLR-induced chromatin modifications. *Nature 2007 447:7147*, *447*(7147), 972–978.

Freed, B. H., Gomberg-Maitland, M., Chandra, S., Mor-Avi, V., Rich, S., Archer, S. L., Jamison, E. B., Lang, R. M., & Patel, A. R. (2012). Late gadolinium enhancement cardiovascular magnetic resonance predicts clinical worsening in patients with pulmonary hypertension. *Journal of Cardiovascular Magnetic Resonance : Official Journal of the Society for Cardiovascular Magnetic Resonance*, *14*(1).

Fučíková, J., Rožková, D., Ulčová, H., Budinský, V., Sochorová, K., Pokorná, K., Bartůňková, J., & Špíšek, R. (2011). Poly I: C-activated dendritic cells that were generated in CellGro for use in cancer immunotherapy trials. *Journal of Translational Medicine*, *9*(1), 1–10.

Fujita, M., Shannon, J. M., Irvin, C. G., Fagan, K. A., Cool, C., Augustin, A., & Mason, R. J. (2001). Overexpression of tumor necrosis factor-α produces an increase in lung volumes and pulmonary hypertension. *American Journal of Physiology - Lung Cellular and Molecular Physiology*, *280*(1 24-1).

Funami, K., Matsumoto, M., Oshiumi, H., Akazawa, T., Yamamoto, A., & Seya, T. (2004). The cytoplasmic “linker region” in Toll-like receptor 3 controls receptor localization and signaling. *International Immunology*, *16*(8), 1143–1154.

Galabru, J., & Hovanessian, A. (1987). Autophosphorylation of the protein kinase dependent on double-stranded RNA. *The Journal of Biological Chemistry*, *262*(32), 15538–15544.

Galiè, N., Hoeper, M. M., Humbert, M., Torbicki, A., Vachiery, J. L., Barbera, J. A., Beghetti, M., Corris, P., Gaine, S., Gibbs, J. S., Gomez-Sanchez, M. A., Jondeau, G., Klepetko, W., Opitz, C., Peacock, A., Rubin, L., Zellweger, M., & Simonneau, G. (2009). Guidelines for the diagnosis and treatment of pulmonary hypertension. In *European Respiratory Journal*. 34(6),1219–1263.

Gan, C. T. J., Lankhaar, J. W., Marcus, J. T., Westerhof, N., Marques, K. M., Bronzwaer, J. G. F., Boonstra, A., Postmus, P. E., & Vonk-Noordegraaf, A. (2006a). Impaired left ventricular filling due to right-to-left ventricular interaction in patients with pulmonary arterial hypertension. *American Journal of Physiology. Heart and Circulatory Physiology*, *290*(4).

Gan, T., Yang, Y., Hu, F., Chen, X., Zhou, J., Li, Y., Xu, Y., Wang, H., Chen, Y., & Zhang, M. (2018). TLR3 Regulated Poly I:C-Induced Neutrophil Extracellular Traps and Acute Lung Injury Partly Through p38 MAP Kinase. *Frontiers in Microbiology*, *9*,(1).

Gantier, M. P., & Williams, B. R. G. (2007). The response of mammalian cells to double-stranded RNA. *Cytokine & Growth Factor Reviews*, *18*(5–6), 363–371.

Gao, X., Chan, P. K. S., Lui, G. C. Y., Hui, D. S. C., Chu, I. M. T., Sun, X., Tsang, M. S. M., Chan, B. C. L., Lam, C. W. K., & Wong, C. K. (2021). Interleukin-38 ameliorates poly(I:C) induced lung inflammation: therapeutic implications in respiratory viral infections. *Cell Death & Disease 2021 12:1*, *12*(1), 1–18.

Gao, X., Gao, S., Guan, Y., Huang, L., Huang, J., Lin, L., Liu, Y., Zhao, H., Huang, B., Yuan, T., Liu, Y., Liang, D., Zhang, Y., Ma, X., Li, L., Li, J., Zhou, D., Shi, D., Xu, L., & Chen, Y.-H. (2019). Toll-like receptor 3 controls QT interval on the electrocardiogram by targeting the degradation of Kv4.2/4.3 channels in the endoplasmic reticulum. *The FASEB Journal*, *33*(5), 6197–6208.

George, P. M., Badiger, R., Shao, D., Edwards, M. R., Wort, S. J., Paul-Clark, M. J., & Mitchell, J. A. (2012). Viral Toll Like Receptor activation of pulmonary vascular smooth muscle cells results in endothelin-1 generation; relevance to pathogenesis of pulmonary arterial hypertension. *Biochemical and Biophysical Research Communications*, *426*(4), 486–491.

George, P. M., Oliver, E., Dorfmuller, P., Dubois, O. D., Reed, D. M., Kirkby, N. S., Mohamed, N. A., Perros, F., Antigny, F., Fadel, E., Schreiber, B. E., Holmes, A. M., Southwood, M., Hagan, G., Wort, S. J., Bartlett, N., Morrell, N. W., Coghlan, J. G., Humbert, M., … Mitchell, J. A. (2014). Evidence for the involvement of type I interferon in pulmonary arterial hypertension. *Circulation Research*, *114*(4), 677–688.

Geraci, M. W., Bull, T. M., & Tuder, R. M. (2010). Genomics of Pulmonary Arterial Hypertension: Implications for Therapy. In *Heart Failure Clinics*. 6(1), 101–114.

Gil, J., & Esteban, M. (2000). The interferon-induced protein kinase (PKR), triggers apoptosis through FADD-mediated activation of caspase 8 in a manner independent of Fas and TNF-α receptors. *Oncogene*, *19*(32), 3665–3674.

Gingles, N. A., Alexander, J. E., Kadioglu, A., Andrew, P. W., Kerr, A., Mitchell, T. J., Hopes, E., Denny, P., Brown, S., Jones, H. B., Little, S., Booth, G. C., & McPheat, W. L. (2001). Role of Genetic Resistance in Invasive Pneumococcal Infection: Identification and Study of Susceptibility and Resistance in Inbred Mouse Strains. *Infection and Immunity*, *69*(1), 426.

Golembeski, S. M., West, J., Tada, Y., & Fagan, K. A. (2005). Interleukin-6 causes mild pulmonary hypertension and augments hypoxia-induced pulmonary hypertension in mice. *Chest*, *128*(6).

Gu, T., Zhao, S., Jin, G., Song, M., Zhi, Y., Zhao, R., Ma, F., Zheng, Y., Wang, K., Liu, H., Xin, M., Han, W., Li, X., Dong, C. D., Liu, K., & Dong, Z. (2021). Cytokine Signature Induced by SARS-CoV-2 Spike Protein in a Mouse Model. *Frontiers in Immunology*, *11*, 621441.

Hajouli, S., Moustafa, M. A., & Memoli, J. S. W. (2019). Pulmonary Veno-Occlusive Disease: A Rare Cause of Pulmonary Hypertension. *Journal of Investigative Medicine High Impact Case Reports*, *7*.

Hamada, K., Teramoto, S., Narita, N., Yamada, E., Teramoto, K., & Kobzik, L. (2000). Pulmonary veno-occlusive disease in pulmonary Langerhans' cell granulomatosis. *European Respiratory Journal*, *15*(2), 421–423.

Hameed, A. G., Arnold, N. D., Chamberlain, J., Pickworth, J. A., Paiva, C., Dawson, S., Cross, S., Long, L., Zhao, L., Morrell, N. W., Crossman, D. C., Newman, C. M. H., Kiely, D. G., Francis, S. E., & Lawrie, A. (2012). Inhibition of tumor necrosis factor-related apoptosis-inducing ligand (TRAIL) reverses experimental pulmonary hypertension. *Journal of Experimental Medicine*, *209*(11), 1919–1935.

Hänel, G., Angerer, C., Petry, K., Lichtenegger, F. S., & Subklewe, M. (2022). Blood DCs activated with R848 and poly(I:C) induce antigen-specific immune responses against viral and tumor-associated antigens. *Cancer Immunology, Immunotherapy*, *71*(7), 1705.

Hardarson, H. S., Baker, J. S., Yang, Z., Purevjav, E., Huang, C. H., Alexopoulou, L., Li, N., Flavell, R. A., Bowles, N. E., & Vallejo, J. G. (2007). Toll-like receptor 3 is an essential component of the innate stress response in virus-induced cardiac injury. *American Journal of Physiology - Heart and Circulatory Physiology*, *292*(1).

Harris, P., Sridhar, S., Peng, R., Phillips, J. E., Cohn, R. G., Burns, L., Woods, J., Ramanujam, M., Loubeau, M., Tyagi, G., Allard, J., Burczynski, M., Ravindran, P., Cheng, D., Bitter, H., Fine, J. S., Bauer, C. M. T., & Stevenson, C. S. (2013). Double-stranded RNA induces molecular and inflammatory signatures that are directly relevant to COPD. *Mucosal Immunology*, *6*(3), 474–484.

Hirsch, K., Nolley, S., Ralph, D. D., Zheng, Y., Altemeier, W. A., Rhodes, C. J., Morrell, N. W., Wilkins, M. R., Leary, P. J., & Rayner, S. G. (2023). Circulating markers of inflammation and angiogenesis and clinical outcomes across subtypes of pulmonary arterial hypertension. *The Journal of Heart and Lung Transplantation : The Official Publication of the International Society for Heart Transplantation*, *42*(2), 173–182.

Hoebe, K., Du, X., Georgel, P., Janssen, E., Tabeta, K., Kim, S. O., Goode, J., Lin, P., Mann, N., Mudd, S., Crozat, K., Sovath, S., Han, J., & Beutler, B. (2003). Identification of Lps2 as a key transducer of MyD88-independent TIR signalling. *Nature*, *424*(6950), 743–748.

Hoffstein, V., Ranganathan, N., & Mullen, J. B. M. (1986). Sarcoidosis simulating pulmonary veno-occlusive disease. *American Review of Respiratory Disease*, *134*(4), 809–811.

Hojda, S. E., Chis, I. C., & Clichici, S. (2022). Biomarkers in Pulmonary Arterial Hypertension. *Diagnostics*, *12*(12).

Holfeld, J., Tepeköylü, C., Reissig, C., Lobenwein, D., Scheller, B., Kirchmair, E., Kozaryn, R., Albrecht-Schgoer, K., Krapf, C., Zins, K., Urbschat, A., Zacharowski, K., Grimm, M., Kirchmair, R., & Paulus, P. (2016). Toll-like receptor 3 signalling mediates angiogenic response upon shock wave treatment of ischaemic muscle. *Cardiovascular Research*, *109*(2), 331–343.

Horton, C. G., & Farris, A. D. (2012). Toll-like receptors in systemic lupus erythematosus: Potential targets for therapeutic intervention. *Current Allergy and Asthma Reports*, *12*(1), 1–7.

Hoshikawa, Y., Nana-Sinkam, P., Moore, M. D., Sotto-Santiago, S., Phang, T., Keith, R. L., Morris, K. G., Kondo, T., Tuder, R. M., Voelkel, N. F., & Geraci, M. W. (2003). Hypoxia induces different genes in the lungs of rats compared with mice. *Physiological Genomics*, *12*(3), 209–219.

Hu, Y., Wang, J., Yang, B., Zheng, N., Qin, M., Ji, Y., Lin, G., Tian, L., Wu, X., Wu, L., & Sun, B. (2011). Guanylate Binding Protein 4 Negatively Regulates Virus-Induced Type I IFN and Antiviral Response by Targeting IFN Regulatory Factor 7. *The Journal of Immunology*, *187*(12), 6456–6462.

Huertas, A., Tu, L., Humbert, M., & Guignabert, C. (2020). Chronic inflammation within the vascular wall in pulmonary arterial hypertension: more than a spectator. *Cardiovascular Research*, *116*(5), 885–893.

Humbert, M., Guignabert, C., Bonnet, S., Dorfmüller, P., Klinger, J. R., Nicolls, M. R., Olschewski, A. J., Pullamsetti, S. S., Schermuly, R. T., Stenmark, K. R., & Rabinovitch, M. (2019). Pathology and pathobiology of pulmonary hypertension: state of the art and research perspectives. *European Respiratory Journal*, *53*(1).

Humbert, M., Monti, G., Brenot, F., Sitbon, O., Portier, A., Grangeot-Keros, L., Duroux, P., Galanaud, P., Simonneau, G., & Emilie, D. (2012). Increased interleukin-1 and interleukin-6 serum concentrations in severe primary pulmonary hypertension. *151*(5), 1628–1631.

Hurst, L. A., Dunmore, B. J., Long, L., Crosby, A., Al-Lamki, R., Deighton, J., Southwood, M., Yang, X., Nikolic, M. Z., Herrera, B., Inman, G. J., Bradley, J. R., Rana, A. A., Upton, P. D., & Morrell, N. W. (2017). TNFα drives pulmonary arterial hypertension by suppressing the BMP type-II receptor and altering NOTCH signalling. *Nature Communications*, *8*(1), 1–14.

Ichimura, K., Santana, E. J., Kuznetsova, T., Cauwenberghs, N., Sabovčik, F., Chun, L., Francisco, N. L. C., Kheyfets, V. O., Salerno, M., Zamanian, R. T., Spiekerkoetter, E., & Haddad, F. (2023). Novel left ventricular mechanical index in pulmonary arterial hypertension. *Pulmonary Circulation*, *13*(2).

Iordanov, M. S., Paranjape, J. M., Zhou, A., Wong, J., Williams, B. R. G., Meurs, E. F., Silverman, R. H., & Magun, B. E. (2000). Activation of p38 Mitogen-Activated Protein Kinase and c-Jun NH2-Terminal Kinase by Double-Stranded RNA and Encephalomyocarditis Virus: Involvement of RNase L, Protein Kinase R, and Alternative Pathways. *Molecular and Cellular Biology*, *20*(2), 617.

Itoh, K., Watanabe, A., Funami, K., Seya, T., & Matsumoto, M. (2008). The Clathrin-Mediated Endocytic Pathway Participates in dsRNA-Induced IFN-β Production. *The Journal of Immunology*, *181*(8), 5522–5529.

ITOH, T., NAGAYA, N., ISHIBASHI-UEDA, H., KYOTANI, S., OYA, H., SAKAMAKI, F., KIMURA, H., & NAKANISHI, N. (2006). Increased plasma monocyte chemoattractant protein-1 level in idiopathic pulmonary arterial hypertension. *Respirology*, *11*(2), 158–163.

Iurescia, S., Fioretti, D., & Rinaldi, M. (2018). Targeting cytosolic nucleic acid-sensing pathways for cancer immunotherapies. In *Frontiers in Immunology* (Vol. 9, Issue APR). Frontiers Media S.A. https://doi.org/10.3389/fimmu.2018.00711

Janeway, C. A., & Medzhitov, R. (2002). Innate Immune Recogntion. *Annual Review of Immunology*, *20*(1), 197–216.

Jelinek, I., Leonard, J. N., Price, G. E., Brown, K. N., Meyer-Manlapat, A., Goldsmith, P. K., Wang, Y., Venzon, D., Epstein, S. L., & Segal, D. M. (2011). TLR3-Specific Double-Stranded RNA Oligonucleotide Adjuvants Induce Dendritic Cell Cross-Presentation, CTL Responses, and Antiviral Protection. *The Journal of Immunology*, *186*(4), 2422–2429.

Jiang, Z., Zamanian-Daryoush, M., Nie, H., Silva, A. M., Williams, B. R. G., & Li, X. (2003). Poly(dI·dC)-induced Toll-like receptor 3 (TLR3)-mediated activation of NFκB and MAP kinase is through an interleukin-1 receptor-associated kinase (IRAK)-independent pathway employing the signaling components TLR3-TRAF6-TAK1-TAB2-PKR. *Journal of Biological Chemistry*, *278*(19), 16713–16719.

Joselson, R., & Warnock, M. (1983). Pulmonary veno-occlusive disease after chemotherapy. *Human Pathology*, *14*(1), 88–91.

Kagoya, Y., Yoshimi, A., Kataoka, K., Nakagawa, M., Kumano, K., Arai, S., Kobayashi, H., Saito, T., Iwakura, Y., & Kurokawa, M. (2014). Positive feedback between NF-κB and TNF-α promotes leukemia-initiating cell capacity. *The Journal of Clinical Investigation*, *124*(2), 528–542.

Kang, M. J., Chun, G. L., Lee, J. Y., Dela Cruz, C. S., Chen, Z. J., Enelow, R., & Elias, J. A. (2008). Cigarette smoke selectively enhances viral PAMP- and virus-induced pulmonary innate immune and remodeling responses in mice. *The Journal of Clinical Investigation*, *118*(8), 2771–2784.

Karakurt, Z. (2010). [Other causes of pulmonary arterial hypertension: pulmonary veno-occlusive disease, pulmonary capillary hemangiomatosis, porto-pulmonary hypertension, HIV- associated pulmonary arterial hypertension]. *Anadolu Kardiyoloji Dergisi : AKD = the Anatolian Journal of Cardiology*, *10*(1), 63–68.

Karikó, K., Ni, H., Capodici, J., Lamphier, M., & Weissman, D. (2004). mRNA Is an Endogenous Ligand for Toll-like Receptor 3. *Journal of Biological Chemistry*, *279*(13), 12542–12550.
Kato, H., Takeuchi, O., Mikamo-Satoh, E., Hirai, R., Kawai, T., Matsushita, K., Hiiragi, A., Dermody, T. S., Fujita, T., & Akira, S. (2008). Length-dependent recognition of double-stranded ribonucleic acids by retinoic acid-inducible gene-I and melanoma differentiation-associated gene 5. *Journal of Experimental Medicine*, *205*(7), 1601–1610.
Kawai, T., & Akira, S. (2006). TLR signaling. In *Cell Death and Differentiation*. 13(5), 816–825.
Kawai, T., & Akira, S. (2009). The roles of TLRs, RLRs and NLRs in pathogen recognition. In *International Immunology*. 21(4),317–337.
Kell, A., Stoddard, M., Li, H., Marcotrigiano, J., Shaw, G. M., & Gale, M. (2015). Pathogen-Associated Molecular Pattern Recognition of Hepatitis C Virus Transmitted/Founder Variants by RIG-I Is Dependent on U-Core Length. *Journal of Virology*, *89*(21), 11056–11068.
Kerbaul, F., Van Der Linden, P., Pierre, S., Rondelet, B., Melot, C., Brimioulle, S., & Naeije, R. (2004). Prevention of hemodilution-induced inhibition of hypoxic pulmonary vasoconstriction by N-acetylcysteine in dogs. *Anesthesia and Analgesia*, *99*(2), 547–551.
Kiely, D. G., Elliot, C. A., Sabroe, I., & Condliffe, R. (2013). Pulmonary hypertension: Diagnosis and management. In *BMJ (Online)*.346.
Kim, H., Yung, G. L., Marsh, J. J., Konopka, R. G., Pedersen, C. A., Chiles, P. G., Morris, T. A., & Channick, R. N. (2000). Endothelin mediates pulmonary vascular remodelling in a canine model of chronic embolic pulmonary hypertension. *European Respiratory Journal*, *15*(4), 640–648.
Kojima, H., Tokunou, T., Takahara, Y., Sunagawa, K., Hirooka, Y., Ichiki, T., & Tsutsui, H. (2019). Hypoxia-inducible factor-1 α deletion in myeloid lineage attenuates hypoxia-induced pulmonary hypertension. *Physiological Reports*, *7*(7), e14025.
Kokturk, N., Demir, N., Demircan, S., Memis, L., Kurul, C., Akyurek, N., & Turktas, H. *Pulmonary Veno-occlusive Disease in a Patient with a History of Hashimoto's Thyroiditis*.
Kulkarni, H. S., Lee, J. S., Bastarache, J. A., Kuebler, W. M., Downey, G. P., Albaiceta, G. M., Altemeier, W. A., Artigas, A., Bates, J. H. T., Calfee, C. S., Cruz, C. S. Dela, Dickson, R. P., Englert, J. A., Everitt, J. I., Fessler, M. B., Gelman, A. E., Gowdy, K. M., Groshong, S. D., Herold, S., … Matute-Bello, G. (2022). *AMERICAN THORACIC SOCIETY DOCUMENTS Update on the Features and Measurements of Experimental Acute Lung Injury in Animals An Official American Thoracic Society Workshop Report*.
Lamia, B., Muir, J. F., Molano, L. C., Viacroze, C., Benichou, J., Bonnet, P., Quieffin, J., Cuvelier, A., & Naeije, R. (2017). Altered synchrony of right ventricular contraction in borderline pulmonary hypertension. *International Journal of Cardiovascular Imaging*, *33*(9), 1331–1339.
Lane, K. B., Machado, R. D., Pauciulo, M. W., Thomson, J. R., Phillips, J. A., Loyd, J. E., Nichols, W. C., Trembath, R. C., Aldred, M., Brannon, C. A., Conneally, P. M., Foroud, T., Fretwell, N., Gaddipati, R., Koller, D., Loyd, E. J., Morgan, N., Newman, J. H., Prince, M. A., … Wheeler, L. (2000). Heterozygous germline mutations in BMPR2, encoding a TGF-β receptor, cause familial primary pulmonary hypertension. *Nature Genetics*, *26*(1), 81–84.
Ledermann, B. (2000). Embryonic Stem Cells and Gene Targeting. *Experimental Physiology*, *85*(6), 603–613.
Lee, H. K., Dunzendorfer, S., Soldau, K., & Tobias, P. S. (2006). Double-stranded RNA-mediated TLR3 activation is enhanced by CD14. *Immunity*, *24*(2), 153–163.
Lee, S. M. Y., Yip, T. F., Yan, S., Jin, D. Y., Wei, H. L., Guo, R. T., & Peiris, J. S. M. (2018). Recognition of double-stranded RNA and regulation of interferon pathway by toll-like receptor 10. *Frontiers in Immunology*, *9*(1).
Li, Y., Li, Y., Li, L., Yin, M., Wang, J., & Li, X. (2021). PKR deficiency alleviates pulmonary hypertension via inducing inflammasomeadaptor ASC inactivation. *Pulmonary Circulation*, *11*(4), 1–13.
Li, Z., Jiang, J., & Gao, S. (2021). Potential of C-X-C motif chemokine ligand 1/8/10/12 as diagnostic and prognostic biomarkers in idiopathic pulmonary arterial hypertension. *The Clinical Respiratory Journal*, *15*(12), 1302–1309.
Liang, L., Ma, G., Chen, K., Liu, Y., Wu, X., Ying, K., & Zhang, R. (2016). EIF2AK4 mutation in pulmonary veno-occlusive disease: A case report and review of the literature. *Medicine*, *95*(39).
Liao, Y., Wang, J., Jaehnig, E. J., Shi, Z., & Zhang, B. (2019). WebGestalt 2019: gene set analysis toolkit with revamped UIs and APIs. *Nucleic Acids Research*, *47*(W1), W199–W205.
Lin, Q., Fang, D., Fang, J., Ren, X., Yang, X., Wen, F., & Su, S. B. (2011). Impaired Wound Healing with Defective Expression of Chemokines and Recruitment of Myeloid Cells in TLR3-Deficient Mice. *The Journal of Immunology*, *186*(6), 3710–3717.

Liu, L., Botos, I., Wang, Y., Leonard, J. N., Shiloach, J., Segal, D. M., & Davies, D. R. (2008). Structural basis of toll-like receptor 3 signaling with double-stranded RNA. *Science*, *320*(5874), 379–381.

López, C. B., Moltedo, B., Alexopoulou, L., Bonifaz, L., Flavell, R. A., & Moran, T. M. (2004). TLR-Independent Induction of Dendritic Cell Maturation and Adaptive Immunity by Negative-Strand RNA Viruses. *The Journal of Immunology*, *173*(11), 6882–6889.

Ma, L., Roman-Campos, D., Austin, E. D., Eyries, M., Sampson, K. S., Soubrier, F., Germain, M., Trégouët, D.-A., Borczuk, A., Rosenzweig, E. B., Girerd, B., Montani, D., Humbert, M., Loyd, J. E., Kass, R. S., & Chung, W. K. (2013). A Novel Channelopathy in Pulmonary Arterial Hypertension. *New England Journal of Medicine*, *369*(4), 351–361.

Machado, R. D., Eickelberg, O., Elliott, C. G., Geraci, M. W., Hanaoka, M., Loyd, J. E., Newman, J. H., Phillips, J. A., Soubrier, F., Trembath, R. C., & Chung, W. K. (2009). Genetics and Genomics of Pulmonary Arterial Hypertension. *Journal of the American College of Cardiology*, *54*(1), S32–S42.

Manaud, G., Nossent, E. J., Lambert, M., Ghigna, M. R., Boet, A., Vinhas, M. C., Ranchoux, B., Dumas, S. J., Courboulin, A., Girerd, B., Soubrier, F., Bignard, J., Claude, O., Lecerf, F., Hautefort, A., Florio, M., Sun, B., Nadaud, S., Verleden, S. E., … Perros, F. (2020). Comparison of human and experimental pulmonary veno-occlusive disease. *American Journal of Respiratory Cell and Molecular Biology*, *63*(1), 118–131.

Manche, L., Green, S. R., Schmedt, C., & Mathews, M. B. (1992). Interactions between double-stranded RNA regulators and the protein kinase DAI. *Molecular and Cellular Biology*, *12*(11), 5238–5248.

Maron, B. A., Brittan, E. L., Hess, E., Waldo, S. W., Barón, A. E., Huang, S., Goldstein, R. H., Assad, T., Wertheim, B. M., Alba, G. A., Leopold, J. A., Olschewski, H., Galiè, N., Simonneau, G., Kovacs, G., Tedford, R. J., Humbert, M., & Choudhary, G. (2020). Pulmonary vascular resistance and clinical outcomes in patients with pulmonary hypertension: a retrospective cohort study. *The Lancet. Respiratory Medicine*, *8*(9), 873–884.

Maston, L. D., Jones, D. T., Giermakowska, W., Resta, T. C., Ramiro-Diaz, J., Howard, T. A., Jernigan, N. L., Herbert, L., Maurice, A. A., & Gonzalez Bosc, L. V. (2018). Interleukin-6 trans-signaling contributes to chronic hypoxia-induced pulmonary hypertension. *Pulmonary Circulation*, *8*(3), 1–11.

Matute-Bello, G., Downey, G., Moore, B. B., Groshong, S. D., Matthay, M. A., Slutsky, A. S., & Kuebler, W. M. (2012). An Official American Thoracic Society Workshop Report: Features and Measurements of Experimental Acute Lung Injury in Animals. *44*(5), 725–738.

McGarry, N., Murray, C. L., Garvey, S., Wilkinson, A., Tortorelli, L., Ryan, L., Hayden, L., Healy, D., Griffin, E. W., Hennessy, E., Arumugam, M., Skelly, D. T., Mitchell, K. J., & Cunningham, C. (2021). Double stranded RNA drives anti-viral innate immune responses, sickness behavior and cognitive dysfunction dependent on dsRNA length, IFNAR1 expression and age. *Brain, Behavior, and Immunity*, *95*, 413.

Medvedev, A. E., Lentschat, A., Wahl, L. M., Golenbock, D. T., & Vogel, S. N. (2002). Dysregulation of LPS-induced Toll-like receptor 4-MyD88 complex formation and IL-1 receptor-associated kinase 1 activation in endotoxin-tolerant cells. *Journal of Immunology. 169*(9), 5209–5216.

Méndez, C., Soler, R., Rodriguez, E., López, M., Álvarez, L., Fernández, N., & Montserrat, L. (2011). Magnetic resonance imaging of abnormal ventricular septal motion in heart diseases: a pictorial review. *Insights into Imaging*, *2*(4), 483.

Meylan, E., Burns, K., Hofmann, K., Blancheteau, V., Martinon, F., Kelliher, M., & Tschopp, J. (2004). RIP1 is an essential mediator of Toll-like receptor 3-induced NF κB activation. *Nature Immunology*, *5*(5), 503–507.

Miller, A. J., & Spence, J. R. (2017). In Vitro Models to Study Human Lung Development, Disease and Homeostasis. *Physiology (Bethesda, Md.)*, *32*(3), 246–260.

Mitchell, W. M. (2016). Efficacy of rintatolimod in the treatment of chronic fatigue syndrome/myalgic encephalomyelitis (CFS/ME). *Expert Review of Clinical Pharmacology*, *9*(6), 755.

Mitchell, W. M., Nicodemus, C. F., Carter, W. A., Horvath, J. C., & Strayer, D. R. (2014). Discordant Biological and Toxicological Species Responses to TLR3 Activation. *The American Journal of Pathology*, *184*(4), 1062–1072.

Monge Garcia, M. I., Jian, Z., Settels, J. J., Hunley, C., Cecconi, M., Hatib, F., & Pinsky, M. R. (2018). Performance comparison of ventricular and arterial dP/dtmax for assessing left ventricular systolic function during different experimental loading and contractile conditions. *Critical Care (London, England)*, *22*(1).

Montani, D., Lau, E. M., Descatha, A., Jaïs, X., Savale, L., Andujar, P., Bensefa-Colas, L., Girerd, B., Zendah, I., Le Pavec, J., Seferian, A., Perros, F., Dorfmüller, P., Fadel, E., Soubrier, F., Sitbon, O., Simonneau, G., & Humbert, M. (2015). Occupational exposure to organic solvents: a risk factor for pulmonary veno-occlusive disease. *European Respiratory Journal*, *46*(6), 1721–1731.

Morimont, P., Lambermont, B., Desaive, T., Janssen, N., Chase, G., & D'Orio, V. (2012). Arterial dP/dtmax accurately reflects left ventricular contractility during shock when adequate vascular filling is achieved. *BMC Cardiovascular Disorders*, *12*, 13.

Murray, L. A., Knight, D. A., McAlonan, L., Argentieri, R., Joshi, A., Shaheen, F., Cunningham, M., Alexopolou, L., Flavell, R. A., Sarisky, R. T., & Hogaboam, C. M. (2008). Deleterious Role of TLR3 during Hyperoxia-induced Acute Lung Injury. *American Journal of Respiratory and Critical Care Medicine*, *178*(12), 1227–1237.

Mutschler, D., Wikström, G., Lind, L., Larsson, A., Lagrange, A., & Eriksson, M. (2006). Etanercept reduces late endotoxin-induced pulmonary hypertension in the pig. *Journal of Interferon & Cytokine Research : The Official Journal of the International Society for Interferon and Cytokine Research*, *26*(9), 661–667.

Nagpal, R., Wang, S., Solberg Woods, L. C., Seshie, O., Chung, S. T., Shively, C. A., Register, T. C., Craft, S., McClain, D. A., & Yadav, H. (2018). Comparative microbiome signatures and short-chain fatty acids in mouse, rat, non-human primate, and human feces. *Frontiers in Microbiology*, *9*(1).

Nair, A. B., & Jacob, S. (2016). A simple practice guide for dose conversion between animals and human. *Journal of Basic and Clinical Pharmacy*, *7*(2), 27.

Nazmi, A., Mukhopadhyay, R., Dutta, K., & Basu, A. (2012). STING mediates neuronal innate immune response following japanese encephalitis virus infection. *Scientific Reports*, *2*.

Netea, M. G., Joosten, L. A. B., Latz, E., Mills, K. H. G., Natoli, G., Stunnenberg, H. G., O'Neill, L. A. J., & Xavier, R. J. (2016). Trained immunity: a program of innate immune memory in health and disease. *Science (New York, N.Y.)*, *352*(6284).

Nishiya, T., & DeFranco, A. L. (2004). Ligand-regulated Chimeric Receptor Approach Reveals Distinctive Subcellular Localization and Signaling Properties of the Toll-like Receptors. *Journal of Biological Chemistry*, *279*(18), 19008–19017.

Nishiya, T., Kajita, E., Miwa, S., & DeFranco, A. L. (2005). TLR3 and TLR7 are targeted to the same intracellular compartments by distinct regulatory elements. *Journal of Biological Chemistry*, *280*(44), 37107–37117.

Nomura, F., Akashi, S., Sakao, Y., Sato, S., Kawai, T., Matsumoto, M., Nakanishi, K., Kimoto, M., Miyake, K., Takeda, K., & Akira, S. (2000). Cutting edge: endotoxin tolerance in mouse peritoneal macrophages correlates with down-regulation of surface toll-like receptor 4 expression. *Journal of Immunology (Baltimore, Md. : 1950)*, *164*(7), 3476–3479.

O'Dwyer, D. N., Armstrong, M. E., Trujillo, G., Cooke, G., Keane, M. P., Fallon, P. G., Simpson, A. J., Millar, A. B., McGrath, E. E., Whyte, M. K., Hirani, N., Hogaboam, C. M., & Donnelly, S. C. (2013). The toll-like receptor 3 L412F polymorphism and disease progression in idiopathic pulmonary fibrosis. *American Journal of Respiratory and Critical Care Medicine*, *188*(12), 1442–1450.

Ormiston, M. L., Chang, C., Long, L. L., Soon, E., Jones, D., Machado, R., Treacy, C., Toshner, M. R., Campbell, K., Riding, A., Southwood, M., Pepke-Zaba, J., Exley, A., Trembath, R. C., Colucci, F., Wills, M., Trowsdale, J., & Morrell, N. W. (2012). Impaired natural killer cell phenotype and function in idiopathic and heritable pulmonary arterial hypertension. *Circulation*, *126*(9), 1099–1109.

Oshiumi, H., Miyashita, M., Okamoto, M., Morioka, Y., Okabe, M., Matsumoto, M., & Seya, T. (2015). DDX60 Is Involved in RIG-I-Dependent and Independent Antiviral Responses, and Its Function Is Attenuated by Virus-Induced EGFR Activation. *Cell Reports*, *11*(8), 1193–1207.

Owen, A. M., Fults, J. B., Patil, N. K., Hernandez, A., & Bohannon, J. K. (2021). TLR Agonists as Mediators of Trained Immunity: Mechanistic Insight and Immunotherapeutic Potential to Combat Infection. *Frontiers in Immunology*, *11*, 622614.

Pacher, P., Nagayama, T., Mukhopadhyay, P., Bátkai, S., & Kass, D. A. (2008a). Measurement of cardiac function using pressure-volume conductance catheter technique in mice and rats. *Nature Protocols*, *3*(9), 1422–1434.

Pakos-Zebrucka, K., Koryga, I., Mnich, K., Ljujic, M., Samali, A., & Gorman, A. M. (2016). The integrated stress response. *EMBO Reports*, *17*(10), 1374–1395.

Palmer, S. M., Robinson, L. J., Wang, A., Gossage, J. R., Bashore, T., & Tapson, V. F. (1998). Massive pulmonary edema and death after prostacyclin infusion in a patient with pulmonary veno-occlusive disease. *Chest*, *113*(1), 237–240.

Pan, H., Deutsch, G. H., & Wert, S. E. (2019). Comprehensive anatomic ontologies for lung development: A comparison of alveolar formation and maturation within mouse and human lung. *Journal of Biomedical Semantics*, *10*(1), 1–21.

Papani, R., Duarte, A. G., Lin, Y. L., Kuo, Y. F., & Sharma, G. (2017). Pulmonary arterial hypertension associated with interferon therapy: A population-based study. *Multidisciplinary Respiratory Medicine*, *12*(1).

Patel, H., Ewels, P., Peltzer, A., Botvinnik, O., Sturm, G., Moreno, D., Vemuri, P., silviamorins, Garcia, M. U., Pantano, L., Binzer-Panchal, M., bot, nf-core, Zepper, M., Syme, R., Kelly, G., Hanssen, F., Yates, J. A. F., Cheshire, C., rfenouil, … F., S. (2023). *nf-core/rnaseq: nf-core/rnaseq v3.11.1 - Plastered Radium Rhino*.

Perros, F., Dorfmüller, P., Montani, D., Hammad, H., Waelput, W., Girerd, B., Raymond, N., Mercier, O., Mussot, S., Cohen-Kaminsky, S., Humbert, M., & Lambrecht, B. N. (2012). Pulmonary lymphoid neogenesis in idiopathic pulmonary arterial hypertension. *American Journal of Respiratory and Critical Care Medicine*, *185*(3), 311–321.

Perros, F., Günther, S., Ranchoux, B., Godinas, L., Antigny, F., Chaumais, M. C., Dorfmüller, P., Hautefort, A., Raymond, N., Savale, L., Jaïs, X., Girerd, B., Cottin, V., Sitbon, O., Simonneau, G., Humbert, M., & Montani, D. (2015). Mitomycin-induced pulmonary veno-occlusive disease: Evidence from human disease and animal models. *Circulation*, *132*(9), 834–847.

Pfeifer, R., Lichte, P., Schreiber, H., Sellei, R. M., Dienstknecht, T., Sadeghi, C., Pape, H. C., & Kobbe, P. (2013). Models of hemorrhagic shock: Differences in the physiological and inflammatory response. *Cytokine*, *61*(2), 585–590.

Pirher, N., Ivičak, K., Pohar, J., Benčina, M., & Jerala, R. (2008). A second binding site for double-stranded RNA in TLR3 and consequences for interferon activation. *Nature Structural and Molecular Biology*, *15*(7), 761–763.

Pope, R. M., & Huang, Q. Q. (2009). The role of Toll-like receptors in rheumatoid arthritis. In *Current Rheumatology Reports*.11(5), 357–364.

Pulko, V., Liu, X., Krco, C. J., Harris, K. J., Frigola, X., Kwon, E. D., & Dong, H. (2009). TLR3-Stimulated Dendritic Cells Up-regulate B7-H1 Expression and Influence the Magnitude of CD8 T Cell Responses to Tumor Vaccination. *The Journal of Immunology*, *183*(6), 3634–3641.

Rabinovitch, M. (2008). Molecular pathogenesis of pulmonary arterial hypertension. In *Journal of Clinical Investigation* (Vol. 118, Issue 7, pp. 2372–2379). https://doi.org/10.1172/JCI33452

Rafikova, O., Al Ghouleh, I., & Rafikov, R. (2019). Focus on Early Events: Pathogenesis of Pulmonary Arterial Hypertension Development. In *Antioxidants and Redox Signaling,*31(13), 933–953.

Rako, Z. A., Kremer, N., Yogeswaran, A., Richter, M. J., & Tello, K. (2023). Adaptive versus maladaptive right ventricular remodelling. *ESC Heart Failure*, *10*(2), 762.

Ramnath, D., Tunny, K., Hohenhaus, D. M., Pitts, C. M., Bergot, A. S., Hogarth, P. M., Hamilton, J. A., Kapetanovic, R., Sturm, R. A., Scholz, G. M., & Sweet, M. J. (2015). TLR3 drives IRF6-dependent IL-23p19 expression and p19/EBI3 heterodimer formation in keratinocytes. *Immunology and Cell Biology*, *93*(9), 771–779.

Ryan, J. J., & Archer, S. L. (2014). The Right Ventricle in Pulmonary Arterial Hypertension. *Circulation Research*, *115*(1), 176–188.

Sahay, S. (2019). Evaluation and classification of pulmonary arterial hypertension. *Journal of Thoracic Disease*. 11, 1789–1799.

Saito, M., Ohshima, N., Matsui, H., Hebisawa, A., & Ohta, K. (2017). Sudden death in a patient with pulmonary veno-occlusive disease (PVOD) and severe pulmonary hypertension. *Internal Medicine*, *56*(15), 2025–2031.

Sakao, S., Tatsumi, K., & Voelkel, N. F. (2009). Endothelial cells and pulmonary arterial hypertension: Apoptosis, proliferation, interaction and transdifferentiation. In *Respiratory Research*. 10(1).

Santamore, W. P., Lynch, P. R., Heckman, J. L., Bove, A. A., & Meier, G. D. (1976). Left ventricular effects on right ventricular developed pressure. *Journal of Applied Physiology*, *41*(6), 925–930.

Santos-Ribeiro, D., Lecocq, M., de Beukelaer, M., Verleden, S., Bouzin, C., Ambroise, J., Dorfmuller, P., Yakoub, Y., Huaux, F., Quarck, R., Karmouty-Quintana, H., Ghigna, M. R., Bignard, J., Nadaud, S., Soubrier, F., Horman, S., Perros, F., Godinas, L., & Pilette, C. (2023). Disruption of GCN2 Pathway Aggravates Vascular and Parenchymal Remodeling during Pulmonary Fibrosis. *American Journal of Respiratory Cell and Molecular Biology*, *68*(3), 326–338.

Sato, S., Sugiyama, M., Yamamoto, M., Watanabe, Y., Kawai, T., Takeda, K., & Akira, S. (2003). Toll/IL-1 Receptor Domain-Containing Adaptor Inducing IFN-β (TRIF) Associates with TNF Receptor-Associated Factor 6 and TANK-Binding Kinase 1, and Activates Two Distinct Transcription Factors, NF-κB and IFN-Regulatory Factor-3, in the Toll-Like Receptor S. *The Journal of Immunology*, *171*(8), 4304–4310.

Savale, L., Sattler, C., Günther, S., Montani, D., Chaumais, M. C., Perrin, S., Jaïs, X., Seferian, A., Jovan, R., Bulifon, S., Parent, F., Simonneau, G., Humbert, M., & Sitbon, O. (2014). Pulmonary arterial hypertension in patients treated with interferon. *European Respiratory Journal*, *44*(6), 1627–1634.

Sawada, H., Saito, T., Nickel, N. P., Alastalo, T. P., Glotzbach, J. P., Chan, R., Haghighat, L., Fuchs, G., Januszyk, M., Cao, A., Lai, Y. J., de Jesus Perez, V., Kim, Y. M., Wang, L., Chen, P. I., Spiekerkoetter, E., Mitani, Y., Gurtner, G. C., Sarnow, P., & Rabinovitch, M. (2014). Reduced BMPR2 expression induces GM-CSF translation and macrophage recruitment in humans and mice to exacerbate pulmonary hypertension. *Journal of Experimental Medicine*, *211*(2), 263–280.

Schaefer, L. (2014). Complexity of danger: The diverse nature of damage-associated molecular patterns. In *Journal of Biological Chemistry*. 289(51),35237–35245.

Scheuner, D., Song, B., McEwen, E., Liu, C., Laybutt, R., Gillespie, P., Saunders, T., Bonner-Weir, S., & Kaufman, R. J. (2001). Translational control is required for the unfolded protein response and in vivo glucose homeostasis. *Molecular Cell*, *7*(6), 1165–1176.

Schirmer, S. H., Bot, P. T., Fledderus, J. O., Van Der Laan, A. M., Volger, O. L., Laufs, U., Böhm, M., De Vries, C. J. M., Horrevoets, A. J. G., Piek, J. J., Hoefer, I. E., & Van Royen, N. (2010). Blocking interferon β stimulates vascular smooth muscle cell proliferation and arteriogenesis. *Journal of Biological Chemistry*, *285*(45), 34677–34685.

Schlee, M., & Hartmann, G. (2016). Discriminating self from non-self in nucleic acid sensing. *Nature Reviews Immunology 2016 16:9*, *16*(9), 566–580.

Seya, T., Funami, K., Taniguchi, M., & Matsumoto, M. (2005). Antibodies against human Toll-like receptors (TLRs): TLR distribution and localization in human dendritic cells. *Journal of Endotoxin Research*, *11*(6), 369–374.

Simonneau, G., Gatzoulis, M. A., Adatia, I., Celermajer, D., Denton, C., Ghofrani, A., Gomez Sanchez, M. A., Krishna Kumar, R., Landzberg, M., Machado, R. F., Olschewski, H., Robbins, I. M., & Souza, R. (2013). Updated Clinical Classification of Pulmonary Hypertension. *Journal of the American College of Cardiology*, *62*(25), D34–D41.

Simonneau, G., Montani, D., Celermajer, D. S., Denton, C. P., Gatzoulis, M. A., Krowka, M., Williams, P. G., & Souza, R. (2019). Haemodynamic definitions and updated clinical classification of pulmonary hypertension. *The European Respiratory Journal*, *53*(1).

Sitbon, O., Humbert, M., Jaïs, X., Ioos, V., Hamid, A. M., Provencher, S., Garcia, G., Parent, F., Hervé, P., & Simonneau, G. (2005). Long-term response to calcium channel blockers in idiopathic pulmonary arterial hypertension. *Circulation*, *111*(23), 3105–3111.

Sitbon, O., & Morrell, N. W. (2012). Pathways in pulmonary arterial hypertension: the future is here. *European Respiratory Review : An Official Journal of the European Respiratory Society*, *21*(126), 321–327.

Soon, E., Holmes, A. M., Treacy, C. M., Doughty, N. J., Southgate, L., MacHado, R. D., Trembath, R. C., Jennings, S., Barker, L., Nicklin, P., Walker, C., Budd, D. C., Pepke-Zaba, J., & Morrell, N. W. (2010). Elevated levels of inflammatory cytokines predict survival in idiopathic and familial pulmonary arterial hypertension. *Circulation*, *122*(9), 920–927.

Southam, D. S., Dolovich, M., O'Byrne, P. M., & Inman, M. D. (2002). Distribution of intranasal instillations in mice: effects of volume, time, body position, and anesthesia. *American Journal of Physiology. Lung Cellular and Molecular Physiology*, *282*(4).

Starkhammar, M., Georén, S., Swedin, L., Dahlén, S. E., Adner, M., & Cardell, L. O. (2012). Intranasal Administration of poly(I:C) and LPS in BALB/c Mice Induces Airway Hyperresponsiveness and Inflammation via Different Pathways. *PLoS ONE*, *7*(2).

Steiner, M. K., Syrkina, O. L., Kolliputi, N., Mark, E. J., Hales, C. A., & Waxman, A. B. (2009). IL-6 Overexpression Induces Pulmonary Hypertension. *Circulation Research*, *104*(2), 236.

Stowell, N. C., Seideman, J., Raymond, H. A., Smalley, K. A., Lamb, R. J., Egenolf, D. D., Bugelski, P. J., Murray, L. A., Marsters, P. A., Bunting, R. A., Flavell, R. A., Alexopoulou, L., San Mateo, L. R., Griswold, D. E., Sarisky, R. T., Mbow, M. L., & Das, A. M. (2009). Long-term activation of TLR3 by Poly(I:C) induces inflammation and impairs lung function in mice. *Respiratory Research*, *10*(1), 1–14.

Sun, B., Sundström, K. B., Chew, J. J., Bist, P., Gan, E. S., Tan, H. C., Goh, K. C., Chawla, T., Tang, C. K., & Ooi, E. E. (2017). Dengue virus activates cGAS through the release of mitochondrial DNA. *Scientific Reports*, *7*(1).

Sun, R., Zhang, Y., Lv, Q., Liu, B., Jin, M., Zhang, W., He, Q., Deng, M., Liu, X., Li, G., Li, Y., Zhou, G., Xie, P., Xie, X., Hu, J., & Duan, Z. (2011). Toll-like receptor 3 (TLR3) induces apoptosis via death receptors and mitochondria by up-regulating the transactivating p63 isoform α (TAP63α). *Journal of Biological Chemistry*, *286*(18), 15918–15928.

Suzuki, S., Asano, R., Aoki, T., Nakayama, S., Ueda, J., Tsuji, A., Noguchi, T., & Ogo, T. (2022). Prognostic impact of follow-up pulmonary vascular resistance in pulmonary arterial hypertension. *Open Heart*, *9*(1).

Tabeta, K., Hoebe, K., Janssen, E. M., Du, X., Georgel, P., Crozat, K., Mudd, S., Mann, N., Sovath, S., Goode, J., Shamel, L., Herskovits, A. A., Portnoy, D. A., Cooke, M., Tarantino, L. M., Wiltshire, T., Steinberg, B. E., Grinstein, S., & Beutler, B. (2006). The Unc93b1 mutation 3d disrupts exogenous antigen presentation and signaling via Toll-like receptors 3, 7 and 9. *Nature Immunology*, *7*(2), 156–164.

Tamosiuniene, R., Tian, W., Dhillon, G., Wang, L., Sung, Y. K., Gera, L., Patterson, A. J., Agrawal, R., Rabinovitch, M., Ambler, K., Long, C. S., Voelkel, N. F., & Nicolls, M. R. (2011). Regulatory T cells limit vascular endothelial injury and prevent pulmonary hypertension. *Circulation Research*, *109*(8), 867.

Tamura, Y., Phan, C., Tu, L., Le Hiress, M., Thuillet, R., Jutant, E. M., Fadel, E., Savale, L., Huertas, A., Humbert, M., & Guignabert, C. (2018). Ectopic upregulation of membrane-bound IL6R drives vascular remodeling in pulmonary arterial hypertension. *The Journal of Clinical Investigation*, *128*(5), 1956–1970.

Taraseviene-Stewart, L., Kasahara, Y., Alger, L., Hirth, P., Mahon, G. M., Waltenberger, J., Voelkel, N. F., & Tuder, R. M. (2001). Inhibition of the VEGF receptor 2 combined with chronic hypoxia causes cell death-dependent pulmonary endothelial cell proliferation and severe pulmonary hypertension. *FASEB Journal : Official Publication of the Federation of American Societies for Experimental Biology*, *15*(2), 427–438.

Tenorio, J., Navas, P., Barrios, E., Fernández, L., Nevado, J., Quezada, C. A., López-Meseguer, M., Arias, P., Mena, R., Lobo, J. L., Alvarez, C., Heath, K., Escribano-Subías, P., & Lapunzina, P. (2015). A founder EIF2AK4 mutation causes an aggressive form of pulmonary arterial hypertension in Iberian Gypsies. *Clinical Genetics*, *88*(6), 579–583.

Tewari, K., Flynn, B. J., Boscardin, S. B., Kastenmueller, K., Salazar, A. M., Anderson, C. A., Soundarapandian, V., Ahumada, A., Keler, T., Hoffman, S. L., Nussenzweig, M. C., Steinman, R. M., & Seder, R. A. (2010). Poly(I:C) is an effective adjuvant for antibody and multi-functional CD4+ T cell responses to Plasmodium falciparum circumsporozoite protein (CSP) and αDEC-CSP in non human primates. *Vaccine*, *28*(45), 7256–7266.

Thenappan, T., Ormiston, M. L., Ryan, J. J., & Archer, S. L. (2018). Pulmonary arterial hypertension: Pathogenesis and clinical management. In *BMJ (Online)* (Vol. 360).

Thompson, A. A. R., & Lawrie, A. (2017). Targeting Vascular Remodeling to Treat Pulmonary Arterial Hypertension. In *Trends in Molecular Medicine*.23(1), 31–45.

Tian, B., Liu, Z., Litvinov, J., Maroto, R., Jamaluddin, M., Rytting, E., Patrikeev, I., Ochoa, L., Vargas, G., Motamedi, M., Ameredes, B. T., Zhou, J., & Brasier, A. R. (2019). Efficacy of novel highly specific bromodomain-containing protein 4 inhibitors in innate inflammation–driven airway remodeling. *American Journal of Respiratory Cell and Molecular Biology*, *60*(1), 68–83.

Tian, B., Patrikeev, I., Ochoa, L., Vargas, G., Belanger, K. A. K., Litvinov, J., Boldogh, I., Ameredes, B. T., Motamedi, M., & Brasier, A. R. (2017). NF-κB mediates mesenchymal transition, remodeling, and pulmonary fibrosis in response to chronic inflammation by viral RNA patterns. *American Journal of Respiratory Cell and Molecular Biology*, *56*(4), 506–520.

Tobal, R., Potjewijd, J., Empel, V. P. M. van, Ysermans, R., Schurgers, L. J., Reutelingsperger, C. P., Damoiseaux, J. G. M. C., & Paassen, P. van. (2021). Vascular Remodeling in Pulmonary Arterial Hypertension: The Potential Involvement of Innate and Adaptive Immunity. *Frontiers in Medicine*, *8*, 806899.

Toshner, M., Dunmore, B., McKinney, E., Southwood, M., Ormiston, M., Nash, G., Rana, A., Upton, P., & Morrell, N. (2013). Analyses of blood outgrowth endothelial cells reveal an endothelial HOX gene signature in human beings. *The Lancet*, *381*, S108.

Tsuchiya, H., Kioka, H., Ozu, K., Ohtani, T., Yamaguchi, O., Yazaki, Y., Yamauchi-Takihara, K., & Sakata, Y. (2017). Interferon therapy exacerbated pulmonary hypertension in a patient with hepatitis C virus infection: Pathogenic interplay among multiple risk factors. *Internal Medicine*, *56*(9), 1061–1065.

Tsuno, T., Mejido, J., Zhao, T., Schmeisser, H., Morrow, A., & Zoon, K. C. (2009). IRF9 is a key factor for eliciting the antiproliferative activity of IFN-α. *Journal of Immunotherapy*, *32*(8), 803–816.

Tuder, R. M., Marecki, J. C., Richter, A., Fijalkowska, I., & Flores, S. (2007). Pathology of Pulmonary Hypertension. In *Clinics in Chest Medicine*. 28,(1), 23–42.

Turton, H. A., Thompson, A. A. R., & Farkas, L. (2020). RNA Signaling in Pulmonary Arterial Hypertension—A Double-Stranded Sword. *International Journal of Molecular Sciences*, *21*(9), 3124.

Vanderpool, R. R., & Naeije, R. (2018). Hematocrit-corrected Pulmonary Vascular Resistance. *American Journal of Respiratory and Critical Care Medicine*, *198*(3), 305–309.

Vassiliou, A. G., Kotanidou, A., Dimopoulou, I., & Orfanos, S. E. (2020). Endothelial Damage in Acute

Respiratory Distress Syndrome. *International Journal of Molecular Sciences 2020.21*(22), 8793.
Vintiñi, E., Haro, C., Palazon, E., & Medina, M. (2022). Nasal administration of a non-viable Lactobacillus casei to infant mice modulates lung damage induced by Poly I:C and hyperreactivity in airways. *Microbes and Infection*, *24*(6–7), 104997.
Vitali, S. H., Hansmann, G., Rose, C., Fernandez-Gonzalez, A., Scheid, A., Mitsialis, S. A., & Kourembanas, S. (2014). The Sugen 5416/hypoxia mouse model of pulmonary hypertension revisited: Long-term follow-up. *Pulmonary Circulation*, *4*(4), 619–629.
Voelkel, N. F., Gomez-Arroyo, J., Abbate, A., Bogaard, H. J., & Nicolls, M. R. (2012). Pathobiology of pulmonary arterial hypertension and right ventricular failure. *The European Respiratory Journal*, *40*(6), 1555.
Voelkel, N. F., Quaife, R. A., Leinwand, L. A., Barst, R. J., McGoon, M. D., Meldrum, D. R., Dupuis, J., Long, C. S., Rubin, L. J., Smart, F. W., Suzuki, Y. J., Gladwin, M., Denholm, E. M., & Gail, D. B. (2006). Right Ventricular Function and Failure. *Circulation*, *114*(17), 1883–1891.
Wang, X., Ha, T., Liu, L., Hu, Y., Kao, R., Kalbfleisch, J., Williams, D., & Li, C. (2018). TLR3 Mediates Repair and Regeneration of Damaged Neonatal Heart through Glycolysis Dependent YAP1 Regulated miR-152 Expression. *Cell Death and Differentiation*, *25*(5), 966–982.
Watanabe, T., Ninomiya, H., Saitou, T., Takanezawa, S., Yamamoto, S., Imai, Y., Yoshida, O., Kawakami, R., Hirooka, M., Abe, M., Imamura, T., & Hiasa, Y. (2020). Therapeutic effects of the PKR inhibitor C16 suppressing tumor proliferation and angiogenesis in hepatocellular carcinoma in vitro and in vivo. *Scientific Reports 2020 10:1*, *10*(1), 1–9.
Wei, H., Lin, C. K., Lu, S. J., Wen, Y. X., Yuan, S., & Liu, Y. L. (2020). CD11b is involved in coxsackievirus B3-induced viral myocarditis in mice by inducing Th17 cells. *Open Life Sciences*, *15*(1), 1024–1032.
Woods, M., Bishop-Bailey, D., Pepper, J. R., Evans, T. W., Mitchell, J. A., & Warner, T. D. (1998). Cytokine and lipopolysaccharide stimulation of endothelin-1 release from human internal mammary artery and saphenous vein smooth-muscle cells. *Journal of Cardiovascular Pharmacology*, *31*(1).
Woods, M., Mitchell, J. A., Wood, E. G., Barker, S., Walcot, N. R., Rees, G. M., & Warner, T. D. (1999). Endothelin-1 is induced by cytokines in human vascular smooth muscle cells: evidence for intracellular endothelin-converting enzyme. *Molecular Pharmacology*, *55*(5), 902–909.
Wort, S. J., Woods, M., Warner, T. D., Evans, T. W., & Mitchell, J. A. (2001). Endogenously released endothelin-1 from human pulmonary artery smooth muscle promotes cellular proliferation: Relevance to pathogenesis of pulmonary hypertension and vascular remodeling. *American Journal of Respiratory Cell and Molecular Biology*, *25*(1), 104–110.
Yamaguchi, S., Harasawa, H., Li, K. S., Zhu, D., & Santamore, W. P. (1991). Comparative significance in systolic ventricular interaction. *Cardiovascular Research*, *25*(9), 774–783.
Yamashita, M., Chattopadhyay, S., Fensterl, V., Zhang, Y., & Sen, G. C. (2012). A TRIF-Independent Branch of TLR3 Signaling. *The Journal of Immunology*, *188*(6), 2825–2833.
Yanagisawa, M., Kurihara, H., Kimura, S., Tomobe, Y., Kobayashi, M., Mitsui, Y., Yazaki, Y., Goto, K., & Masaki, T. (1988). A novel potent vasoconstrictor peptide produced by vascular endothelial cells. *Nature*, *332*(6163), 411–415.
Yanai, H., Chiba, S., Hangai, S., Kometani, K., Inoue, A., Kimura, Y., Abe, T., Kiyonari, H., Nishio, J., Taguchi-Atarashi, N., Mizushima, Y., Negishi, H., Grosschedl, R., & Taniguchi, T. (2018). Revisiting the role of IRF3 in inflammation and immunity by conditional and specifically targeted gene ablation in mice. *Proceedings of the National Academy of Sciences of the United States of America*, *115*(20), 5253–5258.
Yang, P., An, H., Liu, X., Wen, M., Zheng, Y., Rui, Y., & Cao, X. (2010). The cytosolic nucleic acid sensor LRRFIP1 mediates the production of type i interferon via a B-catenin-dependent pathway. *Nature Immunology*, *11*(6), 487–494.
Yang, X., Murthy, V., Schultz, K., Tatro, J. B., Fitzgerald, K. A., & Beasley, D. (2006). Toll-like receptor 3 signaling evokes a proinflammatory and proliferative phenotype in human vascular smooth muscle cells. *American Journal of Physiology-Heart and Circulatory Physiology*, *291*(5), H2334–H2343.
Yang, X., Rutkovsky, A. C., Zhou, J., Zhong, Y., Reese, J., Schnell, T., Albrecht, H., Owens, W. B., Nagarkatti, P. S., & Nagarkatti, M. (2022). Characterization of Altered Gene Expression and Histone Methylation in Peripheral Blood Mononuclear Cells Regulating Inflammation in COVID-19 Patients. *Journal of Immunology*, *208*(8), 1968–1977.
Yang, Z., Stratton, C., Francis, P. J., Kleinman, M. E., Tan, P. L., Gibbs, D., Tong, Z., Chen, H., Constantine, R., Yang, X., Chen, Y., Zeng, J., Davey, L., Ma, X., Hau, V. S., Wang, C., Harmon, J., Buehler, J., Pearson, E., … Zhang, K. (2008). Toll-like receptor 3 and geographic atrophy in age-related macular degeneration. *New England Journal of Medicine*, *359*(14), 1456–1463.

Ying, Z., Li, J., & Li, M. (2011). Astrocyte elevated gene 1: Biological functions and molecular mechanism in cancer and beyond. *Cell and Bioscience*, *1*(1), 1–6.

Zamanian-Daryoush, M., Der, S. D., & Williams, B. R. G. (1999). Cell cycle regulation of the double stranded RNA activated protein kinase, PKR. *Oncogene*, *18*(2), 315–326.

Zamanian-Daryoush, M., Mogensen, T. H., DiDonato, J. A., & Williams, B. R. G. (2000). NF-kappa B Activation by Double-Stranded-RNA-Activated Protein Kinase (PKR) Is Mediated through NF-kappa B-Inducing Kinase and Ikappa B Kinase. *Molecular and Cellular Biology*, *20*(4), 1278–1290.

Zamprogno, P., Wüthrich, S., Achenbach, S., Thoma, G., Stucki, J. D., Hobi, N., Schneider-Daum, N., Lehr, C. M., Huwer, H., Geiser, T., Schmid, R. A., & Guenat, O. T. (2021). Second-generation lung-on-a-chip with an array of stretchable alveoli made with a biological membrane. *Communications Biology 2021 4:1*, *4*(1), 1–10.

Zawia, A., West, L., Turton, H., Iremonger, J., & Cañedo, J. (2020). Altered Macrophage Polarization Induces Experimental Pulmonary Hypertension and Is Observed in Patients With Pulmonary Arterial Hypertension . In *Arteriosclerosis, Thrombosis, and Vascular Biology. 41(*1), 430-445.

Zhang, B., Davis, J. P., & Ziolo, M. T. (2015). Cardiac catheterization in mice to measure the pressure volume relationship: Investigating the Bowditch effect. *Journal of Visualized Experiments*, *2015*(100).

Zhang, C., Lu, W., Luo, X., Liu, S., Li, Y., Zheng, Q., Liu, W., Wu, X., Chen, Y., Jiang, Q., Zhang, Z., Gu, G., Chen, J., Chen, H., Liao, J., Liu, C., Hong, C., Tang, H., Sun, D., … Wang, J. (2021). Mitomycin C induces pulmonary vascular endothelial-to-mesenchymal transition and pulmonary veno-occlusive disease via Smad3-dependent pathway in rats. *British Journal of Pharmacology*, *178*(1), 217–235.

Zhang, L. L., Lu, J., Li, M. T., Wang, Q., & Zeng, X. F. (2016). Preventive and remedial application of etanercept attenuate monocrotaline-induced pulmonary arterial hypertension. *International Journal of Rheumatic Diseases*, *19*(2), 192–198.

Zhang, X., Ha, T., Lu, C., Lam, F., Liu, L., Schweitzer, J., Kalbfleisch, J., Kao, R. L., Williams, D. L., & Li, C. (2015). Poly (I:C) therapy decreases cerebral ischaemia/reperfusion injury *via* TLR3-mediated prevention of Fas/FADD interaction. *Journal of Cellular and Molecular Medicine*, *19*(3), 555–565.

Zhao, J., Wohlford-Lenane, C., Zhao, J., Fleming, E., Lane, T. E., Paul B. McCray, J., & Perlman, S. (2012). Intranasal Treatment with Poly(I·C) Protects Aged Mice from Lethal Respiratory Virus Infections. *Journal of Virology*, *86*(21), 11416.

Zheng, X., & Bevilacqua, P. C. (2004). Activation of the protein kinase PKR by short double-stranded RNAs with single-stranded tails. *RNA*, *10*(12), 1934–1945.

Zhong, Y., & Yu, P. B. (2022). Decoding the Link Between Inflammation and Pulmonary Arterial Hypertension. *Circulation*, *146*(13), 1023–1025.

Zhou, Y., Guo, M., Wang, X., Li, J., Wang, Y., Ye, L., Dai, M., Zhou, L., Persidsky, Y., & Ho, W. (2013). TLR3 activation efficiency by high or low molecular mass poly I:C. *Innate Immunity*, *19*(2), 184–192.

Zimmer, S., Steinmetz, M., Asdonk, T., Motz, I., Coch, C., Hartmann, E., Barchet, W., Wassmann, S., Hartmann, G., & Nickenig, G. (2011). Activation of endothelial toll-like receptor 3 impairs endothelial function. *Circulation Research*, *108*(11), 1358–1366.

9. Appendices

9.1 Appendix I – Clinical characteristics of cell donors

Table 1. Clinical characteristic of donors of human PAECs

Lot number	18TL155113 Ψ	19TL217385*Ψ	0000708987*Ψ	21TL228096*
Sex	Male	Male	Male	Female
Age (years)	42	26	64	56
Race	Caucasian	Caucasian	Caucasian	Caucasian

* Lot numbers were used in RNA-seq experiments.
Ψ Lot numbers were used for other *in vitro* experiments.

9.2 Appendix II – Baseline weights of animals in prophylactic intraperitoneal poly(I:C) experiments

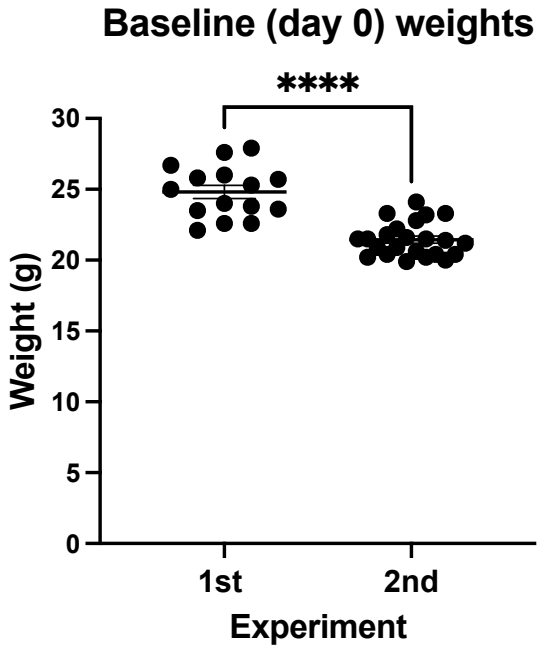

Figure 1. Comparison of baseline weights of C57BL/6J mice previous to prophylactic poly(I:C) and SuHx or Nx induction.

Comparison of baseline (day 0) between both experiments in chapter 3, irrespective of experimental group. Data show mean (top of bar) ± SEM. Unpaired t-test. 1st experiment (bi-weekly poly(I:C)); *n*=15. 2nd experiment (thrice-weekly poly(I:C)); *n*=23.

9.3 Appendix III – Poly(I:C) concentration optimisation in hPAECs

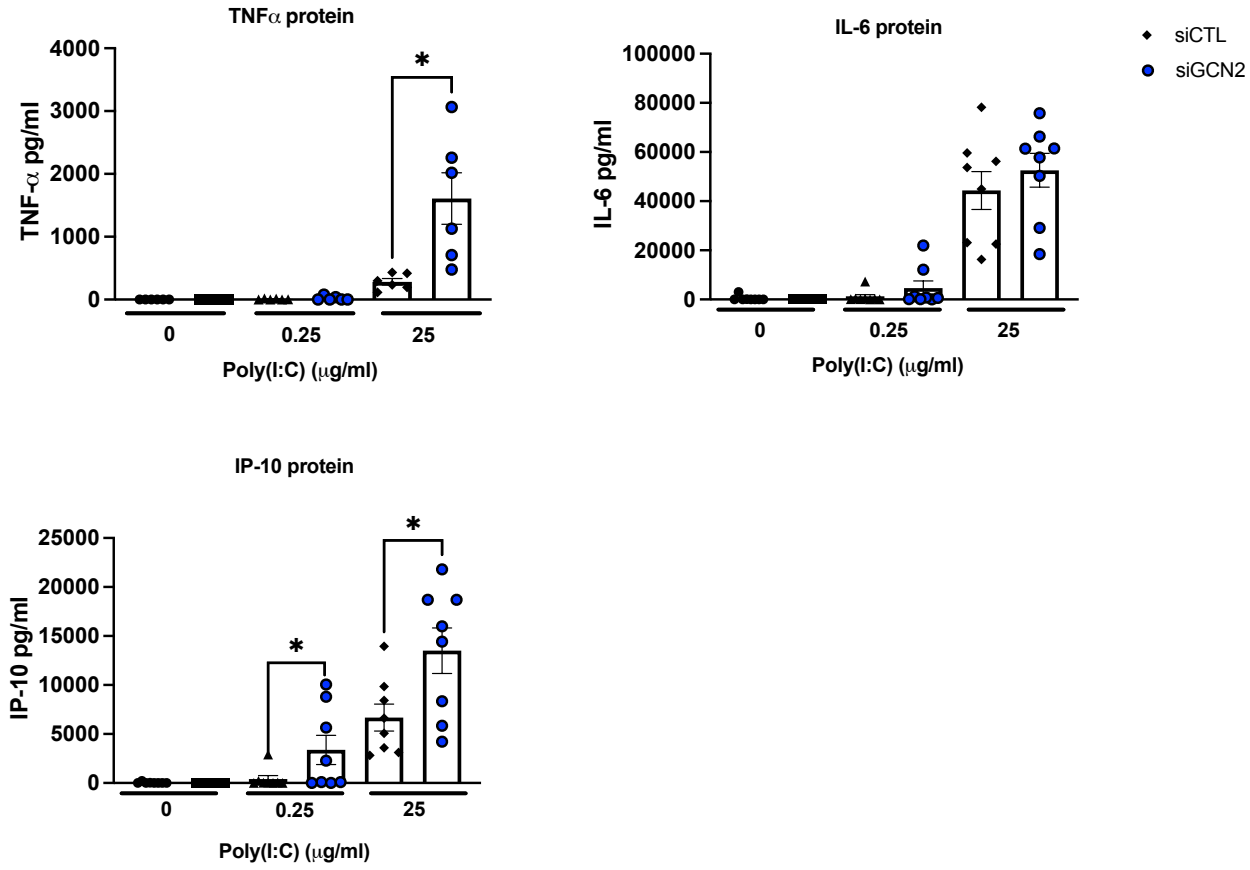

Figure 2. The protein levels of proinflammatory cytokines in supernatant of GCN2-deficient BOECs with and without 24 hours of poly(I:C) stimulation.

Luminex technology assessed pro-inflammatory cytokine release of TNF- α (A), IL-6 (B) and IP-10 (C), in the cell supernatants of si*GCN2*-treated BOECs with and without poly(I:C) (0.25μg/ml or 25μg/ml) stimulation for 24 hours. Data show mean (top of bar) ± SEM. Two-way ANOVA, Šídák's multiple comparisons test*, $p < 0.05$. n=7-9 experimental repeats from 3 donors.

9.4 Appendix IV – RNA sequencing

9.4.1 Table describing quality of RNA sequencing

Table 2. General statistic tables generated by MultiQC

Sample Name	% Aligned	M Aligned	% Dups	% GC	M Seqs	% BP Trimmed	% Dups	% GC	M Seqs
No transfection, unstim (n1)	88.8	41.8	80.2	50	47.1	0.60	80.2	50	47.1
siCTL, unstim (n1)	87.7	43.7	75.1	52	49.9	0.50	75.1	52	49.9
siCTL, poly(I:C) (n1)	89.4	43.8	75.1	51	49	0.50	75.1	51	49
siGCN2, unstim (n1)	87.7	43.2	73.7	51	49.2	0.50	73.7	51	49.2
siGCN2, poly(I:C) (n1)	88.5	37.1	68.4	50	41.9	0.60	68.4	50	41.9
No transfection, unstim (n2)	88.2	39.1	67.8	49	44.3	0.50	67.8	49	44.3
siCTL, unstim (n2)	88.7	37.7	69.4	49	42.6	0.60	69.4	49	42.6
siCTL, poly(I:C) (n2)	87.9	40.5	65.9	50	46.1	0.60	65.9	50	46.1
siGCN2, unstim (n2)	89.0	44.5	71.3	51	50	0.50	71.2	51	50
siGCN2, poly(I:C) (n2)	88.90	48.4	73.1	50	54.5	0.50	73.1	50	54.5
No transfection, unstim (n3)	85.50	35.6	66.0	48	41.6	0.50	66.0	48	41.6
siCTL, unstim (n3)	87.10	39.2	63.9	50	45	0.60	63.9	50	45
siCTL, poly(I:C) (n3)	86.80	41.8	66.1	50	48.2	0.50	66.1	50	48.2
siGCN2, unstim (n3)	86.50	44.5	68.0	49	51.4	0.50	68.0	49	51.4
siGCN2, poly(I:C) (n3)	87.90	38	70.9	49	43.2	0.60	70.9	49	43.2

Orange; salmon analysis. Light blue: FastQC analysis (before trimming). Yellow; FastQC analysis (after trimming).

9.4.2 DEG in untransfected unstimulated versus siCTL-treated unstimulated hPAECs

Table 3. Differentially expressed genes in untransfected unstimulated vs siCTL unstimulated PAECs

Gene Symbol	*Gene Name*	*Log2 Fold Change*	*SE of Log2*	*Adj. p-value*
BIVM-ERCC5	BIVM-ERCC5 Readthrough	3.560	0.517	1.13E-07

Log2 fold change between untransfected hPAECs versus siCTL-treated hPAECs as calculated using DESeq2 bioinformatic package. SE; standard error of Log2 fold change. The *p*-value (not shown in this table) calculated using Wald test was adjusted for multiple hypothesis testing using the Benjamini-Hochberg procedure (adjusted (adj.) *p*-value). Log2 fold change and SE of Log2 presented as 3 decimal places.

9.4.3 Volcano plot of DEGs in untransfected unstimulated versus siCTL-treated unstimulated hPAECs

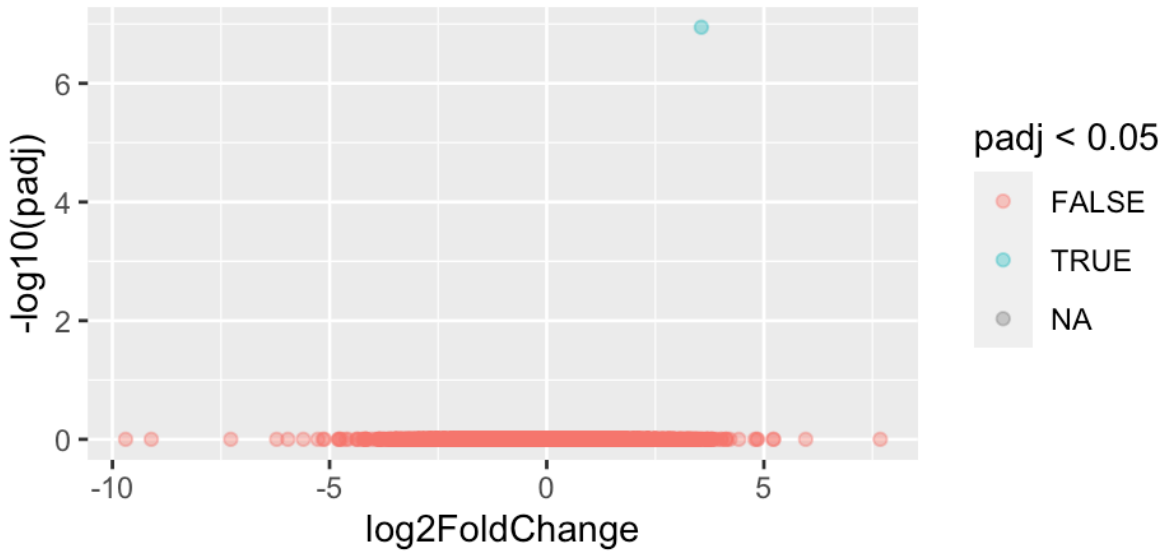

Figure 3 Volcano plot showing differentially expressed gene (DEG) after lipofectamine-based transfection of hPAECs.

Human (h)PAECs subjected to lipofectamine-based transfected of siRNA-targeting non homologous control genes had one DEG when compared to untransfected hPAECs at a 5% level of significance (i.e., adj p<0.05). DEG was quantified by DESeq2 bioinformatic package. Log2 fold change, untransfected hPAECs versus siCTL-treated hPAECs. Adjusted p value is represented as $-\log^{10}$(adj p value) on y axis i.e., $-\log^{10}$(adj p value) >1.3 are significantly different at a 5% significance level.

9.4.4 All DEGs ranked on adjusted p-values in poly(I:C)-stimulated versus unstimulated in siCTL-treated hPAECs

Table 4. All DEGs D (i.e., an adjusted p-value of < 0.05) in poly(I:C)-stimulated versus unstimulated in siCTL-treated hPAECs

Gene Symbol	*Gene Name*	*Log2 (Fold Change)*	*SE of Log2*	*Adj. p-value*
IFIT5	interferon induced protein with tetratricopeptide repeats 5	-4.221	0.196	2.08E-98
RND1	Rho family GTPase 1	-4.714	0.236	4.51E-85
ATF3	activating transcription factor 3	-4.703	0.242	2.05E-80
USP18	ubiquitin specific peptidase 18	-3.172	0.174	2.21E-70
IRF1	interferon regulatory factor 1	-4.330	0.250	1.05E-63
FAM46A	terminal nucleotidyltransferase 5A	-2.822	0.164	2.54E-63
IL6	interleukin 6	-3.771	0.232	3.13E-56
CCRN4L	nocturnin	-3.092	0.201	6.29E-50
CEBPD	CCAAT enhancer binding protein delta	-3.802	0.252	2.84E-48
ZFP36	ZFP36 ring finger protein	-2.428	0.164	2.51E-46
GCH1	GTP cyclohydrolase 1	-3.932	0.289	6.76E-39
NCOA7	nuclear receptor coactivator 7	-2.970	0.219	1.18E-38
SAMD9	sterile alpha motif domain containing 9	-3.918	0.297	1.31E-36
PPM1K	protein phosphatase, Mg2+/Mn2+ dependent 1K	-3.106	0.238	6.93E-36
DHX58	DExH-box helicase 58	-3.743	0.294	4.33E-34
MYD88	MYD88 innate immune signal transduction adaptor	-1.976	0.157	2.19E-33
PMAIP1	phorbol-12-myristate-13-acetate-induced protein 1	-3.423	0.273	3.19E-33
LOC101929758		-4.274	0.345	2.63E-32
DDX60	DExD/H-box helicase 60	-3.488	0.283	5.12E-32
TRIM21	tripartite motif containing 21	-2.467	0.203	5.76E-31
ARID5A	AT-rich interaction domain 5A	-2.600	0.217	3.34E-30
MSX1	msh homeobox 1	-2.158	0.181	7.15E-30
IL7R	interleukin 7 receptor	-4.536	0.381	7.15E-30
PPAP2B	phospholipid phosphatase 3	-1.824	0.154	1.54E-29
SLC7A2	solute carrier family 7 member 2	-2.655	0.226	5.17E-29
IFI44	interferon induced protein 44	-3.676	0.315	1.22E-28
TXNIP	thioredoxin interacting protein	-2.037	0.176	2.96E-28
SOX18	SRY-box transcription factor 18	2.537	0.222	1.60E-27
RCAN1	regulator of calcineurin 1	-1.767	0.160	1.43E-25
JUNB	JunB proto-oncogene, AP-1 transcription factor subunit	-2.334	0.212	2.16E-25
SP110	SP110 nuclear body protein	-2.782	0.253	2.28E-25
CSRNP1	cysteine and serine rich nuclear protein 1	-1.989	0.183	8.07E-25
HLA-F	major histocompatibility complex, class I, F	-3.630	0.335	1.05E-24
TRAFD1	TRAF-type zinc finger domain containing 1	-2.225	0.208	5.21E-24
RIPK2	receptor interacting serine/threonine kinase 2	-3.078	0.289	8.42E-24
LIF	LIF interleukin 6 family cytokine	-2.747	0.262	4.96E-23
SLC25A28	solute carrier family 25 member 28	-2.718	0.260	6.05E-23
IFI35	interferon induced protein 35	-3.362	0.323	1.01E-22
SLFN5	schlafen family member 5	-2.516	0.243	1.90E-22
CCL5	C-C motif chemokine ligand 5	-8.661	0.839	2.13E-22
OASL	2'-5'-oligoadenylate synthetase like	-11.543	1.123	3.09E-22
IL18R1	interleukin 18 receptor 1	-2.394	0.234	4.03E-22
C2CD4B	C2 calcium dependent domain containing 4B	-2.589	0.254	7.20E-22
FGF5	fibroblast growth factor 5	-2.186	0.220	9.47E-21
PLSCR1	phospholipid scramblase 1	-2.555	0.259	2.09E-20
RHOB	ras homolog family member B	-1.556	0.159	3.37E-20
SOCS1	suppressor of cytokine signaling 1	-2.804	0.286	3.45E-20
IFIT3	interferon induced protein with tetratricopeptide repeats 3	-8.265	0.844	3.89E-20
CXCL11	C-X-C motif chemokine ligand 11	-9.567	0.978	3.98E-20

THBD	thrombomodulin	1.528	0.158	1.17E-19
ACTN2	actinin alpha 2	-2.833	0.293	1.21E-19
SPAG9	sperm associated antigen 9	-1.238	0.129	1.98E-19
TNIP3	TNFAIP3 interacting protein 3	-4.281	0.447	2.54E-19
RBM43	RNA binding motif protein 43	-1.668	0.177	9.46E-19
GBP2	guanylate binding protein 2	-2.534	0.270	1.75E-18
HDX	highly divergent homeobox	-2.190	0.235	3.25E-18
GNB4	G protein subunit beta 4	-1.321	0.144	1.26E-17
TRIM38	tripartite motif containing 38	-1.738	0.190	1.39E-17
SGK223	PEAK1 related, kinase-activating pseudokinase 1	1.550	0.170	1.50E-17
TIPARP	TCDD inducible poly(ADP-ribose) polymerase	-1.296	0.142	1.50E-17
DUSP5	dual specificity phosphatase 5	-1.459	0.160	1.75E-17
ZNFX1	zinc finger NFX1-type containing 1	-2.391	0.263	2.46E-17
CCL8	C-C motif chemokine ligand 8	-11.097	1.222	2.61E-17
TNFAIP8	TNF alpha induced protein 8	-2.490	0.276	4.64E-17
SDC4	syndecan 4	-2.648	0.296	7.89E-17
FBXO6	F-box protein 6	-2.362	0.264	9.15E-17
PNPT1	polyribonucleotide nucleotidyltransferase 1	-1.630	0.184	1.60E-16
BCL3	BCL3 transcription coactivator	-1.988	0.225	2.27E-16
STAT1	signal transducer and activator of transcription 1	-2.276	0.259	3.17E-16
CX3CL1	C-X3-C motif chemokine ligand 1	-7.545	0.863	4.92E-16
CD274	CD274 molecule	-2.023	0.232	5.99E-16
NFKBIA	NFKB inhibitor alpha	-2.239	0.260	1.55E-15
VCAM1	vascular cell adhesion molecule 1	-5.410	0.632	2.22E-15
MCTP1	multiple C2 and transmembrane domain containing 1	-1.452	0.171	3.64E-15
SAT1	spermidine/spermine N1-acetyltransferase 1	-1.754	0.207	4.77E-15
STAT2	signal transducer and activator of transcription 2	-2.605	0.310	8.65E-15
TRIM14	tripartite motif containing 14	-2.636	0.315	1.02E-14
IFIT2	interferon induced protein with tetratricopeptide repeats 2	-8.999	1.078	1.34E-14
IL4I1	interleukin 4 induced 1	-2.403	0.288	1.45E-14
ADAMTS4	ADAM metallopeptidase with thrombospondin type 1 motif 4	-2.522	0.304	2.17E-14
TMEM140	transmembrane protein 140	-1.405	0.170	2.38E-14
MSC	musculin	-4.988	0.604	2.59E-14
CSF1	colony stimulating factor 1	-2.353	0.285	2.60E-14
PLA1A	phospholipase A1 member A	-3.722	0.452	3.20E-14
RIN2	Ras and Rab interactor 2	-1.171	0.143	4.20E-14
TREX1	three prime repair exonuclease 1	-1.332	0.163	4.52E-14
CXCL10	C-X-C motif chemokine ligand 10	-14.290	1.765	9.75E-14
DCP1A	decapping mRNA 1A	-1.549	0.192	1.13E-13
RARRES3	phospholipase A and acyltransferase 4	-3.133	0.394	2.93E-13
TMEM106A	transmembrane protein 106A	-1.515	0.191	3.68E-13
CNP	2',3'-cyclic nucleotide 3' phosphodiesterase	-1.816	0.229	3.68E-13
BLZF1	basic leucine zipper nuclear factor 1	-1.616	0.204	4.19E-13
ELF1	E74 like ETS transcription factor 1	-1.288	0.163	4.23E-13
N4BP1	NEDD4 binding protein 1	-1.817	0.230	4.62E-13
LAP3	leucine aminopeptidase 3	-1.914	0.243	4.80E-13
CBR3	carbonyl reductase 3	-1.535	0.195	5.58E-13
ZBTB18	zinc finger and BTB domain containing 18	1.431	0.182	6.00E-13
GATA2	GATA binding protein 2	1.537	0.196	6.52E-13
LOC102723996		-2.569	0.328	7.64E-13
MB21D1	cyclic GMP-AMP synthase	-2.205	0.284	1.20E-12
OGFR	opioid growth factor receptor	-1.904	0.247	2.08E-12
TRIM26	tripartite motif containing 26	-1.753	0.228	2.17E-12
RELB	RELB proto-oncogene, NF-kB subunit	-2.257	0.295	2.85E-12
GTF2B	general transcription factor IIB	-1.335	0.175	3.06E-12
GBP3	guanylate binding protein 3	-2.748	0.360	3.06E-12
TNFAIP6	TNF alpha induced protein 6	-6.359	0.832	3.06E-12
PSMB9	proteasome 20S subunit beta 9	-2.690	0.354	4.15E-12
MAP3K8	mitogen-activated protein kinase 8	-2.662	0.351	4.39E-12
STBD1	starch binding domain 1	-1.445	0.191	5.05E-12
FAM212B	inka box actin regulator 2	1.556	0.206	5.08E-12
IL15RA	interleukin 15 receptor subunit alpha	-1.981	0.262	5.63E-12
GBP1	guanylate binding protein 1	-4.669	0.619	6.10E-12
F3	coagulation factor III, tissue factor	-2.586	0.343	6.29E-12

PDP1	pyruvate dehydrogenase phosphatase catalytic subunit 1	-1.799	0.241	1.15E-11
RNF19B	ring finger protein 19B	-1.858	0.249	1.22E-11
SAV1	salvador family WW domain containing protein 1	-1.254	0.168	1.23E-11
TMCC3	transmembrane and coiled-coil domain family 3	1.535	0.206	1.29E-11
BAK1	BCL2 antagonist/killer 1	-1.331	0.179	1.53E-11
VEGFC	vascular endothelial growth factor C	-2.131	0.288	1.54E-11
SIX1	SIX homeobox 1	-2.712	0.366	1.54E-11
PGF	placental growth factor	1.429	0.194	2.14E-11
BST2	bone marrow stromal cell antigen 2	-1.326	0.181	2.89E-11
PANX1	pannexin 1	-1.598	0.219	3.28E-11
LACTB	lactamase beta	-1.281	0.177	4.73E-11
FHL2	four and a half LIM domains 2	1.000	0.138	4.91E-11
MOB3C	MOB kinase activator 3C	-2.220	0.306	4.92E-11
HES4	hes family bHLH transcription factor 4	-1.901	0.263	5.23E-11
C19orf66	shiftless antiviral inhibitor of ribosomal frameshifting	-2.112	0.293	6.71E-11
RARA	retinoic acid receptor alpha	1.427	0.198	6.83E-11
DNAJA1	DnaJ heat shock protein family (Hsp40) member A1	-1.214	0.169	7.29E-11
TLR3	toll like receptor 3	-2.619	0.365	8.46E-11
CMPK2	cytidine/uridine monophosphate kinase 2	-7.715	1.078	9.42E-11
CXCR4	C-X-C motif chemokine receptor 4	2.116	0.297	1.08E-10
IER5L	immediate early response 5 like	1.474	0.207	1.09E-10
ZNF107	zinc finger protein 107	-1.777	0.249	1.09E-10
TYMP	thymidine phosphorylase	-2.122	0.298	1.19E-10
RSPO3	R-spondin 3	-3.351	0.472	1.30E-10
IRF9	interferon regulatory factor 9	-1.583	0.224	1.67E-10
TDRD7	tudor domain containing 7	-2.014	0.286	1.85E-10
H3F3B	H3.3 histone B	-0.904	0.129	2.17E-10
RSAD2	radical S-adenosyl methionine domain containing 2	-10.240	1.459	2.36E-10
HLA-E	major histocompatibility complex, class I, E	-1.108	0.158	2.56E-10
C22orf29	retrotransposon Gag like 10	1.634	0.233	2.64E-10
ISG15	ISG15 ubiquitin like modifier	-4.548	0.651	2.86E-10
CNKSR3	CNKSR family member 3	-2.002	0.287	3.18E-10
TNFSF10	TNF superfamily member 10	-4.770	0.685	3.28E-10
HLA-B	major histocompatibility complex, class I, B	-1.463	0.210	3.41E-10
SLC41A2	solute carrier family 41 member 2	-1.654	0.238	3.58E-10
TRIM69	tripartite motif containing 69	-2.502	0.361	4.23E-10
PML	PML nuclear body scaffold	-1.891	0.273	4.29E-10
ADM	adrenomedullin	1.473	0.213	4.46E-10
DUSP4	dual specificity phosphatase 4	1.977	0.286	4.48E-10
GBP5	guanylate binding protein 5	-7.564	1.096	4.93E-10
BATF2	basic leucine zipper ATF-like transcription factor 2	-6.591	0.957	5.43E-10
ADPRHL2	ADP-ribosylserine hydrolase	-1.292	0.189	6.99E-10
PSMB8	proteasome 20S subunit beta 8	-1.393	0.205	1.13E-09
CTHRC1	collagen triple helix repeat containing 1	-1.063	0.157	1.17E-09
CCDC88C	coiled-coil domain containing 88C	1.502	0.222	1.28E-09
GCNT4	glucosaminyl (N-acetyl) transferase 4	-4.283	0.635	1.38E-09
PI4K2B	phosphatidylinositol 4-kinase type 2 beta	-1.300	0.193	1.38E-09
CYTH1	cytohesin 1	-1.335	0.199	1.70E-09
C20orf112	nucleolar protein 4 like	1.301	0.194	1.92E-09
UBE2L6	ubiquitin conjugating enzyme E2 L6	-1.721	0.257	1.95E-09
DUSP7	dual specificity phosphatase 7	1.607	0.240	2.06E-09
B4GALT5	beta-1,4-galactosyltransferase 5	-1.276	0.191	2.21E-09
PSMB10	proteasome 20S subunit beta 10	-1.280	0.192	2.28E-09
TRIM5	tripartite motif containing 5	-1.254	0.189	2.60E-09
EIF2AK2	eukaryotic translation initiation factor 2 alpha kinase 2	-2.097	0.315	2.61E-09
CYLD	CYLD lysine 63 deubiquitinase	-1.642	0.247	2.62E-09
XBP1	X-box binding protein 1	-1.099	0.165	2.65E-09
NFKB1	nuclear factor kappa B subunit 1	-1.327	0.200	2.73E-09
ZNF217	zinc finger protein 217	-0.975	0.147	2.79E-09
HES1	hes family bHLH transcription factor 1	1.721	0.259	2.79E-09
FAM101A	refilin A	-1.298	0.196	2.90E-09
IRF2	interferon regulatory factor 2	-1.761	0.266	3.06E-09
BAG1	BAG cochaperone 1	-0.895	0.135	3.22E-09
MCL1	MCL1 apoptosis regulator, BCL2 family member	-0.953	0.145	3.84E-09

MTUS1	microtubule associated scaffold protein 1	0.972	0.149	4.97E-09
TLE1	TLE family member 1, transcriptional corepressor	1.022	0.156	5.19E-09
SH2D3C	SH2 domain containing 3C	1.094	0.167	5.30E-09
SNRK	SNF related kinase	1.006	0.154	5.30E-09
STAT5A	signal transducer and activator of transcription 5A	-1.505	0.231	5.63E-09
CABLES1	Cdk5 and Abl enzyme substrate 1	1.283	0.197	5.89E-09
PTPRK	protein tyrosine phosphatase receptor type K	-0.863	0.133	7.58E-09
CLIC2	chloride intracellular channel 2	-1.451	0.224	7.88E-09
C21orf91	chromosome 21 open reading frame 91	-1.834	0.283	7.88E-09
RAB23	RAB23, member RAS oncogene family	-0.915	0.142	8.90E-09
SSFA2	ITPR interacting domain containing 2	1.147	0.179	1.07E-08
TNFAIP1	TNF alpha induced protein 1	-1.190	0.185	1.07E-08
CD83	CD83 molecule	-2.655	0.415	1.20E-08
STX11	syntaxin 11	-1.704	0.267	1.33E-08
CD69	CD69 molecule	-3.937	0.617	1.38E-08
ZNF703	zinc finger protein 703	1.528	0.240	1.42E-08
IFIT1	interferon induced protein with tetratricopeptide repeats 1	-9.088	1.426	1.42E-08
CASP10	caspase 10	-1.600	0.251	1.46E-08
IFI16	interferon gamma inducible protein 16	-1.444	0.227	1.56E-08
SELE	selectin E	-5.660	0.893	1.75E-08
NABP1	nucleic acid binding protein 1	-1.015	0.160	1.81E-08
SOD2	superoxide dismutase 2	-4.031	0.638	1.94E-08
SHROOM4	shroom family member 4	-0.850	0.135	2.26E-08
WTAP	WT1 associated protein	-1.350	0.215	2.58E-08
HELZ2	helicase with zinc finger 2	-4.096	0.656	3.22E-08
RIN1	Ras and Rab interactor 1	1.657	0.266	3.63E-08
C8orf4	transcriptional and immune response regulator	-1.892	0.304	3.71E-08
ARID5B	AT-rich interaction domain 5B	-1.769	0.285	3.73E-08
CHST1	carbohydrate sulfotransferase 1	1.281	0.206	3.75E-08
TNIP1	TNFAIP3 interacting protein 1	-1.605	0.258	3.75E-08
NRARP	NOTCH regulated ankyrin repeat protein	1.886	0.304	3.93E-08
DDIT4	DNA damage inducible transcript 4	1.289	0.208	4.27E-08
ELL2	elongation factor for RNA polymerase II 2	-1.531	0.248	4.32E-08
PRRG4	proline rich and Gla domain 4	-5.290	0.857	4.66E-08
AJUBA	ajuba LIM protein	1.499	0.243	5.04E-08
Mar-05		-0.897	0.146	5.04E-08
SPRY4	sprouty RTK signaling antagonist 4	1.021	0.166	5.63E-08
TAPSAR1	PSMB8 antisense RNA 1 (head to head)	-2.203	0.360	6.52E-08
SQRDL	sulfide quinone oxidoreductase	-1.486	0.243	6.61E-08
DDX60L	DExD/H-box 60 like	-3.391	0.555	6.61E-08
TNFAIP3	TNF alpha induced protein 3	-4.405	0.721	6.86E-08
ZC3HAV1	zinc finger CCCH-type containing, antiviral 1	-3.382	0.554	7.05E-08
GIMAP7	GTPase, IMAP family member 7	-1.246	0.205	7.80E-08
KIT	KIT proto-oncogene, receptor tyrosine kinase	1.987	0.327	7.85E-08
TLE4	TLE family member 4, transcriptional corepressor	-1.402	0.231	8.49E-08
ANKRD33B	ankyrin repeat domain 33B	-1.671	0.275	8.51E-08
IRG1	aconitate decarboxylase 1	-11.293	1.865	9.17E-08
RAB24	RAB24, member RAS oncogene family	-1.394	0.230	9.39E-08
CACNA1A	calcium voltage-gated channel subunit alpha1 A	-2.583	0.428	1.00E-07
BCL2L13	BCL2 like 13	-1.072	0.178	1.02E-07
CPEB2	cytoplasmic polyadenylation element binding protein 2	-1.131	0.188	1.05E-07
IRAK2	interleukin 1 receptor associated kinase 2	-1.554	0.258	1.16E-07
LINC00984	InaF motif containing 2	1.044	0.174	1.16E-07
CFLAR	CASP8 and FADD like apoptosis regulator	-1.097	0.183	1.32E-07
TIFA	TRAF interacting protein with forkhead associated domain	-1.694	0.283	1.32E-07
FGF2	fibroblast growth factor 2	-1.732	0.289	1.34E-07
PLEKHF1	pleckstrin homology and FYVE domain containing 1	-1.482	0.248	1.37E-07
GIMAP8	GTPase, IMAP family member 8	-1.446	0.242	1.49E-07
ACKR3	atypical chemokine receptor 3	-3.353	0.562	1.51E-07
ITPKB	inositol-trisphosphate 3-kinase B	1.222	0.205	1.57E-07
NRROS	negative regulator of reactive oxygen species	1.967	0.331	1.75E-07
RNF114	ring finger protein 114	-1.382	0.233	1.87E-07

NAV3	neuron navigator 3	-0.821	0.139	1.88E-07
CTSS	cathepsin S	-1.706	0.288	1.95E-07
NNMT	nicotinamide N-methyltransferase	-1.347	0.228	1.98E-07
GTPBP2	GTP binding protein 2	-1.227	0.208	2.06E-07
NFKBIZ	NFKB inhibitor zeta	-1.290	0.218	2.06E-07
SSTR2	somatostatin receptor 2	-6.343	1.075	2.16E-07
CASP1	caspase 1	-1.707	0.290	2.28E-07
FAM26E	calcium homeostasis modulator family member 5	-0.897	0.152	2.34E-07
IFIH1	interferon induced with helicase C domain 1	-5.232	0.890	2.49E-07
APOBEC3G	apolipoprotein B mRNA editing enzyme catalytic subunit 3G	-2.771	0.472	2.49E-07
HLA-C	major histocompatibility complex, class I, C	-1.010	0.172	2.50E-07
IL18BP	interleukin 18 binding protein	-1.652	0.282	2.89E-07
IDO1	indoleamine 2,3-dioxygenase 1	-9.021	1.542	2.89E-07
DDX58	RNA sensor RIG-I	-4.288	0.733	2.92E-07
LAMP3	lysosomal associated membrane protein 3	-2.567	0.441	3.29E-07
PARP10	poly(ADP-ribose) polymerase family member 10	-1.766	0.304	3.66E-07
LONRF1	LON peptidase N-terminal domain and ring finger 1	-1.360	0.234	3.71E-07
LOC101926887		-7.086	1.222	3.88E-07
CXCL9	C-X-C motif chemokine ligand 9	-12.996	2.246	4.14E-07
ZBTB42	zinc finger and BTB domain containing 42	-1.661	0.287	4.21E-07
DLL1	delta like canonical Notch ligand 1	-2.336	0.404	4.32E-07
CSF2RB	colony stimulating factor 2 receptor subunit beta	-1.468	0.255	4.54E-07
NFKB2	nuclear factor kappa B subunit 2	-1.569	0.272	4.57E-07
TAP1	transporter 1, ATP binding cassette subfamily B member	-3.107	0.540	4.93E-07
IFNB1	interferon beta 1	-10.711	1.865	5.18E-07
ZNF792	zinc finger protein 792	1.753	0.305	5.21E-07
LGMN	legumain	-0.920	0.160	5.39E-07
LPHN2	adhesion G protein-coupled receptor L2	-0.812	0.142	5.43E-07
HLA-A	major histocompatibility complex, class I, A	-0.902	0.158	5.98E-07
JAK3	Janus kinase 3	-2.324	0.407	6.27E-07
GFPT2	glutamine-fructose-6-phosphate transaminase 2	-1.195	0.210	6.57E-07
UBE2Z	ubiquitin conjugating enzyme E2 Z	-0.972	0.171	6.59E-07
ADAR	adenosine deaminase RNA specific	-1.406	0.247	6.59E-07
B3GNT2	UDP-GlcNAc:betaGal beta-1,3-N-acetylglucosaminyltransferase 2	-1.013	0.178	6.64E-07
JAK2	Janus kinase 2	-1.863	0.328	7.53E-07
TNFAIP2	TNF alpha induced protein 2	-4.545	0.801	7.53E-07
GIMAP2	GTPase, IMAP family member 2	-1.536	0.271	7.71E-07
MASTL	microtubule associated serine/threonine kinase like	-1.588	0.280	7.83E-07
HIVEP2	HIVEP zinc finger 2	-3.368	0.595	8.02E-07
SMARCA5	SWI/SNF related, matrix associated, actin dependent regulator of chromatin, subfamily a, member 5	-1.000	0.177	8.32E-07
RNF122	ring finger protein 122	-1.289	0.228	8.72E-07
PRICKLE1	prickle planar cell polarity protein 1	1.762	0.312	8.79E-07
SNX18	sorting nexin 18	1.142	0.203	9.64E-07
TICAM1	TIR domain containing adaptor molecule 1	-1.128	0.201	1.00E-06
ZFPM2	zinc finger protein, FOG family member 2	-1.019	0.181	1.02E-06
IFITM1	interferon induced transmembrane protein 1	-5.257	0.937	1.05E-06
KBTBD2	kelch repeat and BTB domain containing 2	-0.881	0.157	1.13E-06
LIPG	lipase G, endothelial type	-1.068	0.191	1.16E-06
TMEM171	transmembrane protein 171	-0.997	0.179	1.25E-06
SERTAD1	SERTA domain containing 1	-0.950	0.171	1.33E-06
TGFBRAP1	transforming growth factor beta receptor associated protein 1	1.050	0.189	1.36E-06
BBC3	BCL2 binding component 3	-1.543	0.278	1.37E-06
XIAP	X-linked inhibitor of apoptosis	-0.849	0.154	1.62E-06
NBN	nibrin	-0.927	0.168	1.65E-06
TOX	thymocyte selection associated high mobility group box	-1.113	0.202	1.69E-06
IL1R1	interleukin 1 receptor type 1	-1.261	0.228	1.71E-06
SECTM1	secreted and transmembrane 1	-5.886	1.069	1.86E-06

EPSTI1	epithelial stromal interaction 1	-6.882	1.252	1.91E-06
BAZ1A	bromodomain adjacent to zinc finger domain 1A	-1.008	0.184	2.04E-06
BMP2	bone morphogenetic protein 2	-1.201	0.219	2.05E-06
IRF2BPL	interferon regulatory factor 2 binding protein like	-1.411	0.257	2.07E-06
MX2	MX dynamin like GTPase 2	-7.857	1.434	2.10E-06
APOL6	apolipoprotein L6	-5.177	0.946	2.19E-06
SLFN12	schlafen family member 12	-1.011	0.185	2.23E-06
FOSL2	FOS like 2, AP-1 transcription factor subunit	-1.150	0.210	2.24E-06
SDPR	caveolae associated protein 2	1.039	0.190	2.25E-06
CCL20	C-C motif chemokine ligand 20	-4.660	0.853	2.25E-06
PLEKHA4	pleckstrin homology domain containing A4	-3.385	0.620	2.30E-06
KLF6	KLF transcription factor 6	-0.706	0.130	2.38E-06
MYCN	MYCN proto-oncogene, bHLH transcription factor	2.403	0.441	2.44E-06
ADCY4	adenylate cyclase 4	-0.900	0.165	2.48E-06
SLC30A7	solute carrier family 30 member 7	-0.899	0.166	2.66E-06
KLF9	KLF transcription factor 9	-0.791	0.146	2.69E-06
PARP12	poly(ADP-ribose) polymerase family member 12	-1.578	0.291	2.70E-06
C5orf56	IRF1 antisense RNA 1	-2.630	0.485	2.74E-06
SH3BP4	SH3 domain binding protein 4	0.889	0.164	2.82E-06
FZD5	frizzled class receptor 5	-1.811	0.334	2.82E-06
SLC31A2	solute carrier family 31 member 2	-1.231	0.228	2.99E-06
NR2F2	nuclear receptor subfamily 2 group F member 2	1.143	0.212	3.02E-06
SERPINB9	serpin family B member 9	-1.381	0.255	3.02E-06
UBD	ubiquitin D	-6.733	1.246	3.02E-06
DTX3L	deltex E3 ubiquitin ligase 3L	-3.066	0.567	3.03E-06
WHAMM	WASP homolog associated with actin, golgi membranes and microtubules	-0.934	0.173	3.15E-06
GMPR	guanosine monophosphate reductase	-1.278	0.237	3.26E-06
LY6E	lymphocyte antigen 6 family member E	-1.195	0.222	3.56E-06
TLDC2	TBC/LysM-associated domain containing 2	-4.414	0.826	4.15E-06
NMI	N-myc and STAT interactor	-1.138	0.213	4.27E-06
HSPA1B	heat shock protein family A (Hsp70) member 1B	-0.942	0.177	4.56E-06
PRR16	proline rich 16	-2.519	0.473	4.56E-06
MEX3B	mex-3 RNA binding family member B	1.317	0.247	4.63E-06
IRF7	interferon regulatory factor 7	-3.285	0.618	4.75E-06
ISG20	interferon stimulated exonuclease gene 20	-4.421	0.832	4.75E-06
CXorf38	chromosome X open reading frame 38	-1.050	0.198	4.91E-06
CXCL2	C-X-C motif chemokine ligand 2	-3.461	0.652	4.91E-06
GBP4	guanylate binding protein 4	-7.803	1.470	4.91E-06
TMEM62	transmembrane protein 62	-1.257	0.237	4.96E-06
BIRC3	baculoviral IAP repeat containing 3	-4.315	0.816	5.39E-06
UGDH	UDP-glucose 6-dehydrogenase	-0.729	0.138	5.55E-06
C3orf52	chromosome 3 open reading frame 52	-1.286	0.244	5.84E-06
NKX3-1	NK3 homeobox 1	-2.534	0.481	5.97E-06
FYTTD1	forty-two-three domain containing 1	-0.878	0.167	6.00E-06
APOL2	apolipoprotein L2	-3.145	0.599	6.45E-06
CCRL2	C-C motif chemokine receptor like 2	-1.009	0.192	6.59E-06
SEMA7A	semaphorin 7A (John Milton Hagen blood group)	-2.258	0.430	6.69E-06
ERCC6	ERCC excision repair 6, chromatin remodeling factor	1.133	0.217	7.41E-06
IFI30	IFI30 lysosomal thiol reductase	-4.446	0.851	7.42E-06
PRKCD	protein kinase C delta	-1.008	0.193	7.44E-06
CDH11	cadherin 11	-0.997	0.191	7.85E-06
SOCS3	suppressor of cytokine signaling 3	-3.362	0.645	7.85E-06
MLKL	mixed lineage kinase domain like pseudokinase	-1.343	0.259	9.13E-06
XRN1	5'-3' exoribonuclease 1	-1.494	0.288	9.25E-06
TRIB1	tribbles pseudokinase 1	-1.377	0.266	9.28E-06
GTPBP1	GTP binding protein 1	-1.366	0.264	9.69E-06
SP140L	SP140 nuclear body protein like	-1.120	0.217	9.79E-06
NUAK1	NUAK family kinase 1	1.343	0.260	1.03E-05
DCUN1D3	defective in cullin neddylation 1 domain containing 3	-1.140	0.221	1.03E-05
PXK	PX domain containing serine/threonine kinase like	-1.313	0.255	1.10E-05

APOBEC3F	apolipoprotein B mRNA editing enzyme catalytic subunit 3F	-1.363	0.266	1.19E-05
CASP7	caspase 7	-1.375	0.268	1.26E-05
ITGAV	integrin subunit alpha V	-0.726	0.142	1.26E-05
CDKN2B	cyclin dependent kinase inhibitor 2B	-0.998	0.195	1.27E-05
NUAK2	NUAK family kinase 2	-3.912	0.765	1.28E-05
CXCL3	C-X-C motif chemokine ligand 3	-4.506	0.883	1.37E-05
ZC3H12C	zinc finger CCCH-type containing 12C	-1.280	0.251	1.41E-05
OAS1	2'-5'-oligoadenylate synthetase 1	-4.940	0.970	1.44E-05
IFI44L	interferon induced protein 44 like	-5.925	1.164	1.46E-05
S100A3	S100 calcium binding protein A3	-2.232	0.439	1.47E-05
BIRC2	baculoviral IAP repeat containing 2	-1.037	0.205	1.61E-05
PFKFB3	6-phosphofructo-2-kinase/fructose-2,6-biphosphatase 3	-1.538	0.303	1.61E-05
GOLPH3	golgi phosphoprotein 3	-0.754	0.149	1.68E-05
PLEKHO2	pleckstrin homology domain containing O2	-0.921	0.182	1.68E-05
TRIM22	tripartite motif containing 22	-1.194	0.236	1.70E-05
ARHGAP18	Rho GTPase activating protein 18	0.856	0.169	1.77E-05
TMEM170B	transmembrane protein 170B	1.283	0.254	1.78E-05
FAM214A	atos homolog A	0.868	0.172	1.87E-05
PPP1R9B	protein phosphatase 1 regulatory subunit 9B	0.860	0.171	1.89E-05
MYCBP2	MYC binding protein 2	-1.215	0.242	2.01E-05
NFKBIE	NFKB inhibitor epsilon	-1.104	0.220	2.03E-05
TSLP	thymic stromal lymphopoietin	-2.562	0.511	2.04E-05
RNF168	ring finger protein 168	0.886	0.177	2.07E-05
LINC01181	long intergenic non-protein coding RNA 1181	-7.393	1.478	2.20E-05
CCDC9	coiled-coil domain containing 9	-1.391	0.278	2.28E-05
NAMPT	nicotinamide phosphoribosyltransferase	-0.796	0.160	2.36E-05
LOC730101		1.520	0.305	2.39E-05
BNC1	basonuclin 1	0.886	0.178	2.46E-05
SPATA13	spermatogenesis associated 13	-0.953	0.191	2.50E-05
SBNO2	strawberry notch homolog 2	-1.266	0.254	2.52E-05
JADE1	jade family PHD finger 1	1.083	0.218	2.52E-05
RIPK1	receptor interacting serine/threonine kinase 1	-1.047	0.211	2.59E-05
SLC20A1	solute carrier family 20 member 1	0.871	0.176	2.65E-05
PVRL2	nectin cell adhesion molecule 2	-0.730	0.147	2.71E-05
NEURL3	neuralized E3 ubiquitin protein ligase 3	-7.965	1.611	2.92E-05
ETV7	ETS variant transcription factor 7	-6.128	1.241	2.97E-05
PPP1R15A	protein phosphatase 1 regulatory subunit 15A	-0.837	0.170	3.09E-05
SOX12	SRY-box transcription factor 12	1.010	0.205	3.13E-05
PDE7B	phosphodiesterase 7B	1.019	0.207	3.14E-05
NDUFC2-KCTD14	NDUFC2-KCTD14 readthrough	-2.538	0.515	3.15E-05
RICTOR	RPTOR independent companion of MTOR complex 2	-1.093	0.222	3.22E-05
APOL1	apolipoprotein L1	-2.767	0.563	3.33E-05
TSHZ1	teashirt zinc finger homeobox 1	1.703	0.347	3.43E-05
CTDSPL	CTD small phosphatase like	0.764	0.156	3.47E-05
MFSD12	major facilitator superfamily domain containing 12	-0.939	0.192	3.53E-05
HAPLN3	hyaluronan and proteoglycan link protein 3	-3.155	0.645	3.62E-05
GIMAP6	GTPase, IMAP family member 6	-1.008	0.206	3.75E-05
GPBP1	GC-rich promoter binding protein 1	-1.009	0.207	3.85E-05
MEF2D	myocyte enhancer factor 2D	0.818	0.168	3.88E-05
FOXP1	forkhead box P1	-0.947	0.194	3.97E-05
HERC5	HECT and RLD domain containing E3 ubiquitin protein ligase 5	-7.425	1.523	3.99E-05
EBI3	Epstein-Barr virus induced 3	-3.193	0.655	3.99E-05
LRIG3	leucine rich repeats and immunoglobulin like domains 3	-1.046	0.215	4.24E-05
BTG3	BTG anti-proliferation factor 3	-0.955	0.197	4.65E-05
PCDH17	protocadherin 17	-1.200	0.248	4.69E-05
F2RL3	F2R like thrombin or trypsin receptor 3	1.361	0.281	4.73E-05
CEACAM1	CEA cell adhesion molecule 1	-2.129	0.441	4.85E-05
LRRC32	leucine rich repeat containing 32	-0.789	0.163	4.86E-05
UNC93B1	unc-93 homolog B1, TLR signaling regulator	-1.503	0.311	4.93E-05
PTPN4	protein tyrosine phosphatase non-receptor type 4	1.021	0.212	5.09E-05
PCDH7	protocadherin 7	-1.373	0.285	5.14E-05

RTP4	receptor transporter protein 4	-7.200	1.496	5.26E-05
RASSF1	Ras association domain family member 1	-0.723	0.150	5.38E-05
DNPEP	aspartyl aminopeptidase	-0.736	0.153	5.38E-05
B4GALT1	beta-1,4-galactosyltransferase 1	-0.915	0.190	5.38E-05
IL6ST	interleukin 6 cytokine family signal transducer	-0.612	0.127	5.51E-05
ATP10A	ATPase phospholipid transporting 10A (putative)	-7.065	1.472	5.55E-05
KBTBD6	kelch repeat and BTB domain containing 6	1.169	0.244	5.59E-05
LOC100294362		-3.189	0.666	5.85E-05
CXCL5	C-X-C motif chemokine ligand 5	-3.046	0.637	5.95E-05
B2M	beta-2-microglobulin	-0.710	0.148	5.99E-05
SP100	SP100 nuclear antigen	-1.022	0.214	6.14E-05
CSRNP2	cysteine and serine rich nuclear protein 2	-0.888	0.186	6.22E-05
ANKRD28	ankyrin repeat domain 28	0.747	0.157	6.24E-05
IL3RA	interleukin 3 receptor subunit alpha	-0.906	0.190	6.29E-05
TFAP4	transcription factor AP-4	2.151	0.451	6.42E-05
DRAM1	DNA damage regulated autophagy modulator 1	-0.929	0.195	6.60E-05
ZEB2	zinc finger E-box binding homeobox 2	-0.955	0.201	7.18E-05
EVA1A	eva-1 homolog A, regulator of programmed cell death	1.066	0.225	7.22E-05
NR2F6	nuclear receptor subfamily 2 group F member 6	0.785	0.166	7.46E-05
KLF4	KLF transcription factor 4	-3.051	0.645	7.50E-05
FAM124B	family with sequence similarity 124 member B	1.320	0.280	7.98E-05
RP2	RP2 activator of ARL3 GTPase	-0.797	0.169	8.02E-05
ORAI3	ORAI calcium release-activated calcium modulator 3	0.990	0.210	8.21E-05
C6orf62	chromosome 6 open reading frame 62	-0.699	0.148	8.37E-05
LINC00338	small nucleolar RNA host gene 20	1.281	0.273	8.67E-05
CMTR1	cap methyltransferase 1	-1.047	0.223	8.67E-05
ANKFY1	ankyrin repeat and FYVE domain containing 1	-1.199	0.255	8.71E-05
THEMIS2	thymocyte selection associated family member 2	-3.059	0.651	8.74E-05
RBMXL1	RBMX like 1	-0.891	0.190	9.22E-05
EFNA1	ephrin A1	-1.547	0.331	9.74E-05
CEMP1	cementum protein 1	0.909	0.195	1.00E-04
SLC7A5	solute carrier family 7 member 5	0.869	0.186	1.02E-04
RGCC	regulator of cell cycle	1.270	0.272	1.03E-04
MX1	MX dynamin like GTPase 1	-6.129	1.315	1.04E-04
UBL4A	ubiquitin like 4A	0.894	0.192	1.04E-04
USP30-AS1	USP30 antisense RNA 1	-7.340	1.576	1.04E-04
CARD10	caspase recruitment domain family member 10	1.055	0.227	1.05E-04
OSBPL7	oxysterol binding protein like 7	0.865	0.186	1.10E-04
PNMA2	PNMA family member 2	0.886	0.191	1.12E-04
CLDN23	claudin 23	-2.541	0.547	1.12E-04
ZNF395	zinc finger protein 395	1.518	0.327	1.13E-04
FAM124A	family with sequence similarity 124 member A	-1.205	0.260	1.13E-04
HERC6	HECT and RLD domain containing E3 ubiquitin protein ligase family member 6	-4.202	0.908	1.20E-04
MN1	MN1 proto-oncogene, transcriptional regulator	1.627	0.352	1.24E-04
TAP2	transporter 2, ATP binding cassette subfamily B member	-1.334	0.289	1.25E-04
HSPA1A	heat shock protein family A (Hsp70) member 1A	-0.885	0.192	1.26E-04
TRIM8	tripartite motif containing 8	0.696	0.151	1.29E-04
IFI6	interferon alpha inducible protein 6	-3.337	0.725	1.33E-04
ODF3B	outer dense fiber of sperm tails 3B	-2.317	0.504	1.35E-04
NUB1	negative regulator of ubiquitin like proteins 1	-1.132	0.246	1.36E-04
FMR1	fragile X messenger ribonucleoprotein 1	-0.940	0.205	1.37E-04
ZNF267	zinc finger protein 267	-0.952	0.207	1.37E-04
RRAD	RRAD, Ras related glycolysis inhibitor and calcium channel regulator	-1.677	0.365	1.40E-04
STC1	stanniocalcin 1	1.007	0.220	1.44E-04
NINJ1	ninjurin 1	-1.405	0.307	1.45E-04
KANK2	KN motif and ankyrin repeat domains 2	1.129	0.247	1.51E-04

STARD4	StAR related lipid transfer domain containing 4	-0.764	0.167	1.56E-04
IL32	interleukin 32	-1.218	0.267	1.56E-04
KIAA1462	junctional cadherin 5 associated	0.776	0.170	1.57E-04
RELA	RELA proto-oncogene, NF-kB subunit	-1.009	0.221	1.61E-04
STOML1	stomatin like 1	-0.768	0.169	1.68E-04
ETS1	ETS proto-oncogene 1, transcription factor	-1.082	0.239	1.85E-04
SAMD4A	sterile alpha motif domain containing 4A	-0.858	0.190	1.93E-04
RBBP6	RB binding protein 6, ubiquitin ligase	-0.973	0.216	1.96E-04
SPHK1	sphingosine kinase 1	-0.639	0.142	2.02E-04
S1PR2	sphingosine-1-phosphate receptor 2	-1.765	0.393	2.12E-04
SMURF1	SMAD specific E3 ubiquitin protein ligase 1	-0.935	0.208	2.13E-04
AZI2	5-azacytidine induced 2	-0.783	0.174	2.13E-04
ACVR1B	activin A receptor type 1B	-1.047	0.233	2.13E-04
TMEM2	cell migration inducing hyaluronidase 2	-0.937	0.209	2.14E-04
HOXA5	homeobox A5	1.298	0.289	2.16E-04
BATF3	basic leucine zipper ATF-like transcription factor 3	-2.948	0.658	2.24E-04
IFI27	interferon alpha inducible protein 27	-1.037	0.232	2.25E-04
IL15	interleukin 15	-2.480	0.554	2.33E-04
TBKBP1	TBK1 binding protein 1	0.906	0.203	2.33E-04
BACH1	BTB domain and CNC homolog 1	-0.952	0.213	2.36E-04
FNDC3B	fibronectin type III domain containing 3B	-0.584	0.131	2.41E-04
HLX	H2.0 like homeobox	0.714	0.160	2.46E-04
FOXO1	forkhead box O1	0.785	0.176	2.48E-04
PSME2	proteasome activator subunit 2	-0.798	0.179	2.49E-04
TTC39B	tetratricopeptide repeat domain 39B	-1.597	0.358	2.49E-04
SERPINB2	serpin family B member 2	-1.451	0.326	2.57E-04
ABCA1	ATP binding cassette subfamily A member 1	-1.478	0.332	2.57E-04
FNBP1L	formin binding protein 1 like	0.669	0.151	2.58E-04
CDKN1A	cyclin dependent kinase inhibitor 1A	-0.600	0.135	2.64E-04
TRAF1	TNF receptor associated factor 1	-4.062	0.916	2.72E-04
IER2	immediate early response 2	-0.766	0.173	2.76E-04
PPA1	inorganic pyrophosphatase 1	-0.771	0.174	2.78E-04
MECOM	MDS1 and EVI1 complex locus	0.670	0.151	2.85E-04
MTSS1L	MTSS I-BAR domain containing 2	1.132	0.256	2.85E-04
KCTD12	potassium channel tetramerization domain containing 12	0.889	0.201	2.86E-04
CH25H	cholesterol 25-hydroxylase	-2.779	0.629	2.88E-04
GBP1P1	guanylate binding protein 1 pseudogene 1	-9.856	2.230	2.88E-04
KIAA1211L	CRACD like	0.906	0.205	2.91E-04
AC009948.5		-0.926	0.210	3.02E-04
CSRP2	cysteine and glycine rich protein 2	-1.442	0.327	3.02E-04
CAB39	calcium binding protein 39	-0.859	0.195	3.19E-04
CNIH3	cornichon family AMPA receptor auxiliary protein 3	1.789	0.407	3.22E-04
BTN3A1	butyrophilin subfamily 3 member A1	-1.256	0.286	3.26E-04
DDIT4L	DNA damage inducible transcript 4 like	1.562	0.356	3.32E-04
LOC102723901		1.959	0.447	3.32E-04
HIST2H2AA3	H2A clustered histone 18	-1.368	0.312	3.38E-04
MID1IP1	MID1 interacting protein 1	0.859	0.196	3.42E-04
TMEM217	transmembrane protein 217	-1.101	0.252	3.44E-04
RGL1	ral guanine nucleotide dissociation stimulator like 1	-0.906	0.207	3.51E-04
SERPINB8	serpin family B member 8	-0.627	0.143	3.54E-04
ARMCX1	armadillo repeat containing X-linked 1	-0.719	0.165	3.58E-04
STC2	stanniocalcin 2	-0.940	0.215	3.60E-04
PHF11	PHD finger protein 11	-1.143	0.262	3.62E-04
NRCAM	neuronal cell adhesion molecule	-0.765	0.176	3.84E-04
PDGFRL	platelet derived growth factor receptor like	-1.048	0.241	3.89E-04
CPEB3	cytoplasmic polyadenylation element binding protein 3	-1.276	0.294	3.89E-04
C1R-2		-1.989	0.458	3.98E-04
CNDP2	carnosine dipeptidase 2	-0.768	0.177	4.01E-04
TJP2	tight junction protein 2	-0.602	0.139	4.09E-04
FAM50B	family with sequence similarity 50 member B	1.343	0.310	4.10E-04
ZNF521	zinc finger protein 521	0.906	0.209	4.16E-04
FAM212A	inka box actin regulator 1	1.111	0.257	4.19E-04
ZBTB1	zinc finger and BTB domain containing 1	0.823	0.190	4.25E-04
NCOA3	nuclear receptor coactivator 3	-1.073	0.248	4.29E-04
RNF31	ring finger protein 31	-0.801	0.186	4.67E-04

C2CD4A	C2 calcium dependent domain containing 4A	-4.028	0.937	4.67E-04
THAP3	THAP domain containing 3	-0.806	0.188	4.69E-04
NEK6	NIMA related kinase 6	0.652	0.152	4.73E-04
TTC38	tetratricopeptide repeat domain 38	-0.700	0.163	4.89E-04
NFIB	nuclear factor I B	0.699	0.163	4.90E-04
CYTH4	cytohesin 4	-3.473	0.810	4.96E-04
ACHE	acetylcholinesterase (Cartwright blood group)	-1.953	0.456	5.03E-04
CFB	complement factor B	-4.521	1.057	5.15E-04
TRIM34	tripartite motif containing 34	-0.855	0.200	5.23E-04
BTN2A1	butyrophilin subfamily 2 member A1	-0.666	0.156	5.38E-04
SH3TC2	SH3 domain and tetratricopeptide repeats 2	1.488	0.350	5.60E-04
LOC102724141		-6.981	1.641	5.63E-04
AGFG2	ArfGAP with FG repeats 2	0.881	0.208	6.10E-04
PTGS2	prostaglandin-endoperoxide synthase 2	-2.617	0.618	6.10E-04
NOD2	nucleotide binding oligomerization domain containing 2	-3.726	0.882	6.41E-04
LYPD5	LY6/PLAUR domain containing 5	-2.481	0.587	6.41E-04
CHSY3	chondroitin sulfate synthase 3	-1.219	0.289	6.45E-04
YAP1	Yes1 associated transcriptional regulator	-0.657	0.156	6.52E-04
RNF24	ring finger protein 24	-0.781	0.185	6.67E-04
HSH2D	hematopoietic SH2 domain containing	-6.980	1.657	6.67E-04
SAMD9L	sterile alpha motif domain containing 9 like	-2.890	0.686	6.69E-04
XAF1	XIAP associated factor 1	-4.191	0.995	6.72E-04
TBC1D8	TBC1 domain family member 8	0.778	0.185	6.91E-04
SOX4	SRY-box transcription factor 4	0.636	0.151	7.06E-04
FILIP1	filamin A interacting protein 1	2.233	0.532	7.13E-04
TTC39A	tetratricopeptide repeat domain 39A	-2.886	0.688	7.17E-04
GBA2	glucosylceramidase beta 2	0.744	0.178	7.43E-04
NCF2	neutrophil cytosolic factor 2	-4.585	1.095	7.43E-04
ARHGEF40	Rho guanine nucleotide exchange factor 40	-1.615	0.386	7.46E-04
SLC15A3	solute carrier family 15 member 3	-3.637	0.869	7.46E-04
FAS	Fas cell surface death receptor	-1.019	0.244	7.80E-04
RFX5	regulatory factor X5	-0.654	0.157	7.86E-04
CCL2	C-C motif chemokine ligand 2	-3.150	0.756	7.96E-04
SERPING1	serpin family G member 1	-4.132	0.993	8.25E-04
ARVCF	ARVCF delta catenin family member	0.831	0.200	8.26E-04
GNA13	G protein subunit alpha 13	-0.752	0.181	8.26E-04
C19orf71	tektin bundle interacting protein 1	-1.214	0.292	8.32E-04
ARL5B	ADP ribosylation factor like GTPase 5B	-1.230	0.296	8.33E-04
ART3	ADP-ribosyltransferase 3 (inactive)	-5.472	1.318	8.47E-04
C19orf26	CACN subunit beta associated regulatory protein	0.808	0.195	8.58E-04
HLA-H	major histocompatibility complex, class I, H (pseudogene)	-1.435	0.346	8.61E-04
BCL6	BCL6 transcription repressor	-1.012	0.244	8.65E-04
RGS20	regulator of G protein signaling 20	-0.992	0.239	8.85E-04
ROBO1	roundabout guidance receptor 1	-0.846	0.205	9.21E-04
LCA5	lebercilin LCA5	1.172	0.284	9.48E-04
CD164	CD164 molecule	-0.574	0.139	9.48E-04
OTUD4	OTU deubiquitinase 4	-0.899	0.218	9.65E-04
DUSP16	dual specificity phosphatase 16	-1.045	0.254	9.79E-04
ZBTB43	zinc finger and BTB domain containing 43	-1.014	0.247	9.83E-04
LIFR	LIF receptor subunit alpha	-1.292	0.314	9.89E-04
OTX1	orthodenticle homeobox 1	3.082	0.750	0.0010059
CREB3	cAMP responsive element binding protein 3	-0.661	0.161	0.0010217
CHST15	carbohydrate sulfotransferase 15	0.894	0.218	0.0010345
USP42	ubiquitin specific peptidase 42	-1.247	0.304	0.0010444
ZNF331	zinc finger protein 331	1.226	0.300	0.001071
KIAA1217	KIAA1217	-1.629	0.399	0.001131
FNDC3A	fibronectin type III domain containing 3A	-0.606	0.149	0.0011417
ARNTL2	basic helix-loop-helix ARNT like 2	-0.899	0.221	0.0011426
SCYL3	SCY1 like pseudokinase 3	-1.109	0.272	0.0011632
PARP9	poly(ADP-ribose) polymerase family member 9	-2.875	0.706	0.0011632
HRH1	histamine receptor H1	-0.880	0.217	0.001248
OTUB2	OTU deubiquitinase, ubiquitin aldehyde binding 2	1.230	0.304	0.0012572
USF1	upstream transcription factor 1	-0.786	0.194	0.0012767
DUSP14	dual specificity phosphatase 14	0.715	0.177	0.0012813
Mar-04		0.846	0.209	0.0012847

ITPRIPL2	ITPRIP like 2	-0.716	0.177	0.0013036
SLC25A36	solute carrier family 25 member 36	0.632	0.156	0.0013296
NR3C1	nuclear receptor subfamily 3 group C member 1	-0.632	0.157	0.0013311
TNIP2	TNFAIP3 interacting protein 2	-0.728	0.180	0.0013328
UBTD1	ubiquitin domain containing 1	0.589	0.146	0.0013384
APOL3	apolipoprotein L3	-2.580	0.641	0.0013906
PTCH1	patched 1	1.665	0.414	0.0013943
JHDM1D-AS1	KDM7A divergent transcript	-1.800	0.448	0.001429
KDM5B	lysine demethylase 5B	0.624	0.155	0.001434
ELOVL7	ELOVL fatty acid elongase 7	-3.982	0.992	0.001434
PLAUR	plasminogen activator, urokinase receptor	-0.829	0.207	0.00146
WSCD1	WSC domain containing 1	1.023	0.255	0.0014716
IFITM3	interferon induced transmembrane protein 3	-0.817	0.204	0.0014716
TNFSF4	TNF superfamily member 4	0.794	0.198	0.0014826
RPS6KC1	ribosomal protein S6 kinase C1	-0.809	0.202	0.0014826
INHBA	inhibin subunit beta A	-1.273	0.318	0.0014947
OAS2	2'-5'-oligoadenylate synthetase 2	-3.768	0.942	0.0014986
DHRS3	dehydrogenase/reductase 3	0.838	0.209	0.0014986
RAB8B	RAB8B, member RAS oncogene family	-0.771	0.193	0.0015083
STAT3	signal transducer and activator of transcription 3	-0.644	0.161	0.0015122
AKAP1	A-kinase anchoring protein 1	0.712	0.179	0.0016284
ZMYND8	zinc finger MYND-type containing 8	0.594	0.149	0.0016344
HIC1	HIC ZBTB transcriptional repressor 1	1.392	0.350	0.0016403
DENND5A	DENN domain containing 5A	-0.719	0.181	0.0016805
SCHIP1	schwannomin interacting protein 1	0.892	0.225	0.0016899
USP53	ubiquitin specific peptidase 53	0.806	0.203	0.0016899
MLH3	mutL homolog 3	0.800	0.201	0.0016899
ATF5	activating transcription factor 5	-1.004	0.254	0.001781
AMIGO2	adhesion molecule with Ig like domain 2	0.807	0.204	0.0017933
CSAG3	CSAG family member 3	-6.694	1.694	0.001807
STAP2	signal transducing adaptor family member 2	-0.905	0.229	0.0018109
TNF	tumor necrosis factor	-4.853	1.228	0.0018149
AGAP3	ArfGAP with GTPase domain, ankyrin repeat and PH domain 3	0.620	0.157	0.0018365
RAB12	RAB12, member RAS oncogene family	-0.657	0.167	0.0018402
HINT3	histidine triad nucleotide binding protein 3	-0.776	0.197	0.0018431
MMP25	matrix metallopeptidase 25	-2.100	0.532	0.0018535
LDLR	low density lipoprotein receptor	-0.563	0.143	0.0018757
ICAM1	intercellular adhesion molecule 1	-3.743	0.950	0.0018833
GSDMD	gasdermin D	-0.795	0.202	0.0019362
TLR2	toll like receptor 2	-2.349	0.598	0.0019499
ARHGAP20	Rho GTPase activating protein 20	-1.290	0.329	0.0019839
HK2	hexokinase 2	-0.856	0.218	0.0019852
GIMAP4	GTPase, IMAP family member 4	-0.736	0.188	0.0019976
ITGB8	integrin subunit beta 8	-1.189	0.303	0.0019977
ARHGAP27	Rho GTPase activating protein 27	0.661	0.168	0.0020094
DIEXF	UTP25 small subunit processome component	0.808	0.206	0.002022
ZNF248	zinc finger protein 248	1.092	0.279	0.0020348
CCND3	cyclin D3	-0.601	0.154	0.0020653
RPP25	ribonuclease P and MRP subunit p25	0.985	0.252	0.0021617
ADAP1	ArfGAP with dual PH domains 1	-2.410	0.618	0.0021617
PPAP2A	phospholipid phosphatase 1	-0.810	0.208	0.0021756
TP53INP1	tumor protein p53 inducible nuclear protein 1	0.614	0.158	0.0021769
APLN	apelin	0.907	0.233	0.0022062
BROX	BRO1 domain and CAAX motif containing	-0.623	0.160	0.0022066
TLK2	tousled like kinase 2	-0.669	0.172	0.0022126
TRADD	TNFRSF1A associated via death domain	-0.732	0.188	0.0022873
PLIN2	perilipin 2	0.727	0.187	0.0022949
ZSCAN31	zinc finger and SCAN domain containing 31	0.685	0.177	0.0023224
KIAA0040	KIAA0040	-0.672	0.173	0.002331
GVINP1	GTPase, very large interferon inducible pseudogene 1	-1.267	0.327	0.002331
JARID2	jumonji and AT-rich interaction domain containing 2	0.974	0.251	0.0023543
MMAA	metabolism of cobalamin associated A	-0.999	0.258	0.0023671
RASSF2	Ras association domain family member 2	0.838	0.216	0.0024248
DESI1	desumoylating isopeptidase 1	-0.541	0.140	0.0024455
ZC3H7B	zinc finger CCCH-type containing 7B	-0.951	0.246	0.0024469

PLD6	phospholipase D family member 6	2.059	0.533	0.0024678
GGA2	golgi associated, gamma adaptin ear containing, ARF binding protein 2	0.577	0.150	0.002545
MYO1E	myosin IE	-0.553	0.143	0.0025633
ST8SIA4	ST8 alpha-N-acetyl-neuraminide alpha-2,8-sialyltransferase 4	-0.731	0.190	0.0025691
PHACTR4	phosphatase and actin regulator 4	-0.840	0.218	0.0025691
RBM38	RNA binding motif protein 38	0.637	0.165	0.0025817
CCNL1	cyclin L1	-0.892	0.232	0.0026189
ERAP2	endoplasmic reticulum aminopeptidase 2	-0.991	0.258	0.0026587
CDCA7L	cell division cycle associated 7 like	0.621	0.162	0.0026727
CDC42EP1	CDC42 effector protein 1	0.534	0.139	0.0026727
PIK3CG	phosphatidylinositol-4,5-bisphosphate 3-kinase catalytic subunit gamma	1.327	0.346	0.0027024
PKIG	cAMP-dependent protein kinase inhibitor gamma	-0.602	0.157	0.0027024
NCF4	neutrophil cytosolic factor 4	-5.256	1.370	0.0027165
TROVE2	Ro60, Y RNA binding protein	-0.666	0.174	0.0027199
CAMKK1	calcium/calmodulin dependent protein kinase 1	1.372	0.358	0.0027385
GPR180	G protein-coupled receptor 180	-0.759	0.198	0.002773
FST	follistatin	-2.366	0.618	0.0028039
IFFO2	intermediate filament family orphan 2	0.692	0.181	0.0028076
CHMP5	charged multivesicular body protein 5	-0.720	0.188	0.0028484
SLC1A3	solute carrier family 1 member 3	-6.479	1.697	0.0029079
LOC101929340		0.871	0.228	0.0029129
ZNF48	zinc finger protein 48	0.870	0.228	0.0029129
OAS3	2'-5'-oligoadenylate synthetase 3	-4.083	1.070	0.0029201
STK17A	serine/threonine kinase 17a	0.625	0.164	0.0029901
FHL3	four and a half LIM domains 3	-0.817	0.215	0.0030132
CCDC117	coiled-coil domain containing 117	-0.922	0.242	0.0030331
RAI1	retinoic acid induced 1	0.739	0.194	0.0030374
RSAD1	radical S-adenosyl methionine domain containing 1	0.589	0.155	0.003064
ZADH2	prostaglandin reductase 3	0.991	0.261	0.0030746
CD2AP	CD2 associated protein	-0.654	0.172	0.0030816
LYL1	LYL1 basic helix-loop-helix family member	1.095	0.288	0.0030848
DIS3L	DIS3 like exosome 3'-5' exoribonuclease	0.802	0.211	0.0031572
ST7-AS1	ST7 antisense RNA 1	-1.502	0.396	0.0031673
LOC101928533		-5.764	1.521	0.0031867
BCAR1	BCAR1 scaffold protein, Cas family member	0.576	0.152	0.0032023
P2RX4	purinergic receptor P2X 4	-0.916	0.242	0.0032023
DNMBP	dynamin binding protein	0.567	0.150	0.0032144
KCTD5	potassium channel tetramerization domain containing 5	-0.556	0.147	0.0032144
ATP6V1B2	ATPase H+ transporting V1 subunit B2	-0.530	0.140	0.0032397
ST3GAL1	ST3 beta-galactoside alpha-2,3-sialyltransferase 1	0.606	0.160	0.0032662
IKBKE	inhibitor of nuclear factor kappa B kinase subunit epsilon	-0.678	0.180	0.0033533
ZHX3	zinc fingers and homeoboxes 3	0.840	0.223	0.0033678
PPP1R3C	protein phosphatase 1 regulatory subunit 3C	2.167	0.575	0.0034327
ACSL3	acyl-CoA synthetase long chain family member 3	-0.731	0.194	0.0034327
TRAM2	translocation associated membrane protein 2	0.966	0.257	0.0034639
SLC2A6	solute carrier family 2 member 6	-0.788	0.210	0.0035216
ITPKC	inositol-trisphosphate 3-kinase C	-0.862	0.230	0.0035744
BTN2A2	butyrophilin subfamily 2 member A2	-0.819	0.218	0.003587
SNX33	sorting nexin 33	0.812	0.216	0.003598
NEXN	nexilin F-actin binding protein	0.609	0.162	0.0036553
KRT19	keratin 19	0.666	0.178	0.0036656
NTNG2	netrin G2	-2.997	0.800	0.0036656
CCL7	C-C motif chemokine ligand 7	-4.747	1.267	0.0036756
ARHGEF37	Rho guanine nucleotide exchange factor 37	0.951	0.254	0.0036908
AGPAT9	lysophosphatidylcholine acyltransferase 1	1.260	0.337	0.0037133
GRINA	glutamate ionotropic receptor NMDA type subunit associated protein 1	-0.692	0.185	0.0037158
CASZ1	castor zinc finger 1	-1.299	0.347	0.0037534
KSR2	kinase suppressor of ras 2	1.023	0.273	0.0037549
WARS	tryptophanyl-tRNA synthetase 1	-2.207	0.590	0.0037549
NUDCD1	NudC domain containing 1	-0.722	0.193	0.0038241

LYRM1	LYR motif containing 1	-0.976	0.261	0.0038277
CCND1	cyclin D1	0.658	0.176	0.0038425
FBXO32	F-box protein 32	0.668	0.179	0.003855
KRT80	keratin 80	0.717	0.193	0.0039591
BCL6B	BCL6B transcription repressor	-0.577	0.155	0.0039704
PREX2	phosphatidylinositol-3,4,5-trisphosphate dependent Rac exchange factor 2	-0.851	0.229	0.0040009
LDLRAD2	low density lipoprotein receptor class A domain containing 2	0.564	0.152	0.0040132
SHROOM3	shroom family member 3	0.920	0.247	0.0040298
RUSC2	RUN and SH3 domain containing 2	0.585	0.157	0.0040407
PATL1	PAT1 homolog 1, processing body mRNA decay factor	-0.905	0.244	0.0040821
LOC101928789		-6.574	1.771	0.0041338
LOC102723726		-4.138	1.117	0.0042521
C1R	complement C1r	-2.205	0.595	0.0042589
JMJD1C	jumonji domain containing 1C	0.531	0.144	0.0042871
BPGM	bisphosphoglycerate mutase	-0.648	0.175	0.0042871
SAMHD1	SAM and HD domain containing deoxynucleoside triphosphate triphosphohydrolase 1	-2.428	0.656	0.0042871
SLMO2-ATP5E		-4.141	1.120	0.0043026
CD68	CD68 molecule	-0.620	0.168	0.0043048
PXDC1	PX domain containing 1	0.527	0.143	0.0043551
PSPH	phosphoserine phosphatase	0.679	0.184	0.0045023
BAMBI	BMP and activin membrane bound inhibitor	-0.989	0.268	0.0045023
NOS3	nitric oxide synthase 3	0.778	0.211	0.0045716
ARHGAP31	Rho GTPase activating protein 31	-0.571	0.155	0.0045987
PGPEP1	pyroglutamyl-peptidase I	0.785	0.213	0.0046449
INTS12	integrator complex subunit 12	-0.745	0.203	0.0046449
SLC45A3	solute carrier family 45 member 3	1.092	0.297	0.0046544
TSPAN5	tetraspanin 5	0.596	0.162	0.0046544
BCL7A	BAF chromatin remodeling complex subunit BCL7A	1.238	0.337	0.0046963
CASP4	caspase 4	-0.677	0.184	0.0046963
KLHL24	kelch like family member 24	0.664	0.181	0.0047819
RNF138	ring finger protein 138	-0.752	0.205	0.0048887
LGALS8	galectin 8	-0.752	0.206	0.0049208
ASAH2B	N-acylsphingosine amidohydrolase 2B	-0.904	0.247	0.0049838
NR1D1	nuclear receptor subfamily 1 group D member 1	1.023	0.280	0.0050921
HIPK3	homeodomain interacting protein kinase 3	-0.701	0.192	0.0051146
SEMA3C	semaphorin 3C	-1.060	0.291	0.0051413
RNF44	ring finger protein 44	0.609	0.167	0.0051772
SPATS2L	spermatogenesis associated serine rich 2 like	-0.548	0.150	0.0051881
HTR1D	5-hydroxytryptamine receptor 1D	1.582	0.435	0.0052345
TUBA4A	tubulin alpha 4a	0.772	0.212	0.0052358
GCA	grancalcin	-1.074	0.295	0.0052358
CD47	CD47 molecule	-0.945	0.260	0.0052753
CCDC109B	mitochondrial calcium uniporter dominant negative subunit beta	-0.538	0.148	0.0053711
TNRC6C	trinucleotide repeat containing adaptor 6C	0.838	0.231	0.0054203
ANGPTL4	angiopoietin like 4	-0.711	0.196	0.0054487
EGR1	early growth response 1	-1.046	0.288	0.0054487
PARP14	poly(ADP-ribose) polymerase family member 14	-2.735	0.754	0.0054487
RANBP6	RAN binding protein 6	0.655	0.181	0.0054945
NRSN2	neurensin 2	-0.592	0.163	0.0055107
LOC102723779		-1.699	0.469	0.0055107
RBM7	RNA binding motif protein 7	-0.713	0.197	0.0055199
ARID4B	AT-rich interaction domain 4B	-0.723	0.200	0.0056301
SLC2A1	solute carrier family 2 member 1	0.689	0.191	0.0056597
MICB	MHC class I polypeptide-related sequence B	-0.569	0.157	0.0056659
NOL6	nucleolar protein 6	-0.599	0.166	0.0056673
RGS4	regulator of G protein signaling 4	0.992	0.275	0.005731
ZNF175	zinc finger protein 175	0.861	0.238	0.005768
ARSJ	arylsulfatase family member J	-0.560	0.155	0.0058593
NAA16	N-alpha-acetyltransferase 16, NatA auxiliary subunit	0.815	0.226	0.005873
FAM122C	PABIR family member 3	-1.262	0.350	0.00592
MESDC1	talin rod domain containing 1	-0.734	0.204	0.0059585

TACC2	transforming acidic coiled-coil containing protein 2	0.767	0.213	0.0059677
TMBIM1	transmembrane BAX inhibitor motif containing 1	-0.498	0.138	0.0060167
FAXDC2	fatty acid hydroxylase domain containing 2	1.319	0.367	0.0060438
ALCAM	activated leukocyte cell adhesion molecule	-0.542	0.151	0.0060452
TANK	TRAF family member associated NFKB activator	-0.643	0.179	0.0060509
TNFRSF25	TNF receptor superfamily member 25	0.777	0.216	0.0060708
GADD45B	growth arrest and DNA damage inducible beta	-0.662	0.184	0.0060708
NIPA1	NIPA magnesium transporter 1	-0.734	0.204	0.0060708
NFKBIB	NFKB inhibitor beta	-0.602	0.168	0.0061087
TRIB3	tribbles pseudokinase 3	0.701	0.195	0.006145
ASB13	ankyrin repeat and SOCS box containing 13	0.955	0.266	0.0062034
LOC100126784		-0.896	0.250	0.0062034
CCL4L1	C-C motif chemokine ligand 4 like 1	-8.643	2.410	0.0062034
GOLM1	golgi membrane protein 1	-0.598	0.167	0.0062094
IL6R	interleukin 6 receptor	1.055	0.295	0.0062604
SERTAD3	SERTA domain containing 3	-0.604	0.169	0.0062681
CXCL16	C-X-C motif chemokine ligand 16	-0.808	0.226	0.0063022
LRRTM2	leucine rich repeat transmembrane neuronal 2	-3.144	0.878	0.0063022
FLT3LG	fms related receptor tyrosine kinase 3 ligand	-1.208	0.338	0.0064261
LRCH2	leucine rich repeats and calponin homology domain containing 2	-1.064	0.298	0.0065731
ABHD16A	abhydrolase domain containing 16A, phospholipase	-0.549	0.154	0.0066795
PPP2R1B	protein phosphatase 2 scaffold subunit Abeta	-0.547	0.154	0.0066842
SPPL2A	signal peptide peptidase like 2A	-0.567	0.159	0.006781
NEDD1	NEDD1 gamma-tubulin ring complex targeting factor	-0.809	0.228	0.0070406
GPATCH11	G-patch domain containing 11	0.944	0.266	0.007067
MYEOV	myeloma overexpressed	0.874	0.246	0.007067
RAB30	RAB30, member RAS oncogene family	1.047	0.296	0.0072111
LOC100996535		-2.935	0.829	0.0072111
CSF2	colony stimulating factor 2	-3.399	0.960	0.0072321
ADAT2	adenosine deaminase tRNA specific 2	0.798	0.226	0.0072844
CAPRIN2	caprin family member 2	0.565	0.160	0.0073394
FAM102A	estrogen-induced osteoclastogenesis regulator 1	0.715	0.202	0.0074007
CLDN5	claudin 5	0.530	0.150	0.0074007
TSC22D3	TSC22 domain family member 3	1.253	0.355	0.0074456
LPIN2	lipin 2	0.595	0.168	0.00746
FAM117B	family with sequence similarity 117 member B	1.377	0.391	0.0075995
TNFRSF9	TNF receptor superfamily member 9	-4.310	1.224	0.0076924
DNAAF2	dynein axonemal assembly factor 2	1.140	0.324	0.0076966
UHRF1BP1	bridge-like lipid transfer protein family member 3A	-1.116	0.317	0.0077673
BCL2A1	BCL2 related protein A1	-2.423	0.689	0.0077801
ZNF652	zinc finger protein 652	0.704	0.200	0.0078934
SH3D19	SH3 domain containing 19	0.568	0.162	0.0078934
PHF12	PHD finger protein 12	0.662	0.188	0.0079019
C3orf38	chromosome 3 open reading frame 38	-0.621	0.177	0.0079673
C5orf15	chromosome 5 open reading frame 15	-0.702	0.200	0.0080357
CDC73	cell division cycle 73	-0.556	0.159	0.0081804
GRIPAP1	GRIP1 associated protein 1	-0.583	0.167	0.0082641
SPRY2	sprouty RTK signaling antagonist 2	1.106	0.316	0.0083308
ASPHD2	aspartate beta-hydroxylase domain containing 2	-1.223	0.350	0.0083308
KYNU	kynureninase	-3.043	0.871	0.0084415
C3orf58	divergent protein kinase domain 2A	0.708	0.203	0.0085308
LRRFIP2	LRR binding FLII interacting protein 2	-0.515	0.148	0.0085451
HMG20A	high mobility group 20A	0.551	0.158	0.0085563
RNF149	ring finger protein 149	-0.787	0.226	0.0086053
ABHD15	abhydrolase domain containing 15	0.843	0.242	0.0087056
OSGIN2	oxidative stress induced growth inhibitor family member 2	-0.747	0.215	0.0087368
PALMD	palmdelphin	0.850	0.244	0.0088188

LOC728769		-1.118	0.321	0.0088188
N4BP3	NEDD4 binding protein 3	0.863	0.249	0.009124
CDK6	cyclin dependent kinase 6	-0.576	0.166	0.0091529
GRAMD3	GRAM domain containing 2B	-1.118	0.323	0.0092684
ZFYVE26	zinc finger FYVE-type containing 26	-0.908	0.262	0.0092966
TBC1D2B	TBC1 domain family member 2B	0.627	0.181	0.0093628
ARID4A	AT-rich interaction domain 4A	0.675	0.195	0.0093911
SLFN11	schlafen family member 11	-0.845	0.245	0.0094813
RIF1	replication timing regulatory factor 1	-0.756	0.219	0.0094973
AMD1	adenosylmethionine decarboxylase 1	0.544	0.158	0.0095699
SIDT2	SID1 transmembrane family member 2	-0.795	0.230	0.0096027
EVI2B	ecotropic viral integration site 2B	1.247	0.361	0.0096117
RNF213	ring finger protein 213	-2.554	0.740	0.0096117
ADNP	activity dependent neuroprotector homeobox	0.510	0.148	0.0096336
BTN3A3	butyrophilin subfamily 3 member A3	-0.974	0.282	0.0096513
RET	ret proto-oncogene	-4.578	1.328	0.0096824
RANGAP1	Ran GTPase activating protein 1	-0.592	0.172	0.0097443
ANP32A	acidic nuclear phosphoprotein 32 family member A	0.507	0.147	0.0097754
FAM109A	PH domain containing endocytic trafficking adaptor 1	0.739	0.215	0.0098719
MAP2K3	mitogen-activated protein kinase kinase 3	-0.591	0.172	0.0099208
TMEM110	STIM activating enhancer	-0.736	0.214	0.0099443
KDM7A	lysine demethylase 7A	-1.023	0.298	0.0101898
DPYSL2	dihydropyrimidinase like 2	0.450	0.131	0.0102987
MOB1A	MOB kinase activator 1A	-0.629	0.184	0.01034
DOK5	docking protein 5	-0.704	0.205	0.0103706
DEDD	death effector domain containing	-0.681	0.199	0.0103875
PDE4B	phosphodiesterase 4B	-0.531	0.155	0.0103963
SELM	selenoprotein M	-0.727	0.212	0.0104406
PCGF5	polycomb group ring finger 5	-0.770	0.225	0.0104406
SGK1	serum/glucocorticoid regulated kinase 1	-0.803	0.234	0.0104576
SCO2	synthesis of cytochrome C oxidase 2	-0.659	0.193	0.0105416
PDCD1LG2	programmed cell death 1 ligand 2	-0.759	0.222	0.0105416
Mar-01		1.466	0.429	0.010559
CDK5R1	cyclin dependent kinase 5 regulatory subunit 1	1.282	0.375	0.0105745
NR5A2	nuclear receptor subfamily 5 group A member 2	1.040	0.304	0.0105745
ARHGEF28	Rho guanine nucleotide exchange factor 28	0.699	0.204	0.0105927
PANK1	pantothenate kinase 1	1.100	0.322	0.0106154
EGFL7	EGF like domain multiple 7	0.542	0.159	0.0106154
IPMK	inositol polyphosphate multikinase	-0.658	0.193	0.0106154
OPTN	optineurin	-0.908	0.266	0.0106421
INPP1	inositol polyphosphate-1-phosphatase	0.565	0.166	0.0107698
NOX4	NADPH oxidase 4	0.791	0.232	0.0108744
BEND3	BEN domain containing 3	1.097	0.322	0.0109185
ZBTB10	zinc finger and BTB domain containing 10	-0.590	0.173	0.0109686
KIAA1671	KIAA1671	0.855	0.251	0.0110547
ZNF589	zinc finger protein 589	0.931	0.274	0.0111712
HIF1A	hypoxia inducible factor 1 subunit alpha	-0.777	0.229	0.0112096
KLF7	KLF transcription factor 7	-0.614	0.181	0.0112241
ZC3H12A	zinc finger CCCH-type containing 12A	-0.984	0.290	0.0112295
MED13L	mediator complex subunit 13L	-0.814	0.240	0.0113016
ELMSAN1	mitotic deacetylase associated SANT domain protein	0.684	0.201	0.0113355
WEE1	WEE1 G2 checkpoint kinase	0.894	0.263	0.0114201
UBE2D3	ubiquitin conjugating enzyme E2 D3	-0.477	0.141	0.0114201
SUGT1P1	SUGT1 pseudogene 1	-1.244	0.367	0.0114574
C1S	complement C1s	-2.730	0.806	0.0115875
LIMD2	LIM domain containing 2	-0.552	0.163	0.0116169
PPP4R2	protein phosphatase 4 regulatory subunit 2	-0.576	0.170	0.0116169
PEAR1	platelet endothelial aggregation receptor 1	0.815	0.241	0.0118402
SERPINB1	serpin family B member 1	-0.969	0.287	0.0118807
CCNJL	cyclin J like	0.660	0.195	0.0120041
BMPR2	bone morphogenetic protein receptor type 2	-0.646	0.191	0.0120497
DCBLD1	discoidin, CUB and LCCL domain containing 1	0.585	0.173	0.0120619
ZNF195	zinc finger protein 195	0.659	0.195	0.0122447
RAD9A	RAD9 checkpoint clamp component A	-1.062	0.315	0.0122684
NUMA1	nuclear mitotic apparatus protein 1	0.535	0.159	0.0126183

SLC46A1	solute carrier family 46 member 1	1.262	0.376	0.0126226
BDNF	brain derived neurotrophic factor	1.248	0.372	0.0127561
CTNNBL1	catenin beta like 1	-0.532	0.159	0.0127561
IFNGR1	interferon gamma receptor 1	-0.827	0.246	0.0127561
BBS7	Bardet-Biedl syndrome 7	-0.569	0.170	0.0128168
NFE2L3	NFE2 like bZIP transcription factor 3	-0.731	0.218	0.012827
PNRC1	proline rich nuclear receptor coactivator 1	-0.741	0.221	0.012827
IBA57	iron-sulfur cluster assembly factor IBA57	-0.665	0.198	0.0128406
CASP8	caspase 8	-0.703	0.210	0.0128587
CDR2	cerebellar degeneration related protein 2	0.601	0.180	0.0131095
SKIDA1	SKI/DACH domain containing 1	-2.230	0.666	0.0131095
NCEH1	neutral cholesterol ester hydrolase 1	-0.694	0.207	0.0131477
FAM131A	family with sequence similarity 131 member A	0.793	0.237	0.0131676
PSEN1	presenilin 1	-0.707	0.211	0.0131745
TNFRSF10B	TNF receptor superfamily member 10b	-0.682	0.204	0.0131886
FAM45A	DENN domain containing 10	0.497	0.149	0.0131892
TPRN	taperin	0.794	0.238	0.0132401
PPARGC1B	PPARG coactivator 1 beta	1.611	0.483	0.0136144
ICAM4	intercellular adhesion molecule 4 (Landsteiner-Wiener blood group)	-2.407	0.722	0.0136947
ANKIB1	ankyrin repeat and IBR domain containing 1	-0.728	0.219	0.013902
SLC30A4	solute carrier family 30 member 4	-0.984	0.296	0.013902
ZNF362	zinc finger protein 362	0.609	0.183	0.0139401
TNFSF9	TNF superfamily member 9	-1.255	0.377	0.014061
SHC3	SHC adaptor protein 3	0.740	0.223	0.0142146
REST	RE1 silencing transcription factor	0.590	0.178	0.0142146
VPS37B	VPS37B subunit of ESCRT-I	0.616	0.185	0.0142146
TINF2	TERF1 interacting nuclear factor 2	-0.518	0.156	0.0142935
UGCG	UDP-glucose ceramide glucosyltransferase	-0.686	0.207	0.0143101
TOR1AIP1	torsin 1A interacting protein 1	-0.479	0.144	0.0143107
THAP11	THAP domain containing 11	0.638	0.192	0.014323
IL7	interleukin 7	-1.705	0.515	0.0144924
AIDA	axin interactor, dorsalization associated	-0.593	0.179	0.0145642
ARRDC2	arrestin domain containing 2	0.693	0.210	0.0147514
PRKAB1	protein kinase AMP-activated non-catalytic subunit beta 1	0.611	0.185	0.0147581
MTMR11	myotubularin related protein 11	-0.744	0.226	0.0151533
SWT1	SWT1 RNA endoribonuclease homolog	-0.913	0.277	0.0151945
PPP2R5A	protein phosphatase 2 regulatory subunit B'alpha	0.576	0.175	0.0157122
ADAM17	ADAM metallopeptidase domain 17	-0.615	0.187	0.0157767
CORO7-PAM16	CORO7-PAM16 readthrough	-4.862	1.481	0.0159502
HSF2	heat shock transcription factor 2	0.790	0.241	0.0160428
MDGA1	MAM domain containing glycosylphosphatidylinositol anchor 1	-1.043	0.318	0.0160996
SSH1	slingshot protein phosphatase 1	-0.597	0.182	0.0161437
SLC4A7	solute carrier family 4 member 7	0.540	0.165	0.0161473
PPP1R16B	protein phosphatase 1 regulatory subunit 16B	0.972	0.296	0.016155
MAP3K4	mitogen-activated protein kinase kinase kinase 4	0.626	0.191	0.0161991
LRFN5	leucine rich repeat and fibronectin type III domain containing 5	-3.012	0.919	0.0162217
MEDAG	mesenteric estrogen dependent adipogenesis	0.921	0.281	0.0164517
FRAT2	FRAT regulator of WNT signaling pathway 2	0.815	0.249	0.0164644
TRIM2	tripartite motif containing 2	0.805	0.246	0.0164954
RASA4B	RAS p21 protein activator 4B	-1.074	0.329	0.0167861
LGALS3BP	galectin 3 binding protein	-0.967	0.296	0.0168222
LOC101929668		-1.429	0.438	0.0168618
SCYL2	SCY1 like pseudokinase 2	-0.477	0.146	0.0169215
GIT2	GIT ArfGAP 2	0.508	0.156	0.0169569
RELN	reelin	-0.654	0.200	0.0169569
WFS1	wolframin ER transmembrane glycoprotein	0.555	0.170	0.0169991
SESN1	sestrin 1	0.637	0.196	0.0170479
NFATC2	nuclear factor of activated T cells 2	1.032	0.317	0.0172656
GLUL	glutamate-ammonia ligase	-0.443	0.136	0.0172989
FAM177A1	family with sequence similarity 177 member A1	-0.509	0.156	0.0172989

FGD4	FYVE, RhoGEF and PH domain containing 4	0.886	0.273	0.0174133
SH3BP5	SH3 domain binding protein 5	0.591	0.182	0.0174349
SLC35E4	solute carrier family 35 member E4	0.591	0.182	0.0174349
PTX3	pentraxin 3	-0.655	0.201	0.0175279
SLC19A1	solute carrier family 19 member 1	0.551	0.170	0.0176906
TAPBP	TAP binding protein	-0.844	0.260	0.0177174
SLC5A3	solute carrier family 5 member 3	0.741	0.228	0.0177292
FAM60A	SIN3-HDAC complex associated factor	0.580	0.179	0.0178132
POLR3D	RNA polymerase III subunit D	-0.499	0.154	0.0178162
TNFRSF10A	TNF receptor superfamily member 10a	-0.562	0.173	0.0178162
TMX4	thioredoxin related transmembrane protein 4	-0.522	0.161	0.0182044
PNPLA8	patatin like phospholipase domain containing 8	-0.583	0.180	0.0182508
ETV1	ETS variant transcription factor 1	0.962	0.298	0.0186681
RBCK1	RANBP2-type and C3HC4-type zinc finger containing 1	-0.760	0.235	0.0187653
CBX4	chromobox 4	-0.786	0.244	0.0191597
ZNF850	zinc finger protein 850	1.177	0.365	0.019183
DSE	dermatan sulfate epimerase	-0.535	0.166	0.019183
ETAA1	ETAA1 activator of ATR kinase	0.643	0.200	0.0191899
GAS2L1	growth arrest specific 2 like 1	0.633	0.197	0.0192124
ARHGAP25	Rho GTPase activating protein 25	1.251	0.389	0.0192429
NFE2L1	NFE2 like bZIP transcription factor 1	-0.544	0.169	0.0192429
PATZ1	POZ/BTB and AT hook containing zinc finger 1	0.809	0.252	0.0192689
C12orf68	coiled-coil domain containing 184	-1.977	0.615	0.0193446
DUSP8	dual specificity phosphatase 8	-0.945	0.294	0.019411
UPP1	uridine phosphorylase 1	-0.681	0.212	0.0194693
FNIP2	folliculin interacting protein 2	-0.755	0.235	0.0194693
HID1	HID1 domain containing	0.658	0.205	0.0200271
BHLHB9	G protein-coupled receptor associated sorting protein family member 3	0.788	0.247	0.021113
KIAA0247	sushi domain containing 6	-1.055	0.331	0.0213866
ANKZF1	ankyrin repeat and zinc finger peptidyl tRNA hydrolase 1	0.674	0.212	0.021414
SMAD5	SMAD family member 5	0.529	0.166	0.021414
SCARB2	scavenger receptor class B member 2	-0.438	0.137	0.021414
FAM86B1	family with sequence similarity 86 member B1	1.187	0.373	0.0214883
CDV3	CDV3 homolog	-0.621	0.195	0.0214883
RHEBL1	RHEB like 1	-1.507	0.474	0.0216766
EHMT2	euchromatic histone lysine methyltransferase 2	0.627	0.197	0.0219014
JMY	junction mediating and regulatory protein, p53 cofactor	0.826	0.260	0.0219856
MKNK2	MAPK interacting serine/threonine kinase 2	0.563	0.177	0.0219998
SQSTM1	sequestosome 1	-0.645	0.203	0.0219998
LOC100129034		0.732	0.231	0.0221957
LHFP	LHFPL tetraspan subfamily member 6	-0.499	0.157	0.0222082
PCNX	pecanex 1	-0.856	0.270	0.0222653
PAOX	polyamine oxidase	-0.989	0.312	0.0223539
SEC24D	SEC24 homolog D, COPII coat complex component	-0.429	0.135	0.0224214
DDO	D-aspartate oxidase	-2.240	0.707	0.0224717
HLTF	helicase like transcription factor	0.611	0.193	0.0225341
TRIM25	tripartite motif containing 25	-1.909	0.603	0.0226332
SLC1A1	solute carrier family 1 member 1	0.696	0.220	0.0229996
SIAH2	siah E3 ubiquitin protein ligase 2	-0.563	0.178	0.0230716
G0S2	G0/G1 switch 2	-1.655	0.524	0.0231592
ATXN7	ataxin 7	-0.863	0.274	0.0235176
PRDM8	PR/SET domain 8	-1.219	0.387	0.0235701
GATA3	GATA binding protein 3	1.079	0.342	0.0235822
CAMK2G	calcium/calmodulin dependent protein kinase II gamma	0.611	0.194	0.0238757
SOHLH2	spermatogenesis and oogenesis specific basic helix-loop-helix 2	6.008	1.910	0.0239305
APOL4	apolipoprotein L4	-1.595	0.507	0.0239705
AKAP7	A-kinase anchoring protein 7	-1.094	0.348	0.0243381
HIAT1	major facilitator superfamily domain containing 14A	-0.619	0.197	0.0244257
ABL2	ABL proto-oncogene 2, non-receptor tyrosine kinase	-0.554	0.177	0.0244692

POMGNT1	protein O-linked mannose N-acetylglucosaminyltransferase 1 (beta 1,2-)	-0.439	0.140	0.024569
TRANK1	tetratricopeptide repeat and ankyrin repeat containing 1	-2.192	0.699	0.024569
TGIF2	TGFB induced factor homeobox 2	-0.557	0.178	0.0246186
RALGAPA2	Ral GTPase activating protein catalytic subunit alpha 2	-0.728	0.232	0.0246186
ATP13A3	ATPase 13A3	-0.732	0.234	0.0246186
LNPEP	leucyl and cystinyl aminopeptidase	-0.857	0.273	0.0246186
CA13	carbonic anhydrase 13	-1.113	0.355	0.0246186
KIAA0922	transmembrane 131 like	0.667	0.213	0.0247178
APH1A	aph-1 homolog A, gamma-secretase subunit	-0.419	0.134	0.0249235
ASAP2	ArfGAP with SH3 domain, ankyrin repeat and PH domain 2	0.561	0.179	0.0250379
TBX20	T-box transcription factor 20	-1.415	0.453	0.0251678
TNFSF18	TNF superfamily member 18	-0.604	0.193	0.025183
STX12	syntaxin 12	-0.516	0.165	0.0253169
GLTPD1	ceramide-1-phosphate transfer protein	0.480	0.154	0.0254718
PPP3CC	protein phosphatase 3 catalytic subunit gamma	-0.562	0.180	0.0254718
LOC101928262		1.393	0.447	0.0258913
AMPD2	adenosine monophosphate deaminase 2	0.521	0.167	0.0260095
CHML	CHM like Rab escort protein	0.623	0.200	0.0262519
AHNAK2	AHNAK nucleoprotein 2	0.780	0.251	0.0263933
FLJ31306	PSMA3 antisense RNA 1	0.738	0.237	0.0263933
MERTK	MER proto-oncogene, tyrosine kinase	0.902	0.290	0.0266297
SLC9A8	solute carrier family 9 member A8	-0.608	0.196	0.0267182
FZD8	frizzled class receptor 8	0.564	0.182	0.02685
TMEM38B	transmembrane protein 38B	-0.769	0.248	0.0269955
MIR155HG	MIR155 host gene	-3.043	0.982	0.0272874
PIK3R3	phosphoinositide-3-kinase regulatory subunit 3	-0.816	0.263	0.0273094
RBMS1	RNA binding motif single stranded interacting protein 1	-0.439	0.142	0.0273353
LOC284837		1.591	0.514	0.0275483
KCTD1	potassium channel tetramerization domain containing 1	0.700	0.226	0.0275483
AP4B1	adaptor related protein complex 4 subunit beta 1	0.609	0.197	0.0275483
SMARCA5-AS1	SMARCA5 antisense RNA 1	-3.406	1.101	0.0275483
CARD16	caspase recruitment domain family member 16	-0.476	0.154	0.027791
PKP2	plakophilin 2	0.613	0.198	0.0278617
ERCC5	ERCC excision repair 5, endonuclease	0.508	0.165	0.0282828
MSRB1	methionine sulfoxide reductase B1	-0.543	0.176	0.0282965
SLC25A25	solute carrier family 25 member 25	-0.779	0.253	0.0285059
NPAS3	neuronal PAS domain protein 3	-2.146	0.696	0.0285059
EFR3A	EFR3 homolog A	-0.454	0.147	0.0286159
MAP3K13	mitogen-activated protein kinase kinase kinase 13	-0.532	0.173	0.0290787
MAD2L1BP	MAD2L1 binding protein	-0.597	0.194	0.0292192
EPN3	epsin 3	2.821	0.918	0.0292836
PURG	purine rich element binding protein G	1.339	0.436	0.0292836
LINC00961	small regulatory polypeptide of amino acid response	0.817	0.266	0.0296278
TMC7	transmembrane channel like 7	1.125	0.367	0.0297948
STOM	stomatin	-0.472	0.154	0.0297948
DPYSL3	dihydropyrimidinase like 3	-0.483	0.157	0.0297948
ZNF30	zinc finger protein 30	1.402	0.457	0.0298392
CASP2	caspase 2	0.515	0.168	0.0301375
MALT1	MALT1 paracaspase	-0.632	0.206	0.0301619
APBA1	amyloid beta precursor protein binding family A member 1	0.673	0.220	0.0302224
ELF4	E74 like ETS transcription factor 4	-0.861	0.282	0.0303776
MOV10	Mov10 RISC complex RNA helicase	-0.756	0.247	0.0304004
LOC90784		0.590	0.193	0.0305011
CD3EAP	RNA polymerase I subunit G	0.762	0.249	0.0306518
EPOR	erythropoietin receptor	0.625	0.205	0.0306518
IFNGR2	interferon gamma receptor 2	-0.657	0.215	0.0307963
ORAI1	ORAI calcium release-activated calcium modulator 1	0.519	0.170	0.030826
EFHC1	EF-hand domain containing 1	0.551	0.181	0.0310274
TNFSF13B	TNF superfamily member 13b	-3.850	1.262	0.0310274

STK40	serine/threonine kinase 40	-0.585	0.192	0.0312842
CYP1B1	cytochrome P450 family 1 subfamily B member 1	-3.063	1.006	0.0316038
B4GALT4	beta-1,4-galactosyltransferase 4	-0.807	0.265	0.031744
FRY	FRY microtubule binding protein	0.690	0.227	0.0318875
LRRC59	leucine rich repeat containing 59	-0.390	0.128	0.0319603
CBX2	chromobox 2	0.695	0.229	0.0319901
BCAT1	branched chain amino acid transaminase 1	0.440	0.145	0.0320104
USP3	ubiquitin specific peptidase 3	0.640	0.211	0.0321637
CDKL5	cyclin dependent kinase like 5	-0.829	0.273	0.0323975
ZNF692	zinc finger protein 692	0.630	0.208	0.0331292
SOAT1	sterol O-acyltransferase 1	-0.473	0.156	0.0331292
UAP1L1	UDP-N-acetylglucosamine pyrophosphorylase 1 like 1	0.586	0.193	0.0331644
TSPAN14	tetraspanin 14	0.515	0.170	0.0331927
IER5	immediate early response 5	-0.649	0.214	0.0332578
SPOCD1	SPOC domain containing 1	-0.641	0.212	0.0332754
TRAK2	trafficking kinesin protein 2	0.489	0.162	0.0333626
FIGN	fidgetin, microtubule severing factor	1.116	0.370	0.0338362
LOC101927085		1.431	0.474	0.0340232
RILP	Rab interacting lysosomal protein	-0.673	0.223	0.0340232
MAD2L2	mitotic arrest deficient 2 like 2	-0.501	0.166	0.0344731
PPAT	phosphoribosyl pyrophosphate amidotransferase	0.743	0.247	0.0344968
LGALS9	galectin 9	-2.089	0.694	0.0345397
CSRP2BP	lysine acetyltransferase 14	0.707	0.235	0.0349024
GIT1	GIT ArfGAP 1	0.491	0.163	0.0352006
NOTCH2	notch receptor 2	-0.573	0.191	0.0352284
FAM129A	niban apoptosis regulator 1	-1.207	0.402	0.0353476
DDX52	DExD-box helicase 52	-0.478	0.159	0.0356506
C2CD2L	C2CD2 like	0.612	0.204	0.0357243
MXD1	MAX dimerization protein 1	-0.623	0.208	0.0357311
LDLRAP1	low density lipoprotein receptor adaptor protein 1	0.560	0.187	0.0357793
PELI1	pellino E3 ubiquitin protein ligase 1	-0.781	0.260	0.0358059
CDKN1B	cyclin dependent kinase inhibitor 1B	0.594	0.198	0.0362327
TMEM170A	transmembrane protein 170A	-0.814	0.272	0.0362327
ST3GAL6	ST3 beta-galactoside alpha-2,3-sialyltransferase 6	0.733	0.245	0.0368621
IMPA1	inositol monophosphatase 1	-0.473	0.158	0.0369514
NRBP1	nuclear receptor binding protein 1	-0.455	0.152	0.0371203
SETD8	lysine methyltransferase 5A	0.517	0.173	0.0371306
NHSL2	NHS like 2	0.672	0.225	0.0371324
GPR37	G protein-coupled receptor 37	-0.584	0.196	0.037207
ATXN1L	ataxin 1 like	-0.737	0.247	0.0374822
FAM78A	family with sequence similarity 78 member A	1.468	0.492	0.0375792
ADPRH	ADP-ribosylarginine hydrolase	-0.716	0.240	0.0378456
PIK3IP1	phosphoinositide-3-kinase interacting protein 1	0.605	0.203	0.0379183
EEF1E1-BLOC1S5	EEF1E1-BLOC1S5 readthrough (NMD candidate)	-2.310	0.776	0.038126
PAQR4	progestin and adipoQ receptor family member 4	0.633	0.213	0.0391805
ARL4C	ADP ribosylation factor like GTPase 4C	0.818	0.276	0.0393356
UBXN2A	UBX domain protein 2A	-0.517	0.174	0.0396244
RRAGC	Ras related GTP binding C	-0.495	0.167	0.039666
HJURP	Holliday junction recognition protein	0.553	0.187	0.0398267
ITIH4	inter-alpha-trypsin inhibitor heavy chain 4	-2.179	0.736	0.0398729
DNAJB5	DnaJ heat shock protein family (Hsp40) member B5	-0.688	0.232	0.0400539
AKIRIN2	akirin 2	-0.491	0.166	0.040767
FAM43A	family with sequence similarity 43 member A	0.589	0.200	0.0409482
ZNF205	zinc finger protein 205	0.570	0.193	0.0412267
SNIP1	Smad nuclear interacting protein 1	-0.532	0.181	0.0419524
PLCD3	phospholipase C delta 3	0.564	0.192	0.0419699
WDFY1	WD repeat and FYVE domain containing 1	-0.410	0.139	0.0419699
TMEM87A	transmembrane protein 87A	-0.448	0.152	0.0419699
STAT6	signal transducer and activator of transcription 6	-0.585	0.199	0.0419699
PNMA1	PNMA family member 1	0.493	0.168	0.0424843
AMER1	APC membrane recruitment protein 1	-0.987	0.336	0.0426109

STX5	syntaxin 5	-0.468	0.160	0.0428651
YPEL2	yippee like 2	-0.806	0.275	0.0428748
PALD1	phosphatase domain containing paladin 1	0.872	0.297	0.0429661
CCNYL1	cyclin Y like 1	-0.481	0.164	0.0432701
AKAP2	A-kinase anchoring protein 2	-0.680	0.232	0.0433002
NFIA	nuclear factor I A	0.628	0.214	0.0434272
KIAA0226	rubicon autophagy regulator	-0.746	0.255	0.043631
HOXA9	homeobox A9	1.368	0.467	0.0437123
REV1	REV1 DNA directed polymerase	0.591	0.202	0.0437375
LRRC58	leucine rich repeat containing 58	0.499	0.170	0.0439431
HIST2H4A	H4 clustered histone 14	-1.766	0.604	0.0440328
TRIM36	tripartite motif containing 36	-1.106	0.378	0.0441069
USP9X	ubiquitin specific peptidase 9 X-linked	-0.553	0.189	0.0446369
PDE5A	phosphodiesterase 5A	-0.651	0.223	0.044754
C15orf52	coiled-coil domain containing 9B	0.759	0.261	0.0456999
SHE	Src homology 2 domain containing E	0.658	0.226	0.0457902
TSEN2	tRNA splicing endonuclease subunit 2	0.746	0.256	0.0458884
TMEM201	transmembrane protein 201	0.542	0.186	0.0464065
COL4A1	collagen type IV alpha 1 chain	-0.494	0.170	0.047068
SNHG7	small nucleolar RNA host gene 7	0.502	0.173	0.0470822
TXNL4B	thioredoxin like 4B	-0.572	0.197	0.0471684
RAB10	RAB10, member RAS oncogene family	-0.397	0.137	0.0472358
KDM2A	lysine demethylase 2A	-0.547	0.189	0.0472358
BAZ2A	bromodomain adjacent to zinc finger domain 2A	-0.720	0.249	0.0472543
ZBTB14	zinc finger and BTB domain containing 14	0.605	0.209	0.0473667
NEDD4	NEDD4 E3 ubiquitin protein ligase	-0.550	0.190	0.0473674
SLK	STE20 like kinase	-0.414	0.143	0.0474361
IL8	C-X-C motif chemokine ligand 8	-3.323	1.148	0.0476292
TGIF1	TGFB induced factor homeobox 1	-0.501	0.173	0.0478644
HTR7P1	5-hydroxytryptamine receptor 7 pseudogene 1	0.853	0.295	0.0479455
IL16	interleukin 16	2.350	0.813	0.0480058
CYP1A1	cytochrome P450 family 1 subfamily A member 1	0.981	0.339	0.0480058
TIGD5	tigger transposable element derived 5	0.697	0.241	0.0480058
RBM8A	RNA binding motif protein 8A	-0.386	0.133	0.0480058
HES2	hes family bHLH transcription factor 2	0.599	0.207	0.0481464
ZCCHC2	zinc finger CCHC-type containing 2	-0.830	0.287	0.0482585
MED13	mediator complex subunit 13	-0.592	0.205	0.0486786
MAFK	MAF bZIP transcription factor K	0.522	0.181	0.0488436
VAMP5	vesicle associated membrane protein 5	-0.396	0.137	0.0488857
PDLIM4	PDZ and LIM domain 4	-0.475	0.165	0.0489333
POLRMT	RNA polymerase mitochondrial	0.525	0.182	0.0489381
TMEM37	transmembrane protein 37	1.239	0.430	0.0490082
C19orf12	chromosome 19 open reading frame 12	-0.650	0.226	0.0490082
SAMD10	sterile alpha motif domain containing 10	1.039	0.361	0.0492581
FAM217B	family with sequence similarity 217 member B	0.819	0.284	0.0493655
NANP	N-acetylneuraminic acid phosphatase	0.677	0.235	0.0493655
EPT1	selenoprotein I	-0.523	0.182	0.0493655
LRRC3	leucine rich repeat containing 3	-0.741	0.258	0.0493655
PLCXD1	phosphatidylinositol specific phospholipase C X domain containing 1	0.705	0.245	0.0495184

Log2 fold change between siCTL unstimulated versus siCTL poly(I:C)-treated (4 hours) hPAECs as calculated using DESeq2 bioinformatic package. SE; standard error of Log2 fold change. The *p*-value (not shown in this table) calculated using Wald test and adjusted for multiple hypothesis testing using the Benjamini-Hocberg procedure (adjusted (adj.) *p*-value).

9.4.5. List of DEGs from siGCN2-treated unstimulated versus siCTL unstimulated hPAECs

Table 5. DEGs (i.e., an adjusted p-value ≤ 0.05) in si*GCN2*-treated unstimulated versus siCTL unstimulated hPAECs

Gene Symbol	*Gene Name*	*Log2 (Fold Change)*	*SE of Log2*	*Adj. p-value*
CNN1	Calponin 1	2.459	0.412	1.78E-05
PTX3	Pentraxin 3	-0.903	0.151	1.78E-05
COL4A6	Collagen, Type IV, Alpha 6	-0.991	0.176	9.29E-05
FABP4	Fatty Acid Binding Protein 4	1.067	0.205	5.84E-04
STC1	Stanniocalcin 1	-1.145	0.219	5.84E-04
COL1A2	Collagen Type I Alpha 2 Chain [2]	0.877	0.175	0.00126879
ADIRF	Adipogenesis Regulatory Factor	-0.817	0.169	0.00276475
GABBR2	Gamma-Aminobutyric Acid Type B Receptor Subunit 2	-0.782	0.165	0.00331717
HMOX1	Heme Oxygenase 1	0.590	0.124	0.00331717
TGM2	Transglutaminase 2	-0.520	0.111	0.00365164
CCDC81	Coiled-Coil Domain Containing 81	1.942	0.424	0.00596214
FAM107A	Family With Sequence Similarity 107 Member A	-0.663	0.145	0.00611615
PLAT	Plasminogen Activator, Tissue Type	-0.647	0.144	0.00793738
COL4A5	Collagen Type IV Alpha 5 Chain	-0.575	0.129	0.00825337
RGS5	Regulator Of G Protein Signaling 5	-0.563	0.127	0.0086703
IRF6	Interferon Regulatory Factor 6	0.863	0.197	0.01090639
VCAN	Versican	0.998	0.230	0.01173688
EIF2AK4	Eukaryotic Translation Initiation Factor 2 Alpha Kinase 4 (GCN2)	-2.063	0.489	0.0196308
HTRA1	HtrA Serine Peptidase 1	0.442	0.107	0.02966995
SEMA3F	Semaphorin 3F	-0.526	0.129	0.03156357
BGN	Biglycan	0.451	0.112	0.03669423
FBLN5	Fibulin 5	0.799	0.202	0.04781618
FLJ41200	Long Intergenic Non-Protein Coding RNA 1235	-0.828	0.209	0.04781618
LYVE1	Lymphatic Vessel Endothelial Hyaluronan Receptor 1	-0.803	0.204	0.04781618
CLDN11	Claudin 11	-0.574	0.147	0.04950342
PIEZO2	Piezo Type Mechanosensitive Ion Channel Component 2	-0.558	0.142	0.04950342

Log2 fold change between si*GCN2*-treated unstimulated versus siCTL unstimulated hPAECs as calculated using DESeq2 bioinformatic package. SE; standard error of Log2 fold change. The *p*-value (not shown in this table) calculated using Wald test and adjusted for multiple hypothesis testing using the Benjamini-Hocberg procedure (adjusted (adj.) *p*-value